January 2015

Influence of Architecture Design on the Performance and Fuel Efficiency of Hydraulic Hybrid Transmissions

Michael Wayne Sprengel
Purdue University

Graduate School Form 30
Updated 1/15/2015

PURDUE UNIVERSITY
GRADUATE SCHOOL
Thesis/Dissertation Acceptance

This is to certify that the thesis/dissertation prepared

By Michael W. Sprengel

Entitled

Influence of Architecture Design on the Performance and Fuel Efficiency of Hydraulic Hybrid Transmissions

For the degree of Doctor of Philosophy

Is approved by the final examining committee:

Dr. Monika Ivantysynova
Chair

Dr. Dennis Buckmaster

Dr. John Starkey

Dr. Andrea Vacca

To the best of my knowledge and as understood by the student in the Thesis/Dissertation Agreement, Publication Delay, and Certification Disclaimer (Graduate School Form 32), this thesis/dissertation adheres to the provisions of Purdue University's "Policy of Integrity in Research" and the use of copyright material.

Approved by Major Professor(s): Dr. Monika Ivantysynova

Approved by: Dr. Bernie Engel 11/18/2015

Head of the Departmental Graduate Program Date

INFLUENCE OF ARCHITECTURE DESIGN ON THE PERFORMANCE AND FUEL EFFICIENCY OF HYDRAULIC HYBRID TRANSMISSIONS

A Dissertation

Submitted to the Faculty

of

Purdue University

by

Michael W. Sprengel

In Partial Fulfillment of the

Requirements for the Degree

of

Doctor of Philosophy

December 2015

Purdue University

West Lafayette, Indiana

ACKNOWLEDGEMENTS

I must first thank my advisor Dr. Monika Ivantysynova for all of the opportunities she has provided me with over the past five plus years. Her guidance, support, and willingness to repeatedly engage with me in long discussions against conventional viewpoints has helped me grow both personally and professionally. Further her generosity and kindness has provided me with more opportunities than I ever thought possible. Thank you.

Advancing the state of the art is rarely an individual affair and my experience has certainly been no different. There are many graduate researchers at the Maha Fluid Power Research Center that I would like to thank including Michael (Mac) Cross for introducing me to, and passing on his knowledge regarding, hydraulic hybrids. I would also like to thank Naseem Daher, Paul Kalbfleisch, Dan Mizell, Tim Opperwall, Andrew Schenk, and many other lab members for providing suggestions when I was stuck, as well as a willingness to serve as sounding boards for my various thoughts. I also greatly appreciate all the researchers who helped make the blended hybrid demonstration vehicle a reality including the team lead Tyler Bleazard along with Hiral Haria, Ryan Jenkins, Nate Keller, and Ning Liu. Certainly very little of my physical testing and validation work would have been fully realized without the exceptionally hard work and dedication of the Maha lab manager Anthony Franklin. Similarly Susan Granger consistently went well beyond her administrative responsibilities to provide me with unmatched support and kindness. I would also like to thank my committee members including especially Dr. Andrea Vacca as well as Dr. Dennis Buckmaster and Dr. John Starkey.

Finally I would like to thank my family for their unwavering support and encouragement leading up to, and throughout, my graduate education.

TABLE OF CONTENTS

Page

Page

LIST OF SYMBOLS

a_D	System dynamics	[-]
A_f	Vehicle frontal area	[m^2]
A	Vehicle inclination	[rad]
α_{wheel}	Wheel acceleration	[rad/s^2]
β	Normalized unit displacement	[-]
β_1	Normalized Unit 1 displacement	[-]
β_2	Normalized Unit 2 displacement	[-]
β_3	Normalized Unit 3 displacement	[-]
C	Number of control combinations	[-]
C_d	Aerodynamic drag coefficient	[-]
$C_{H\ acm}$	Accumulator capacitance	[m^3/Pa]
C_r	Coefficient of rolling resistance	[-]
C_V	Valve flow coefficient	[$m^3/Pa{\cdot}s$]
C_v	Specific heat	[J/kmol·k]
$e_{\omega_{CE}}$	Engine speed error	[rpm]
F_d	Aerodynamic drag	[N]
F_g	Grading force	[N]
F_{rr}	Rolling resistance	[N]
f_M	Torque losses	[Nm]
f_Q	Flow losses	[m^3/s]
$fuel_{CE}$	Engine fuel consumption	[m^3/s]
g	Gravitational constant	[m/s^2]
g_D	DP transitional cost	[-]
$grade$	Vehicle inclination	[-]
i	Gear ratio	[-]
i_0	PGT standing gear ratio	[-]
i_{axle}	Axle ratio	[-]
I_{CE}	Engine inertia	[$kg{\cdot}m^2$]

i_{gear}	Gear ratio	[-]
i_{HST}	Hydrostatic transmission ratio	[-]
$i_{pmp\ drv}$	Pump drive ratio	[-]
J^*	DP optimal cost matrix	[-]
K	DP stage counter	[-]
k_d	Derivative gain	[-]
k_i	Integral gain	[-]
kmol	Kilomoles of gas	[kmol]
K_{oil}	Bulk modulus of oil	[Pa]
k_p	Proportional gain	[-]
$K_{p\ ref}$	Reference pressure gain	[Pa]
k_{split}	Desired Unit 2/3 torque split	[-]
K_{TQ}	Torque converter K factor	[-]
λ	Linear scaling term	[-]
M_2	Unit 2 torque	[Nm]
M_3	Unit 3 torque	[Nm]
$M_{3\ des}$	Desired Unit 3 torque	[Nm]
$M_{2,3}$	Unit 2 and 3 torque	[Nm]
$M_{2,3\ des}$	Desired Unit 2 and 3 torque	[Nm]
m_{air}	Air mass flowrate	[kg/s]
$M_{brake\ torque\ map}$	Desired brake torque map	[Nm]
M_{CE}	Engine torque	[Nm]
$M_{CE\ load}$	Engine load	[Nm]
M_{eff}	Effective torque	[Nm]
M_I	Torque converter impeller torque	[Nm]
M_{in}	Spur gear torque	[Nm]
M_{load}	Load simulator torque	[Nm]
$M_{load\ des}$	Desired load simulator torque	[Nm]
M_{out}	Spur gear torque	[Nm]
$M_{pmp\ drv}$	Pump drive torque	[Nm]
M_S	Torque losses	[Nm]
$M_{S\ scaled}$	Scaled torque losses	[Nm]
M_T	Torque converter turbine torque	[Nm]
M_{th}	Theoretical torque	[Nm]
M_{trans}	Transmission torque	[Nm]
m_{veh}	Vehicle mass	[kg]
M_{wheel}	Wheel torque	[Nm]

$M_{\text{wheel front}}$	Front wheel torque	[Nm]
$M_{\text{wheel rear}}$	Rear wheel torque	[Nm]
M_{WOT}	Wide open throttle torque	[Nm]
n	Polytropic coefficient	[-]
N	Number of DP stages	[-]
η_{acm}	Accumulator efficiency	[-]
η_{hm}	Hydromechanical efficiency	[-]
η_{vol}	Volumetric efficiency	[-]
ω	Angular speed	[rpm]
ω_1	Unit 1 speed	[rpm]
ω_2	Unit 2 speed	[rpm]
ω_3	Unit 3 speed	[rpm]
ω_{C}	Carrier gear speed	[rpm]
ω_{CE}	Engine speed	[rpm]
$\omega_{\text{CE des}}$	Desired engine speed	[rpm]
$\omega_{\text{CE des map}}$	Desired engine speed	[rpm]
ω_{I}	Torque converter impeller speed	[rpm]
ω_{in}	Spur gear speed	[rpm]
ω_{load}	Load simulator speed	[rpm]
$\omega_{\text{load des}}$	Desired load simulator speed	[rpm]
ω_{out}	Spur gear speed	[rpm]
ω_{R}	Ring gear speed	[rpm]
ω_{S}	Sun gear speed	[rpm]
ω_{T}	Torque converter turbine speed	[rpm]
ω_{wheel}	Wheel speed	[rpm]
$\omega_{\text{wheel des}}$	Desired wheel speed	[rpm]
ρ	Density	[kg/m^3]
p	Pressure	[Pa]
Δp	Differential pressure	[Pa]
p_0	Effective gas pressure	[Pa]
p_{A}	Pressure in Line A	[Pa]
p_{acm}	High pressure accumulator pressure	[Pa]
p_{B}	Pressure in Line B	[Pa]
p_{C}	Pressure in Line C	[Pa]
p_{HP}	High pressure accumulator pressure	[Pa]
$p_{\text{HP ref}}$	High pressure accumulator reference pressure	[Pa]
p_{in}	Valve inlet pressure	[Pa]

p_{LP}	Low pressure accumulator pressure	[Pa]
p_{out}	Valve outlet pressure	[Pa]
$p_{optimal}$	Optimal pressure	[Pa]
p_{ref}	Reference pressure	[Pa]
p_{set}	Relief valve set pressure	[Pa]
p_{therm}	Accumulator pressure thermal model	[kPa]
$P_{CE\ ref}$	Reference engine power	[kW]
$P_{CE\ scaled}$	Scaled engine power	[kW]
Q	Flow rate	[m^3/s]
Q_1	Unit 1 flow rate	[m^3/s]
Q_2	Unit 2 flow rate	[m^3/s]
Q_3	Unit 3 flow rate	[m^3/s]
$Q_{Unit1\ max}$	Unit 1 maximum flow rate	[m^3/s]
$Q_{Unit2\ max}$	Unit 2 maximum flow rate	[m^3/s]
$Q_{Unit2,\ 3\ max}$	Unit 2 and 3 maximum flow rate	[m^3/s]
Q_A	Port A flow	[m^3/s]
Q_{acm}	Accumulator flow rate	[m^3/s]
Q_B	Port B flow	[m^3/s]
Q_{CE}	Fuel consumption flow rate	[kg/s]
Q_{eff}	Effective flow rate	[m^3/s]
Q_S	Flow losses	[m^3/s]
$Q_{S\ scaled}$	Scaled flow losses	[m^3/s]
Q_{Se}	External flow losses	[m^3/s]
Q_{Si}	Internal flow losses	[m^3/s]
Q_{th}	Theoretical flow rate	[m^3/s]
R	Universal gas constant	[$kPa \cdot m^3/\ kmol \cdot K$]
r_{dyn}	Tire dynamic rolling radius	[m]
R_{TQ}	Torque converter torque ratio	[-]
S	Number of state combinations	[-]
t	Time	[s]
T	Temperature	[k]
T_{acm}	Ambient Temperature	[k]
τ	Thermal time constant	[s]
u	Control	[-]
U	Array of controls	[-]
U^*	DP optimal control matrix	[-]
$u_{brake\ pedal}$	Normalized brake pedal position	[-]

u_{CE}	Engine throttle	[-]
u_{clutch}	Clutch force	[N]
$u_{clutch\ lockup}$	Clutch lockup command	[-]
u_{enab}	Enabling valve command	[-]
$u_{throttle\ pedal}$	Normalized throttle pedal position	[-]
$u_{\omega_{CE}}$	Controller output	[-]
V	Volume	[m^3]
V_0	Effective gas volume	[m^3]
V_1	Unit 1 displacement	[m^3/rev]
V_2	Unit 2 displacement	[m^3/rev]
V_3	Unit 3 displacement	[m^3/rev]
V_{acm}	Accumulator volume	[m^3]
V_i	Derived displacement	[m^3/rev]
V_{ref}	Reference unit displacement	[m^3/rev]
V_{scaled}	Scaled unit displacement	[m^3/rev]
v_{veh}	Vehicle velocity	[km/h]
v	Molar density	[m^3/kmol]
X	State	[-]
X	Array of states	[-]

LIST OF ABBREVIATIONS

BSFC	Brake Specific Fuel Consumption
CAD	Computer Aided Design
cRIO	Compact Reconfigurable Input Output
CVT	Continuously Variable Transmission
DAQ	Data Acquisition
DP	Dynamic Programming
EoS	Equations of State
EPA	Environmental Protection Agency
FB	Feedback
FF	Feedforward
GVM	Gross Vehicle Mass
HIL	Hardware-in-the-Loop
HP	High Pressure
HST	Hydrostatic Transmission
ICE	Internal Combustion Engine
JC08	Japanese JC08 Driving Schedule
LA92	Unified Dynamometer Driving Schedule
LP	Low Pressure
NI	National Instruments
NN	Neural Network
NVH	Noise, Vibration, Harshness
PGT	Planetary Gear Train
PID	Proportional, Integral, Derivative
PST	Power Split Transmission
SC03	EPA Speed Corrected SC03 Driving Schedule
SDP	Stochastic Dynamic Programming
UDDS	Urban Dynamometer Driving Schedule
VFD	Variable Frequency Drive
WOT	Wide Open Throttle

ABSTRACT

Sprengel, Michael W. Ph.D., Purdue University, December 2015. Influence of Architecture Design on the Performance and Fuel Efficiency of Hydraulic Hybrid Transmissions. Major Professor: Monika Ivantysynova.

Diminishing oil reserves coupled with increasing concern over the environmental impacts of burning fossil fuels has spurred renewed interest in increasing the efficiency of on-road vehicles. One approach which has shown much promise is powertrain hybridization by means of a hydraulic hybrid transmission. While lesser known than their electrical counterparts, hydraulic hybrid transmissions have many benefits over competing technologies.

The aim of this work is to devise and investigate novel hydraulic hybrid transmission architectures and control strategies with improved efficiency and performance for on-road applications. While hydraulic hybrids possess the ability to reduce fuel consumption when compared to conventional and electric hybrids, their full potential can only be realized through the use of effective power management strategies. In this work a novel implementable power management strategy is proposed and investigated which seeks to predict and track a hydraulic hybrid's globally optimal state trajectories. This is achieved by training a neural network to generalize the trends between vehicle velocity and optimal accumulator pressure generated by dynamic programming for a known cycle. The neural network is then used for online prediction of the optimal accumulator pressure for new and untrained cycles which serves as the core of an implementable power management strategy. In simulation the neural network based power management strategy was able to achieve an average fuel consumption rate within 6.69% of the

globally optimal value for two untrained evaluation cycles. Further when evaluated on a hardware-in-the-loop transmission dynamometer the neural network approach was able to decrease the average fuel consumption rate by 25.51% when compared to a baseline 275 bar constant pressure control strategy for the same two untrained evaluation cycles.

To further improve the efficiency and performance of hydraulic hybrids it is necessary to move beyond conventional architectures. An analysis of conventional hydraulic hybrids found inherently inefficient modes of operation resulting from the base system architectures. Additionally these same conventional transmissions are in some instances limited in their dynamic response due to the high compliance imparted by their high pressure accumulators. To address these and other shortcomings a novel transmission architecture termed a Blended Hydraulic Hybrid is proposed and investigated in this work. This novel architecture partially separates power transmission from energy recovery and storage yielding a system with improved efficiency and performance over conventional hydraulic hybrid transmissions. The concept is further enhanced by adding a planetary gear resulting in an advanced power split version of the blended hybrid transmission.

A better understanding of how the proposed architectures compare with existing systems is gained by performing an energetic analysis on two baseline mechanical transmissions, two conventional hydraulic hybrids, and the two blended hybrid transmissions. To eliminate the influence of control on fuel efficiency all six transmissions are optimally controlled over a predefined cycle using dynamic programming. This analysis showed both blended hybrid architectures achieved superior fuel efficiencies relative to their respective conventional hydraulic hybrid transmissions. Next two system level control schemes are proposed and investigated for the blended hybrid with special attention paid to ensuring a positive driver experience. These system level controls are then enhanced with two implementable power management schemes. The top performing power management scheme combines instantaneous optimization with rule-based controls yielding a simulated fuel consumption rate within 1.65% of the globally optimal value.

The blended hybrid's feasibility is further explored by constructing and testing a blended hybrid on a hardware-in-the-loop transmission dynamometer. Measurement results confirm the viability and benefits of the blended hybrid concept. Finally the question of drivability and driver perception is explored by constructing a blended hydraulic hybrid demonstration vehicle and successfully testing it in an on-road environment.

CHAPTER 1. INTRODUCTION

Rising fuel prices, diminishing oil reserves, and increased awareness of the environmental impacts related to consuming fossil fuels necessitates new and proactive measures. Multiple technologies and approaches are available and essential to reducing carbon emissions. Some of these include increased energy generation from renewable energy sources, increased nuclear energy, increased biofuel usage, increased carbon sequestration, and reduced deforestation among others. However the greatest potential lies with increasing the efficiency of components and systems already in use (Pacala and Socolow, 2004). In 2013 69% of all petroleum consumed in the US went into the transportation sector (Davis et al., 2014). Thus increasing the efficiency of on-road vehicles can significantly contribute to an overall reduction (or at lease minimizing the increase) in fossil fuel consumption.

One approach to increasing vehicle efficiency which has met with much success is powertrain hybridization. A hybrid vehicle refers to a powertrain which contains both a primary energy source (typically an internal combustion engine) and a secondary energy store. Currently electric hybrids dominate the on-road hybrid vehicle market, however hydraulic hybrids are a competing technology with many benefits over their electric counterparts. Numerous investigations have demonstrated the advantages of hydraulic hybrids over electric hybrids. In 2012 the US Federal Transit Administration developed a modified series hydraulic hybrid transmission for city busses in collaboration with industrial partners. Independent 3rd party measurements showed a 29% increase in fuel efficiency over the most efficient electric hybrids, a 47% increase over an identical non-hybrid bus, and a 109% increase in fuel efficiency over conventional city busses (Heskitt

et al., 2012). Heskitt et al. also projected the hydraulic hybrid bus would have a lifecycle cost 24% less than a conventional diesel bus, 27% less than a compressed natural gas bus, and 36% less than an electric hybrid bus. Benefits in terms of fuel efficiency between electric and hydraulic hybrids largely come down to differences in their energy storage media. These differences are well illustrated in a Ragone diagram (Figure 1.1) which plots energy density vs. power density of various storage devices on a log-log scale. Apparent from inspection are the differences between the low power/ high energy density of batteries used in electric hybrids, and the high power/ low energy density of hydropneumatic accumulators used in hydraulic hybrids. The high power density of these accumulators enables hydraulic hybrids to capture virtually all of a vehicle's kinetic energy by means of regenerative braking, energy which is normally dissipated as heat in electric hybrids. It is this increase in regenerative braking which largely contributes to the increased fuel efficiency of hydraulic over electric hybrids.

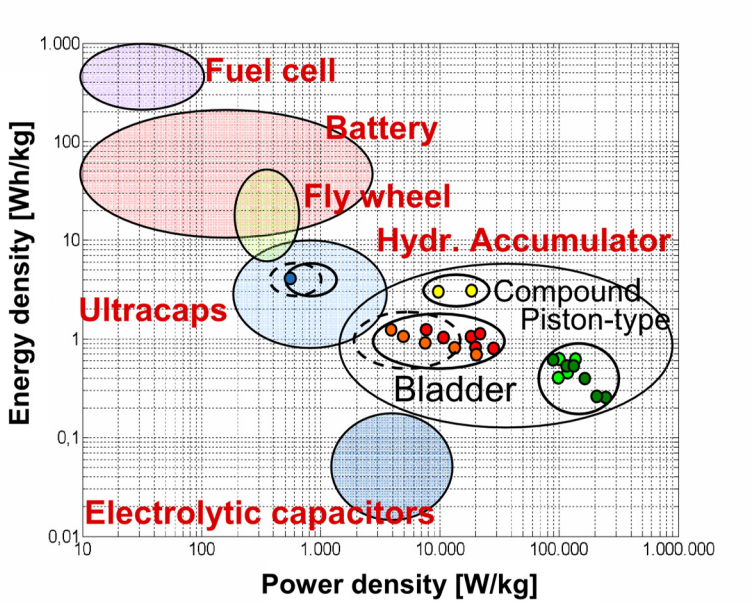

Figure 1.1 Ragone Diagram (Baseley et al., 2007)

While hydraulic hybrids have the ability to achieve greater fuel efficiency than either conventional or electric hybrid vehicles, in order to fully realize their potential effective power management is essential. Power management refers to the manner in which free

states such as engine speed and accumulator pressure are managed while balancing vehicle performance with fuel consumption. For hydraulic hybrids a number of power management strategies have been proposed to date, yet none of these approaches can be considered markedly superior to competing strategies. Only dynamic programming stands out as being capable of producing globally optimal state and control trajectories. Yet dynamic programming's requirement for complete *a priori* cycle knowledge precludes its use as an implementable control strategy. To that end a novel power management strategy is proposed in this dissertation which seeks to generalize the optimal state trajectories generated by dynamic programming for use as the basis of an implementable control strategy. The proposed strategy trains a neural network to generalize the optimal state trajectories of known cycles and then predict how dynamic programming would respond to new and unique cycles. Research into this novel approach to power management is detailed in Chapter 5.

In order to further improve the efficiency and performance of hydraulic hybrid transmissions it essential to move beyond conventional architectures. Conventional hydraulic hybrid transmissions can be broadly grouped into three categories: parallel hybrids, series hybrids, and series hybrid power split transmissions. While each of these architectures have certain benefits they also have intrinsic deficiencies. The efficiency and performance of both series hybrids and series hybrid power split transmissions are inherently linked with their accumulator's current state of charge. When their accumulators are at a high state of charge, but only low to moderate power demand exists, the positive displacement machines in these hybrid transmissions are forced to operate inefficiently at low displacements and high pressures. Conversely in situations where high power demand exists, but the accumulators lack a sufficient state of charge, a delay may be experienced while the accumulators are being charge to a sufficient level to supply the requested power. To address these and other issues a novel transmission architecture was proposed by the author during the course of this research termed a Blended Hydraulic Hybrid which possess benefits over existing configurations. This novel

architecture addresses the relationship between efficiency, performance, and state of charge by uniquely separating power transmission from energy storage while still permitting these systems to be connected under opportune conditions. Research into the blended hybrid concept is presented in Chapters 6 and 8.

This dissertation is divided into nine chapters. A background on powertrains and hydraulic hybrid is covered in Chapter 2. Chapter 3 details the state of the art in hydraulic hybrid transmissions and power management. An investigation into the efficiency of conventional hydraulic hybrid transmissions is covered in Chapter 4. A novel neural network based power management control strategy is presented in Chapter 5. Chapter 6 investigates the novel blended hydraulic hybrid transmission architecture. Chapter 7 covers the design and implementation of a hardware-in-the-loop transmission dynamometer used during both the neural network and blended hybrid investigations. While Chapter 8 covers the design, implementation, and testing of a blended hybrid demonstration vehicle. Finally Chapter 9 concludes this work with a summary and final thoughts.

CHAPTER 2. BACKGROUND

Transmissions are an essential component of a vehicle's powertrain task with converting the higher speed/ lower torque output from the engine to a lower speed/ higher torque input to the wheels. While their function appears simple, a transmission's operation substantially affects the entire vehicle's performance and fuel efficiency. This chapter begins with a general discussion of a transmission's influence on powertrain operation. Next conventional mechanical transmissions are introduced followed by an overview of hybrid transmissions. Finally both hydraulic, and hydraulic hybrid, transmissions are discussed.

2.1 Powertrain Operation

Transmissions provide a variable connection between a vehicle's engine and wheels (Figure 2.1). This location between the vehicle's primary power source (engine) and primary power consumer (wheels) grants the transmission a great deal of influence over the entire powertrain's operation.

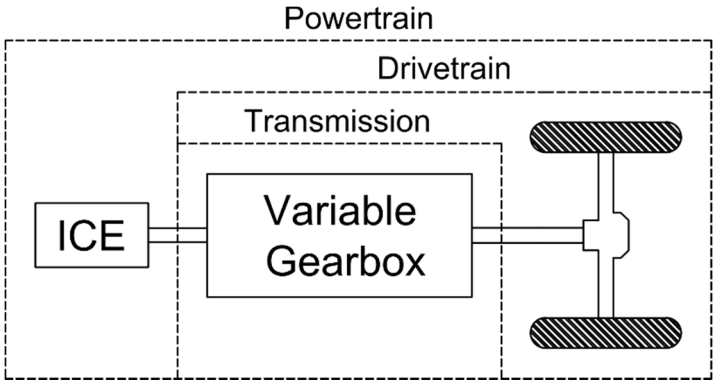

Figure 2.1 Vehicle powertrain overview

In order to understand the transmission's influence one must first understand the basics of engine operation. Internal Combustion Engines (ICEs) convert fuel into mechanical (rotational) power through combustion. Engines do not convert fuel into power with constant efficiency, rather the engine's operating point heavily influences the conversion efficiency. Figure 2.2 shows the brake thermal efficiency (i.e. the efficiency of converting the fuel's chemical energy into useful mechanical energy) of a representative diesel and gasoline engine (based on data from ANL, 2015). Especially note the constant power curves in Figure 2.2. Along these curves the engines produce the same quantity of brake power, albeit with widely varying efficiencies.

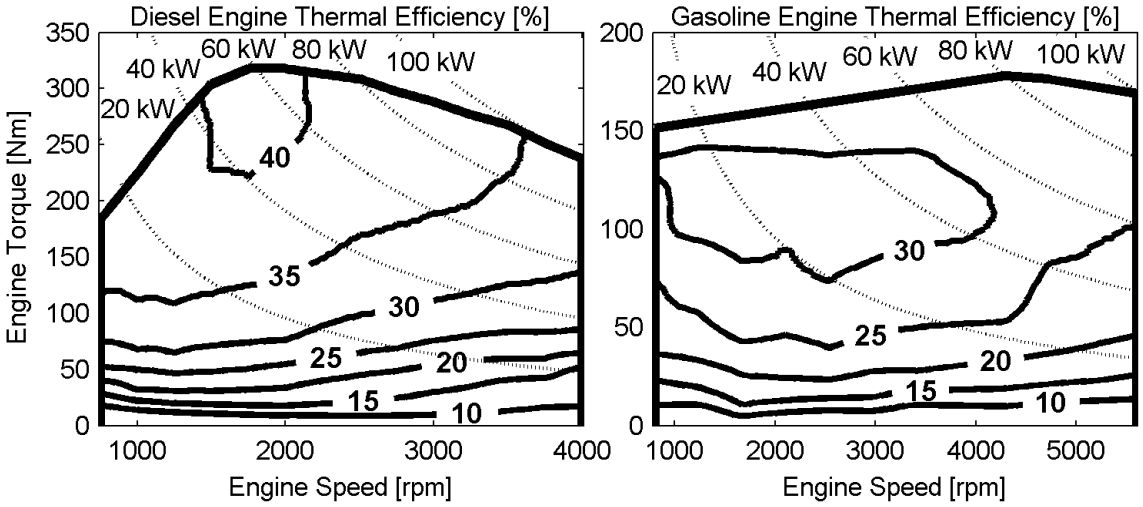

Figure 2.2: Brake thermal efficiency of a typical diesel and gasoline engine

While transmissions have no affect on engine efficiency, they directly influence the engine's location of operation. At all points in time while driving a vehicle will require a certain wheel power comprised of a specific speed and torque. Consider an idealized mechanical transmission consisting of an infinitely variable gear ratio connecting the engine and wheels. While the combination of speed and torque at the wheels is specified, any feasible combination of speed and torque at the engine which yields the required wheel power is permissible. Consequently for a given wheel speed and torque there exists at least one optimal transmission ratio which will minimize fuel consumption. Consider now an idealized mechanical transmission with internal energy storage which permits

power to be absorbed or released as desired. For the same required wheel speed and torque, power may now be released from the transmission's internal energy store to supplement the engine thereby permitting the engine to operate at a more efficient point. Alternatively the engine may produce more power than required by the wheels and store the excess in the transmission, once again operating the engine in a more efficient manner than would be possible without additional energy storage. Collectively adjusting the transmission ratio, and storing/releasing excess engine energy from the transmission, is referred to as engine management.

2.2 Conventional Mechanical Transmissions

Manual Transmissions

Conventional mechanical transmissions are generally classified as either manual or automatic transmissions. Manual transmissions consist of a driver controlled friction clutch and multiple driver selectable gear ratios (Figure 2.3).

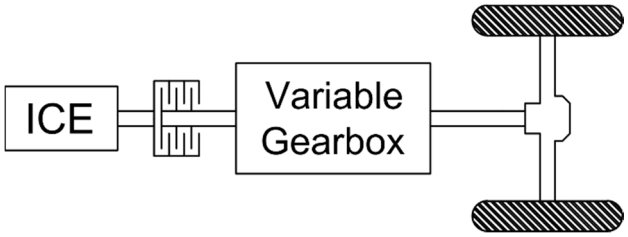

Figure 2.3 Manual transmission

Today five to six discrete gear ratios are common in passenger vehicles while commercial vehicles may have between nine and twenty one depending on application. The move towards more gear ratios in recent years is largely a function of the desire to improve fuel efficiency. The more gear ratios which are available, the closer to the optimal engine operating point the vehicle is capable of being operated at. An example of a transmission with four discrete gear ratios compared to a Continuously Variable Transmission (CVT) and an engine operating along its maximum power curve is presented in Figure 2.4.

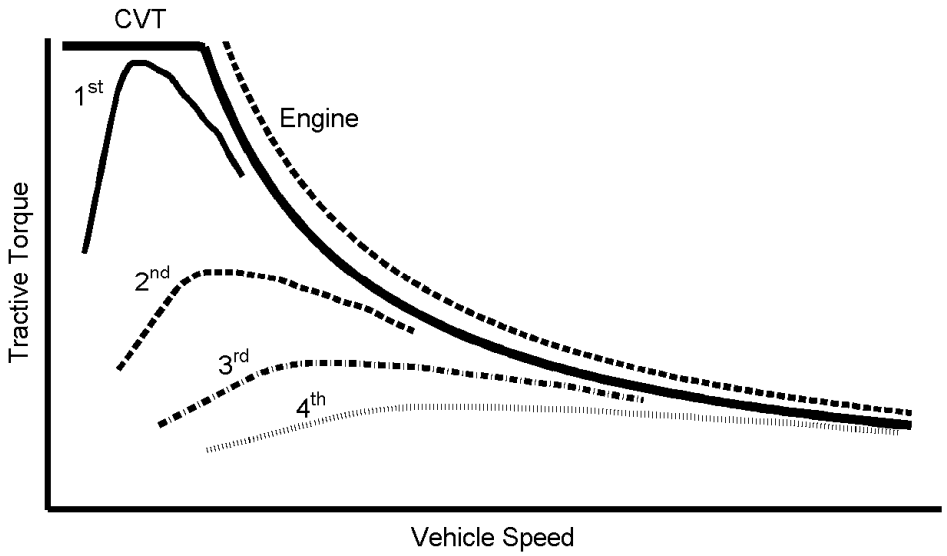

Figure 2.4 Discrete gear ratio performance vs. a CVT

Automatic Transmissions

Automatic transmissions (Figure 2.5) provide many benefits over manual transmissions in terms of performance but at the cost of a generally lower peak fuel efficiency. A key element of automatic transmissions is the torque converter located between the engine and the variable gearbox.

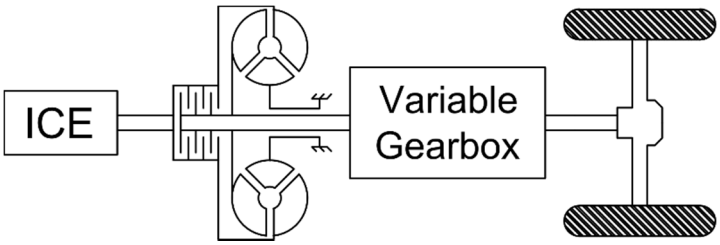

Figure 2.5 Automatic transmission

A torque converter, sometimes referred to as hydrokinetic or hydrodynamic drive, is a transmission element which uses a fluid coupling to partially decouple the engine's speed and torque from the transmission's speed and torque. Torque converters are comprised of six primary elements: an impeller connected to the engine, a turbine connected to the transmission, a stator positioned between the input and output shafts, a lock-up clutch, oil as the working fluid, and a housing which containing all of the components (Figure 2.6).

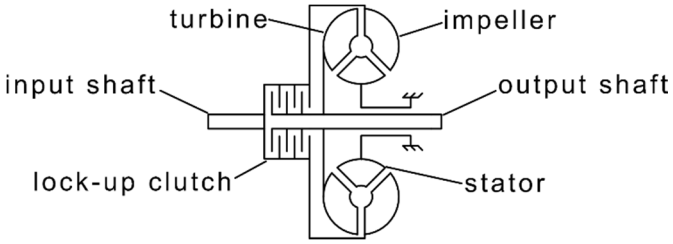

Figure 2.6 Torque converter

While in operation the impeller accelerates oil, converting rotational power from the engine to kinetic energy in the fluid. This high velocity fluid then proceeds to the turbine which converts much of the fluid's kinetic energy back into rotational power for the transmission. The fluid, which still possesses some kinetic energy, is redirected back to the impeller by means of the stator. The impeller then reaccelerates this fluid adding additional kinetic energy to the system. It is this recycling of energy which enables torque converters to multiply torque under certain conditions. The power and torque transmitted through a torque converter, and the efficiency of this process, is a function of the speed ratio between impeller and turbine (Figure 2.7).

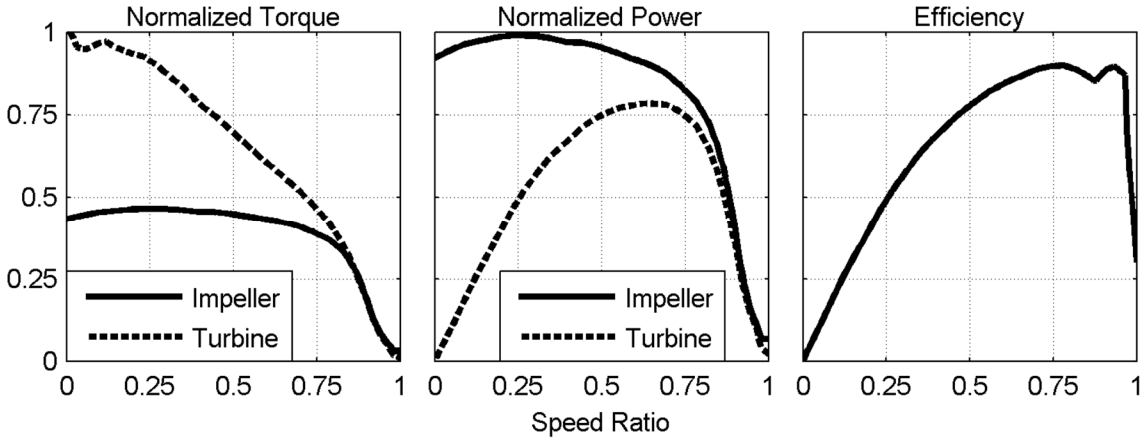

Figure 2.7 Torque converter performance

When the engine (impeller) is rotating significantly faster than the transmission (turbine) a torque multiplication of 2.5 or even higher is possible. This torque multiplication enables automatic transmissions to dramatically increase maximum output torque in certain conditions thereby increasing peak performance targets for any transmission which aims

to meet the same maximum output torque. While torque converters provide benefits in terms of increased torque and a decoupling of engine and vehicle speeds, they do so at the cost of system efficiency. For this reason many modern automatic transmissions contain a lock-up clutch which rigidly couples the impeller and turbine while not in use. When engaged the clutch transfers power mechanical instead of hydrokinetically thereby reducing losses from the torque converter such that only churning losses remain.

2.3 Hybrid Transmissions

Hybrid transmissions, that is transmissions which combine two or more distinct power sources, are becoming increasingly prevalent as a means to improve fuel efficiency. Hybrid transmissions typically operate in either the electrical, rotational (mechanical), or fluid domains. Any transmission which operates outside of the rotational domain requires energy conversion device(s) to convert between the rotational domain of the engine and wheels, and the transmission's alternative domain. In electrical systems these conversions devices are known as generators/motors while in hydraulic systems they are known as pumps/motors. Because no energy conversion is ever 100% efficient it is generally best to minimize the overall number of energy conversions.

Hybrid systems are somewhat arbitrarily classified based on either the domain of their transmission or energy storage device. In electric hybrids energy is stored either chemically in batteries or electrically in capacitors (and sometimes in both) while using generators/motors to convert between the electrical and rotational domains. In mechanical hybrids energy is stored mechanically in the inertia of a flywheel which is coupled to the primary transmission by means of a mechanical, electrical, or hydraulic transmission. In hydraulic hybrids energy is stored by further compressing highly pressurized gas in a hydropneumatic accumulator.

A major difference between hybrid technologies is the energy and power density of their energy storage media. These difference are well visualized using a Ragone Diagram (Figure 1.1). Differentiating energy from power is useful when discussing hybrids as each

quantity, while closely related, influences overall system operation in different ways. Energy density refers to the total quantity of energy which can be stored per unit mass while power density indicates how quickly that energy can be stored or released. For example electric hybrids typically use some form of battery, which while relatively energy dense, is only mildly power dense. In terms of transmission operation the battery's high energy density allows prolonged charging using excess engine power, and prolonged discharging for aiding the engine. This flexibility results in electric hybrids gaining the majority of their improved fuel efficiency through effective engine management. Recovering all of a vehicle's kinetic energy during regenerative braking requires storing energy at a far higher rate than that experienced during load leveling and engine management. Consequently due to the relatively low power density of batteries typically found in electric hybrids, only a small quantity of the available regenerative braking energy is typically stored. This forces the vehicle's remaining kinetic energy to be dissipated through friction brakes.

Regardless of the fundamental energy storage technology employed, most hybrids are based on one of three transmission architectures. These include parallel hybrids, series hybrids, and series hybrid power split transmissions.

Parallel Hybrids

Parallel hybrids consist of a single energy conversion device, and related energy storage media, placed in parallel with a primary transmission (Figure 2.8).

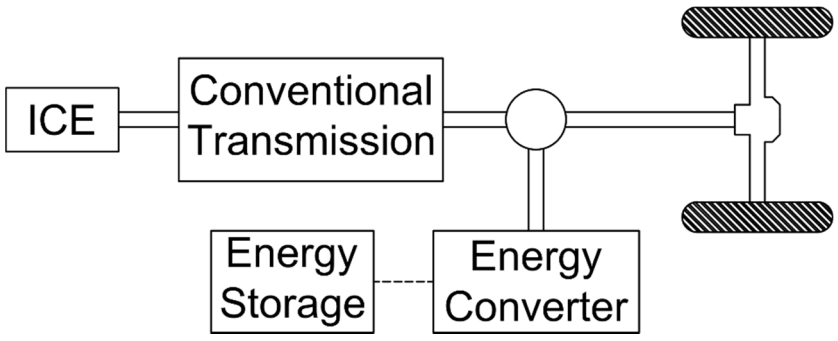

Figure 2.8 Generic parallel hybrid

This energy conversion device, often placed after a conventional automatic transmission, serves as a junction where excess power can be absorbed or released as needed. One of the primary benefits of parallel hybrids is the ease in which they can be retrofitted into existing conventional transmissions. Additionally because all of the engine power can still be transmitted through the conventional transmission there is no minimum size requirement for the parallel hybrid's energy converter. However because the conventional transmission remains, so to do the losses inherent with that transmission. Moreover many conventional transmissions still possess discrete gear ratios which limit this architecture's engine management when compared to more advanced hybrid architectures.

Series Hybrids

Series hybrids contain two energy conversion devices, along with energy storage, in series with the ICE (Figure 2.9).

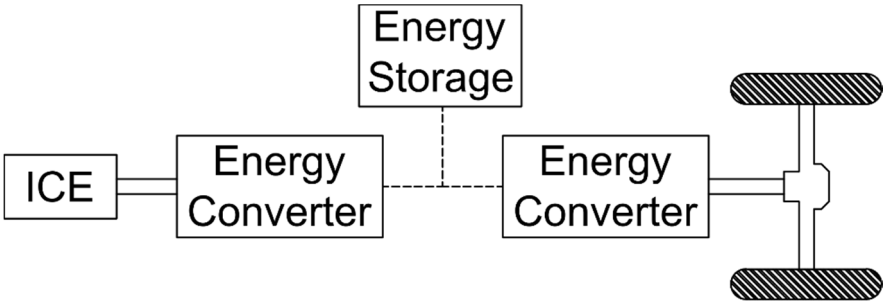

Figure 2.9 Generic series hybrid

Unlike parallel hybrids where power from the ICE remains in the rotational domain as it travels to the wheels, series hybrids require all of the engine power to be converted into a secondary domain at the first energy conversion device. From here power flows either to an energy storage device, or onto the second energy conversion device where it is converted back into rotational power and sent to the wheels. While multiple energy conversions reduce transmission efficiency, the continuously variable nature of many of these devices also enables a continuously variable transmission ratio between the engine and wheels. This yields the primary advantage in terms of fuel economy offered by series

hybrids over parallel hybrids as the increased potential for engine management. A downside of series hybrids is that the energy conversion devices must be sized to absorb the full power of the engine while providing the maximum power required to the wheels.

Power Split Hybrids

While a hybrid transmission may transmit power less efficiently than a mechanical transmission, overall powertrain efficiency may be greatly improved due to benefits gained from engine management and regenerative braking. Reduced transmission efficiency stems primarily from the inherent inefficiency of converting power between the rotational domain of the engine and wheels, and the secondary domain of the hybrid transmission. Hybrid Power Split Transmissions (PSTs) are a class of architectures which seeks to combine the benefits of series hybrids and mechanical transmissions. At the core of power split transmissions are Planetary Gear Trains (PGTs), devices which enable power to be split and combined between three separate mechanical paths. PGTs, also known as epicyclic gear trains, rely on specific configurations of gears which rotate about one another yielding multi degree of freedom systems (Figure 2.10).

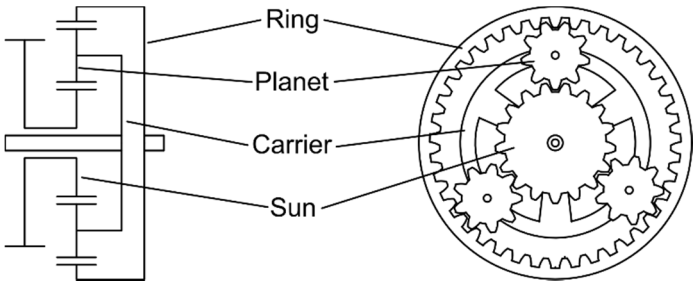

Figure 2.10 Planetary gear train

A PGT's two degrees of freedom refers to the ability to specify without constraint angular velocities for any two gear sets with the remaining gear set's angular velocity a function of kinematics. In contrast the torque passed through a PGT possess only one degree of freedom. Due to the required force balance between gears, specifying torque on one gear set yields specific torques on the remaining two gear sets. PGT's variable speed and fixed

torque ratios enable the power split between the three gears sets to be continuously varied by adjusting the relative speed of the input and output shafts.

Power split hybrid transmissions use the PGT to split power between an efficient mechanical path and a flexible continuously variable hybrid path. Several configurations of PSTs exist depending on the location and number of PGTs employed. The simplest PST configurations are known as input and output coupled (Figure 2.11 A & B respectively) with additional PGTs and clutches yielding compound and dual stage architectures.

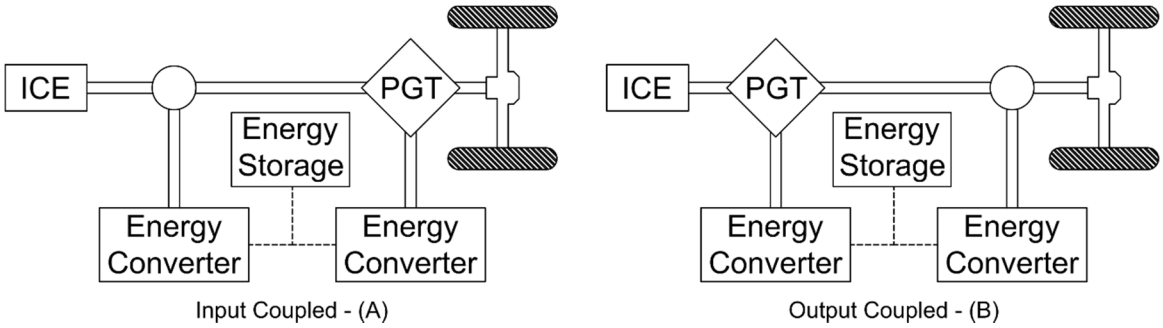

Figure 2.11 Generic input and output coupled power split transmissions

While various PST architectures exist and have been heavy investigated, in interest of brevity the discussion of PSTs in this dissertation will be confined to output coupled power split transmissions. Output coupled PSTs use a PGT located directly after the engine to split power between the mechanical and continuously variable hybrid paths. After power has passed through the two parallel paths it is recombined at a fixed gear ratio coupling point. Near zero vehicle speed almost all of the power transmitted to the wheels passes through the continuously variable hybrid path. However as vehicle speed increases a greater percentage of power passes through the mechanical path up until the aptly named full mechanic point at which point all power passing through the transmission is transmitted mechanically.

2.4 Hydraulic (Non-Hybrid) Transmissions

Hydrostatic Transmissions

Hydrostatic Transmissions (HSTs), in contrast to the hydrokinetic transmission of a torque converter, transmit power by moving pressurized fluid under hydrostatic equilibrium. HSTs use positive displacement machines (i.e. hydraulic units) to convert power between the rotational and fluid domains. These positive displacement machines come in two varieties; fixed displacement machines which move a defined volume of fluid per revolution, and variable displacement machines which can continuously adjust the volume displaced per revolution thus controlling their effective flow rate. Arranging two positive displacement machines in series, at least one of which is variable displacement, yields a continuously variable hydrostatic transmission. Figure 2.12 shows a schematic of a typical hydrostatic transmission, in this case a design which uses two variable displacement machines.

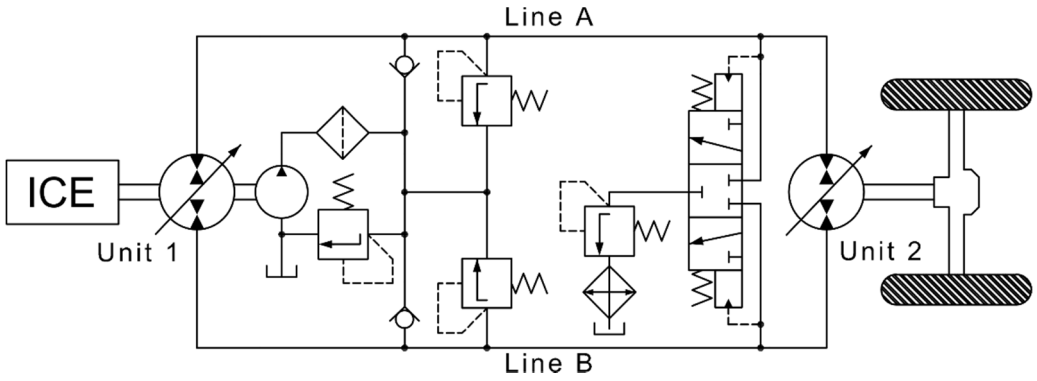

Figure 2.12 Hydrostatic transmission circuit

Hydrostatic transmissions operate in a manner referred to as flow control. In a flow controlled system whatever flow leaves one machine must (almost) immediately pass through the second machine. During operation a given combination of engine speed and pump displacement (Unit 1) will produce a certain flow rate. This flow will then pass through the second machine operating as a motor (Unit 2) which is coupled to the axle/wheels. The (attempted) wheel speed will thus be a function of the pump's flow rate,

the motor displacement, and the associated volumetric losses. Required wheel torque is a function of speed, acceleration, and grade and is back propagated to the HST where, along with motor displacement and hydromechanical losses, it determines system pressure. HSTs are typically controlled using sequential, as opposed to simultaneous, control. In sequential control only the displacement of one machine is adjusted at a time with the second machine remaining at full displacement (Figure 2.13).

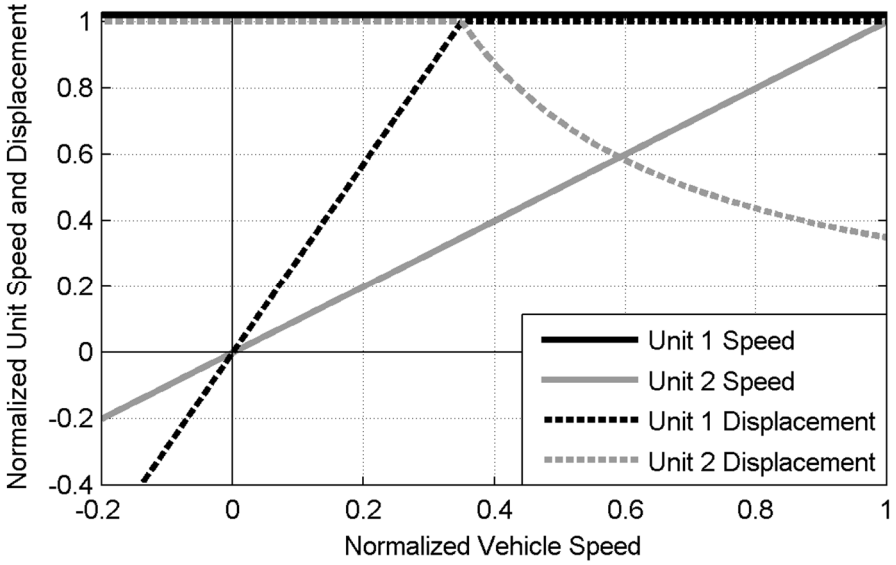

Figure 2.13 Sequential control

HSTs operate in a closed circuit configuration, that is a configuration where flow recirculates predominantly between the two machines. A characteristic of closed circuit configurations is that both primary transmission lines may operate at high pressure. While driving one line of a HST (commonly referred to as Line A) operates under high pressure while the other line (Line B) operates at low pressure. During braking Unit 2 automatically transitions from motoring to pumping mode and pressurizes Line B while Line A reverts to low pressure. The transition between driving and braking occurs when the flow (i.e. speed) controlled transmission is adjusted to a lower speed or external loads (e.g. gravity) act on the wheels with a greater opposing force than the transmission. Another characteristic of closed circuit configurations is that the primary transmission lines are

always pressurized to some nominal low pressure (e.g. 20 bar). Maintaining this minimum pressure is essential for preventing cavitation within the system but also serves to increase overall transmission stiffness and response.

Hydrostatic Power Split Transmissions

Hydrostatic power split transmissions (Figure 2.14) are similar to the hybrid PSTs discussed in Section 2.3 PST with the exception of a hydrostatic transmission replacing the series hybrid path.

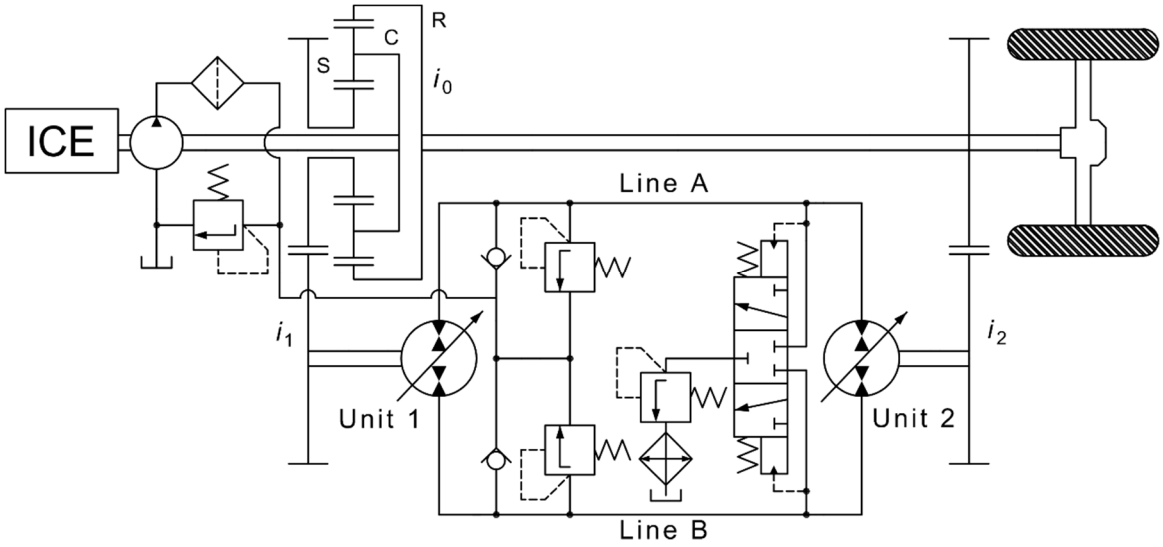

Figure 2.14 Hydrostatic power split transmission circuit

Hydraulic output coupled PSTs operate in a manner both similar and markedly different from HSTs. Similar in that hydraulic PSTs operate under flow control where the positive displacement machines' displacements dictate vehicle speed. Different in that changes in both engine and vehicle speed alters power flow through the PGT resulting in several distinct modes of operation. This influence of PGT kinematics on transmission operation is well conveyed through the use of lever diagrams. In lever diagrams an arrow is placed at the pitch radius of each gear set in the PGT with the arrow's length corresponding to the gear set's current angular velocity. As previously discussed the angular velocity of any two gear sets within a PGT can be freely set with kinematics determining the third gear

set's velocity. This kinematic relationship is expressed graphically in lever diagrams by connecting the terminal point of each arrow with a straight line. Lever diagrams of four distinct modes of PST operation are shown in Figure 2.15. These include power recirculation (reverse), power additive, full mechanical, and power recirculation (forward). For these lever diagrams engine speed (ω_C) was held constant while ω_R increased proportionally with vehicle speed and Unit 1's speed (ω_S) varied with kinematics.

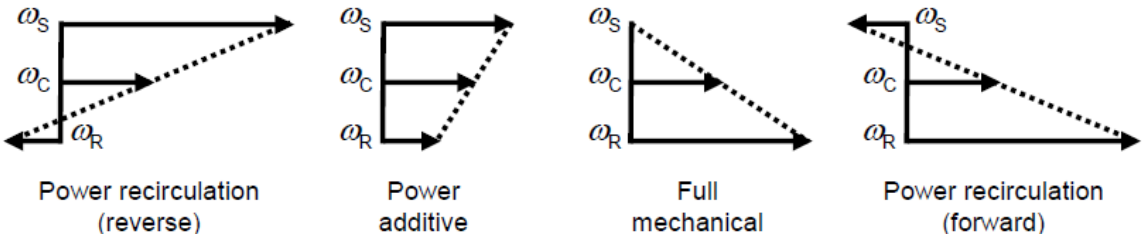

Figure 2.15 Lever diagrams

These four modes of PST operation (summarized in Figure 2.16) function as follows:

Power recirculation (reverse): To reverse Unit 1 moves over center and begins pumping while Unit 2 motors at full displacement. Pumping over center causes oil to flow from Line A to Line B in a counterclockwise direction (per Figure 2.14) resulting in Unit 2 (and consequently the vehicle) operating in reverse. Some of the power leaving Unit 2 flows to the wheels however as the ring gear is now rotating backwards kinematics dictate some power also flows back to the PGT through the mechanical path, hence the name recirculation. Once back at the PGT power from the mechanical path combines with power from the engine before flowing back out to Unit 1 and the HST path. As reverse vehicle speed increases so too does the power recirculating through the less efficient HST path. In this way the entire power flowing from the engine to the wheels passes through the HST path at least once while some portion of this power must pass through the HST path multiple times.

Power additive: In power additive mode Unit 1 pumps from Line B to Line A in clockwise direction while Unit 2 motors at full displacement resulting in forward driving. This causes

power from the engine to be split at the PGT and flow to the wheels through both the mechanical and HST path. To increase vehicle speed Unit 1 continues to increase displacement until both Units 1 and 2 are at full displacement, a point referred to as saturation. To further increase vehicle speed Unit 1 remains at full displacement while Unit 2's displacement is decreased. Near zero vehicle speed almost all of the power flowing through the PST transits the HST path. However as vehicle speed increases, kinematics cause the sun gear to slow down resulting in a greater percentage of power passing through the more efficient mechanical path.

Full mechanical: As vehicle speed further increases through power additive mode Unit 2 will eventually reach zero displacement. At this point Unit 1 is locked at zero velocity and Unit 2 freewheels. Known as the full mechanical point this is a PST's most efficient mode of operation as the entire power flow through the PST transits solely the mechanical path. However this is not to say that the PST's most efficient mode corresponds with a given powertrain's most efficient mode of operation. Rather once all components in a powertrain are viewed holistically then certain components will invariably operate in a suboptimal manner in order to maximize overall powertrain efficiency.

Power recirculation (forward): To increase vehicle speed past the full mechanical point Unit 2 moves over center and begins pumping from Line B to Line A in a counterclockwise direction. Unit 1, remaining at full displacement, now begins motoring in reverse. With the sun gear rotating in reverse PGT kinematics dictates that power from the HST path now flows into the PGT. This results in some of the power flowing from the engine through the mechanical path to the wheels being diverted through the HST path were it flows back to the PGT. As vehicle speed further increases a greater percentage of power recirculates through the less efficient HST path lowering overall transmission efficiency.

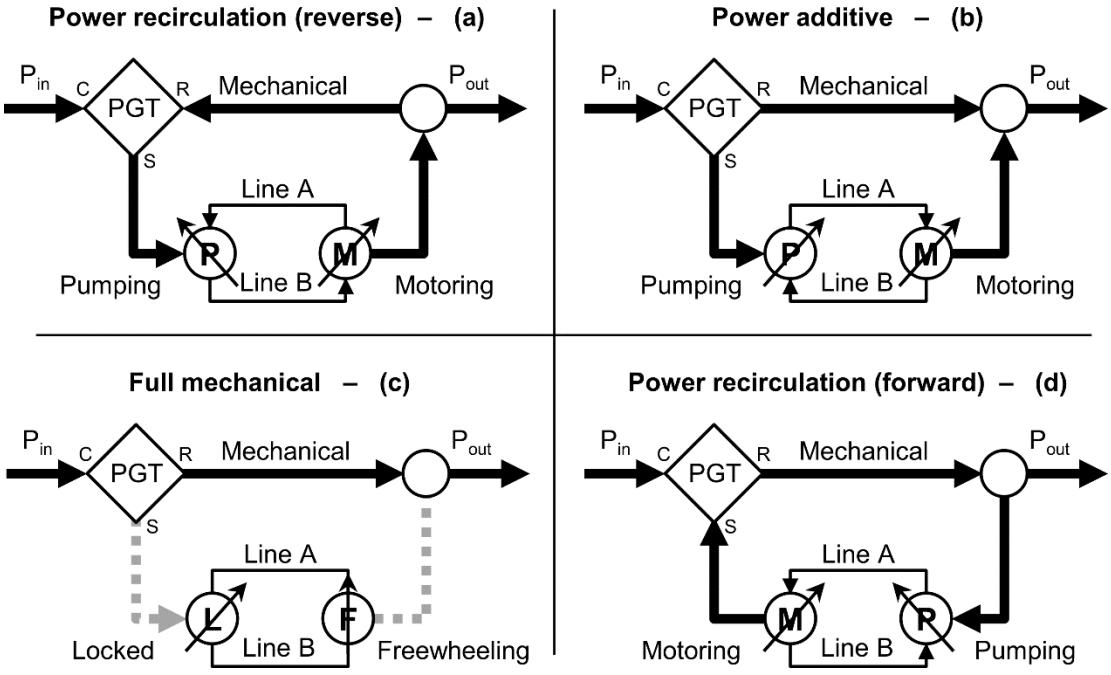

Figure 2.16 Hydrostatic PST modes of operation

A more in depth view of hydraulic PST operation can be gained from examining how the positive displacement machines are controlled as they move continuously through distinct modes of operation (Figure 2.17).

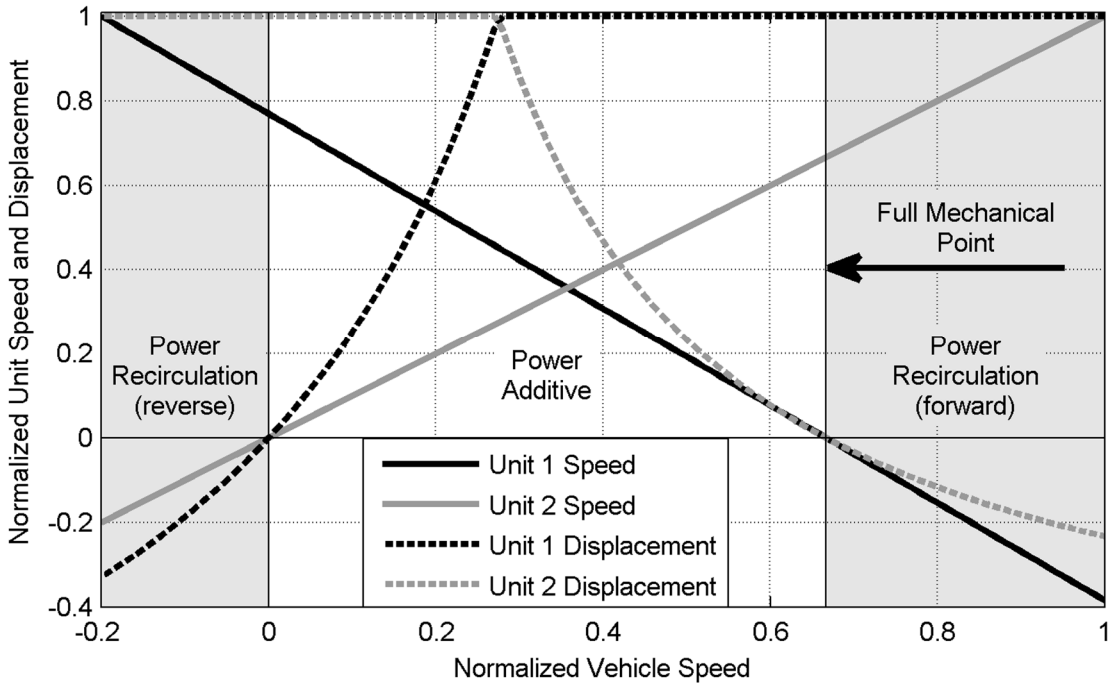

Figure 2.17 Hydrostatic PST control

2.5 Hydraulic Hybrid Transmissions

Hydraulic hybrid transmissions, while investigated since the 1970s, are receiving renewed interest as their benefits over competing hybrid technologies becomes more apparent. Compared to electric hybrids, hydraulic hybrids should always be able to be manufactured at a lower overall cost. This is due in large part to the materials used in their construction. Electric hybrids contain large quantities of expensive copper and various rare earth elements within their electric motors and batteries. In contrast hydraulic hybrids contain predominantly steel with natural or synthetic oil serving as the working fluid. In terms of recycling hydraulic hybrids are more environmentally friendly than electric hybrids due to the general lack of toxic materials used in their construction. Hydraulic accumulators also have a longer lifecycle than batteries with electric hybrids potentially requiring one or more battery replacements depending on application over their anticipated lifetime (Clark et al., 2007). These replacements are required as a battery's performance degrades over time with repeated charging and discharging cycles. In contrast hydraulic accumulators experience minimal degradation in performance over time with some

accumulator technologies such as welded metal bellows lasting the lifetime of a vehicle without maintenance. If bladder style accumulators are used instead then occasional recharging of the nitrogen may be required, however this can be likened to filling a car tire and could be done at roughly the same expense. Hydraulic hybrids also have benefits in terms of required thermal management over electric hybrids. The battery's temperature in an electric hybrid must be carefully controlled to maximize lifetime requiring complex heating and cooling systems. In contrast hydraulic hybrids can operate over a wide range of temperatures with a simple oil cooler as the only required thermal management component in most situations. Finally hydraulic hybrids offer improved safety during maintenance or in an accident as the energy contained within the accumulator can easily be dissipated. Electric hybrids do not have this option as their batteries must always maintain some nominal charge or sustain battery degradation.

Parallel Hydraulic Hybrid

Parallel hydraulic hybrids consist of a positive displacement machine coupled to a conventional transmission and a high pressure accumulator (Figure 2.18).

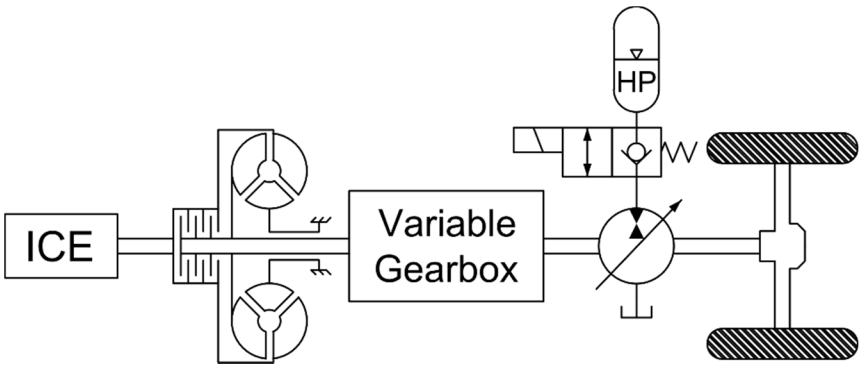

Figure 2.18 Parallel hydraulic hybrid

Parallel hybrids operate by storing excess energy generated by the engine, along with energy recovered during regenerative braking, and then releasing this energy as needed. This architecture stores energy by pumping fluid into a high pressure accumulator and

then using this highly pressurized fluid to motor the positive displacement machine thereby releasing energy as needed.

Series Hydraulic Hybrids

Series hydraulic hybrids consist of two positive displacement machines connected in series with a high pressure accumulator facilitating energy storage (Figure 2.19).

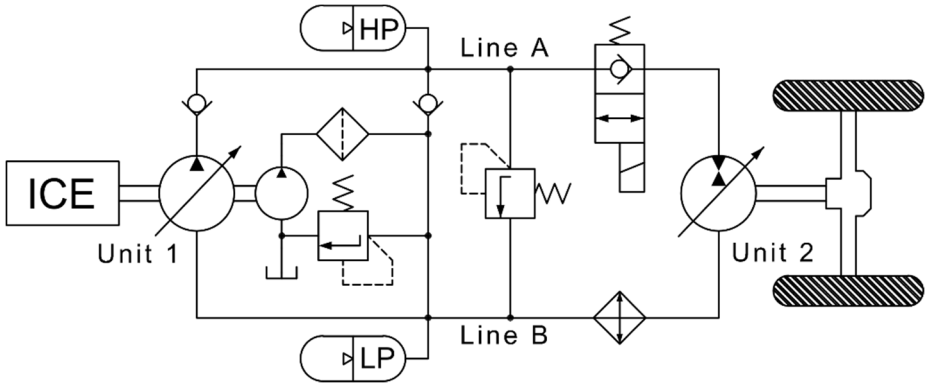

Figure 2.19 Series hydraulic hybrid circuit

Due to the high pressure accumulator's presence all hydraulic hybrid transmissions, including series hybrids, operate in a manner known as secondary (also known as torque or pressure) control. Unlike HSTs in which all of the flow leaving one unit must almost immediately pass through the second unit, the increased capacitance afforded by the HP accumulator allows part or all of the fluid leaving either positive displacement machine to be stored in the accumulator. As fluid is stored or released from the accumulator its pressure (and by association the system's pressure) increases or decreases according to the laws governing the compression and expansion of the accumulator's nitrogen gas. Thus system pressure in hydraulic hybrid transmissions is a function of the cumulative net flow between both positive displacement machines rather than a function of external loads as is the case with HSTs. The HP accumulator's high capacitance limits the influence each positive displacement machine's instantaneous speed and displacement has on the other machine requiring both machines to be controlled independently. Typically Unit 1 is tasked with controlling system pressure whereas Unit 2 controls wheel torque by

adjusting its displacement based on the current system pressure. Unlike HSTs in which either primary line may operate at high pressure, the high and low pressure accumulators' presence necessitates each line be confined to either high or low pressure. To brake in a series hybrid Unit 2 moves over center which reverses the direction of fluid flow causing Unit 2 to pump fluid into the high pressure accumulator. Braking torque is thus controlled by adjusting Unit 2's displacement with regards to desired torque and the accumulator's current pressure.

Series Hydraulic Hybrid Power Split Transmissions

Series hydraulic hybrid power split transmissions (commonly referred to as hydraulic hybrid power split transmissions) are often considered the most efficient, and most complex, general class of hydraulic hybrid transmissions. PST's aim to combine the flexibility and energy recovery potential of series hydraulic hybrids with the efficiency of mechanical transmissions. Output coupled series hydraulic hybrid power split transmissions combine a series hydraulic hybrid transmission with planetary gear train located directly after the engine (Figure 2.20).

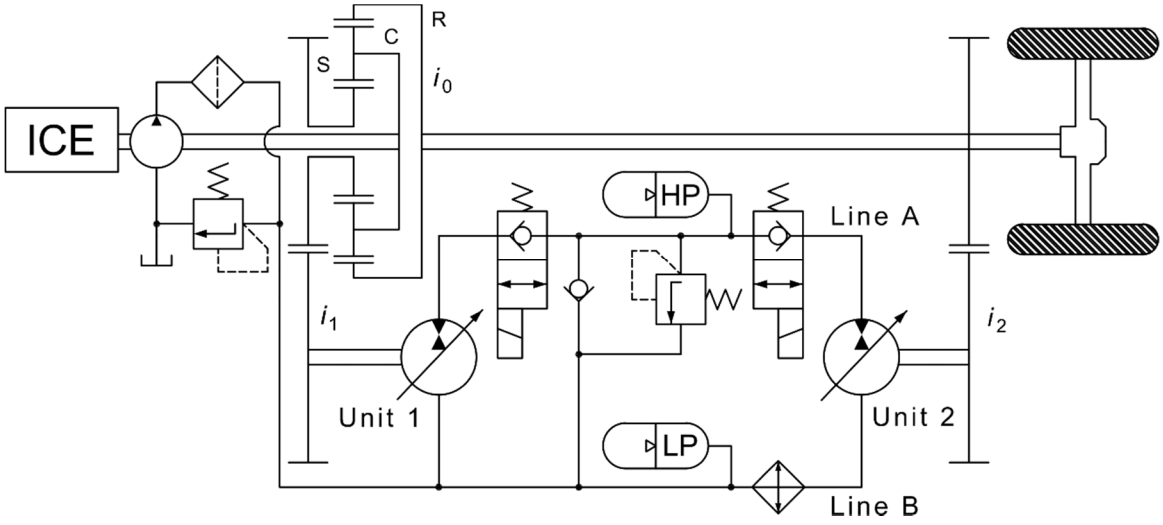

Figure 2.20 Series hydraulic hybrid power split transmission circuit

Power flow within the hybrid PST largely mirrors that of the non-hybrid PST described in Section 2.4**.** However the addition of energy storage and the decoupling of unit

displacements from vehicle speed through secondary control necessitates a modified control strategy. In a series hybrid Unit 1 is generally task with controlling system pressure while Unit 2 is controlled to provide the desired wheel torque. However due to PGT kinematics any charging action by Unit 1 in a hybrid PST will invariably cause a proportional torque to flow from the engine, through the PGT, and onto the mechanical path and ultimately to the wheels. Thus wheel torque is a combination of both mechanical path torque resulting from Unit 1, and torque coming from Unit 2. In the simplest control scheme Unit 1 is still task with controlling system pressure while Unit 2 controls wheel torque, albeit with some knowledge of the torque passing through the mechanical path. During forward power recirculation the roles of Units 1 and 2 reverse with Unit 2 task with controlling system pressure while Unit 1 controls wheel torque. Figure 2.21 shows several select modes of operation.

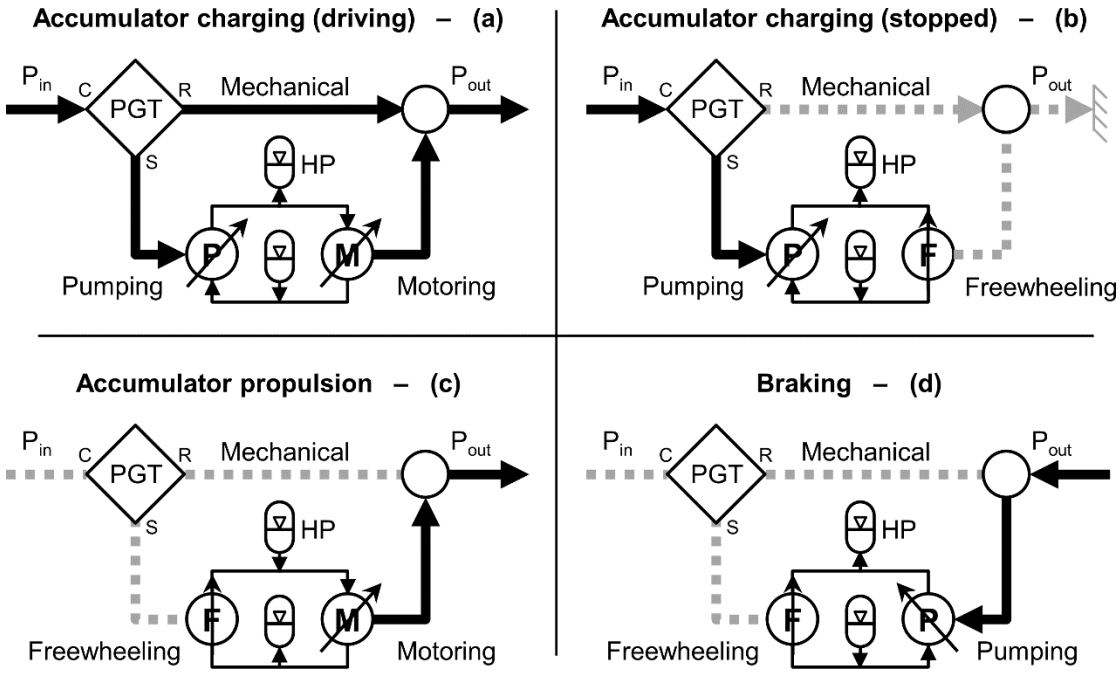

Figure 2.21 Series hydraulic hybrid PST modes of operation

CHAPTER 3. STATE OF THE ART

A summary of the state of the art in hydraulic hybrid transmissions, and their associated power management strategies, is covered in Chapter 3.

3.1 Conventional Hydraulic and Hydraulic Hybrid Transmissions

Hydrostatic Transmissions

Early work on HSTs for off-highway application began in the early 1950's at the National Institute of Agricultural Engineering in Silsoe, UK with the development of a research tractor (Hamblin, 1952). Around the same time period several US tractor manufactures also investigated HSTs for off-highway applications though no products were brought to market (Meile, 1961). In 1956 Linde introduced one of the first commercially available vehicles with a HST (Linde, 2015). In 1967 International Harvester in cooperation with Sundstrand Corporation began commercial production of HSTs for agricultural tractors (Morris, 1967). While this design met with some success it was eventually discontinued due to inefficiencies and high production costs when compared to conventional mechanical transmissions (Renius and Resch, 2005). Eventually HSTs found commercial success in relatively low power (up to ~30 kW) off-highway applications (Renius and Resch, 2005). Today HSTs are still widely available in such applications as lawn and utility tractors and small wheel loaders. For larger working machines the efficiency of HSTs is such that more advanced hydraulic architectures (i.e. hydrostatic PSTs) or conventional mechanical transmissions are preferred (Renius and Resch, 2005).

Hydrostatic Power Split Transmissions

Hydrostatic PSTs were first applied to the transportation sector when Louis Renault introducing a hydrostatic PST for automotive applications in 1907. However this concept failed to gain acceptance due to manufacturing difficulties and production costs (Molly, 1966). The first commercially successful application of hydrostatic PSTs came in 1962 with Sundstrand Corporation's introduction of a transmission used for converting the variable speed of an aircraft engine to the fix speed required for power generation (Reynolds et al., 1966). Later Sundstrand used their knowledge of hydraulic transmissions to co-develop notable hydrostatic and hydrostatic PSTs for the off-highway market. One early example includes the Cummins-Sundstrand "Responder" output coupled hydrostatic PST (Ross, 1972). However the Responder transmission was only a pilot program and did not enter commercial production (Wadman, 1973). In 1995 Fendt introduced the first commercially successful hydrostatic PST their "Vairo" transmission for agricultural tractors (Dziuba and Honzek, 1997; Renius and Resch, 2005). Subsequently multiple manufactures released various hydrostatic PST configurations. Some of these include Styer's compound input coupled "S-Matic" in 2000, ZF's dual stage input coupled "Eccom" in 2001, and John Deere's dual stage input coupled "AutoPowr" in 2001 among others (Renius and Resch, 2005).

Parallel Hydraulic Hybrid Transmissions

Research into parallel hybrids began when Dunn and Wojciechowski (1972) set about determining the architecture's round trip energy storage efficiency. Using an experimental setup consisting of a hydraulic unit, accumulator, and flywheel they found round trip efficiency exceeded 50%. Later studies by Dunn and Wojciechowski (1974, 1975) on an improved test rig found an average round trip efficiency of 66%. They determined that 71% of the energy lost was attributed to the hydraulic unit. A subsequent study by Dewey et al. (1974) found a round trip efficiency of 75% was achieved once the flywheel's aerodynamic drag was properly accounted for.

Vehicle simulations began in 1979 when Buchwald et al. modeled a parallel hydraulic hybrid bus, which they validated using a small delivery van, and found fuel savings of 25-30% were possible. In 1985 Tollefson et al. simulated a parallel hydraulic hybrid passenger car on two urban cycles (Federal Urban Driving Schedule and the New York City Cycle) and one highway cycle (Federal Highway Cycle). They found that while fuel economies up to 65 mpg were possible for an urban drive cycle, few benefits were gained from highway driving due to the lack of regenerative braking events. It should be noted that many early simulations were somewhat limited in their fidelity due to computational constraints so the exact magnitudes of their findings should be considered with this in mind.

Prototype development of parallel hydraulic hybrids began in the early 1980s at Maschinenfabrik Augsburg-Nürnberg (MAN) in Berlin, Germany. The MAN Hydrobus I demonstrated fuel savings of 25% compared to a baseline MAN bus while driving around the inter city of Berlin (Martini, 1984). Next Mitsubishi Motors developed their Braking Energy Storage and Regeneration System (BER System) for city busses. Dynamometer testing of a new bus over the M15 Japanese driving cycle with a 24% downsized engine and the BER System demonstrated fuel savings of 30% over a baseline system (Nakazawa et al., 1987). During this same time Volvo developed their Cumulo Brake Energy Drive (CBED) with measured fuel savings of 16% to 25% during normal operation (Hugosson, 1993). The Canadian National Research Council also developed a parallel hydraulic hybrid bus which yielded a 19% improvement in fuel efficiency with an average traveling speed of 48 km/h and 3.1 stops per kilometer (Davies 1987, 1989). More recently Ford Motor Company in cooperation with Eaton Corporation and the United States Environmental Protection Agency (EPA) developed the Ford Launch Assist. Dynamometer testing of Ford's transmission in an SUV over the Federal Test Procedure cycle yielded 23.6% fuel savings (Kepner, 2002). In 2003 Permo-Drive Technologies developed the Permo-Drive Regenerative Energy Management System (PDREMS). When implemented in an A1 Army Tactical Vehicle the PDREMS yielded fuel savings of 26.8% in an acceleration/ deceleration cycle (Matheson and Stecki, 2003). In 2008 Waste Management Inc. field tested a parallel

hydraulic hybrid developed by Eaton Corporation yielded fuel savings of 30% (Eaton, 2010). Recently numerous other companies have also developed parallel hydraulic hybrid transmission, many of which are not listed here.

Series Hydraulic Hybrid Transmissions

In one of the earliest works on series hydraulic hybrids Elder and Otis (1973) developed a simulation model for passenger cars which indicated substantial fuel savings were possible using the architecture. In 1979 Heggie and Sandri investigated using a mechanical bypass in parallel with a series hybrid. Their simulation showed fuel savings between 17% and 22% were possible over a more conventional series hydraulic hybrid configuration. In 1985 Wu et al. simulated a series hybrid in a passenger car and found a fuel economy of 60 mpg was possible over the Federal Urban Driving Schedule cycle.

Prototype work on series hydraulic hybrids began in the early 1990s with Volvo introducing their Cumulo Hydrostatic Drive. Dynamometer testing of the concept on a bus over a trapezoidal drive cycle showed potential fuel savings of 48% (Hugosson, 1993). In 2006 the EPA, Eaton Corporation, United Postal Service (UPS), and other industrial partners equipped a Class 5 UPS delivery truck with series hydraulic hybrid transmission and a more advanced engine. Together these technologies yielded 60% to 70% fuel savings during field testing in Detroit (Wendel et al., 2007). In 2008 Artemis Intelligent Power Ltd equipped a BMW 530i with its Digital Displacement hybrid transmission which consumed 34% less fuel over the US FTP 72 drive cycle (Artemis, 2008). While the Artemis's digital displacement units operate somewhat differently from traditional axial piston units, the transmission was still in a series hydraulic hybrid configuration. In 2012 the US Federal Transit Administration (FTA) partnered with Altair Product Design and Parker Hannifin among others to develop a modified series hydraulic hybrid transmission for city busses. This modified series hybrid featured a bypass shaft which could be clutched in to rigidly couple the transmission's input and output shafts thereby improving efficiency for certain driving conditions. In addition to a new transmission, FTA's bus

included a more efficient engine and reduced vehicle mass. Together these technologies demonstrated a 29% increase in fuel economy over the most efficient electric hybrids, a 47% increase over an identical non-hybrid bus, and a 109% increase in fuel economy over conventional city busses (Heskitt et al., 2012). As with parallel hybrids, many companies and institutions have develop series hydraulic hybrids over the last decade which have not been included here.

Series Hydraulic Hybrid Power Split Transmissions

Early work on series hybrid power split transmissions began when Shiber (1979, 1980) developed and patented a prototype transmission for a passenger car. Schiber reported a 100% increase in fuel economy though this number seems high with respect to other published values. Subsequently research moved back to larger vehicles when Bowns et al. (1981) and Dorey and Vaughan (1984) simulated various transmission configurations for city buses. Their simulations showed a hydrostatic PST improved fuel economy by 5%, a compound hydrostatic PST improved fuel economy by 14%, and a compound series hydraulic hybrid PST improved fuel economy by 28% compared to a baseline bus. MAN in Berlin Germany also developed a series hydraulic hybrid PST for their Hydrobus II which yielded an 18 to 33% increase in fuel economy compared to a baseline MAN bus (Martini, 1984). In 2010 researchers at the Maha Fluid Power Research Center constructed and tested a series hydraulic hybrid PST sized for a compact passenger car on a hardware-in-the-loop transmission dynamometer (Kumar, 2010). In 2012 Ivantysynova et al. was granted a patent for a power split transmission with energy recovery. Also in 2012 UPS equipped 20 Baltimore, Maryland based deliver vehicles with Parker Hannifin series hydraulic hybrid PSTs. From these vehicles 484 days worth of velocity profiles were recorded and used to generate a representative drive cycle. Dynamometer testing by the National Renewable Energy Lab demonstrated a 19% improvement in fuel economy for the hydraulic hybrid vehicles during the Baltimore Cycle and a 52% improvement during a New York City Composite Cycle (Lammert et al., 2014). More recently PSA-Peugeot-Citroen unveiled their concept series hydraulic hybrid PST passenger car. Marketed as a

"Hybrid Air" vehicle the car obtained fuel economy improvement of 45% in city driving (PSA, 2015). Multiple other companies have developed series hydraulic hybrid power split which are not listed here. However fewer PST based hydraulic hybrids have been developed than parallel and series hybrids likely due to increased system complexity.

3.2 Unique Hydraulic Hybrid Transmissions

A number of unique hydraulic hybrid transmissions have been proposed which cannot be clearly grouped into the aforementioned categories. In 2004 a patent was issued to the US Environmental Protection Agency for the transmission shown in Figure 3.1 (Gray, 2004).

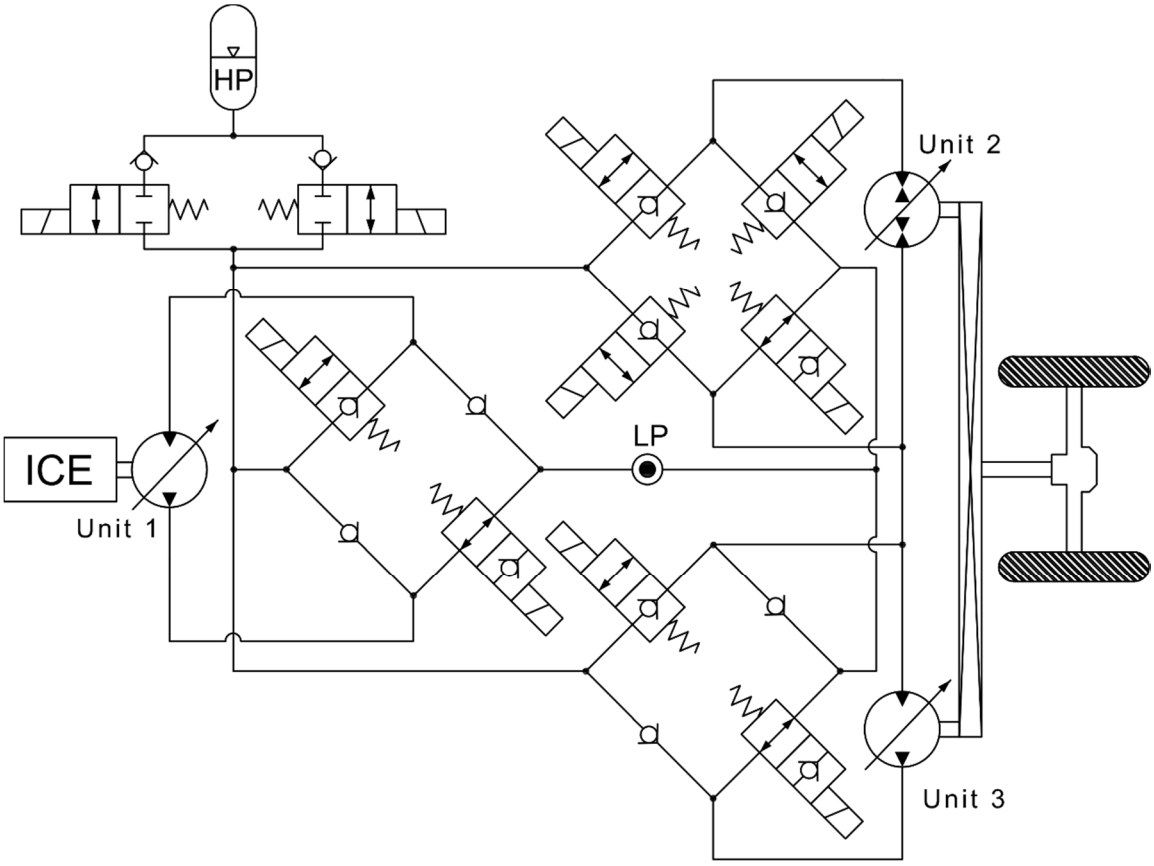

Figure 3.1 EPA hydraulic hybrid circuit (Gray, 2004)

This transmission features two positive displacement machines connected to the wheels which can be separately activated and deactivated. A series of passive and actively

controlled valves allow for four modes of operation: hybrid, hydrostatic, hydrostatic above hybrid pressure, and hydrostatic below hybrid pressure. While braking pressure automatically switches lines removing the need for over center units. However both Units 2 and 3 must operate in the same mode.

Another unique system architecture is Liebherr's Pactronic hybrid drive system (Liebherr, 2015) (Figure 3.2). This system, which powers a winch drum instead of a vehicle, consists of a hydrostatic transmission in parallel with a series hybrid transmission. Liebherr's system provides a stiff response via the hydrostatic transmission although only allows pure hydrostatic transmission through one of the units connected to the winch.

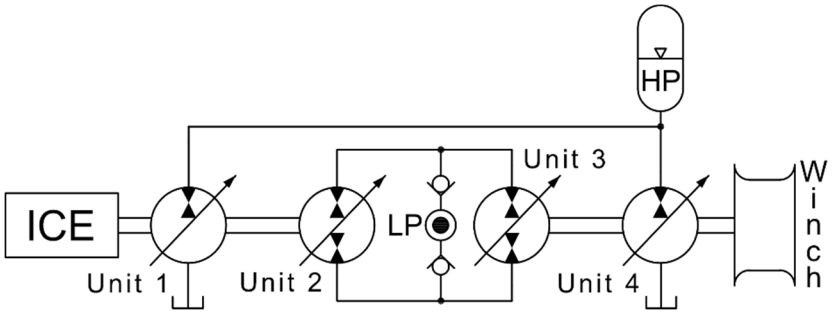

Figure 3.2 Liebherr Pactronic hybrid drive system (Liebherr, 2015)

A hybrid architecture created by HYDAC was used in a case study by Bauer et al., 2011. This system (Figure 3.3) allows operation in three modes; full hydrostatic, full hybrid, and hydrostatic between Units 1 and 2 and hybrid Unit 3. Per Bauer et al. (2011) only Unit 3 is used to recover energy while braking and must move over center to do so.

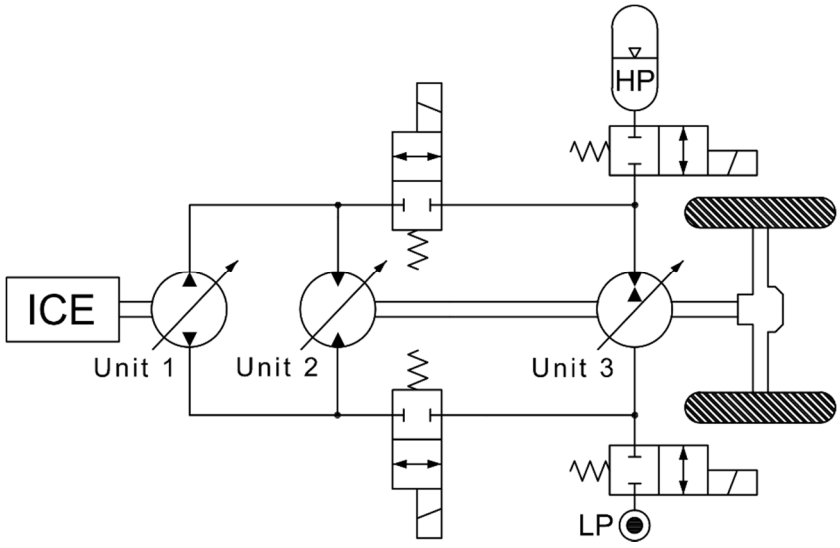

Figure 3.3 HYDAC transmission circuit (Bauer et al., 2011)

In 2012 Schneider and Krautler filled a patent application which shows a concept similar to HYDAC, though one purposed for a winch instead of a vehicle (Figure 3.4). Per the patent three modes of operation are possible (by inspection additional modes are feasible though they were not described). These include hydrostatic between Units 1 and 2, hybrid charging and discharging through Unit 3, and hybrid charging though Unit 1. In this concept Unit 3 is always connected to the HP accumulator. Not only does this increase losses but it also prevents Unit 3 from acting as part of the hydrostatic transmission. Additionally only Unit 3 is referenced as moving over center to store recovered energy in the accumulator.

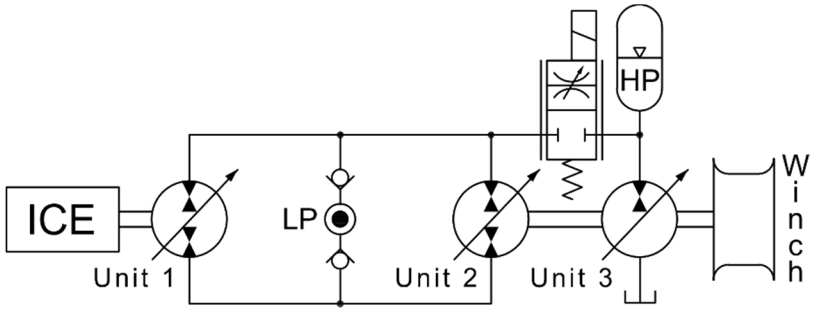

Figure 3.4 Schneider and Krautler patent (Schneider and Krautler, 2012)

3.3 Power Management of Hydraulic Hybrid Powertrains

All hydraulic hybrids require at least a rudimentary power management scheme to control engine speed and accumulator pressure. One of the simplest set of approaches are known as rule-based, that is when certain conditions are met predefined actions are taken. Although because no real optimization takes place the resulting actions are inherently suboptimal. Early examples of rule-based power management include work by Buchwald et al. (1979) where three strategies were evaluated for a parallel hybrid. Buchwald et al. proposals included using accumulator power until depleted and then switching to ICE power, operating the ICE at a constant torque with the hydraulic unit adding or absorbing torque as needed, and using the power source with the most efficient instantaneous conversation efficiency. This last approach bears an early resemblance to the modern Equivalent Consumption Minimization Strategy proposed by Musardo et al. (2005) which has been heavily investigated for electric hybrids. In 2004 Wu et al. proposed extracting rule-based control strategies for a parallel hybrid from optimally controlled DP results. The use of DP yielded improved fuel economy yet the rules remained suboptimal. Another simple suboptimal power management strategy used by Kim and Filipi (2007) for series hybrids is known as thermostatic or bang-bang control. In thermostatic control the accumulator begins to be charged by the engine once the accumulator pressure hits a lower limit and continues to be charge until the accumulator pressure reaches some upper bound.

More advance power management strategies include instantaneous optimization such as the work conducted by Kumar and Ivantysynova (2010) on a series hybrid power split transmission. Kumar and Ivantysynova proposed an online locally optimal control strategy which considered the entire powertrain efficiency in determining the optimal engine speed and power split between ICE and accumulator. Even more advanced are the Stochastic Dynamic Programming (SDP) approaches proposed by Kumar and Ivantysynova (2010) and Johri et al. (2011) for series hybrid power split and parallel hybrids respectively. Both of these approaches used Markov chains to approximate the stochastic

transition probability of the driver's power demand for the next instance in time based solely on the vehicle's current states. In both papers the authors statistically sampled various drive cycles to obtain transitional probabilities which were included as a state variable within a power management controller. These control schemes were then optimized offline and used to generate implementable control maps. However the SDP controller's transition probabilities were calculated based on the same cycles for which the controller was evaluated, thus it is unknown how well this approach can be generalized to unknown cycles.

Another example of sophisticated power management includes work by Bender et al. (2013) which was implemented on a parallel hybrid refuse truck. The proposed controller consisted of several components including online cycle prediction based on vehicle data including GPS and a database of previously measured cycles. Once a cycle was identified the corresponding optimized power management strategy was applied to the vehicle. To further improve performance an automatic offline optimization based on measured vehicle data was used to continuously update the database of optimized power management strategies. In this way the power management controller could learn and adapt online to novel vehicle profiles and usage patterns.

3.4 Research Objectives

The current state of the art in hydraulic hybrid transmissions can be summarized as follows:

- Parallel hybrids, series hybrids, and series hybrid power split transmissions have demonstrated considerable fuel savings in real world applications. In general both fuel efficiency and system complexity increase when transitioning from parallel to series to power split architecture. There also exists a wide variety of alternative hybrid transmission architectures with certain benefits which have not been as thoroughly investigated. However there exist deficiencies intrinsic to each of these architecture which limits performance and fuel efficiency.

- Numerous fuel efficiency results have been presented throughout literature on a wide variety of transmission architectures and applications. However the wide range of component sizings, application vehicles, drive cycles, and control methodologies employed makes it difficult to fairly compare transmission architectures.
- A number of power management controllers have been investigated to date for hydraulic hybrid powertrains. While in general the performance of various power management controllers increase with the controller's complexity, none of the approaches can achieve the same degree of fuel efficiency as globally optimal dynamic programming.

This work aims to discover how the performance, fuel efficiency, and controllability of hydraulic hybrid powertrains can be improved through novel hybrid architectures. To that end the following research objectives were pursued:

- Investigate how various transmission architectures compare to one another when the influence of control is removed.
- Investigate and introduce improved power management control schemes for conventional hydraulic hybrids.
- Investigate and introduce novel hydraulic hybrid transmission architectures to address the deficiencies present in conventional hydraulic hybrid transmissions.
- Investigate and introduce supervisory and system level control schemes for these novel hydraulic hybrid architectures with a specific focus on fuel efficiency and driver perception.
- Investigate these novel hydraulic hybrid architectures by constructing and implementing them in both a hardware-in-the-loop transmission dynamometer as well as a full scale on-road demonstration vehicle.

CHAPTER 4. ANALYSIS OF CONVENTIONAL HYDRAULIC HYBRID POWERTRAINS

Chapter 4 details an energetic analysis comparing baseline mechanical transmissions and conventional hydraulic hybrid transmissions in an on-road vehicle following a predefined cycle.

An energetic analysis of baseline manual and automatic transmissions, along with conventional series hybrid and series hybrid power split transmissions, provides a better understanding of how transmission architecture influences powertrain efficiency. In order to eliminate the controller's influence on fuel efficiency, all four transmission were optimally controlled over a predefined drive cycle using dynamic programming. Further each transmission was sized for, and evaluated in, a compact Sports Utility Vehicle (SUV). Reference vehicle parameters are located in Table 4.1.

Table 4.1 Reference vehicle parameters

Axle ratio:	4.53:1	Engine:	110 kW @ 4000 rpm
Tire rolling radius:	0.346 m	Engine:	350 Nm @ 1750 rpm
Frontal area:	2.82 m^2	Fuel:	Diesel
Drag coefficient:	0.39	GVM:	2505 kg
Rolling resistance:	0.01		

Each transmission was evaluated on the US industry standard Urban Dynamometer Driving Schedule (UDDS) (EPA, 2015). This drive cycle provides sufficient periods of acceleration and deceleration to assess the hybrid transmission's potential. A plot of the UDDS drive cycle can be found in Figure 4.1.

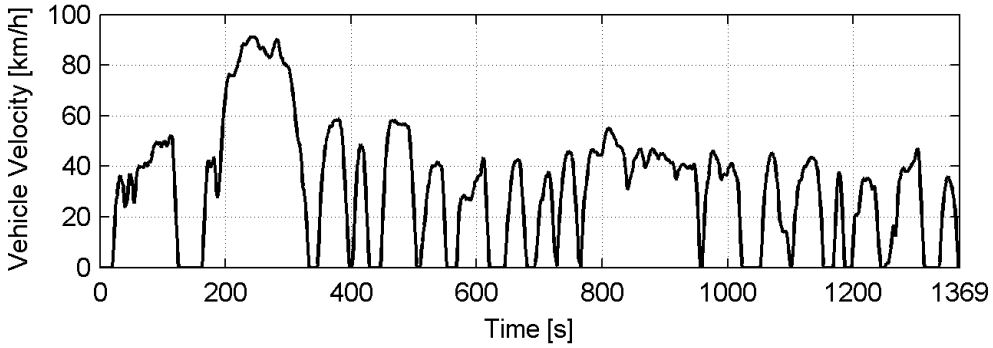

Figure 4.1 Urban Dynamometer Driving Schedule

4.1 Investigated Transmission Architectures

Simplifications were made to each transmission in interest of computational expense by removing components which did not directly influence the relative fuel consumption. These include the omission of parasitic loads such as air conditioning along with the neglection of suspension and tire dynamics. In addition none of the transmissions were allowed to unload the engine while braking. It should be noted that the intention for this investigation was to provide a fair comparison between different transmission architectures, not to precisely predict the fuel consumption of a specific vehicle. Consequently the assumptions made are acceptable as they were applied equally to all four powertrains.

Manual Transmission

A manual transmission, along with an automatic transmission, served as a baseline for comparing the two hybrid architectures. The manual transmission also provided performance specifications for the hybrid transmissions. Specifically the hybrid transmissions were sized to provide the same maximum torque as the manual transmission in 1st gear. Sizing hybrid transmissions is made difficult by the general lack of concrete performance specifications. Determining performance requirements with regards to an existing manual transmission may not be ideal for all applications but it does provide a fair baseline for comparison. Parameters for the manual transmission were

taken from an optional configuration of the reference vehicle. A schematic of the manual transmission, along with select parameters, can be found in Figure 4.2.

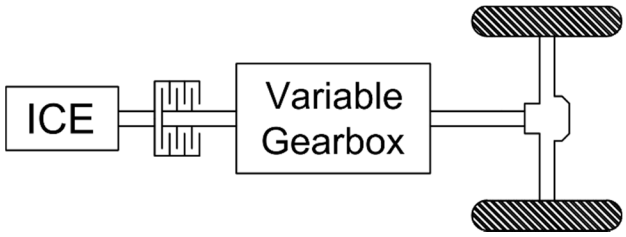

1st: 3.75:1 2nd: 1.91:1 3rd: 1.18:1 4th: 0.84:1 5th: 0.65:1 6th: 0.54:1

Figure 4.2 Manual transmission

Automatic Transmission

As automatic transmissions are a dominant transmission configuration one was included in this work to provide an understanding of how hydraulic hybrid transmissions compare with conventional systems. Parameters for the automatic transmission were taken from an optional configuration of the reference vehicle. Note that this transmission uses a different axle ratio than the other three configurations. A schematic, and select parameters, are provided in Figure 4.3.

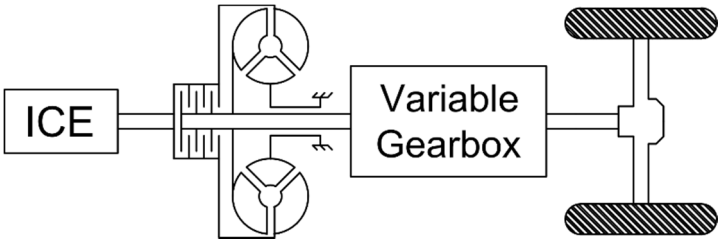

1st: 4.15:1 2nd: 2.37:1 3rd: 1.57:1 4th: 1.16:1
5th: 0.86:1 6th: 0.69:1 Axle: 3.33:1

Figure 4.3 Automatic transmission

Series Hybrid Transmission

Series hydraulic hybrid transmissions are the most common full hybrid architecture. For this investigation Unit 1 was sized to fully load the engine while Units 2 and 3 were sized to provide the same maximum torque as the manual transmission in 1st gear. The high pressure accumulator was sized to fully capture all of the braking energy in the reference

driving cycle. Further the high pressure accumulator's minimum pressure was set to provide a minimum of 0.3 g's of deceleration while braking. This level of deceleration corresponds to the transition between light and moderate braking and ensures some level of regenerative braking is always available. A schematic and select parameters can be found in Figure 4.4.

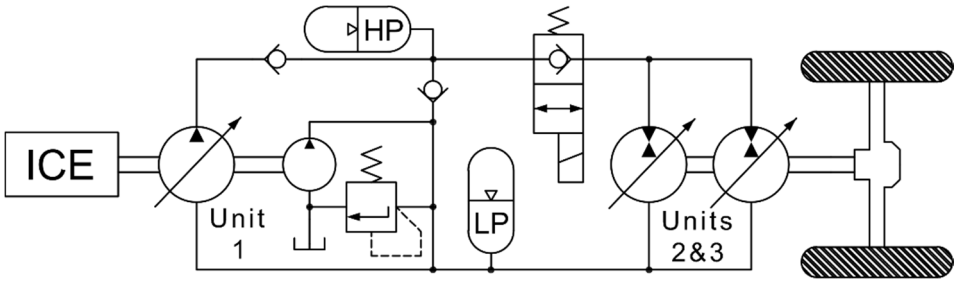

Unit 1:	60 cc/rev	Max pressure:	370 bar
Unit 2,3:	120 cc/rev	HP/LP accumulator volume:	25 l
Charge:	15 cc/rev	HP accumulator precharge:	130 bar
Low pressure:	20 bar	HP accumulator min pressure:	145 bar

Figure 4.4 Series hybrid

Series Hybrid Power Split Transmission

Series hybrid PSTs represent an advanced class of hybrid transmissions. Their planetary gear train splits engine power into an efficient mechanical path and a flexible hydraulic path. This enables PSTs to combine some of the benefits of both mechanical and series hybrid transmissions into a single advanced transmission architecture. Due to differences in operation the series hybrid PST's sizing resulted in different hydraulic components than the series hybrid. However the positive displacement machines and accumulators were still sized using the same methodology as the series hybrid. A schematic of the series hybrid PST, along with select parameters, is located in Figure 4.5.

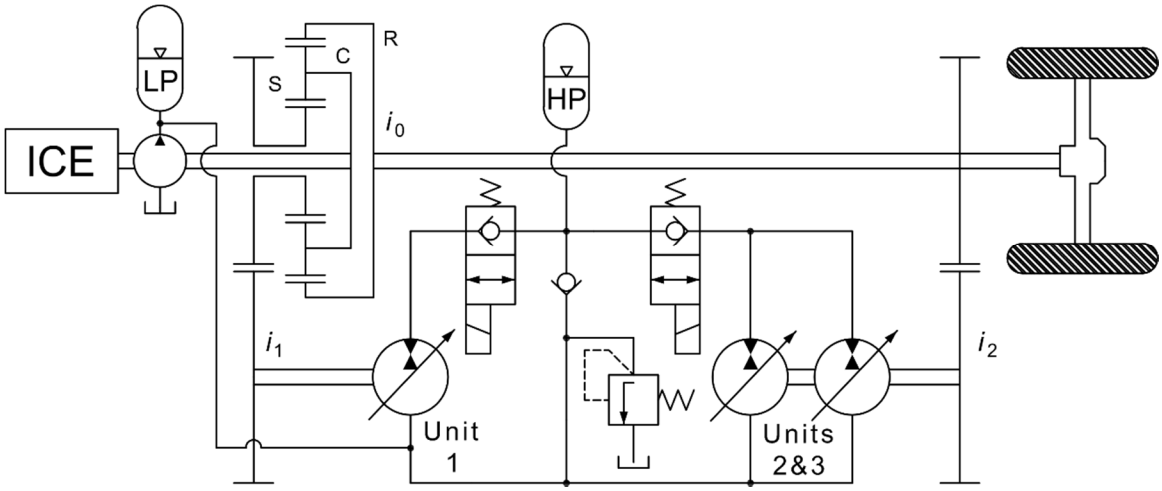

Unit 1:	60 cc/rev	Max pressure:	370 bar
Unit 2,3:	85 cc/rev	HP/LP accumulator volume:	25 l
Charge:	15 cc/rev	HP accumulator precharge:	160 bar
Low pressure:	20 bar	HP accumulator min pressure:	180 bar
PGT i_0:	0.5	i_1: 1.82:1	i_2: 1:1

Figure 4.5 Series hybrid power split transmission

4.2 Component Modeling

The following mathematical equations describe components which form the basis of powertrain models used through this work.

Positive displacement machines form the basis of hydraulic systems where theoretical flow and torque are given by Eq. 4.1 and 4.2 respectively.

$$Q_{th} = \beta \frac{\omega V_i}{2\pi} \tag{4.1}$$

$$M_{th} = \beta \frac{\Delta p V_i}{2\pi} \tag{4.2}$$

Real world performance and efficiency of these machines is captured by combining the theoretical flow and torque equations with flow and torque losses obtained through measurements. To obtain this loss information the positive displacement machine of interest is placed on a test rig and instrumented (speed, torque, flows, temperatures,

pressures). The machine is then run under steady state conditions for a wide range of speeds, pressures, and displacements. This data is then used to build polynomial losses models which can predict the actual machine losses under a range of operating conditions (Mikeska and Ivantysynova, 2002). Denoted by Q_S and M_S these losses are always positive and a function of machine speed, differential pressure, and relative machine displacement.

$$Q_S = f_Q\left(\omega, \Delta p, \beta\right) \tag{4.3}$$

$$M_S = f_M\left(\omega, \Delta p, \beta\right) \tag{4.4}$$

Positive displacement machines are capable of operating in eight distinct modes of operation defined by certain physical parameters. These modes of operation arise from specific combinations of direction of rotation, location of high pressure port (A or B), and swashplate position (nominal or over center). Out of these eight modes four combinations behave as pumps and four as motors. An example of one pumping unit and one motoring unit where port A is always high pressure, the swashplate does not move over center, and the direction of rotation changes is given in Figure 4.6.

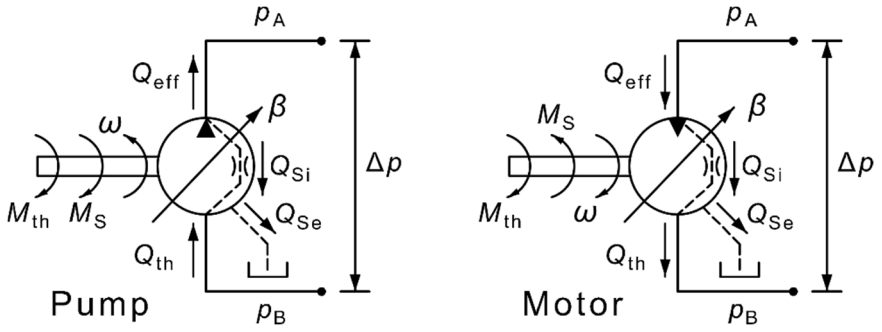

Figure 4.6 Positive displacement pump and motor schematics

While pumping effective flow rate and torque are given by:

$$Q_{eff} = Q_{th} - Q_S = \beta\frac{\omega V_i}{2\pi} - f_Q\left(\omega, \Delta p, \beta\right) \tag{4.5}$$

$$M_{\text{eff}} = M_{\text{th}} + M_{\text{S}} = \beta \frac{\Delta p V_{\text{i}}}{2\pi} + f_{\text{M}}\left(\omega, \Delta p, \beta\right) \tag{4.6}$$

While motoring effective flow rate and torque are given by:

$$Q_{\text{eff}} = Q_{\text{th}} + Q_{\text{S}} = \beta \frac{\omega V_{\text{i}}}{2\pi} + f_{\text{Q}}\left(\omega, \Delta p, \beta\right) \tag{4.7}$$

$$M_{\text{eff}} = M_{\text{th}} - M_{\text{S}} = \beta \frac{\Delta p V_{\text{i}}}{2\pi} - f_{\text{M}}\left(\omega, \Delta p, \beta\right) \tag{4.8}$$

For clarity sign convention in the previous four equations is provided by the arrow directions in Figure 4.6. A more generalized sign conventional for port flows and effective torque during all eight modes of operation is provided in Table 4.2.

Table 4.2 Port flows and effective torques for eight quadrant operation

Rotation	**Pressure**	**Swashplate**	**Flow**	**Pumping/ motoring**	Q_A	Q_B	M_{eff}
$+\omega$	$+\Delta p$	$+\beta$	B to A	P	Q_{th}-Q_{S}	-Q_{th}	-M_{th}-M_{S}
		$-\beta$	A to B	M	-Q_{th}-Q_{S}	Q_{th}	M_{th}-M_{S}
	$-\Delta p$	$+\beta$	B to A	M	Q_{th}	-Q_{th}-Q_{S}	M_{th}-M_{S}
		$-\beta$	A to B	P	-Q_{th}	Q_{th}-Q_{S}	-M_{th}-M_{S}
$-\omega$	$+\Delta p$	$+\beta$	A to B	M	-Q_{th}-Q_{S}	Q_{th}	-M_{th}-M_{S}
		$-\beta$	B to A	P	Q_{th}-Q_{S}	-Q_{th}	M_{th}-M_{S}
	$-\Delta p$	$+\beta$	A to B	P	-Q_{th}	Q_{th}-Q_{S}	M_{th}-M_{S}
		$-\beta$	B to A	M	Q_{th}	-Q_{th}-Q_{S}	-M_{th}-M_{S}

Empirically derived loss models are scaled between positive displacement machines of varying sizes using linear scaling laws (Eq. 4.9). This equation is composed of both the desired (scaled) and original (reference) displacements.

$$\lambda = \sqrt[3]{\frac{V_{\text{scaled}}}{V_{\text{ref}}}} \tag{4.9}$$

Linear scaling laws are used to predict how measured volumetric and torque losses will change with machine size. First the actual speed of the desired machine is scaled and applied to the polynomial loss models (differential pressure and normalized displacement are not scaled). Then the losses predicted by the polynomial loss model for the reference machine are scaled to the desired machine size.

$$Q_{\text{S scaled}} = f_{\text{Q}}\left(\lambda\omega, \Delta p, \beta\right)\lambda^2 \tag{4.10}$$

$$M_{\text{S scaled}} = f_{\text{M}}\left(\lambda\omega, \Delta p, \beta\right)\lambda^3 \tag{4.11}$$

Other than charge pumps, all of the positive displacement machines discussed in this dissertation are variable displacement. A simplified swashplate adjustment system is shown in Figure 4.7.

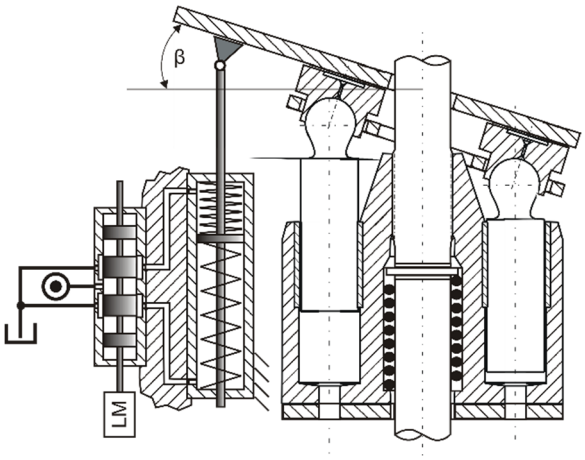

Figure 4.7 Swashplate adjustment system (Ossyra, 2004)

Simplifications can be made when modeling the swashplate adjustment system of hydraulic transmissions due to their relatively slow system dynamics. For these cases the swashplate adjustment system is modeled using a 1st order transfer function with a step response corresponding to the 0-100% step response of the respective positive displacement machine (typically 50-250 ms).

Pressure buildup in a control volume is calculated by:

$$\dot{p} = \frac{K_{\text{oil}}}{V} Q \tag{4.12}$$

Where the oil's bulk modulus K_{oil} is given by:

$$K_{\text{oil}}(p) = (p + b)\left[\frac{1}{\text{a}} - \ln\left(1 + \frac{p}{\text{b}}\right)\right]$$
$$\text{with:} \tag{4.13}$$
$$\text{a} = 0.0733 \text{ (for HLP32 at 52°c (20 cSt))}$$
$$\text{b} = 999.93 \text{ bar (for HLP32 at 52°c (20 cSt))}$$

Relief valves limit a line's maximum pressure:

$$Q = \begin{cases} C_{\text{V}} \sqrt{\dfrac{2(p_{\text{in}} - p_{\text{set}})}{\rho}} & ;(p_{\text{in}} - p_{\text{set}}) > 0 \\ 0 & ;(p_{\text{in}} - p_{\text{set}}) \le 0 \end{cases} \tag{4.14}$$

Check valves allow flow in only one direction:

$$Q = \begin{cases} C_{\text{V}} \sqrt{\dfrac{2(p_{\text{in}} - p_{\text{out}})}{\rho}} & ;(p_{\text{in}} - p_{\text{out}}) > 0 \\ 0 & ;(p_{\text{in}} - p_{\text{out}}) \le 0 \end{cases} \tag{4.15}$$

Two different approaches were used in this work for describing accumulators depending on the desired model fidelity and allowable computational expense. First a higher fidelity thermal accumulator model was used whenever accurate accumulator dynamics and efficiency characteristics were of interest. Second a polytropic accumulator model was used whenever the additional state (temperature) required by the thermal accumulator model yielded an undesirable computational burden such as during the dynamic programming simulations presented in this chapter. Polytropic models are derived from the ideal gas law where after several manipulations V_0 and p_0 represent the effective gas volume and pressure respectively when the accumulator is completely discharged.

$$\dot{p}_{\text{acm}} = \frac{Q_{\text{acm}}}{C_{\text{H acm}}} \tag{4.16}$$

$$C_{\text{H acm}} = \begin{cases} \left(1 + \frac{1-\eta_{\text{acm}}}{2}\right)\frac{V_0}{n}\left(\frac{p_0}{p^{n+1}}\right)^{1/n} & Q_{\text{acm}} \geq 0 \\ \left(1 - \frac{1-\eta_{\text{acm}}}{2}\right)\frac{V_0}{n}\left(\frac{p_0}{p^{n+1}}\right)^{1/n} & Q_{\text{acm}} < 0 \end{cases} \tag{4.17}$$

In the above equation n is the polytropic coefficient which in part determines how quickly pressure builds in the accumulator. Typical values for n range from 1 (isothermal) to 1.4 (adiabatic) with 1.3 an acceptable choice for hybrid applications due to charging/discharging times. A constant accumulator efficiency term η_{acm} is included which results in pressure decreasing faster while discharging then while charging (for a given flowrate).

A more precise description of an accumulator's response to varying cycles can be obtained by using more advanced gas models. These gas models come in the form of Equations of State (EoS) which express the relationship between a gas's pressure, temperate, and volume. In this work it was found that the Beattie-Bridgeman EoS (Eq. 4.18) provided the best agreement with measurement results.

$$p_{\text{therm}} = \frac{\text{R}T}{\nu^2}\left(1 - \frac{\text{c}}{\nu T^3}\right)\left(\nu + \text{B}\right) - \frac{\text{A}}{\nu^2} \tag{4.18}$$

With empirically derived parameters:

$$\begin{gathered} \text{A} = \text{A}_0\left(1 - \frac{\text{a}}{\nu}\right), \quad \text{B} = \text{B}_0\left(1 - \frac{\text{b}}{\nu}\right) \\ \text{R} = 8.314 \qquad \text{A}_0 = 136.2315 \quad \text{B}_0 = 0.05046 \\ \text{c} = 4.2 \times 10^4 \qquad \text{a} = 0.02617 \qquad \text{b} = -0.00691 \end{gathered} \tag{4.19}$$

Here ν is defined as the gas's molar density:

$$\nu = \frac{V}{kmol} \tag{4.20}$$

The number of moles of gas present in the accumulator is a fixed value which is calculated using the accumulator's precharge pressure, effective gas volume, and ambient temperature. Once known the accumulator's pressure becomes a function of current gas volume and temperature.

Energy losses in an accumulator are predominately due to thermal losses and to a lesser extent frictional losses. Thermal losses stem from the nitrogen gas heating up as it is compressed and then cooling if it rests before being discharging resulting in a pressure drop. Consequently a thermal model such as Eq. 4.21 is important for accurately capturing accumulator efficiency.

$$\dot{T} = \frac{T_{amb} - T}{\tau} - \frac{T}{C_v}\left(\frac{\partial p_{\text{therm}}}{\partial T}\right)_{v} \frac{dv}{dt}\,dt \tag{4.21}$$

Where $\frac{\partial p_{\text{therm}}}{\partial T}$ is derived from the Beattie-Bridgeman EoS:

$$\frac{\partial p_{\text{therm}}}{\partial T} = \frac{\mathrm{R}\left(T^3 v + 2\mathrm{c}\right)\left(v + \mathrm{B}\right)}{T^3 v^3} \tag{4.22}$$

The thermodynamics of a specific accumulator are captured using an experimentally determined thermal time constant τ. Model fidelity is further improved by using a variable rather than fixed value for C_V. This approximation is valid for pressures of 2.5-500 bar (with bar used in the equation) and temperatures ranging from 200-400 k and was generated based on empirical data published by Jacobsen et al., 1986:

$$\begin{aligned} C_v = {} & -4.0992\times10^{-11}p^4 - 3.0818\times10^{-10}p^3T + 1.547\times10^{-7}p^3 \\ & -5.6663\times10^{-10}p^2T^2 + 6.4072\times10^{-7}p^2T - 0.00017348p^2 \\ & -3.3645\times10^{-10}pT^3 + 6.5889\times10^{-7}pT^2 - 0.00039843pT \\ & +0.079046p + 7.0769\times10^{-10}T^4 - 9.486\times10^{-7}T^3 \\ & +0.00047681T^2 - 0.10488T + 29.194 \end{aligned} \tag{4.23}$$

Engine dynamics are given by Eq. 4.24 where wide open throttle torque $M_{\text{WOT}}(\omega_{\text{CE}})$ is typically determined experimentally. As with hydraulic unit measurements, empirical

engine measurements are not always available for the desired engine displacement. In these cases engine WOT curves can be scaled linearly with engine power.

$$\omega_{CE} = \int \frac{u_{CE} M_{WOT}\left(\omega_{CE}\right)\left(\frac{P_{CE\ scaled}}{P_{CE\ ref}}\right) - M_{CE\ load}}{I_{CE}\left(\frac{P_{CE\ scaled}}{P_{CE\ ref}}\right)} dt \tag{4.24}$$

Engine fuel consumption is determined experimentally:

$$Q_{CE} = fuel_{CE}\left(\omega_{CE}, u_{CE}\right)\left(\frac{P_{CE\ scaled}}{P_{CE\ ref}}\right) \tag{4.25}$$

Spur gears are modeled as a simple ratio:

$$\omega_{out} = \frac{\omega_{in}}{i} \tag{4.26}$$

Planetary gears are modeled using the Willis equation:

$$\omega_S - i_0 \omega_R - \left(1 - i_0\right)\omega_C = 0 \tag{4.27}$$

Friction clutches, such as those used in the manual and automatic transmission models, were modeled in function only. Regardless of whether or not a clutch is slipping, no torque is dissipated through friction. This, and the requirement that all torques exist in equilibrium, necessitates input and output torques are equal. Simplifications can be made by assuming the clutch is capable of transmitting the desired torque and a precise clamping force is always supplied. Following these assumptions the clutch was modeled as a device which normally behaved as a rigid connection while allowing different input and output speeds as required and always transmitting the desired torque.

Torque converters are an integral component of automatic transmission and largely modeled using empirical data. Both the K factor K_{TQ} and the torque ratio R_{TQ} are determined experimentally.

$$M_{\mathrm{I}} = \left(\frac{\omega_{\mathrm{I}}}{K_{\mathrm{TQ}}\left(\omega_{\mathrm{T}}/\omega_{\mathrm{I}}\right)} \right)^2 \tag{4.28}$$

$$M_{\mathrm{T}} = R_{\mathrm{TQ}}\left(\omega_{\mathrm{T}}/\omega_{\mathrm{I}}\right) \tag{4.29}$$

One dimensional vehicle dynamics are determined through a force balance between applied and resistive forces. Resistive forces include aerodynamic drag F_{d}, rolling resistance F_{rr}, and grading force F_{g}.

$$F_{\mathrm{d}} = \frac{1}{2}\rho A_{\mathrm{f}} C_{\mathrm{d}} \left(\frac{v_{\mathrm{veh}}}{3.6 r_{\mathrm{dyn}}} \right)^2 \tag{4.30}$$

$$F_{\mathrm{rr}} = m_{\mathrm{veh}} g C_{\mathrm{r}} \cos\left(\arctan\left(\frac{grade}{100} \right) \right) \tag{4.31}$$

$$F_{\mathrm{g}} = m_{\mathrm{veh}} g \sin\left(\arctan\left(\frac{grade}{100} \right) \right) \tag{4.32}$$

A road's inclination is often given in terms of grade:

$$grade = 100\frac{\mathrm{rise}}{\mathrm{run}} = 100\tan(\alpha) \tag{4.33}$$

Applied and resistive forces are balanced by inertial loading. In Eq. 4.34 linear vehicle inertia is transformed to rotational inertia by condensing vehicle inertia into a thin hoop with a radius equal to the tire's dynamic rolling radius.

$$\omega_{\mathrm{wheel}} = \int \frac{M_{\mathrm{wheel}} - F_{\mathrm{d}} r_{\mathrm{dyn}} - F_{\mathrm{rr}} r_{\mathrm{dyn}} - F_{\mathrm{g}} r_{\mathrm{dyn}}}{m_{\mathrm{veh}} r_{\mathrm{dyn}}^2} dt \tag{4.34}$$

In interest of simplification weight transfer, tire dynamics, and suspension dynamics were omitted in this research. However as much of this work focuses on comparing transmission architectures over a predefined cycle in simulation, and these simplifications

were applied uniformly, the relative differences between these architectures remain valid thought at a marginally reduced model fidelity.

4.3 System Modeling

Lumped parameter system models for each powertrain investigated in this work were formed by connecting together the previously described component models. These models were realized using MathWork's MATLAB Simulink environment which enabled dynamic (time domain) simulations of the multi-domain lumped parameter models. An example a series hydraulic hybrid lumped parameter model configured for a causal solver is shown in Figure 4.8.

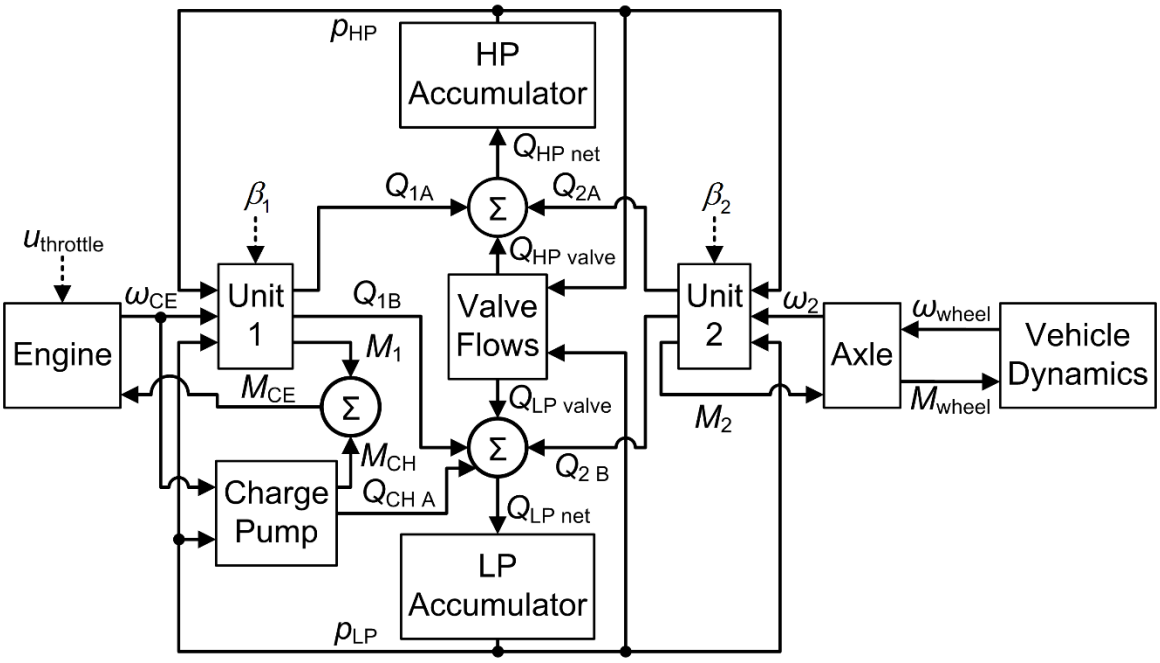

Figure 4.8 Series hybrid block diagram

4.4 Optimal Model Control via Dynamic Programming

It is well documented that the manner in which a hybrid powertrain is controlled has a major impact on fuel efficiency. This problem can be address by optimally controlling the powertrains in question thus eliminating the influence of controller design on fuel

efficiency thereby ensuring a fair system comparison (Lin et al., 2001). Optimally controlling a powertrain model has several benefits which include among others:

- Determining globally optimal state and control trajectories which can be used to baseline other control strategies.
- Designing controllers based on, and extracting control rules from, the optimal state and control trajectories.
- Eliminating the influence of suboptimal controllers on system performance thus determining the maximum possible performance.

In this work optimal model control was achieved through Dynamic Programming (DP) based on Bellman's principle of optimality. Bellman (1956) states this principle as "An optimal policy has the property that whatever the initial state and initial decision are, the remaining decisions must constitute an optimal policy with regard to the state resulting from the first decision".

Discrete time dynamic programming requires a system to be expressed using a state space representation. In a state space system key system parameters and controls are represented by state variables $x_i(t)$ and control inputs $u_i(t)$ respectively. The state variables represent the minimum number of parameters which must be known to fully describe a system at any point in time while control inputs refer to system inputs which serve to alter these states. Together the set of all states and controls for a system are expressed through state vector $x(t)$ and control vector $u(t)$.

$$x(t) \equiv \left[x_1(t) \quad x_2(t) \quad \cdots \quad x_n(t) \right]^T \qquad u(t) \equiv \left[u_1(t) \quad u_2(t) \quad \cdots \quad u_n(t) \right]^T \tag{4.35}$$

In this work the DP powertrains models were created in Simulink using a modified lumped parameter approach. During dynamic programming the previously identified states within the lumped parameter models were initialized to the value specified by DP while

the respective controls from the control vector (also specified by DP) were applied. The simulation model was then run for the prescribed length of time after which the final values of each state were extracted.

Dynamic programming requires both the continuous time and states of an optimal control problem to be discretized. Throughout this work time was discretized in one second intervals due to the relatively slow dynamics present within a drive cycle. The discretization of individual states and controls varied depending on the application but are detailed for each powertrain later on in this chapter.

The principle of optimally is expressed mathematically for discrete time dynamic programming through the functional recurrence equation of dynamic programming:

$$J^{*}_{\text{N-K,N}}\left(x\left(N-K\right)\right)=\min_{\text{u(N-K)}}\left\{\overbrace{g_{\text{D}}\left(x\left(N-K\right),u\left(N-K\right)\right)}^{\text{Transitional Cost}}+\overbrace{J^{*}_{\text{N-(K-1),N}}\left(a_{\text{D}}\left(x\left(N-K\right),u\left(N-K\right)\right)\right)}^{\text{Cost to Finish}}\right\}$$

(4.36)

Where N is the number of stages, K is the stage counter, g_{D} is the transitional cost function to be minimized between the current and subsequent state, and a_{D} represents the system dynamics. As fuel efficiency was of principle interest throughout this work, the transitional cost function g_{D} being minimized contained the engine's fuel consumption.

The DP algorithm begins one time step before the final time step. The model is then initialized at each combination of discrete states before every combination of discrete controls are applied in turn. For the first stage (N-1) the total cost being minimized is simply the transitional fuel consumption between the current stage and the final stage. After all sets of controls are applied for a specific state the DP algorithm selects and records the minimum cost in the J^{*} matrix and the associated optimal control values in their respective optimal control matrices U^{*}. Once all of the states have been optimized the DP algorithm steps back in time to stage (N-2) and begins again. Once again the model

is initialized at a given state and controls are applied, however now the resulting states after the DP time step (now at stage *N*-1) are used to determine the cost to finish contained within the *J** matrix. This projection of states by means of various controls for a representative hybrid transmission is illustrated in Figure 4.9. The optimal controls are now those which minimize both the transitional fuel consumption and the cost to finish.

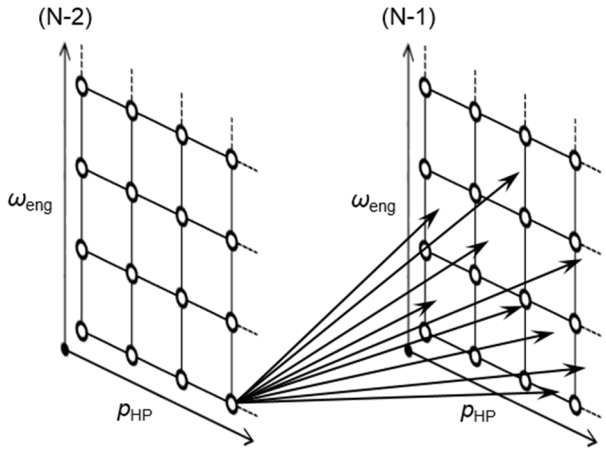

Figure 4.9 Dynamic programming state projection

This recursive process is repeated from stage to stage until the initial time step is reach thus concluding the DP algorithm. Once the initial time step is reached both the *J** and *U** matrices are filled. However the *J** matrix is of little use as the cost to finish values provide little information regarding the optimal path through the states. The only information which can be extracted from the *J** matrix is the optimal initial states and the minimum cycle cost. In order to determine the optimal state trajectory the model must be run forward in time using the optimal *U** controls to control the transmission. This is accomplished by constructing a lookup table from the *U** matrices where the current states and time are inputs and the controls are outputs. This forward looking process further improves accuracy by continually interpolating between the discrete points optimized in the backwards stepping algorithm. When the DP algorithm is followed as specified the results are guaranteed to be globally optimal down to the level the system

is discretized to. A flowchart of the just described dynamic programming algorithm can be found in Figure 4.10.

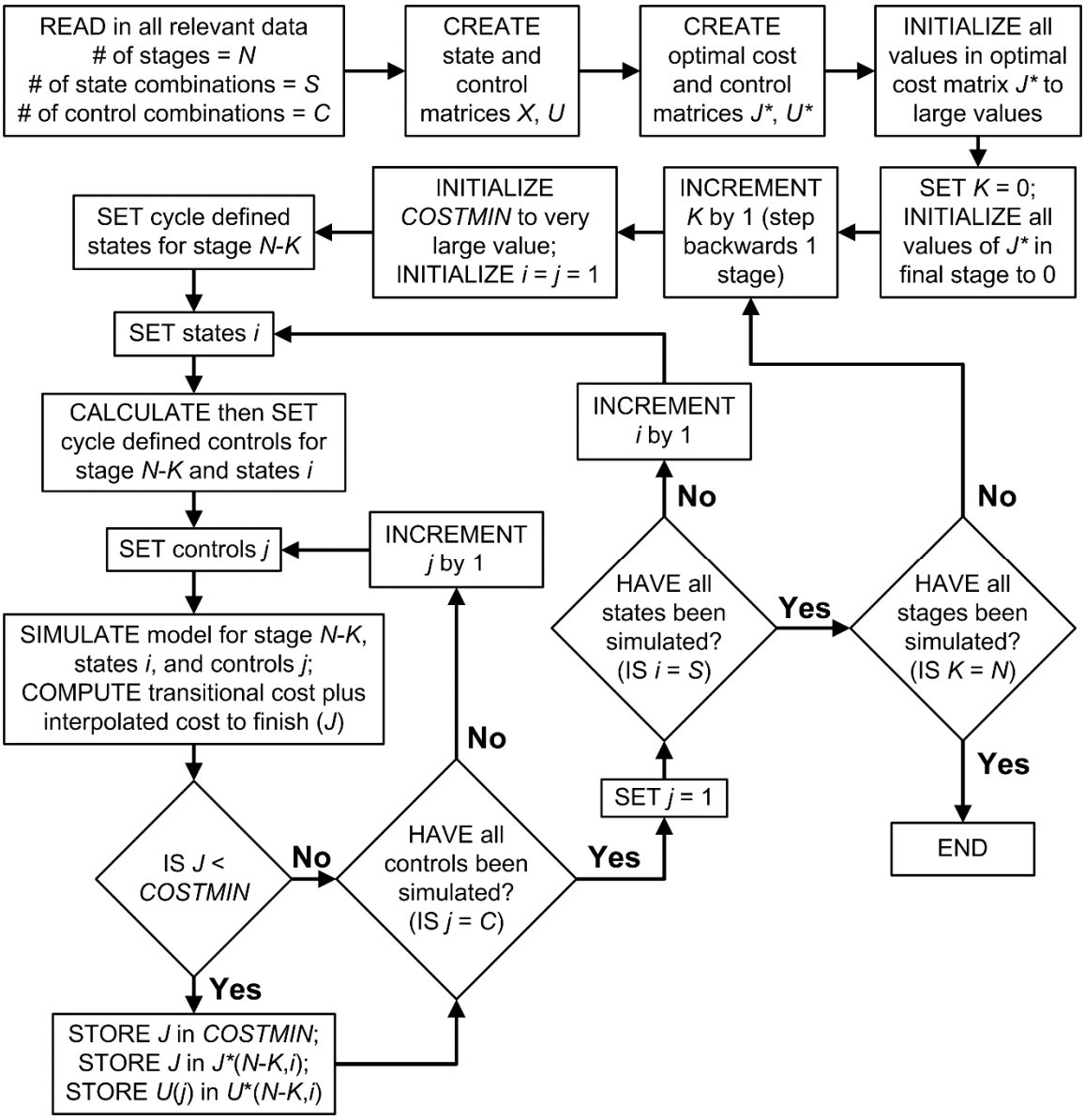

Figure 4.10 Dynamic programming flowchart

One of the primary disadvantages of dynamic programming is the significant computational expense inherent in the technique. For reference the DP optimization of the series hybrid presented in this chapter required ~1.8e9 dynamic simulations. Likewise the DP optimization of series hybrid for a neural network (Chapter 5) required ~3.7e11

dynamic simulations. In order to improve the viability of DP several techniques were used throughout this work. First the computational expense of DP grows exponentially with each additional state and control (often referred to as the “Curse of Dimensionality”). A significant decrease in computational burden was achieved in this work by eliminating superfluous states and controls whenever possible. For example small variance in the LP accumulator’s pressure will not significantly influence fuel consumption and therefore a constant low pressure can be used eliminating that pressure as a state. Overall runtime can be further improved through parallelization as every state and control evaluation within a given stage is completely independent of one another. One form of parallelization used was to place the entire Simulink model in a repeating subsystem block (as proposed by Liu and Peng, 2006). This enabled Simulink to be opened once and then simultaneously run several hundred thousand discrete simulations (varying combinations of states and controls). Depending on model complexity simulation rates of 30-50k+ simulations per second on a single processor have been achieved in this work using this method. Runtime was further reduced by simultaneously running simulations on multiple processors. MATLAB’s Parallel Computing Toolbox enabled a single primary algorithm to split the full set of simulations required for a DP stage into subsets which were then distributed to multiple processors (e.g. up to 8 on a PC, 64 on a server). Once the simulations were complete the results (i.e. transitional plus cost to finish) were sent back to the primary algorithm where the optimal controls were chosen and recorded. An overview of the parallelized DP algorithm is shown in Figure 4.11.

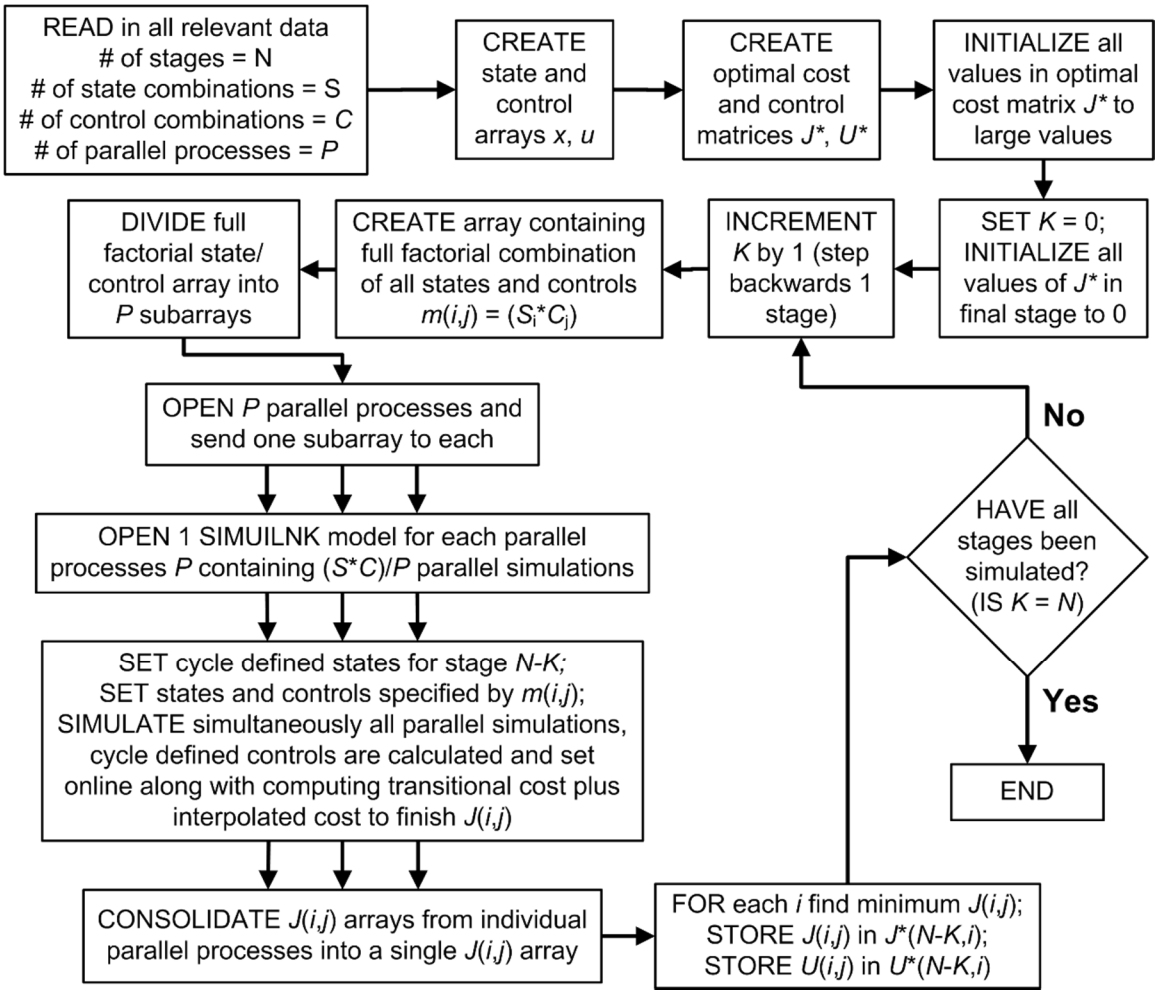

Figure 4.11 Parallelized dynamic programming flowchart

4.5 System Modeling for Dynamic Programming

Several simplifications and assumptions were made to reduce the computational expense of the simulation models used in the DP analysis. The simplifications are detailed below but generally involved either neglecting system dynamics faster than the DP time step, or imposing certain cycle defined states and controls. These cycle defined states and controls result from the assumption that the driving cycle was being perfectly tracked. Consequently wheel speed and torque were known at every time step.

Manual Transmission

The manual transmission's state space representation is given by:

$$x \equiv \begin{bmatrix} \omega_{CE} & \omega_{wheel} \end{bmatrix}^T \qquad u \equiv \begin{bmatrix} u_{CE} & i_{gear} & u_{clutch} \end{bmatrix}^T \tag{4.37}$$

Where ω_{CE} is the engine speed, ω_{wheel} is the wheel speed, u_{CE} is the engine throttle, i_{gear} is the current gear ratio, and u_{clutch} is the clutch force.

The manual transmission's reduced state space representation used in the DP algorithm is given by:

$$x \equiv [\ ] \qquad u \equiv \begin{bmatrix} i_{gear} \end{bmatrix} \tag{4.38}$$

Where ω_{CE}, ω_{wheel}, u_{CE}, and u_{clutch} were all removed as they were defined by the cycle. Since wheel speed and torque were known for every instance in time, each gear selection resulted in a defined engine speed and torque (i.e. throttle). Certain clutch dynamics were neglected as the system's overall energetic consumption was of more interest than highly transient events. Instead a simplified clutch model was developed which always transmitted the required level of torque. When the clutch was engaged the engine and transmission where rigidly coupled. However during gear shifts, and low speed vehicle operation, the clutch model permitted an appropriate level of slip.

Gear shifts were modeled using a predefined sequence of events. Once a gear shift was initiated the clutch disengaged, the engine cut its brake output power to zero, and the transmission switched gears. Simultaneously a controller applied an appropriate throttle to accelerate (or decelerate) the engine such that it arrived at the new transmission speed in 600 ms. 300 ms after the shift was initiated the clutch was partially reengaged and the engine resumed supplying the specified wheel torque, plus or minus the torque required to finish accelerating or decelerating the engine. 600 ms after the shift was initiated the clutch fully engaged and resumed providing a rigid connection between engine and transmission.

Modeling the manual transmission in this manner required violating one of the principle assumptions made to reduce computational expense. Specifically when changing gears

the engine torque was cut preventing the drive cycle from being perfectly followed. This issue was mitigated by requiring the transmission to resume perfectly following the drive cycle within one second of the gear shift's initiation.

The control vector for the manual transmission was discretized as follows for the DP analysis:

$$u \equiv \left[i_{\text{gear}} \right] \left[1:6 \right] \tag{4.39}$$

Automatic Transmission

The automatic transmission's state space representation is given by:

$$x \equiv \left[\omega_{\text{CE}} \quad \omega_{\text{wheel}} \right]^{\text{T}} \qquad u \equiv \left[u_{\text{CE}} \quad i_{\text{gear}} \quad u_{\text{clutch lockup}} \right]^{\text{T}} \tag{4.40}$$

Where $u_{\text{clutch lockup}}$ is the torque converter's lockup clutch.

The automatic transmission's reduced state space representation is given by:

$$x \equiv \left[\ \right] \qquad u \equiv \left[i_{\text{gear}} \quad u_{\text{clutch lockup}} \right]^{\text{T}} \tag{4.41}$$

Where engine speed and throttle were removed from the reduced state space representation as they were defined by the cycle. For a given transmission gear ratio there was a defined engine speed which resulted in the required torque being transmitted through the torque converter. During simulation an internal feed forward controller determined the required engine speed and applied the appropriate throttle to meet the specified drive cycle torque.

An automatic transmission's lockup clutch improves efficiency by rigidly coupling the torque converter's impeller and turbine. While locked transmission efficiency increases to near that of a mechanical transmission, albeit with some churning and pumping losses remaining. The DP algorithm was allowed to engage the lockup clutch at any point above second gear so long as no constraints were violated.

Gear shifts were handled differently in the automatic transmission than in the manual transmission due to differences in transmission construction. In a conventional manual transmission power can only be transmitted through one gear ratio at a time. However during an automatic transmission's gear shift power can be transmitted with little interruption through multiple gear ratios by precisely controlling various clutch pressures. For the dynamic programming algorithm these dynamics were simplified with the transmission shifting gears in 300 ms without cutting engine power.

The control vector for the automatic transmission was discretized as follows for the DP analysis:

$$u \equiv \begin{bmatrix} i_{\text{gear}} \\ u_{\text{clutch lockup}} \end{bmatrix} \begin{bmatrix} 1:6 \\ 0:1 \end{bmatrix} \tag{4.42}$$

Series Hybrid Transmissions

Both the series hybrid, and series hybrid power split transmission, are represented by the same state space:

$$x \equiv \begin{bmatrix} \omega_{\text{CE}} & \omega_{\text{wheel}} & p_{\text{HP}} & p_{\text{LP}} \end{bmatrix}^{\text{T}} \qquad u \equiv \begin{bmatrix} u_{\text{CE}} & \beta_1 & \beta_2 & \beta_3 & u_{\text{enab}} \end{bmatrix}^{\text{T}} \tag{4.43}$$

Where p_{HP} is the high pressure accumulator's pressure, p_{LP} is the pressure in the low pressure system, $\beta_1, \beta_2, \beta_3$ are the normalized displacements for Units 1-3 respectively, and u_{enab} is the enabling valve command.

The reduced state spaced representation used in the DP algorithm is given by:

$$x \equiv \begin{bmatrix} \omega_{\text{CE}} & p_{\text{HP}} \end{bmatrix}^{\text{T}} \qquad u \equiv \begin{bmatrix} \omega_{\text{CE des}} & \beta_1 \end{bmatrix}^{\text{T}} \tag{4.44}$$

Where p_{LP} was removed as the low pressure system was assumed to maintain a fixed pressure, and desired engine speed $\omega_{\text{CE des}}$ replaced engine throttle u_{CE}. β_2 and β_3 were removed as they were defined be the cycle. Instead a feedforward controller internal to

the Simulink model controlled Units 2 and 3 to provide the required wheel torque based on cycle demands and current accumulator pressure. To reduce computational expense it was assumed that both units would provide half of the required cycle torque. While in some instances it may be optimal to operate the units at different displacements, to determine this would have required an additional control and associated increase in the DP algorithm's computation expense. The enabling valve commands (one for the series hybrid and two for the series hybrid PST) were also removed. Instead an internal controller opened the valves any time a unit displacement other than zero was commanded.

The state and control vectors for the series hybrid were discretized as follows for the DP analysis:

$$x \equiv \begin{bmatrix} \omega_{CE} \\ p_{HP} \end{bmatrix} \begin{bmatrix} 750-4000 \text{ rpm} \\ 145-370 \text{ bar} \end{bmatrix} \begin{bmatrix} 750{:}25{:}1000,\ 1050{:}50{:}1500,\ 1600{:}100{:}4000 \\ 145:5:370 \end{bmatrix}$$
$$u \equiv \begin{bmatrix} \omega_{CE\ des} \\ \beta_1 \end{bmatrix} \begin{bmatrix} 750-4000 \text{ rpm} \\ 0-100\ \% \end{bmatrix} \begin{bmatrix} 750{:}25{:}1000,\ 1050{:}50{:}1500,\ 1600{:}100{:}4000 \\ 0:10:100 \end{bmatrix}$$

(4.45)

The state and control vectors for the series hybrid PST were discretized as follows for the DP analysis:

$$x \equiv \begin{bmatrix} \omega_{CE} \\ p_{HP} \end{bmatrix} \begin{bmatrix} 750-4000 \text{ rpm} \\ 180-370 \text{ bar} \end{bmatrix} \begin{bmatrix} 750{:}25{:}1000,\ 1050{:}50{:}1500,\ 1600{:}100{:}4000 \\ 180:5:370 \end{bmatrix}$$
$$u \equiv \begin{bmatrix} \omega_{CE\ des} \\ \beta_1 \end{bmatrix} \begin{bmatrix} 750-4000 \text{ rpm} \\ 0-100\ \% \end{bmatrix} \begin{bmatrix} 750{:}25{:}1000,\ 1050{:}50{:}1500,\ 1600{:}100{:}4000 \\ 0:10:100 \end{bmatrix}$$

(4.46)

Due to the limited and rather long time steps employed by the DP algorithm it is important to have highly accurate feedforward controllers determine unit displacements within a model. This task is complicated by the highly nonlinear nature of the loss models used in

this research which are dependent on unit speed, pressure, and displacement. Previous researchers (Zimmerman, 2012 and Hippalgaonkar, 2014) have used techniques such as Golden Section and Fibonacci searches to determine the required unit displacement to yield a desired torque or flow. While accurate, these and similar search techniques require multiple iterations to converge upon a solution, an obvious downside when computational expense is of interest. In this research precomputed lookup tables were used extensively any time a feedforward controller was required which depended upon nonlinear loss models. Generation of a lookup table which specified required Unit 2 and 3 displacement based on desired output torque began by placing a pump and associated loss model in a separate simulation model. Next a finely discretized full factorial array of the full range of possible unit speeds, pressures, and displacements was generated. The pump and loss model was then simulated for each combination of speed, pressure, and displacement and the resulting output torques recorded. Lookup table generation began by creating a monotonically spaced array of torques ranging from the minimum to the maximum value recorded in the model. Then for each combination of speed and pressure a 1D interpolation was performed between unit displacement and the new discretized torque array. Once completed this yielded a lookup table with indices of speed, pressure, and output torque and table data containing required unit displacements. A similar process was performed for each DP model which required a feedforward controller for one of the hydraulic units.

4.6 Dynamic Programming Energetic Analysis Results

Dynamic programming determines the optimal controls for each discretized state at every time step. However it is the optimal state and control trajectories which are of the most interest and presented here.

Manual Transmission

Optimally controlled on the UDDS cycle the manual transmission yielded a fuel consumption rate of 8.12 l/100 km while consuming 9.38 MJ of energy from the engine.

Energy consumption, defined as total brake energy produced by the engine, was included to help differentiate transmission efficiency from overall powertrain efficiency. For reference smaller fuel consumption rates and larger fuel economy numbers both indicate lower fuel consumption for a given driving segment.

While DP provides valuable insight into various transmission architectures, implementable control schemes are ultimately required. These sub-optimal controllers result in higher fuel consumption rates but more accurately reflect real world vehicle performance. To aid the reader in interpreting DP results, as was done in Johri et al. (2011), the manual transmission was also controlled using a manufacturer's recommended shifting schedule (Table 4.3). This schedule provides recommended shift points based on vehicle velocity for both casual cruising and more aggressive acceleration events.

Table 4.3 Manufacture recommended shifting schedule

	Shift Point (km/h)	
Gear	Cruise	Acceleration
1 to 2	16	24
2 to 3	31	39
3 to 4	43	55
4 to 5	60	76
5 to 6	66	90

Following the UDDS cycle using the cruise shift points the manual transmission obtained a fuel consumption rate of 9.06 l/100 km while consuming 9.69 MJ. The acceleration shifting schedule resulted in a fuel consumption rate of 10.19 l/100 km with an energy consumption of 9.89 MJ.

Automatic Transmission

Optimally controlled with dynamic programming the automatic transmission obtained a fuel consumption rate of 9.01 l/100 km while consuming 11.14 MJ of energy from the

engine. Though torque converter lock-up clutches have become commonplace due to their impact on efficiency, not every automatic transmission contains one. An automatic transmission without a lockup clutch was optimally controlled with DP resulting in a fuel consumption rate of 11.37 l/100 km while consuming 13.37 MJ of energy.

Series Hybrid Transmission

DP yielded a fuel consumption rate of 8.09 l/100 km with an energy consumption of 11.28 MJ for the series hybrid transmission. Figure 4.12 shows a plot of vehicle velocity, engine speed, and accumulator pressure for the optimally controlled series hybrid. During regenerative braking the accumulator's pressure increased as energy was recovered and stored. Subsequently this energy was release to help propel the vehicle resulting in a decreased accumulator pressure. By inspection it can be seen that the accumulator pressure often dropped down to the minimum allowed system pressure of 145 bar. This is an important observation as it indicates that a system pressure below 145 bar would quite likely improve fuel efficiency.

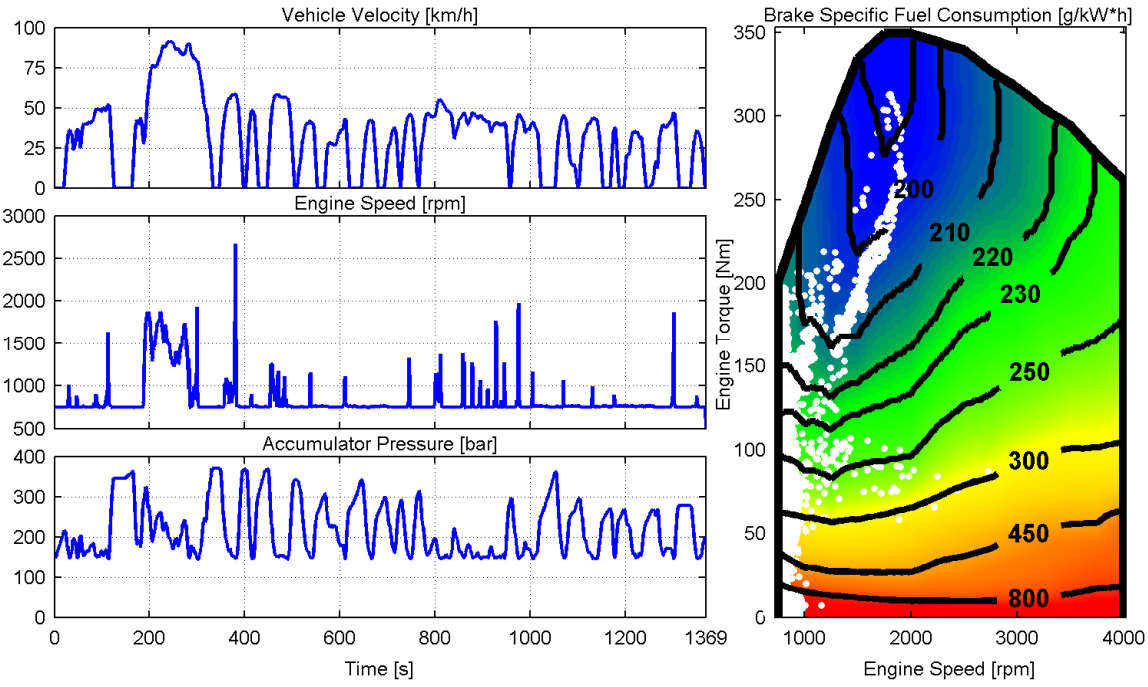

Figure 4.12 Series hybrid dynamic programming results

An engine operation map for the series hybrid is also shown in Figure 4.12. This map includes the engine's Brake Specific Fuel Consumption (BSFC) with lower numbers indicating more efficient engine operation. Superimposed on the BSFC map is a two dimensional histogram of the series hybrid's engine operation over the UDDS cycle. The white dots indicate where the engine operated with their size proportional to the cumulative duration of operation. This plot shows the series hybrid preferred to maintain a minimum engine speed except when operating near the engine's region of peak efficiency.

Series Hybrid Power Split Transmission

Optimally controlled the series hybrid PST achieved a fuel consumption rate of 7.77 l/100 km while consuming 10.55 MJ of energy from the engine. Select transmission parameters for the series hybrid PST are located in Figure 4.13. For the power split transmission the angular velocities of each planetary gear set have also been plotted. This includes the carrier gear (engine speed), the ring gear (mechanical path speed), and the sun gear (hydraulic path speed). Note the sun gear often operated below 0 rpm indicating power recirculation. While it is well know that power recirculation is less efficient than power additive mode, DP found that operating the transmission in a less efficient manner yielded an overall increase in powertrain fuel efficiency. The primary driver behind this method of operation is the strong dependence of fuel efficiency on engine operating conditions. Examining the BSFC map in Figure 4.13 shows the while fuel efficiency declines somewhat with increased speed, fuel efficiency improves considerably with increased torque. Therefore operating at the lowest permissible engine speed has not only the benefit of operating at a slightly more efficient engine speed, but more significantly as the same engine power is required a considerably higher (and more fuel efficient) torque is necessary. This relationship for PSTs between engine speed and fuel efficiency will be discussed in more detail in Section 6.3.1.

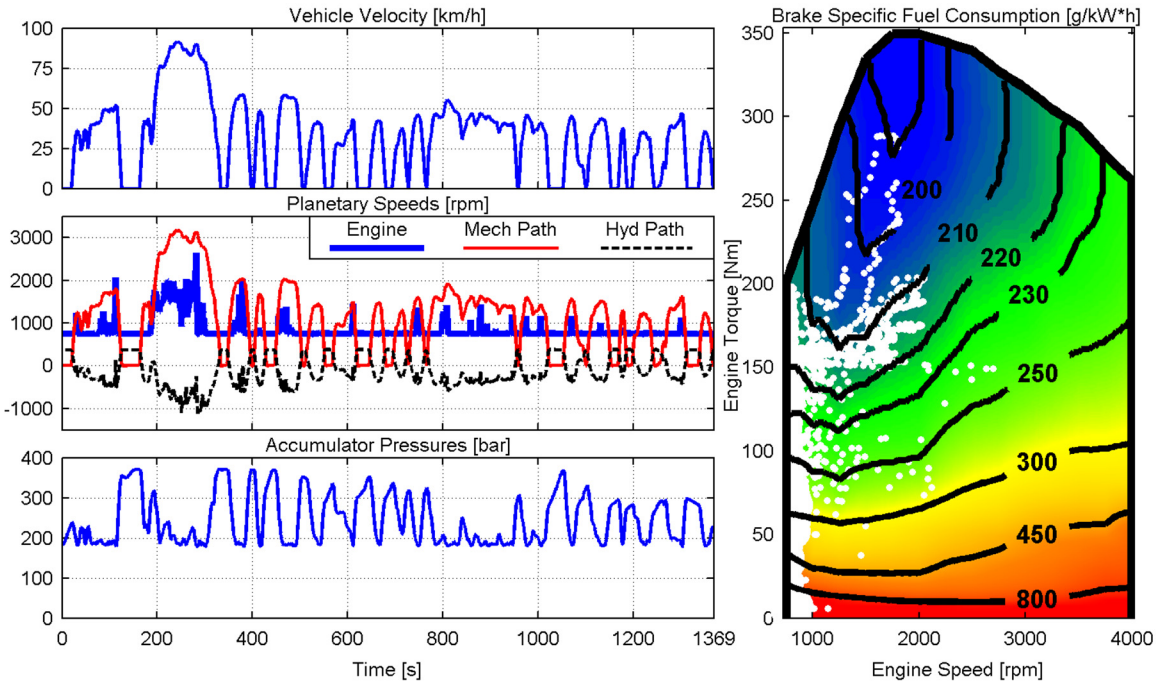

Figure 4.13 Series hybrid PST dynamic programming results

Another interesting result from the DP analysis were the similarities in accumulator pressure between the series hybrid and series hybrid PST. Superimposing these two pressure profiles on the same plot (Figure 4.14) shows that trends in both pressure profiles were nearly identical, albeit with the series hybrid PST operating at a slightly higher pressure. Differences in pressure can largely be attributed to the series hybrid and series hybrid PST's minimum pressure of 145 bar and 180 bar respectively (specified to provide 0.3 g's of braking torque). Similarities in both engine speed and accumulator pressure indicate a similar power management scheme would be optimal for both architectures.

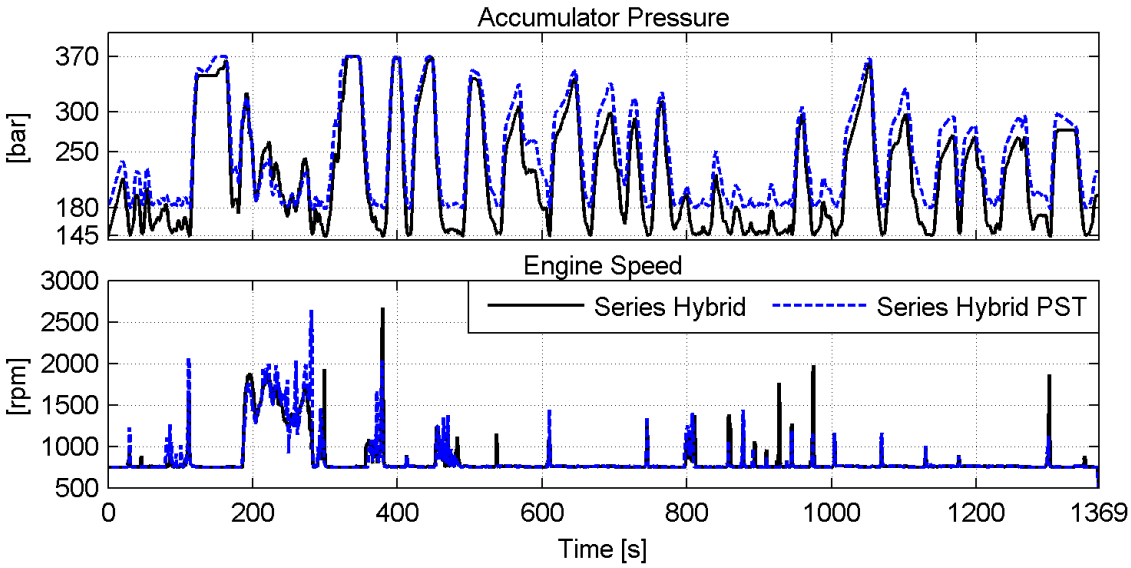

Figure 4.14 Series and series hybrid PST comparison

4.7 Summary of Dynamic Programming Results

A summary of fuel consumption rates and transmission energy consumption for all four transmission architectures is located in Table 4.4. As anticipated both hybrid transmission architectures improved fuel efficiency over the baseline manual and automatic transmissions. However both hybrid transmission also consumed more energy from the engine than the manual transmission (results were mixed for the automatic transmission). Engine energy generation is an interesting metric which can be viewed in two ways. From one prospective it shows that the hybrid transmissions were able to operate the engine in a more efficient manner since they were able to extract more energy from less fuel. Alternatively it shows that the hybrid transmissions themselves were less efficient than the manual transmission as they required more energy from the engine to complete the same drive cycle. As such it is the hybrid transmission's ability to operate the engine in a more efficient manner, along with their ability to recover energy during braking, that results in lower overall fuel consumption. These results also help to illustrate the importance of having and effective power management strategy as the hybrid transmissions themselves are not inherently more efficient than the baseline manual transmission.

Table 4.4 Summary of fuel efficiency and energy consumption

	Fuel Consumption Rate [l/100 km]	Engine Energy Generation (transmission consumption) [MJ]
Automatic	9.01	11.14
Automatic (no lockup clutch)	11.37	13.37
Manual* (acceleration)	10.19	9.89
Manual* (cruise)	9.06	9.69
Manual	8.12	9.38
Series Hybrid	8.09	11.28
Series Hybrid PST	7.77	10.55

*suboptimally controlled using predefined shifting schedule

Dynamic programming results provide valuable insight, but only part of the story, when comparing transmission architectures. DP provides optimal results by using *a priori* drive cycle knowledge. Without this future knowledge an implementable controller will not be able to achieve the same degree of fuel efficiency. It should be expected that implementable controllers for different architectures will achieve fuel efficiencies within varying degrees of the DP optimal results due to inherent differences in their operation. Finally controlling transmissions in the same manner as the DP algorithm may result in an unacceptable transmission feel. For example the manual transmission was operated at low engine speeds and high throttles. To an unknowledgeable driver this may be interpreted as an unresponsive and poorly performing vehicle. During real world operation both the absolute fuel efficiencies, and the relative differences in fuel efficiencies would be expected to change.

The lower improvements in fuel efficiency for the hybrid architectures shown in this work, as compared to other sources, result from the manner in which this investigation was carried out. First in this work the hybrid transmissions were sized to meeting the same performance as the reference manual transmission. In some other studies the hybrid transmissions were sized to meet some specific cycle. In these other studies this resulted

in less demanding performance requirements and yielded smaller, and more efficient, transmissions. For some applications such as taxis and urban delivery vehicle this sizing approach may be more realistic and appropriate. Secondly in this investigation the hybrid transmissions were optimally controlled and compared to baseline transmissions which were also simulated and optimally controlled. In some other studies the simulated hybrid transmissions have been compared to published fuel efficiencies of real world vehicles. Comparing measured fuel efficiency of one architecture to the simulated fuel efficiency of another architecture introduces some uncertainty into the results. This investigation was conducted in such a way as to provide as fair of a comparison between different transmission architectures as possible.

The outcomes in this investigation should not be taken as a definitive comparison between different transmission architecture but rather viewed as the result of a specific system sizing and control methodology. Numerous sources, such as those detail in Chapter 3, have clearly demonstrated the improvements in fuel efficiency possible with hydraulic hybrids through dynamometer and on-road testing.

4.8 Chapter Summary

- Chapter 4 covered component modeling, system modeling, optimal control through dynamic programming, and an energetic analysis of several conventional transmissions.
- The energetic analysis showed that optimally controlled series hybrids and series hybrid PSTs often operated at their minimum accumulator pressure. This indicates that fuel efficiency could further be improved if the transmissions were able to operate at pressures below their minimum accumulator pressure.
- The optimal accumulator pressure and engine speed were similar for both the series hybrid and series hybrid PST indicating a similar power management scheme would be effective for both architectures.

- The optimally controlled engine generally operated at the minimum permissible engine speed. When higher engine speeds were required the engine operated at a moderate to high torque thereby operating the engine in an efficient manner.
- Both hybrid transmissions yielded higher fuel efficiencies than either baseline mechanical transmission. However both hybrid transmissions were also less efficient than a manual transmission. This shows that the overall improvement in fuel efficiency comes not from improved transmission efficiency, but rather from more efficient engine operation along with the ability to recover braking energy. This also highlights the need for effective power management to maximize the fuel efficiency of hydraulic hybrid powertrains.

CHAPTER 5. NEURAL NETWORK BASED POWER MANAGEMENT

As shown in the preceding chapter effective power management is key to maximizing the efficiency and performance of hydraulic hybrid vehicles. Power management can be generalized as the manner in which a powertrain is operated excluding those controls which directly affect vehicle speed. For conventional hydraulic hybrids, power management involves balancing the energy generated by the engine with the energy stored and released from the high pressure accumulator. Generally speaking engine speed and accumulator pressure are the two principle free states which determine how energy is split between these sources. Prior works have investigated a number of methods for optimizing these free states including dynamic programming which remains the only feasible approach capable of determining globally optimal state and control trajectories. However as discussed in the Chapter 4, DP depends on *a priori* knowledge of every driving event and therefore is not applicable as an implementable power management strategy.

Yet exploring these dynamic programming optimizations still provides valuable information regarding effective power management. Analysis of multiple DP optimizations has shown that peak fuel efficiency is obtained by generally operating the engine at the minimum speed required to satisfy the instantaneous power demand irrespective of the broader drive cycle. Only the accumulator pressure is significantly influenced by past, present, and future cycle demands. Therefore if the optimal accumulator pressure profile could be predicted online and combined with a minimum engine speed strategy then an implementable power management controller could achieve near globally optimal fuel efficiency.

A novel approach is proposed in this dissertation which aims to generalize the optimal state trajectories obtained from dynamic programming through the use of a Neural Network (NN). The generalized trends contained within this neural network can then be used as part of an implementable power management strategy which is capable of achieving near optimal fuel efficiency even on new and untrained drive cycles. Specifically a neural network was constructed with the goal of predicting the optimal accumulator pressure based on a short history of vehicle velocity.

5.1 Reference Application and Transmission Sizing

A compact passenger car served as a reference vehicle for investigating the neural network based power management controller. A smaller reference vehicle was chosen for the neural network investigation than was used in the previous DP analysis due to power limitations imposed by the HIL transmission dynamometer used to evaluate the proposed control strategy. Select vehicle parameters can be found in Table 5.1.

Table 5.1: Reference vehicle parameters

Tire rolling radius:	0.321 m	Engine:	103 kW @ 5600 rpm
Frontal area:	2.2 m^2	Engine:	185 Nm @ 4300 rpm
Drag coefficient:	0.31	Fuel:	Gasoline
Rolling resistance	0.01	Mass:	1400 kg
Axle ratio:	3.94:1		

The series hybrid transmission used in the NN investigation was sized to meet roughly the same performance as the reference vehicle. Unit 1 was sized to fully load the engine at moderate pressure. In order to enable higher speed and power operation two identical units (Units 2 and 3) were connected to the axle/wheels. These units were sized to provide a similar peak tractive torque (at the units maximum rated pressure of 450 bar) as the reference vehicle. Finally the high pressure accumulator was sized to capture the energy present in a moderate braking event. Select parameters for the series hybrid transmission are located in Figure 5.1.

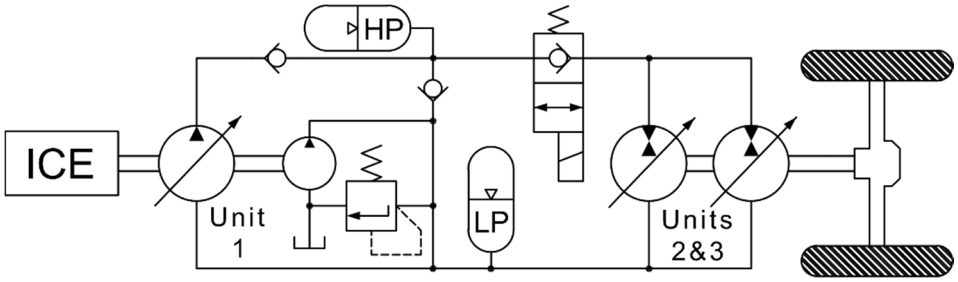

Unit 1,2,3:	42 cc/rev	HP/LP accumulator effective volume:	18.4 l
Charge:	15 cc/rev	HP accumulator precharge:	130 bar
Max pressure:	350 bar	HP accumulator min pressure:	140 bar
Low pressure:	20 bar	LP accumulator precharge:	10 bar

Figure 5.1: Series hybrid transmission

5.2 Optimal Control Generation and Pressure Validation

5.2.1 Reference Cycle Generation

Creating an effective power management controller began by first optimally controlling the series hydraulic hybrid vehicle over a reference drive cycle. Optimally controlling the powertrain provided two functions. First the optimally controlled vehicle defined the best case fuel consumption rate which served as a baseline for comparing power management strategies. Second the optimally controlled vehicle produced an optimal state profile which the neural network could be trained on.

A power management controller should be general and operate effectively in many situations, not just on a single drive cycle. However many industry standard cycles are relatively short and therefore offer a rather small number of driving events. In addition, developing a power management scheme based on one of these standard driving cycles may result in over training or cycle beating. Two industry standard cycles, the Urban Dynamometer Drive Schedule (UDDS), and the Unified Dynamometer Driving Schedule (LA92) (EPA, 2015) are shown in Figure 5.2. Both of these cycles are relatively short with the UDDS traveling 12.0 km over 22.8 minutes while the LA92 travels 15.8 km over 23.9 minutes.

To train the power management controller on a broader spectrum of driving events a new composite drive cycle was created based on these two standard cycles. Drive cycle generation began by splitting each cycle into individual driving events containing the vehicle's velocity from start to stop. In total these two drive cycles contain 33 individual driving events. A 24 hour long drive cycle was arbitrarily chosen to provide a sufficient variety of driving events which helped to prevent over training. Generation of the 24 hour composite cycle began with an algorithm randomly selecting one of the 33 "seed" driving events. Next this seed profile's velocity was randomly compressed or expanded by -50 to 50%. Simultaneously another random number generator compressed or expanded the seed profile's time by -50 to 50%. Finally a stop between 2 and 5 seconds was randomly chosen and placed at the end of the segment before appending the modified driving segment to the end of composite cycle. This process was repeated until the desired 24 hour cycle duration was reached. This random cycle generation resulted in a large variety of realistic driving event on which to train the power management controller. For reference the first 25 minutes of the 24 hour/750.6 km long composite cycle can be seen in Figure 5.2. The composite cycle is unique through its duration though only the first 25 minutes are show here for clarity.

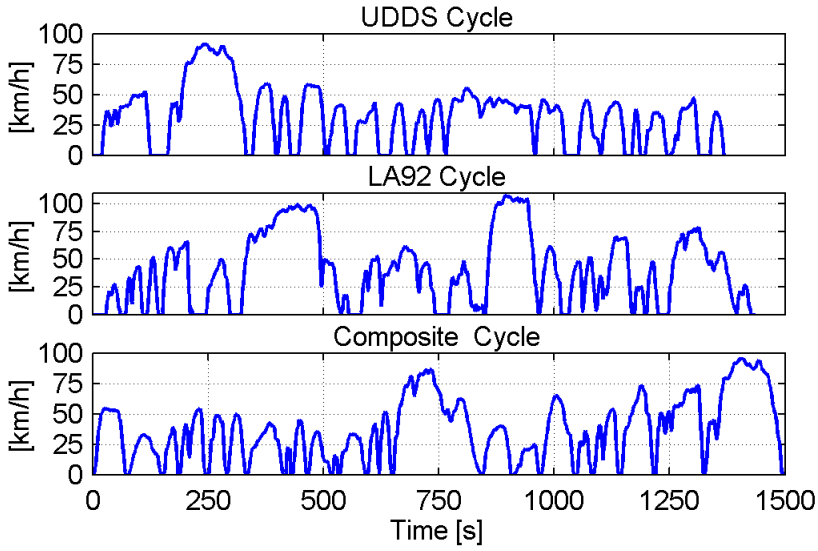

Figure 5.2: Standard and composite drive cycles

It should be mentioned at this point that the purpose of this work was to investigate the feasibility of a neural network based power management strategy, not to optimize the approach's training and implementation. A further investigation might likely show that a shorter duration training segment would be equally effective as would a broader variety of driving events.

5.2.2 Dynamic Programming Optimal State Generation

The series hybrid used for the NN investigation is represented by the follow state space:

$$\begin{aligned} x &\equiv \begin{bmatrix} \omega_{CE} & \omega_{wheel} & V_{acm} & T_{acm} & p_{LP} \end{bmatrix}^T \\ u &\equiv \begin{bmatrix} u_{CE} & \beta_1 & \beta_2 & \beta_3 & u_{enab} \end{bmatrix}^T \end{aligned} \tag{5.1}$$

Where V_{acm} is the high pressure accumulator's gas volume, T_{acm} is the high pressure accumulator's gas temperature.

The reduced state space representation used in the DP algorithm is given by:

$$x \equiv \begin{bmatrix} \omega_{CE} & V_{acm} & T_{acm} \end{bmatrix}^T \qquad u \equiv \begin{bmatrix} \omega_{CE\ des} & \beta_1 \end{bmatrix}^T \tag{5.2}$$

The state and control vectors for the series hybrid were discretized as follows for the DP analysis:

$$\begin{aligned} x &\equiv \begin{bmatrix} \omega_{CE} \\ V_{acm} \\ T_{acm} \end{bmatrix} \begin{bmatrix} 800-3900\ \text{rpm} \\ 0.00743-0.01843\ \text{m}^3 \\ 265-355\ \text{k} \end{bmatrix} \begin{bmatrix} 800{:}50{:}1000,\ 1100{:}100{:}2500,\ 2700{:}200{:}3900 \\ 0.00743 : 0.000275 : 0.01843 \\ 265 : 15 : 355 \end{bmatrix} \\ u &\equiv \begin{bmatrix} \omega_{CE\ des} \\ \beta_1 \end{bmatrix} \begin{bmatrix} 800-3900\ \text{rpm} \\ 0-100\ \% \end{bmatrix} \begin{bmatrix} 800{:}50{:}1000,\ 1100{:}100{:}2500,\ 2700{:}200{:}3900 \\ 0 : 10 : 100 \end{bmatrix} \end{aligned} \tag{5.3}$$

Optimally controlled over the 24 hour composite cycle the series hybrid achieved a fuel consumption rate of 6.77 l/100 km.

5.2.3 Optimal Pressure Validation

A key assumption for the power management controller presented in this work was that if a series hybrid followed its optimal pressure profile then the vehicle would achieve near optimal fuel efficiency. Validating this assumption began by implementing a pressure controller for Unit 1. This controller adjusted Unit 1's displacement in order to track the reference accumulator pressure profile. Examination of the optimal DP results showed a minimum fuel consumption rate was achieved by maintaining a minimum engine speed whenever possible. An engine speed controller was then implemented in the model which maintained a minimum engine speed unless Unit 1 required more speed or torque to track the reference pressure profile. A simplified block diagram of the controller used in both simulation and measurements for engine speed and Unit 1 displacement is located in Figure 5.3.

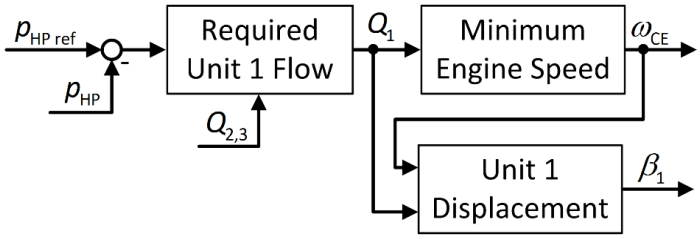

Figure 5.3: Engine speed and Unit 1 controller

Units 2 and 3 were operated together in secondary control based on the current accumulator pressure to provide the tractive torque required by the drive cycle. This controller ensured the drive cycle was tracked but remained separate from the power management controller. The series hybrid was then simulated on the 24 hour composite drive cycle using the DP optimal pressure profile as the reference pressure. Suboptimally controlled the series hybrid still yielded a fuel consumption rate of 6.84 l/100 km, only 0.99% lower than the DP optimal results. These results provided motivation for this research by showing that the closer the optimal pressure profile can be predicted, the nearer a series hybrid can approach its globally optimal fuel consumption rate.

5.3 Overview of Neural Networks

Neural networks contain three distinct but interconnected layers: an input layer, one or more hidden layers, and an output layer. The input layer provides one input for each input variable and preprocesses all incoming data. Next the hidden layer(s) acts on data from the input layer to perform the majority of the NN's computations. Finally data from the hidden layer(s) is post processed and output in the output layer. A generalized schematic of a NN can be found in Figure 5.4.

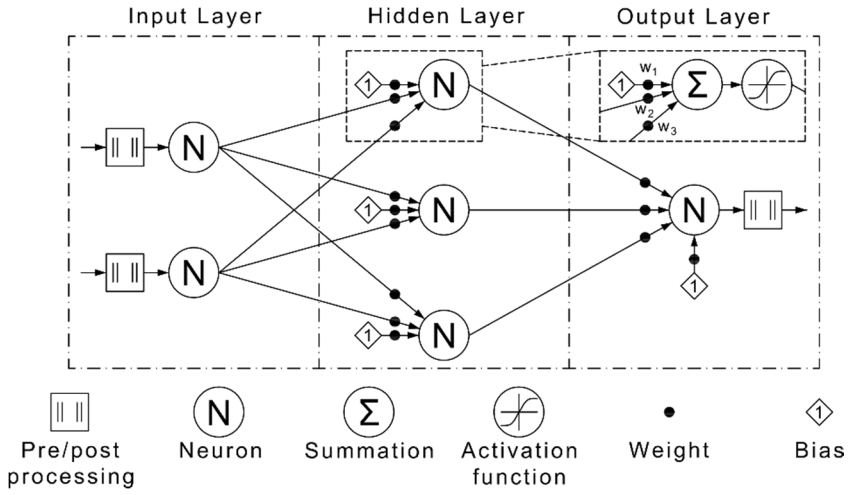

Figure 5.4: Generalized neural network schematic

Interconnected neurons are the fundamental component of every NN. Each neuron is composed of several elements beginning with a summation function which adds together all of the inputs connected to the neuron. Next an activation function (generally a sigmoidal transfer function) constrains the cumulative inputs to some predefined range (typically -1:1 or 0:1) before passing along the resulting value. Neurons may also contain a static bias value connected to the summation element which shifts the cumulative inputs by some predefined amount. Finally every connection outside of a neuron possesses an individual weight (i.e. gain). It is these weights which are adjusted to store information within the neural network.

NN's come in a wide variety of configurations, for this research a NN architecture was employed which specializes in regression analysis. That is the network aims to reproduce a predefined response based on an associated set of input data. As such these types of NN's must first be trained on an existing data set before they are of use. Prior to training this existing input/output data set is divided into three subsets; a training set, a validation set, and a testing set. A substantial advantage of NN's, and one that makes NN's well suited for this research, is their ability to generalize trends in the data rather than simply memorize input/output sets. A well structured and trained NN will have the ability to interpolate and extrapolate an output response based on new input sets which bear a resemblance to previously trained data sets.

Training begins by first defining the configuration of neurons then randomly initializing each weight's value. In a process known as supervised learning inputs for the training set are applied to the network with their response compared to the desired output values. This output response error is then back propagated through the network and used to update the NN's weights. After the weights are updated the validation data set is ran through the network. Training concludes once the maximum number of training iterations is reached, the NN yields an acceptably low error in response to the training data, the error gradient between successive training iterations drops below a predefined value, the training set's error beings to rise, or the validation set's error begins to rise. This last condition helps to prevent memorization of the training set by ending the training once the NN beings to perform worse on generalizing trends. Finally the testing data set is ran through the network as an additional check of the NN's performance on data sets which it was not exposed to.

5.4 Neural Network Based Power Management Controller Development

Designing a neural network for power management began with determining the network's inputs and outputs. There exists no methodical approach for designing an optimal NN. Therefore both the selection of inputs and outputs, and the network's

configuration, was determined through trial and error. It was found that a NN which predicted the optimal accumulator pressure profile based solely on a history of the vehicle's velocity yielded satisfactory results. Many NNs use not only the instantaneous value of an input variable, but also the temporal history of said variable. For this research the last thirty seconds of vehicle velocity, discretized to one second intervals, served as inputs to the NN. It was found through experimentation that for this application a vehicle velocity history longer than thirty seconds did not markedly increase the network's predictive performance.

A cascading feedforward neural network architecture was created for the power management controller featuring two hidden layers. The input layer contained thirty neurons (one for each input time) while the first and second hidden layers contained thirty and fifteen neurons respectively with a single neuron in the output layer. Each neuron in a given layer was connect to every other neuron in each of the subsequent layers. Hence the output of the input layer neurons were inputs to every neuron in both of the hidden layers and the output layer and so on. Both the input and hidden layer neurons featured log sigmoidal activation functions while the output layer neuron used a saturating linear activation function. Bias values were included for every neuron in each of the layers. Finally input and output variables were pre/post processed to normalize their maximum values to one. A schematic of this neural network can be found in Figure 5.5.

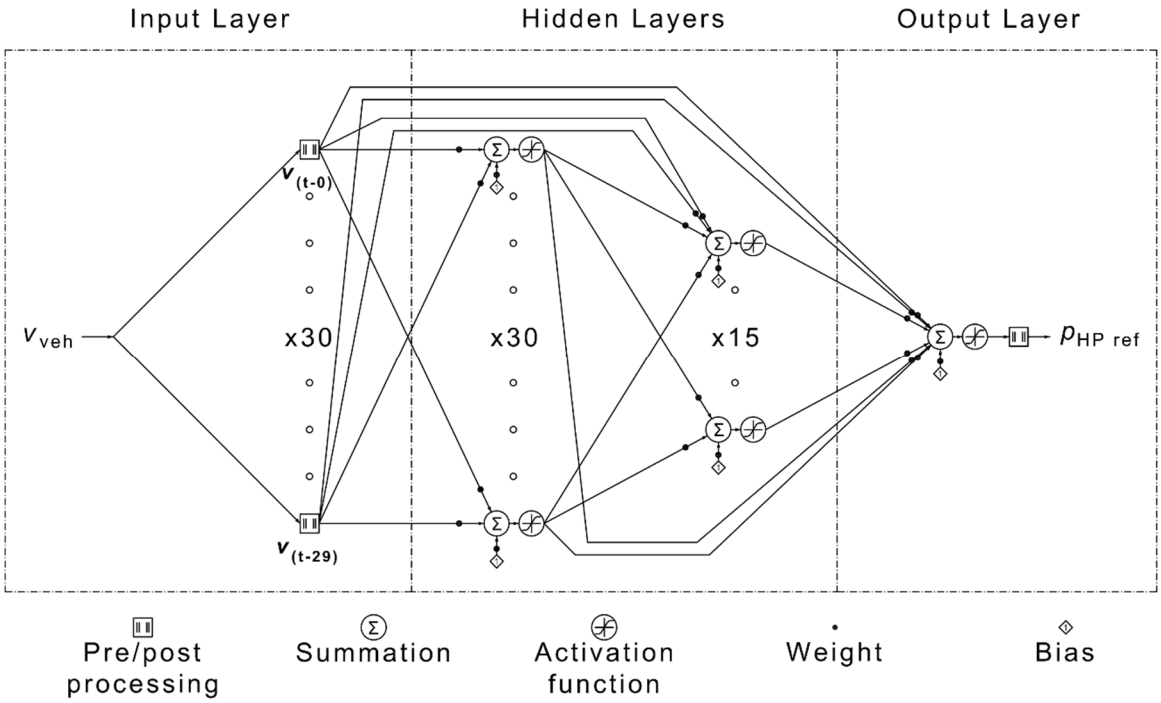

Figure 5.5: Neural network architecture

For this research the NN was constructed, trained, and implemented using MATLAB's Neural Network Toolbox. This toolbox provided an easy to use, yet powerful, interface for developing NNs. The author needed only define the network's architecture, the input/ output data set, and which training algorithms to use and the toolbox took care of training the network. In the network's final configuration the first 17 hours of the 24 hour DP optimal data set was used as the training set while two subsequent 3.5 hour blocks were used as the validation and testing sets respectively. For training the Levenberg-Marquardt backpropagation algorithm was chosen due to its high performance and relatively low computational expense.

Once training concluded the resulting NN was compiled into a Simulink model by the toolbox. This model took in vehicle velocity and output the predicted optimal accumulator pressure. This Simulink model, which required relatively low computational expense to evaluate, was exported and used in both simulation testing and HIL evaluation of the

proposed power management controller. An example of the NN's ability to predict near optimal accumulator pressure for the training cycle can be seen in Figure 5.6.

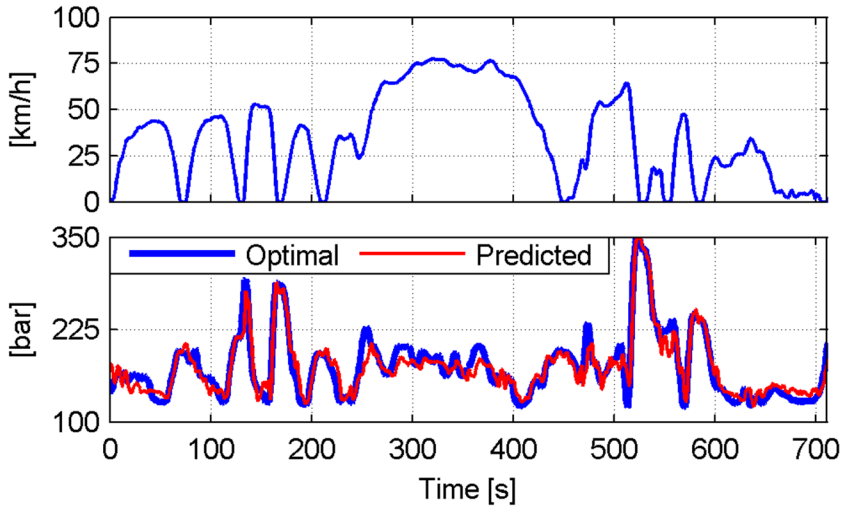

Figure 5.6: Predictive performance of the NN on a segment of the composite training cycle

5.5 Simulation Based Neural Network Power Management Controller Evaluation

Valuable insight was gained by assessing the NN's performance on both drive cycles for which it had, and had not, been trained on. It is the NN's performance on these untrained cycles which is of the most interest as it provides an indication of the network's performance in real world conditions. In total three cycles were evaluated in both simulation and experimental measurements (Section 5.6) including the first 25 minutes of the 24 hour composite cycle. This initial segment of the composite cycle demonstrated the NN's performance on a cycle for which it had been trained. Then both the Japanese JC08 and the EPA's speed corrected SC03 cycles (Figure 5.7) were run to test the network's performance in new and untrained conditions.

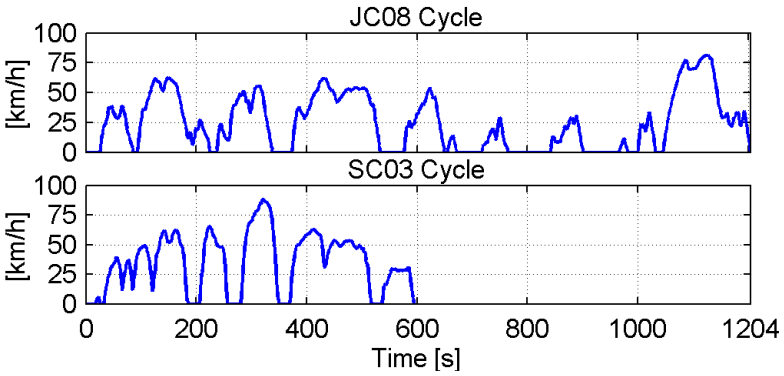

Figure 5.7: Evaluation cycles

The neural network's predictive performance on an untrained cycle can be seen graphically in Figure 5.8. Here the NN predicted the optimal accumulator pressure for the SC03 evaluation cycle. While the prediction error was greater than the training cycle (Figure 5.6), it was still sufficiently close to provide meaningful reductions in fuel consumption.

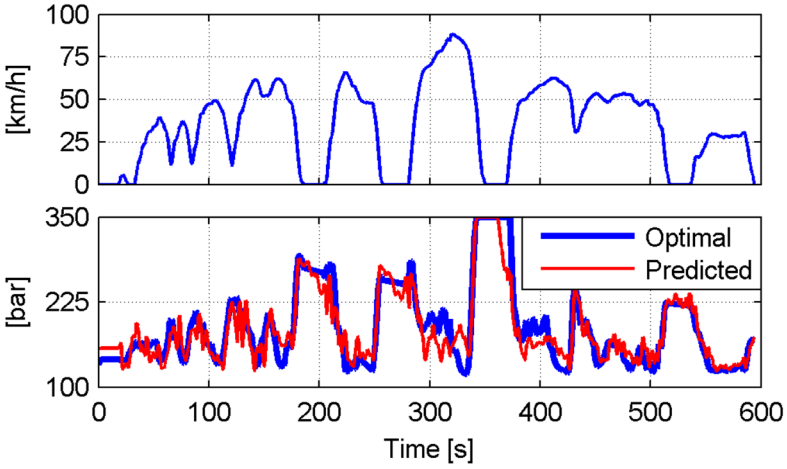

Figure 5.8: NN performance on the SC03 evaluation cycle

The neural network based power management controller was further explored by comparing its performance (again in both simulation and measurements) with a baseline constant pressure power management strategy. Here two constant reference pressures of 200 and 275 bar supplanted the variable reference pressure provided by the NN. Both the constant pressure and NN power management controllers used the same controller

(described in Section 5.2) to adjust Unit 1's displacement and the engine speed. Therefore differences in fuel efficiency between the various control strategies can be attributed primarily to difference in the reference pressure. It is important to note that Unit 1's controller only provided flow when the accumulator pressure dropped below the reference valve. It did not attempt to remove fluid from the system if the accumulator pressure exceeded the reference value as occurs during regenerative braking.

Simulation based evaluation of the NN controller began by baselining the reference vehicle over each of the three drive cycles using dynamic programming. Each drive cycle was then controlled to track the DP optimal pressure profile ($p_{optimal}$) (Table 5.2).

Table 5.2: Simulated fuel consumption rate [l/100 km]

		Drive cycle		
		Composite	JC08	SC03
Control strategy	DP	6.83	7.52	6.72
	$p_{optimal}$	6.97	7.59	6.83

This comparison evaluated the power management controller's performance if the NN was able to perfectly predict the DP optimal pressure profile. Table 5.3 summarizes the optimal pressure controller's performance relative to the globally optimal dynamic programming results.

Table 5.3: Percent change in fuel consumption rate when using optimal pressure controller compared to dynamic programming results

		Drive cycle		
		Composite	JC08	SC03
Control strategy	$p_{optimal}$	-2.10	-0.94	-1.63

Each drive cycle was then individually controlled using both constant reference pressures as well as the NN's predicted pressure. Fuel consumption rates for all of these simulations can be found in Table 5.4.

Table 5.4: Simulated fuel consumption rate [l/100 km]

		Drive cycle		
		Composite	JC08	SC03
Control strategy	DP	6.83	7.52	6.72
	$p_{optimal}$	6.97	7.59	6.83
	200 bar	7.58	8.15	7.51
	275 bar	9.57	10.20	9.37
	NN	7.30	7.90	7.28

In simulation the NN was able to achieve an average fuel consumption rate within 6.69% of the globally optimal value for the two untrained evaluation cycles. Furthermore for the same two evaluation cycles the NN was able to improve the average fuel consumption rate by 3.08% and 22.43% for the 200 and 275 bar cases respectively. These results are summarized in Table 5.5.

Table 5.5: Percent change in fuel consumption rate when using the neural network based controller over competing control strategies

		Drive cycle		
		Composite	JC08	SC03
Control strategy	DP	-6.85	-5.07	-8.30
	200 bar	3.78	3.06	3.10
	275 bar	23.79	22.60	22.26

5.6 Experimental Validation of the Neural Network Power Management Controller

During modeling every effort is made to ensure that the simulation models accurately reflect real world physics. However there is always the possibility that control methodologies developed and evaluated in simulation will not perform well when implemented in an actual vehicle. To address this point a series hybrid transmission was constructed on a Hardware-in-the-Loop (HIL) transmission dynamometer. HIL refers to testing configurations where components of interest are physically present while ancillary components are simulated. In this case a complete series hybrid transmission was present while the engine and drivetrain components after the transmission were simulated using

two electric motor/generators. During operation real time simulations of both the engine and vehicle dynamics were ran in response to measured speeds and torques with their resulting outputs used to control the two electric units. In this way the series hybrid transmission operated in manner quite similar to the way in which it would function when implemented in a real vehicle. More information on the HIL transmission dynamometer can be found in Chapter 7.

A HIL transmission dynamometer is an ideal tool for investigating the neural network based power management controller. This is in large part due to the exceptionally high degree of control, and especially repeatability, which this testing method offers. Specifically this testing configuration allows the transmission to be run identically multiple time over a given drive cycle while altering only the power management controller. Such an approach eliminates many of the unavoidable uncertainties present when evaluating power management controllers through on-road vehicle testing. Another benefit of HIL testing is the high precession measurements obtained though lab quality instrumentation. While instrumentation such as torque meters and gear type flow meters are suitable for stationary testing, they may not be appropriate for mobile applications.

5.6.1 Hardware-In-The-Loop Transmission Dynamometer

Figure 5.9 shows a comprehensive circuit diagram of the HIL test rig. In practice there are additional components and lines required compared to the idealized circuit given in Figure 5.1. Additional components include a high pressure relief valve, filters, an oil cooler, drain lines, and control pressure lines among others. Additionally the typically integrated charge pump was replaced with an external low pressure supply. For consistency the torque losses from this charge pump were estimated and taken into account when calculating fuel consumption. All of the principle hydraulic components on the HIL test rig are the same as were used in the neural network simulations and can be found in Table 5.1 and Figure 5.1.

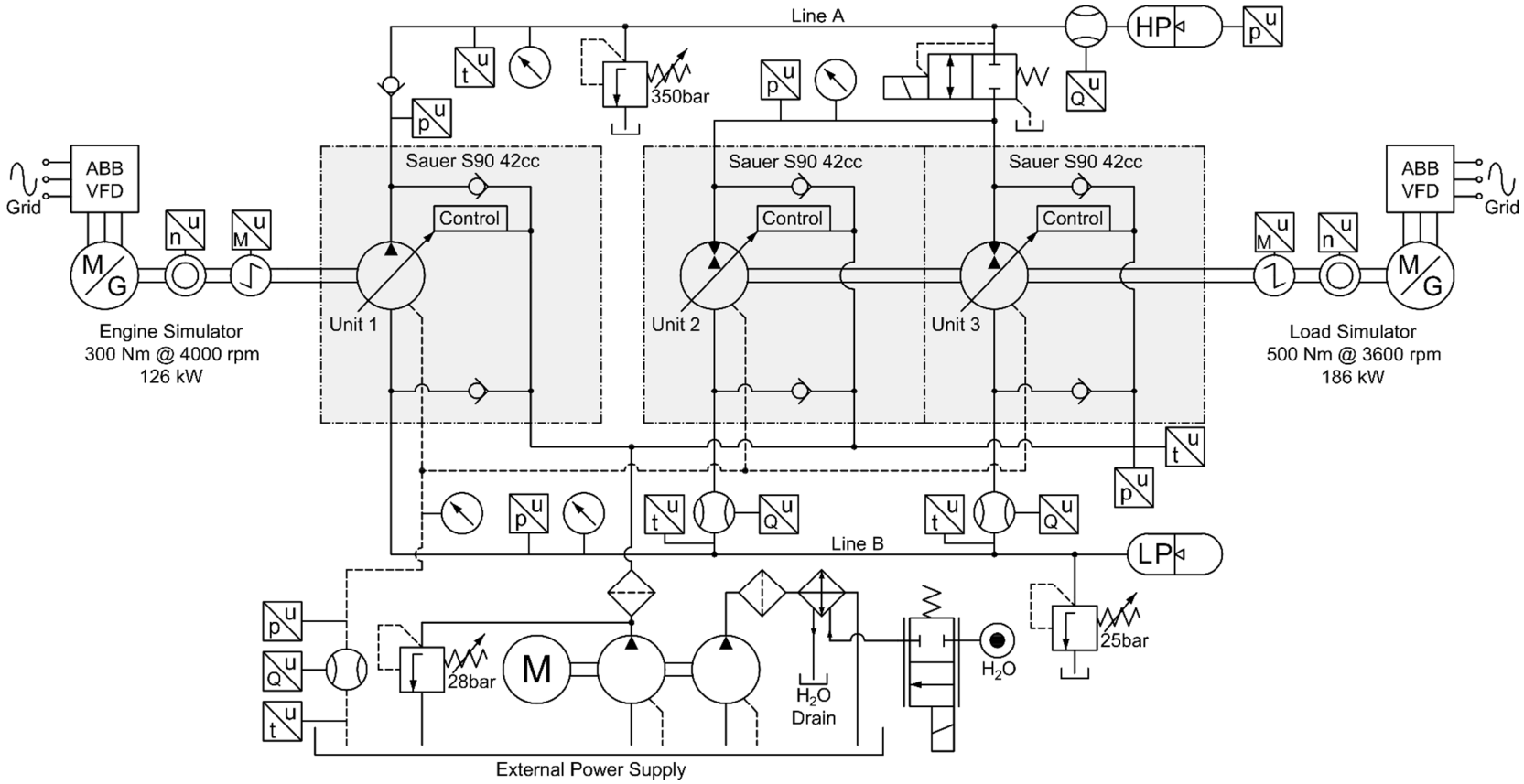

Figure 5.9: Hardware-in-the-loop hydraulic circuit

5.6.2 Measurement Results

Evaluation of the NN controller on the HIL transmission dynamometer was conducted in a manner similar to the simulation based evaluations. Again the NN controller and both constant pressure control strategies were used to control all three drive cycles. However additional consideration such as operating the transmission at a constant control pressure inlet line viscosity (i.e. temperature) was necessary to ensure valid comparisons between the various cycles and controllers. Fuel consumption for the HIL cycles was estimated using measured engine simulator speed and torque in conjunction with the same fuel consumption maps used in the simulation study. Table 5.6 summarizes the measurement results from the HIL transmission dynamometer.

Table 5.6: Hardware-in-the-loop test rig estimated fuel consumption rates [l/100 km]

		Drive cycle		
		Composite	JC08	SC03
Control strategy	200 bar	10.57	11.73	10.05
	275 bar	13.51	14.79	12.75
	NN	10.35	11.04	9.48

Measurement results demonstrate the feasibility and energy saving potential of the proposed neural network power management controller in near real world conditions. For the two untrained evaluation cycles the NN controller was able to improve fuel consumption rates on average by 5.75% and 25.51% for the 200 and 275 bar cases respectively (Table 5.7).

Table 5.7: Performance improvements of the neural network power management controller over constant pressure control strategies

		Drive cycle		
		Composite	JC08	SC03
Control strategy	200 bar	2.02	5.82	5.68
	275 bar	23.37	25.35	25.66

One point which must be addressed in the disparity between simulation and HIL fuel consumption rates. Several factors likely influenced these differences including a less aggressive engine speed controller on the HIL dynamometer which failed to optimize engine speed. A greater contributing factor was likely that the hydraulic units chosen for the HIL dynamometer exhibit exceedingly high leakages through the slippers at very low displacements and high pressures (a characteristic not fully captured by the empirical loss models used in simulation). This issue could be addressed by either formulating a component level controller which avoids low displacement operation, or exchanging the hydraulic units for units with better characteristics in this regime.

Another item which should be addressed is the relatively high fuel consumption rates compared to some modern vehicles. This is largely a function of an outdated fuel consumption map which fails to account for the substantial gains in efficiency seen in modern engines over the past decade. However this does not affect the NN controller's performance relative to the baseline power management strategies. Instead it is anticipated that if this approach were applied to a modern powertrain the fuel consumption rates would improve across the board.

Regardless of these shortcomings the implementable NN power management controller was demonstrated to substantially improve fuel consumption rates over baseline strategies in new and untrained cycles. Further the moderate improvements over the 200 bar case may be somewhat misleading as 200 bar is too low of a pressure for more aggressive driving events. Consequently improvements over the 275 bar case are likely to more accurately reflect an implemented control scheme.

Another benefit of the proposed power management strategy which has not been discussed in detail is the increase in engine management offered. Specifically the DP algorithm stored excess engine energy in the accumulator when it was beneficial and released it during periods of high demand. Because the NN's pressure prediction is based on the DP results it too incorporates some aspects of this form of engine management. In

addition to improving fuel efficiency, the NN power management approach may potentially result in greater overall powertrain performance. Unlike many power management controllers the NN approach attempts to predict when high power demand will be requested and then proactively increases pressure during these periods. Likewise the NN controller is potentially capable of reducing pressure during periods of low demand to ensure the lowest possible fuel consumption rate is obtained.

Neural networks also have the advantage of providing near optimal control while imposing a relatively low computational burden on the vehicle's controller. This is in contrast to certain instantaneous optimization approaches which suffer from comparatively high computational loads during use. One of the proposed approach's key demonstrated advantages is its ability to generalize optimal power management strategies from a training cycle and apply it effectively in novel environments. This is an essential aspect of any implementable power management controller which various control approaches have struggled with in the past. This advantage could further be improved with a more advanced version of the neural network controller in which periodically the network is partially retrained based on an optimization of recently measured cycles. Finally while this investigation focused on series hybrids the proposed NN approach is equally well suited for series hybrid power split transmissions as well as parallel hybrids with some modifications.

5.7 Chapter Summary

- Chapter 5 detailed the development of a neural network based power management controller for conventional hydraulic hybrid transmissions.
- An accumulator's current optimal pressure is heavy influence by prior and upcoming driving events (e.g. braking, hill climbing, coasting, accelerating, etc.). However if the optimal accumulator pressure is known, tracked, and combined with a minimum engine speed strategy then a hybrid vehicle can achieve near globally optimal fuel efficiency.

- A novel approach to power management was proposed in this work which aimed to generalize the optimal state trajectories obtained from dynamic programming through the use of a neural network. The neural network could then be used as part of an implementable power management strategy which predicted the optimal state trajectory for new and untrained cycles. In this way many of the benefits of dynamic programming could be applied to novel cycles without need for offline optimization through DP.

- An online power management controller was devised which used the trained neural network to predict the optimal accumulator pressure for new and untrained cycles. This estimated optimal accumulator pressure could then be tracked and combined with a minimum engine speed strategy. In simulation two evaluation cycle were controlled using the proposed NN power management control strategy along with baseline 200 and 275 bar constant pressure control strategies. In simulation the NN power management controller achieved average fuel consumption rates within 6.69% of the globally optimal value for the two evaluation cycles. Further over these same cycles the NN controller was able to improve average fuel consumption rates by 3.08% and 22.43% for the 200 and 275 bar baseline control strategies respectively.

- A HIL test rig was constructed to experimentally validate the neural network based controller. Measurement results showed the NN power management controller was able to improve average fuel consumption rates on the untrained evaluation cycles by 5.75% and 25.51% for the 200 and 275 bar baseline control strategies respectively.

- Select benefits of the proposed neural network based controller include the ability to generalize globally optimal controls and apply them to untrained cycles, potentially predict future driving events based on a history of past events, and operate at low computational expense once trained. Further this approach can be applied to multiple hydraulic hybrid architectures such as parallel hybrids, series hybrids, and series hybrid power split transmissions.

CHAPTER 6. NOVEL BLENDED HYDRAULIC HYBRID TRANSMISSION

In the previous chapter a neural network based power management controller was presented for a series hybrid. While effective, the improvements gained through the advanced power management controller were fundamentally limited by the base architecture employed. In order to further improve fuel efficiency more advanced system architectures are required. To address the shortcomings of conventional hydraulic hybrids a novel transmission architecture termed a Blended Hydraulic Hybrid is proposed and investigated within this work.

This chapter begins by exploring the deficiencies of conventional series hybrids followed by an introduction and examination of the blended hybrid concept. Next the optimally controlled energetic analysis conducted in Chapter 4 is extended to the blended hybrid transmissions. Following this, a steady state optimization of a series hybrid, blended hybrid, and blended hybrid PST offers further insight into optimal powertrain operation. Two system level control schemes focusing on drivability are then proposed for the blended hybrid. Next two implementable power management control schemes are proposed for the blended hybrid architecture. This chapter concludes with an exploration of the blended hybrid concept using a hardware-in-the-loop transmission dynamometer.

6.1 Novel Blended Hydraulic Hybrid Transmission

Conventional series hydraulic hybrid transmissions have several fundamental drawbacks, first the hydraulic units must always operate at the high pressure accumulator's current pressure. This often results in inefficient operation of the units at high pressures and low displacements. Another possible drawback of series hybrids is the potential for a "spongy" feel which becomes more pronounced as vehicle, and consequently accumulator size,

increases. This spongy feel originates in the relationship between maximum wheel torque and current system pressure. In order to increase system pressure more flow must enter the high pressure line than exits. In series hybrids a delay on the order of seconds may be experienced in responding to the driver's demanded wheel torque when system pressure is below that required potentially resulting in a spongy or sluggish feel. This inherent delay in increasing system pressure is in contrast to hydrostatic transmissions which increase pressure virtually instantaneously, a feature which forms the basis of the blended hybrid architecture presented below. Series hybrids also require over center units connected to the axle/wheels in order to recover energy while braking. This limits the units which are compatible especially if off the shelf bent axis units are desired

To address the aforementioned issues a novel blended hydraulic hybrid transmission was proposed by the author (first published in Sprengel and Ivantysynova, 2012b). It is so named for the blending of a hydrostatic transmission, a parallel hybrid, and a uniquely connected high pressure accumulator. A series of active and passively controlled logic elements enable the HP accumulator to be selectively connected and disconnected from various sections of the transmission. Disconnecting the HP accumulator reduces losses by allowing the units to operate efficiently at pressures below the accumulator's current pressure. In contrast the units in a conventional series hybrid often operate less efficiently at higher pressures and lower displacements. Selectively disconnecting the HP accumulator also permits a higher accumulator precharge with little detriment to system efficiency. Increasing precharge, and by association minimum accumulator pressure, ensures a greater degree of regenerative braking torque is always available further improving energy recovery. Additionally operating the blended hybrid as a HST increases system stiffness (i.e. driver response) over a series hybrid enabling rapid increases in transmission torque. Finally the uniquely connected HP accumulator removes the need for over center units connected to the axle/wheels.

6.1.1 Blended Hybrid Architecture

A schematic of the proposed blended hybrid architecture can be found in Figure 6.1. The blended hybrid is in essence a hydrostatic transmission with an additional unit attached to the transmission's output shaft. A series of check valves connect this third unit to either Unit 1, thereby increasing the hydrostatic transmission's displacement, or to a high pressure accumulator which allows for secondary control of the unit. An additional check valve connects Line B to the high pressure accumulator while braking permitting energy recovery without the need for over center units.

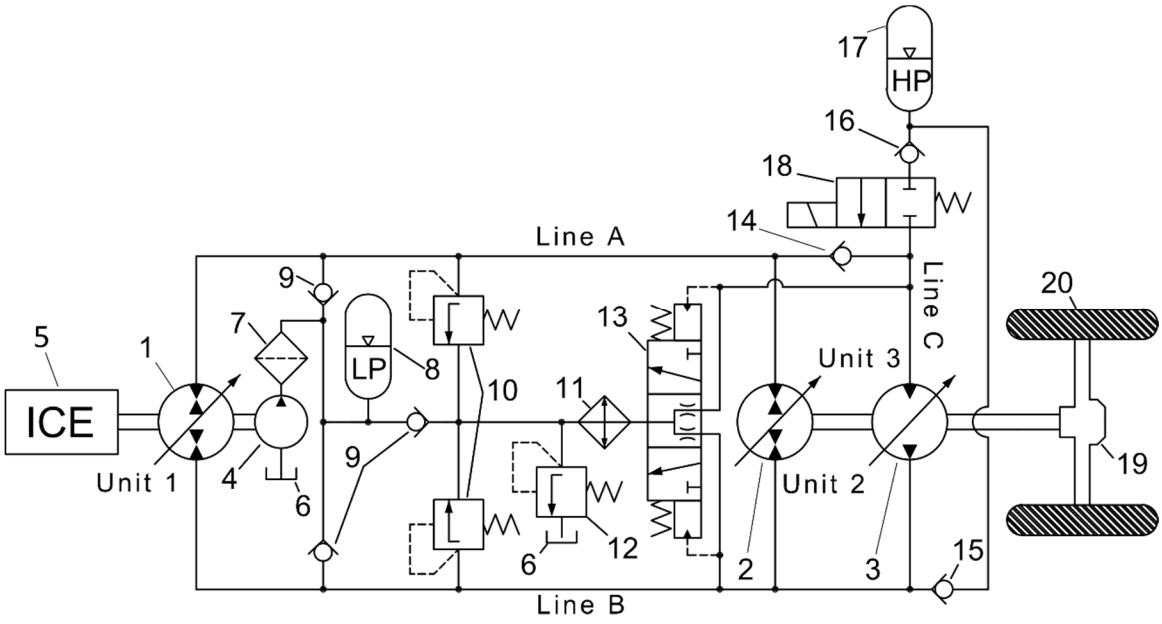

1	hydraulic unit 1	2	hydraulic unit 2	3	hydraulic unit 3
4	charge pump	5	engine	6	reservoir
7	filter	8	LP accumulator	9	LP check valve
10	HP relief valve	11	oil cooler	12	LP relief valve
13	flushing valve	14	check valve	15	check valve
16	check valve	17	HP accumulator	18	enabling valve
19	axle	20	wheels		

Figure 6.1 Blended hydraulic hybrid circuit

The low pressure system accomplishes several tasks in addition to the standard replenishing and flushing functions. While braking (i.e. charging the HP accumulator (17)) the charge pump (4) and LP accumulator (8) supply flow to Units 2 and 3 through check

valve (9). When Unit 3 consumes flow from the HP accumulator, flushing valve (13) shifts so that Line B is connected to the low pressure system. Excess flow from the HP accumulator is now cooled with oil cooler (11) before exiting through LP relief valve (12) or recharging the LP accumulator through check valve (9) if required.

The blended hybrid operates in several distinct modes:

Hydrostatic Driving: The engine (5) provides power to Unit 1 which supplies flow to Line A. With the enabling valve closed, check valve (14) opens and connects Line A to Line C. Both Units 2 and 3 use this flow to rotate at a speed determined by a combination of their displacement. In effect both units operate as a single motor.

Blended Driving: With the enabling valve open, Line C is exposed to the HP accumulator's pressure. As long as the pressure in Line C is higher than Line A, check valve (14) remains closed. Unit 3 is then able to use power from the accumulator to supply torque to the wheels. Power is also supplied by the engine with Unit 1 providing flow to Unit 2 forming a hydrostatic transmission. Pressure in Line A is a function of Unit 2's displacement and the resistive load on the wheels minus the torque contribution from Unit 3. If pressure in Line A exceeds that of the high pressure accumulator, check valve (14) opens and check valve (16) closes causing Units 1, 2, and 3 to operate as a hydrostatic transmission.

Hybrid Driving: With Units 1 and 2 at zero displacement all of the power required for driving comes from the HP accumulator. With the enabling valve open, Unit 3 is exposed to the HP accumulator's pressure. Unit 3 then supplies the required torque to the wheels using power from the HP accumulator.

Braking: While braking Unit 1 moves to zero displacement and the enabling valve is closed. The high pressure then automatically switches from Lines A and C to Line B (a feature inherent in hydrostatic transmissions). When the pressure in Line B exceeds that of the HP accumulator, check valve (15) opens allowing flow from Units 2 and 3 into the HP accumulator. In this manner energy recovered during regenerative braking is stored for later use.

Reverse Operation: To reverse Unit 1 moves over center and supplies flow to Line B. Unit 2 then uses this flow to drive the wheels. If Unit 2 requires a pressure in Line B higher than that of the high pressure accumulator, check valve (15) opens and flow from Unit 1 is used to charge the accumulator until a suitable pressure for Unit 2 is achieved. When braking in reverse high pressure switches to Line A and can be used to power patristic loads on the engine or pass through relief valve (10). Alternatively Units 2 and 3 can move over center rendering all reverse functionality identical to forward operation. While this alternative strategy requires over center units, the possibility for full power reverse and regenerative braking may be well suited for certain applications.

6.1.2 Blended Hybrid Power Split Transmission

The blended hybrid concept can be further expanded on by replacing the hydraulic path of a power split transmission with the blended hybrid architecture (Figure 6.2).

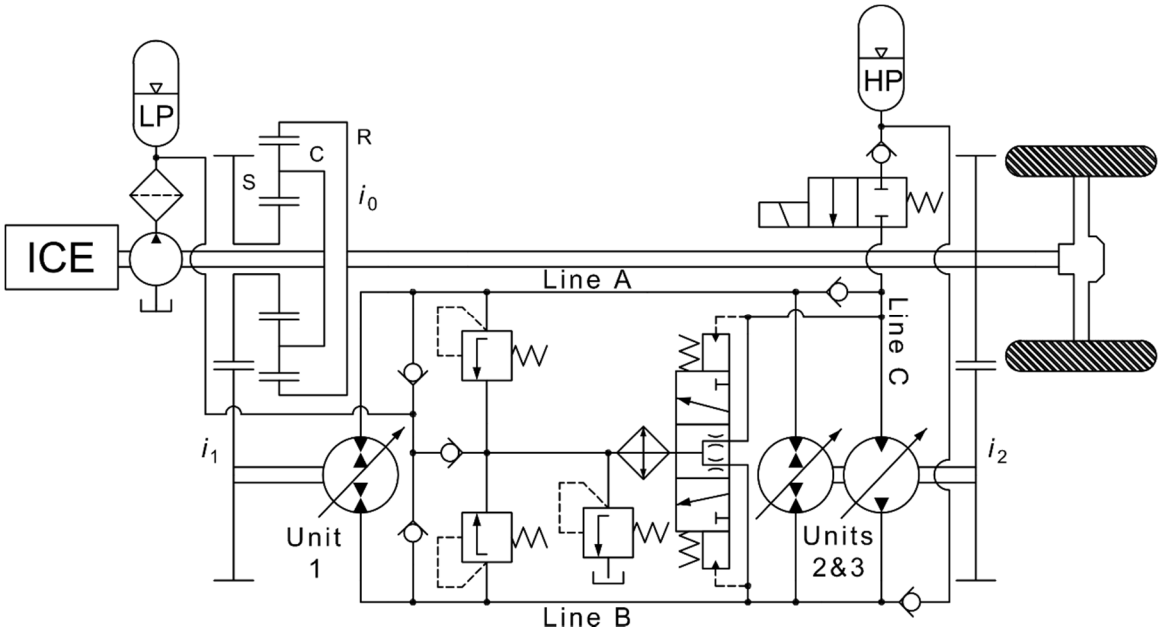

Figure 6.2 Blended hydraulic hybrid power split transmission circuit

This novel blended hybrid PST combines the efficient operation of a conventional series hybrid PST with the improved efficiency and performance of the blended hybrid architecture. As the blended hybrid PST's circuit operation is similar to that of a standard

blended hybrid it will not be detailed here. However an in depth investigation into the performance and fuel efficiency of a blended hybrid PST is conducted later on in this chapter.

6.2 System Analysis and Energetic Comparison

The energetic analysis present in Chapter 4 was extended to a blended hybrid and a blended hybrid PST in order to gain a better understanding of how these concepts compare with conventional architectures. To ensure a fair comparison both the blended hybrid, and blended hybrid PST, were simulated using the same component sizes as their respective series hybrid, or series hybrid PST, transmission architectures (described in Section 4.1). This enabled any variance in fuel efficiency to be attributed solely to differences in system architecture.

The following state space represents both the blended hybrid, and blended hybrid power split transmissions:

$$x \equiv \begin{bmatrix} \omega_{CE} & \omega_{wheel} & p_A & p_B & p_C & p_{HP} & p_{LP} \end{bmatrix}^T \quad u \equiv \begin{bmatrix} u_{CE} & \beta_1 & \beta_2 & \beta_3 & u_{enab} \end{bmatrix}^T \tag{6.1}$$

Where $p_{A,}$ p_B, and p_C are the pressures in Lines A, B, and C respectively.

Several simplifications were made to the blended hybrid transmissions in order to be compatible with the DP algorithm. These simplifications were required due to the stiff nature of HSTs and the presence of hydraulic logic elements (i.e. check valves). Sequential control was used for both transmission configurations. That is Unit 2 and 3's displacements were only decreased after Unit 1 reached its maximum displacement (Figure 2.13). By using sequential control the displacements of all three units became a function of the engine and wheel speeds (along with volumetric losses). Due to the HST's stiff nature the pressure build up equations in the lines were neglected. Instead it was assumed that pressure in the lines built up instantaneously in response to the applied load. With unit displacements set by sequential control, the line pressures were set as a

function of the required wheel torque. Both unit displacements and line pressures were set in regards to empirically derived volumetric and torque loss models.

The reduced state space representation for both blended hybrid transmissions is given by:

$$x \equiv \begin{bmatrix} \omega_{CE} & p_{HP} \end{bmatrix}^T \qquad u \equiv \begin{bmatrix} \omega_{CE\ des} & \beta_3 \end{bmatrix}^T \tag{6.2}$$

Where the line pressures and unit displacements were removed as they were defined by the cycle. β_3 remains and was used to specify Unit 3's displacement during blended and hybrid operation. u_{enab} was removed in interest of computational efficiency, instead a value of β_3 greater than zero was used to open the enabling valve. As with the series hybrid transmissions, β_2 and β_3 were adjusted together while braking to provide the required resistive torque.

The state and control vectors for the blended hybrid were discretized as follows for the DP analysis:

$$x \equiv \begin{bmatrix} \omega_{CE} \\ p_{HP} \end{bmatrix} \begin{bmatrix} 750-4000\ \text{rpm} \\ 145-370\ \text{bar} \end{bmatrix} \begin{bmatrix} 750{:}25{:}1000,\ 1050{:}50{:}1500,\ 1600{:}100{:}4000 \\ 145:5:370 \end{bmatrix}$$
$$u \equiv \begin{bmatrix} \omega_{CE\ des} \\ \beta_1 \end{bmatrix} \begin{bmatrix} 750-4000\ \text{rpm} \\ 0-100\ \% \end{bmatrix} \begin{bmatrix} 750{:}25{:}1000,\ 1050{:}50{:}1500,\ 1600{:}100{:}4000 \\ 0:10:100 \end{bmatrix}$$

(6.3)

The state and control vectors for the blended hybrid PST were discretized as follows for the DP analysis:

$$x \equiv \begin{bmatrix} \omega_{CE} \\ p_{HP} \end{bmatrix} \begin{bmatrix} 750-4000\ \text{rpm} \\ 180-370\ \text{bar} \end{bmatrix} \begin{bmatrix} 750{:}25{:}1000,\ 1050{:}50{:}1500,\ 1600{:}100{:}4000 \\ 180:5:370 \end{bmatrix}$$
$$u \equiv \begin{bmatrix} \omega_{CE\ des} \\ \beta_1 \end{bmatrix} \begin{bmatrix} 750-4000\ \text{rpm} \\ 0-100\ \% \end{bmatrix} \begin{bmatrix} 750{:}25{:}1000,\ 1050{:}50{:}1500,\ 1600{:}100{:}4000 \\ 0:10:100 \end{bmatrix}$$

(6.4)

6.2.1 Dynamic Programming Energetic Comparison Results

Blended Hybrid Transmission

During the UDDS cycle the blended hybrid transmission obtained a fuel consumption rate of 8.02 l/100 km while requiring 10.58 MJ of energy from the engine. Figure 6.3 shows a plot of select transmission parameters for the blended hybrid. Here the pressure plot illustrates key differences between the series and blended hybrids. First this plot shows the blended hybrid operating at pressures below the HP accumulator's pressure. Lower pressures and higher displacements reduce losses, a fact demonstrated quantitatively by the blended hybrid requiring 6.21% less energy from the engine than the series hybrid over the same cycle. This same plot shows another benefit of blended hybrids in that they can operate above the accumulator's current pressure. With maximum transmission pressure no longer dictated by the HP accumulator, the blended hybrid is capable of rapidly providing maximum transmission torque. In contrast series hybrids must charge their HP accumulator to reach maximum pressure which may result in a significant delay when responding to the driver's requested torque. This figure also highlights one advantage of series hybrids over blended hybrids. Namely series hybrids, unlike blended hybrids, are capable of storing energy from the engine in the accumulator thereby operating the powertrain in a more efficient manner. From inspection the HP accumulator pressure in the series hybrid (Figure 4.12) generally operated over a wider range of pressures than the blended hybrid. As both hybrid transmissions used the same size components, and assuming all braking energy was recovered, the only way for the series hybrid to operate over a wider range of pressures was for the HP accumulator to store additional energy from the engine. Figure 6.3 also shows a plot of the blended hybrid's engine operation over the UDDS cycle. As with the series hybrid, the blended hybrid tended to run at a minimum engine speed except when operating in more efficient regions of the engine map.

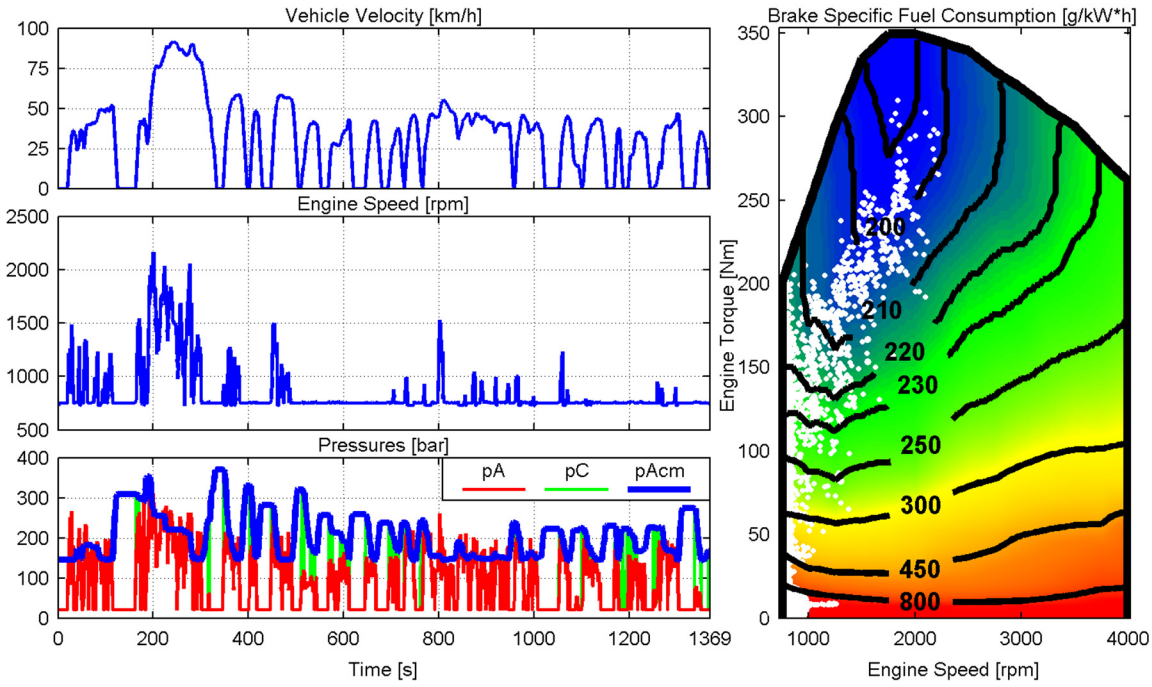

Figure 6.3 Blended hybrid dynamic programming results

Blended Hybrid Power Split Transmission

Over the UDDS cycle the blended hybrid PST obtained a fuel consumption rate of 7.68 l/100 km while consuming 9.28 MJ of energy from the engine. Dynamic programming results for the blended hybrid PST are similar to those seen in the three other hybrid transmissions. Specifically the blended hybrid PST followed a similar minimum engine speed strategy where the transmission was often in a power recirculating mode. Likewise the pressure profile followed a similar trend to the standard blended hybrid although once again with a slightly higher magnitude due to difference in minimum system pressure. However similarities in the pressure profiles between both blended hybrid architectures were to be expected as charging the accumulator only occurs during braking.

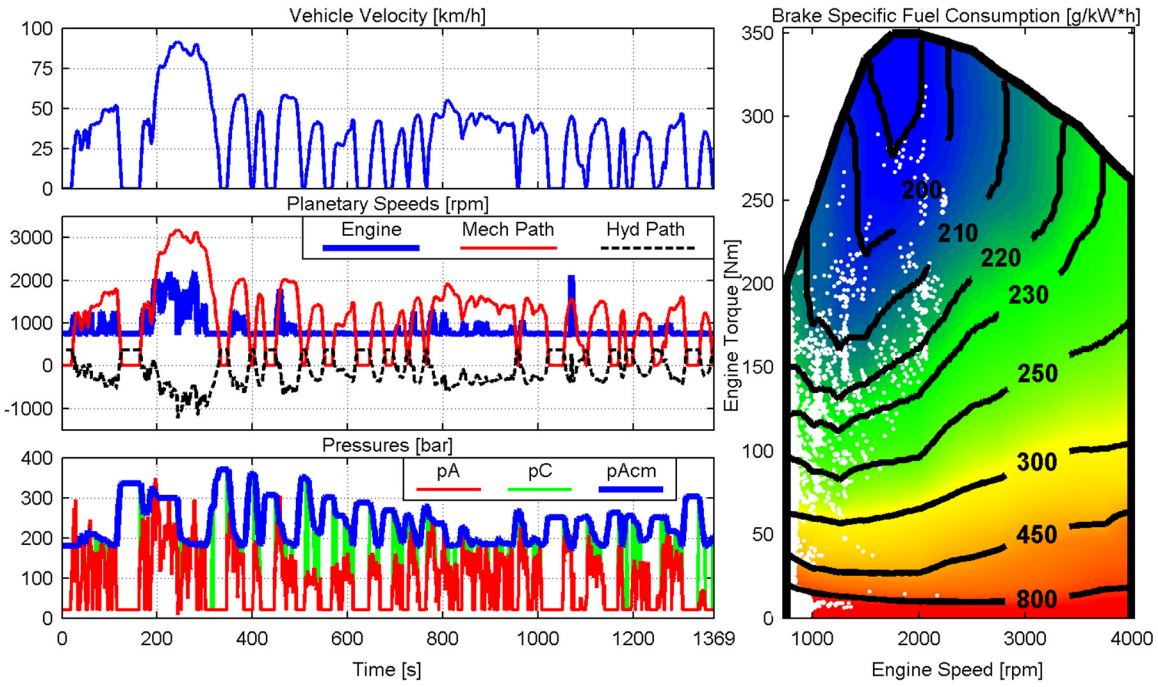

Figure 6.4 Blended hybrid PST dynamic programming results

6.2.2 Summary of Dynamic Programming Results

A summary of fuel consumption rates and transmission energy consumption for all six transmission architectures is included in Table 6.1. Optimally controlled over the UDDS cycle the blended hybrid transmission yielded a 10.99% decrease in the fuel consumption rate over a baseline automatic transmission and a 29.46% decrease over an automatic transmission without a lock-up clutch while consuming 6.21% less energy than a conventional series hybrid transmission. The blended hybrid PST achieved a fuel consumption rate 14.76% less than the automatic transmission while consuming 12.04% less energy than the series hybrid PST.

Table 6.1 Summary of fuel economy and energy consumption

	Fuel Consumption Rate [l/100 km]	Engine Energy Generation (transmission consumption) [MJ]
Automatic	9.01	11.14
Automatic (no lockup clutch)	11.37	13.37
Manual* (acceleration)	10.19	9.89
Manual* (cruise)	9.06	9.69
Manual	8.12	9.38
Series Hybrid	8.09	11.28
Blended Hybrid	8.02	10.58
Series Hybrid PST	7.77	10.55
Blended Hybrid PST	7.68	9.28

*suboptimally controlled using predefined shifting schedule

6.3 System Control

Determining how to control the novel blended hybrid transmission is just as important as understanding the architecture itself. Section 6.3 begins with steady state optimal control of the blended hybrid which provides further insight into how best to operate the transmission from an efficiency perspective. Next two implementable system level control strategies are detailed which focus on converting driver inputs into powertrains commands. Finally two implementable power management strategies are investigated which focus on maximizing a vehicle's fuel efficiency. It should be noted that while the implementable control schemes discussed in this section focus on the blended hybrid, they are equally well suited for the blended hybrid PST with only minor changes to the equations.

6.3.1 Steady State Optimal Control

Determining the fuel efficiency of hybrid transmissions is difficult in large part due to the presence of two power sources. How power is managed between these two sources (and

additionally how all of the other transmission components are controlled) has a large influence on overall fuel efficiency but is intricately linked to the vehicle's past, present, and future driving demands. This dependency of fuel efficiency on a specific drive cycle can obscure some aspects of transmission performance such as instantaneous efficiency. It is important to note that instantaneous transmission efficiency is not directly proportional to fuel efficiency. For example a manual transmission may have higher instantaneous transmission efficiency than a series hybrid but overall fuel efficiency falls short due to a lack of engine management along with the inability to recover braking energy. Instantaneously optimal control provides valuable insight into the steady state performance of a transmission (as presented in Dorey and Vaughan, 1984).

To gain a deeper understanding of the blended hybrid architectures, an instantaneous optimization was performed on the series, blended, and blended hybrid PST studied in Sections 4.6 and 6.2. As vehicle propulsion is the primary function of any transmission it is most useful to analyze a powertrain's performance and operation in terms of tractive torque and vehicle velocity. The instantaneous optimization was conducted by first finely discretizing a mesh of tractive torque vs. velocity (e.g. discretized to 25 Nm and 1 km/h). At each discrete combination of tractive torque and velocity the powertrain's efficiency was optimized under steady state conditions (i.e. no power was allowed to flow into or out of an accumulator). For each of these combinations the full range of permissible engine speeds and system pressures were discretized using a fine mesh (e.g. discretized to 10 rpm and 2.5 bar). At each combination of engine speed and system pressure Units 2 and 3 were controlled to provide the required tractive torque (using a 50/50 torque split) at the specified vehicle velocity and system pressure. Unit 1 was then controlled at the specified engine speed and system pressure to provide the flow consumed by Units 2 and 3. Any combination of the aforementioned controls which failed to provide the required tractive torque, or violated any other system constraint, were considered infeasible and eliminated. This process was repeated for every combination of engine speed and system pressure for a given combination of vehicle velocity and tractive torque.

Throughout each optimization the transmission's efficiency was calculated (power out of Units 2 and 3 divided by power into Unit 1) and used to determine the most efficient combination of engine speed, system pressure, and unit displacements which were then recorded. This process was then repeated for every combination of vehicle velocity and tractive torque. A flowchart of this optimization process is located in Figure 6.5.

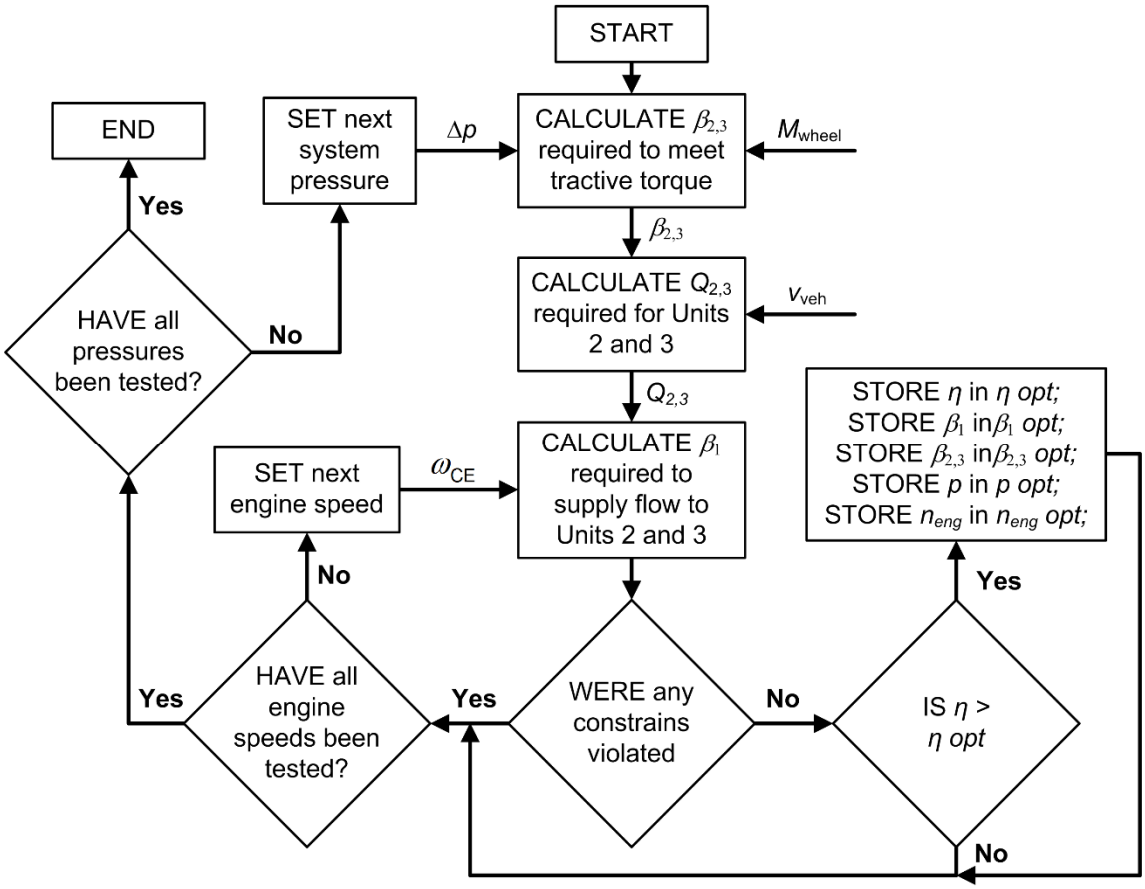

Figure 6.5: Steady state optimization flowchart

The system performance and controls shown below are those which met all optimization constraints while simultaneously maximizing transmission efficiency. Differences in operation between a blended hybrid and series hybrid can be seen by examining differences in their respective steady state optimal pressures (Figure 6.6).

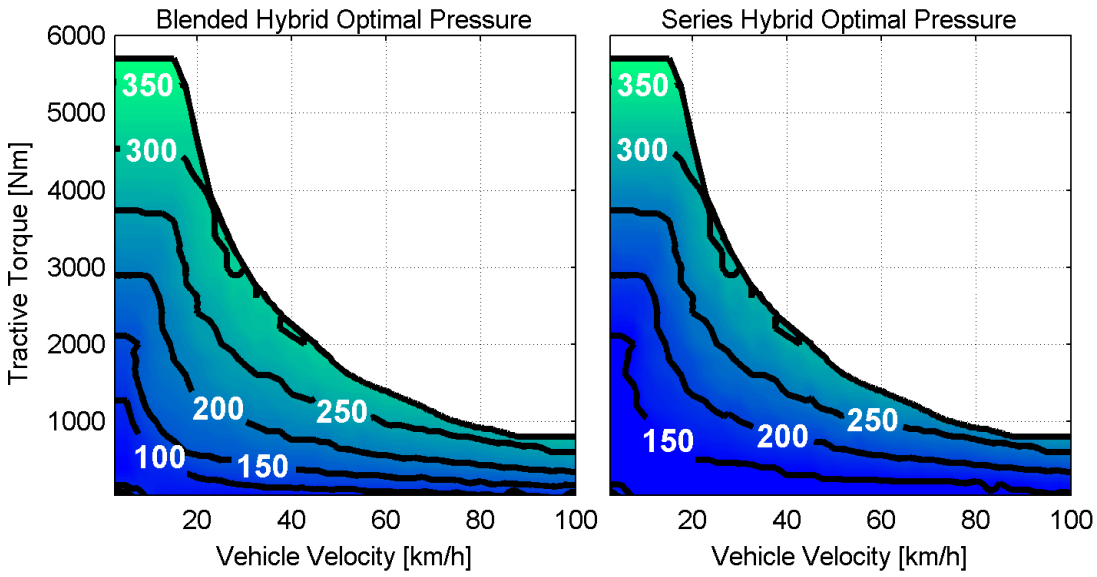

Figure 6.6 Steady state optimal pressure

In terms of efficiency one of the major benefits of blended hybrids over series hybrids is their ability to operate at pressures independent and below that of the high pressure accumulator. The minimum accumulator pressure for the series hybrid used in this investigation was 145 bar. From Figure 6.6 is can be seen that during certain operations optimal efficiency for the blended hybrid is obtained by operating at pressures below 145 bar. While this difference is most apparent at relatively low tractive torques, it is an important mode of operation which often occurs while vehicles are cruising (i.e. not accelerating). Examination of these and subsequent steady state optimizations yields a deeper understanding of transmission operation. The parabolic curve seen in these figures is a result of power limitations imposed by the engine. Only below ~15 km/h where the maximum tractive torque curves is flat was the transmission the power limiting factor. In general hydraulic units have a relatively high corner power, that is the power which they are capable of generating at maximum pressure, speed, and displacement. Units 2 and 3 used for this investigation were 120 cc/rev units with a rated top speed at full displacement of 2800 rpm and 450 bar differential pressure. Together these two units had a corner power of 500 kW, in contrast the engine had a maximum power output of only 110 kW. This fact, coupled with Figure 6.6 which shows high pressure is only optimal

where the transmission was power limited, results in the conclusion that an optimal transmission configuration would possess multiple hydraulic units connected to the wheels. In this configuration one of these units would only be used for low speed driving where additional torque is needed and then would be isolated from the high pressure source to reduce losses when not require.

Figure 6.7 shows the steady state optimal Unit 2 and 3 displacements for both the blended and series hybrids.

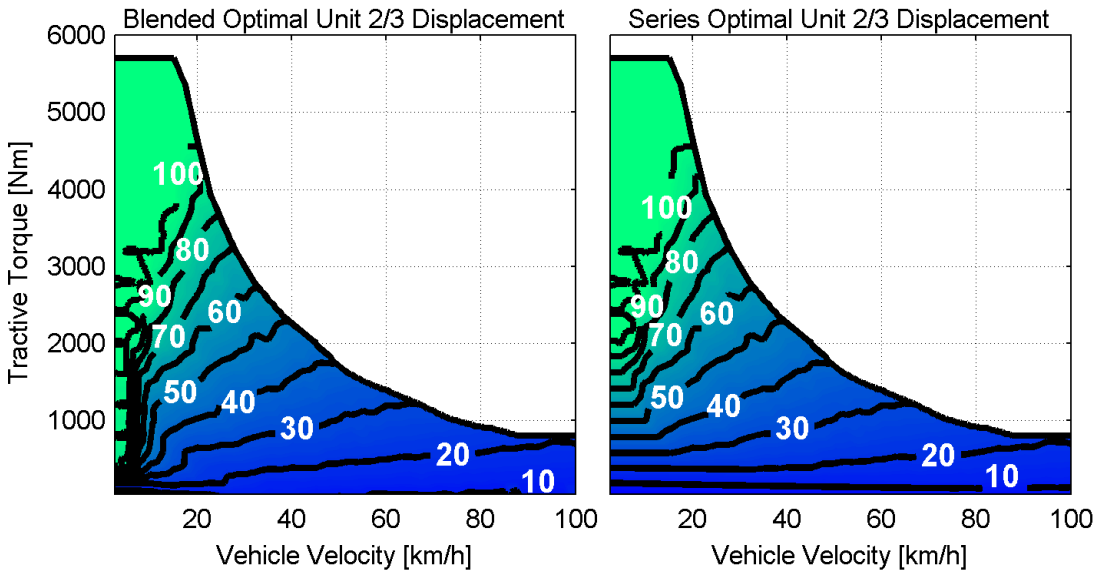

Figure 6.7 Steady state optimal Unit 2 and 3 displacement

Apparent from inspection is the intuitive general trend which reduces Unit 2 and 3's displacement as the required tractive torque decreases. Less intuitive though is the trend to reduce displacement as vehicle speed increases for a specific tractive torque. As tractive torque is a function of pressure and displacement any decrease in displacement must be met with a proportional increase in pressure as seen in Figure 6.6. Also of interest is the observation that above ~20 km/h the required tractive torque is met with combinations of pressures and Unit 2 and 3's displacements which fall between their respective minimum and maximum values. This indicates there is an optimal combination of these two parameters with respect to transmission efficiency. Not only are there cases

where increasing displacement and reducing pressures yield higher efficiency as may be expected, there are also cases where efficiency may be improved by increasing pressure and reducing Unit 2 and 3's displacements. This effect can be seen within these plots at any point where pressure is above its minimum value and unit displacements are below their maximum value. While potentially counterintuitive, it should be remember that this steady state optimization took into account the efficiency of the entire transmission, not just the efficiency of Units 2 and 3 which may be negatively influence by this operation. Complex interactions exist between all of the components within a transmission where decreasing the operating efficiency of a given component may further increases the efficiency of another component to a point where the overall transmission efficiency is improved.

Steady state optimal Unit 1 displacement and engine speed can be found in Figure 6.8 and Figure 6.9 respectively.

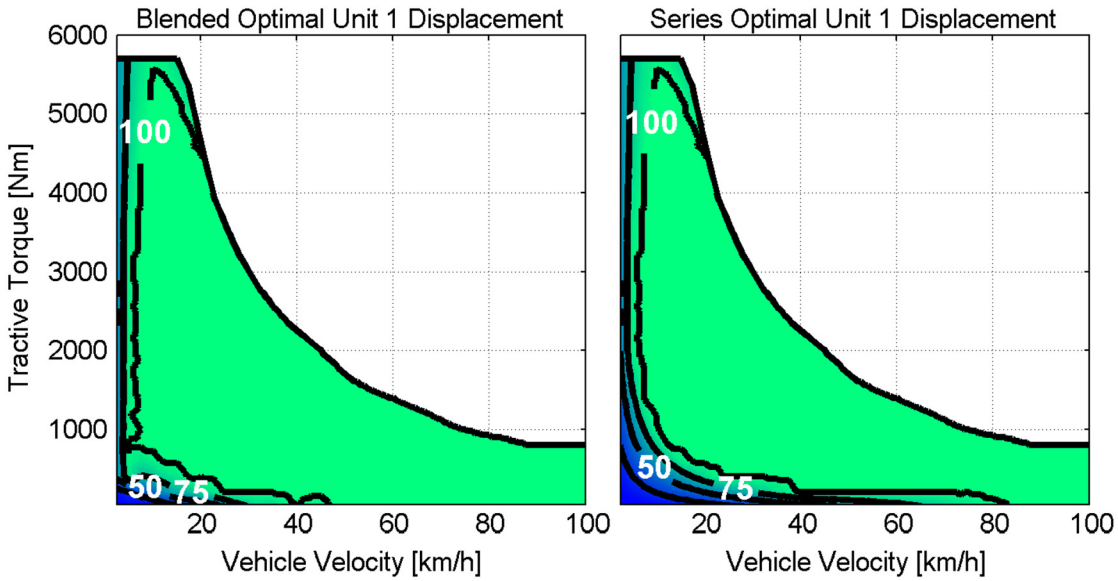

Figure 6.8 Steady state optimal Unit 1 displacement

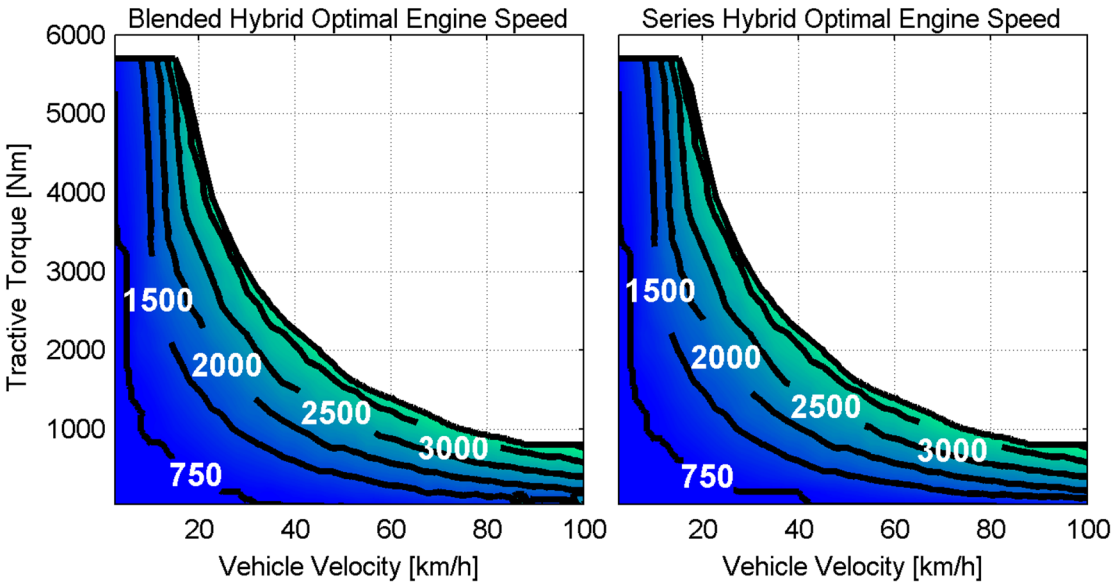

Figure 6.9 Steady state optimal engine speed

Both Unit 1 displacement and engine speed are closely linked. It is generally optimal to increase Unit 1's displacement to maximum as soon as possible and then increase engine speed as more flow is required. This control methodology, often referred to as a minimum engine speed strategy, is commonly cited as an effective means of increasing instantaneous transmission efficiency. While this steady state optimization was conducted in regards to maximizing transmission efficiency, when an engine's fuel efficiency is taken into consideration there is an even stronger tendency to minimize engine speed. Going back to the prior optimal pressure and Unit 2 and 3 displacements, had a lower pressure and higher displacements been commanded for a specific operation then a higher engine speed would have been necessary to meet the flow requirement. This point helps to illustrate the complexities present in determining the optimal set of transmission controls to meet the driver's demand. Also of interest is that that transmission's maximum power curve occurs at an engine speed a little over 3000 rpm whereas maximum engine power occurs at 4000 rpm. This means maximum transmission output power (which is limited by the engine) occurs somewhat below the engine's maximum power point. A closer examination revels that a little after 3000 rpm the transmission's losses increase faster than engine power increases. It must be noted that

these results are for a specific combination of engine and transmission and may not hold true for all combinations. Though it does illustrate the point that for maximum performance a transmission's operating parameters must be carefully selected.

Insight into the differences in efficiency between the blended and series hybrid architectures can be obtained by comparing their efficiency under different operating conditions. To provide a more realistic comparison the series hybrid was operated at four discrete pressures (145, 220, 295, and 370 bar) while the blended hybrid was allowed to optimize its operating pressure. This more accurately replicates real world performance as series hybrids are often forced to operate at higher than optimal pressures, a condition which frequently occurs as driver demand changes as well as following a braking event. Conversely during hydrostatic driving blended hybrids are capable of operating at an optimal pressure independent of the pressure in the HP accumulator.

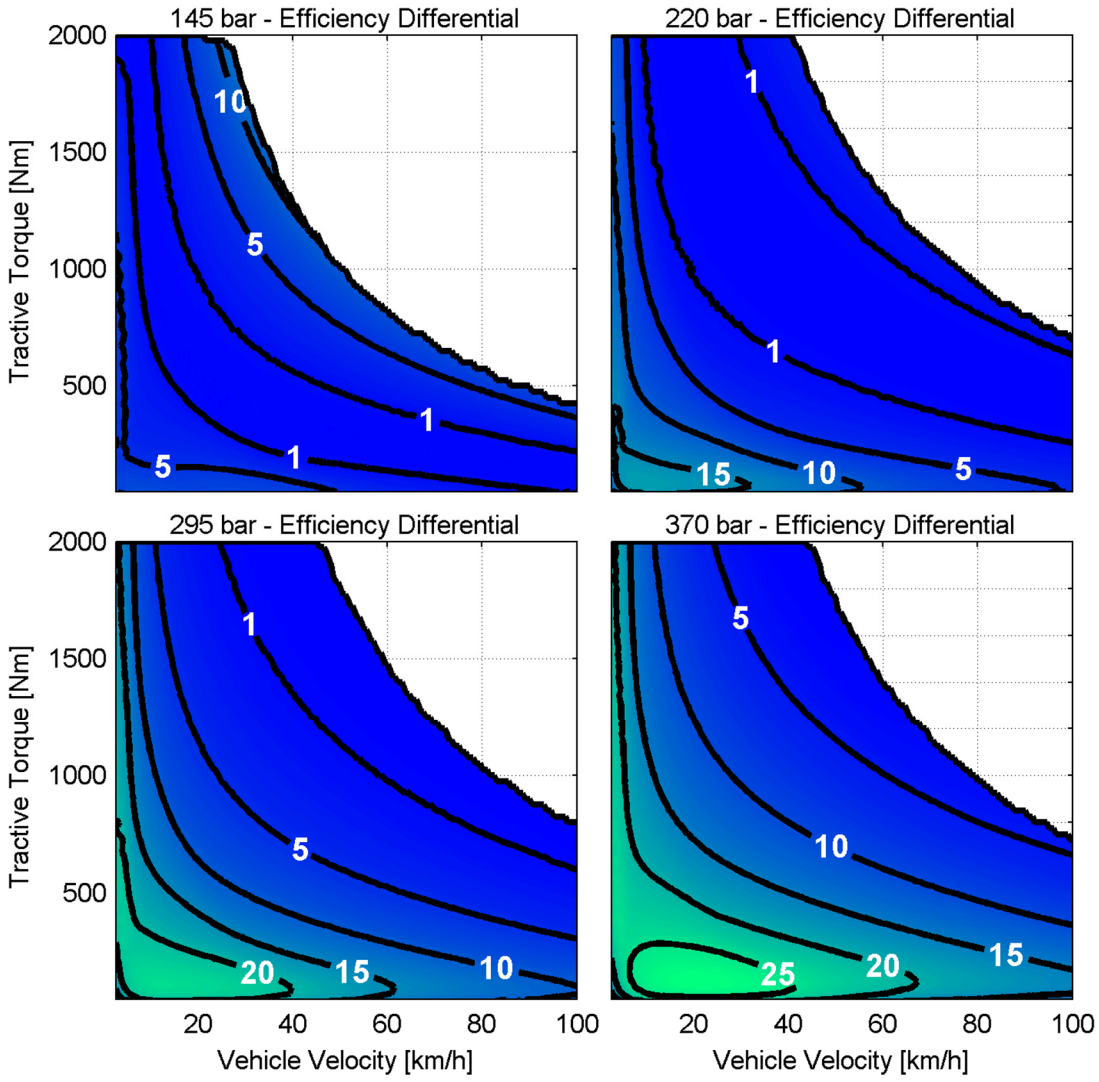

Figure 6.10 Steady state optimal differential efficiency

The plots in Figure 6.10 show the increased efficiency of the blended hybrid over the series hybrid in terms of percentage points (e.g. increasing transmission efficiency from 50% to 75% would show up as 25% on these plots). When operating at the minimum accumulator pressure (145 bar) the series hybrid only lags behind the blended hybrid by a few percentage points. However as accumulator pressure increases so too does the efficiency differential between the blended and series hybrids. Once the series hybrid's accumulator is full, as is possible following a braking event, the percentage point differential efficiency exceeds 25% for some operating conditions.

Similar insight can be gained by examining steady state optimal characteristics of a blended hybrid power split transmission. Previous steady state optimizations for the blended and series hybrids were conducted with respect to maximizing transmission efficiency, ultimately though minimizing engine fuel consumption is the primary goal. The following example highlights a case where operating a transmission in the most efficient manner is not optimal for the powertrain. In this example a blended hybrid PST was controlled to provide a constant output torque at a specific vehicle speed while engine speed was varied (Figure 6.11).

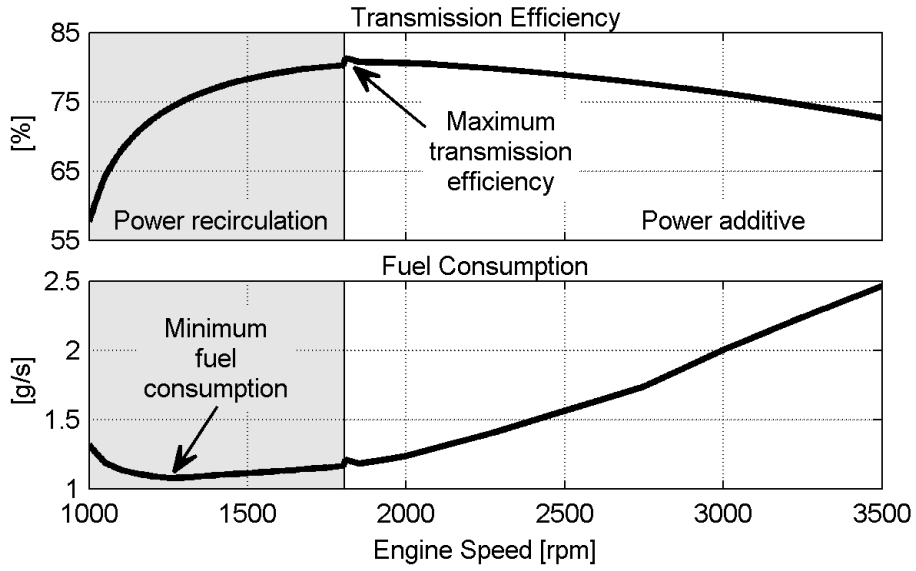

Figure 6.11 Blended hybrid PST engine sweep

Transmission efficiency is shown on the top section of this plot with peak transmission efficiency occurring at the full mechanical point. At engine speeds above the full mechanical point efficiency drops off as a greater percentage of power flows through the power additive mode. Likewise at engine speeds below the full mechanical point transmission efficiency drops off rapidly as more power is recirculated through a mode known to be less efficient. However when fuel consumption is examined on the same plot it becomes apparent that powertrain fuel consumption is best minimized by operating the transmission in the less efficient power recirculation mode.

A steady state optimization was performed on a blended hybrid PST with the objective function minimizing fuel consumption. Figure 6.12 shows steady state optimal transmission efficiency and performance. Note how the transmission's efficiency remains relatively constant as vehicle speed increases, this is a direct result of the PST's efficient mechanical path. Trends in optimal pressure also vary between the previous blended hybrid and the new blended hybrid PST. In the blended hybrid PST optimal system pressure generally decreases as a function of transmission power rather than as a function of tractive torque as is the case with the blended hybrid.

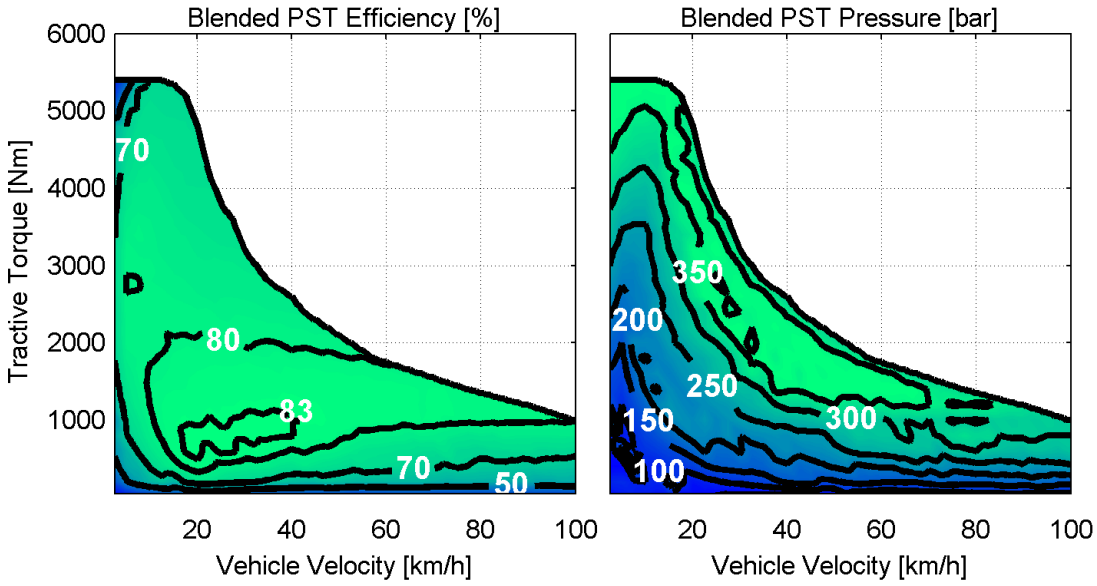

Figure 6.12 Steady state optimal operation

Figure 6.13 shows plots of steady state optimal engine and Unit 1 speeds. Here zero Unit 1 speed denotes the full mechanical point while a negative speed indicates power recirculation. In general vehicle speeds above 20 km/h and tractive torques below 1000 Nm achieve the greatest fuel efficiency by operating in recirculation mode. From the engine speed plot and subsequent Unit 1 displacement plot it can be seen that a minimum engine speed strategy is also optimal for the blended hybrid PST.

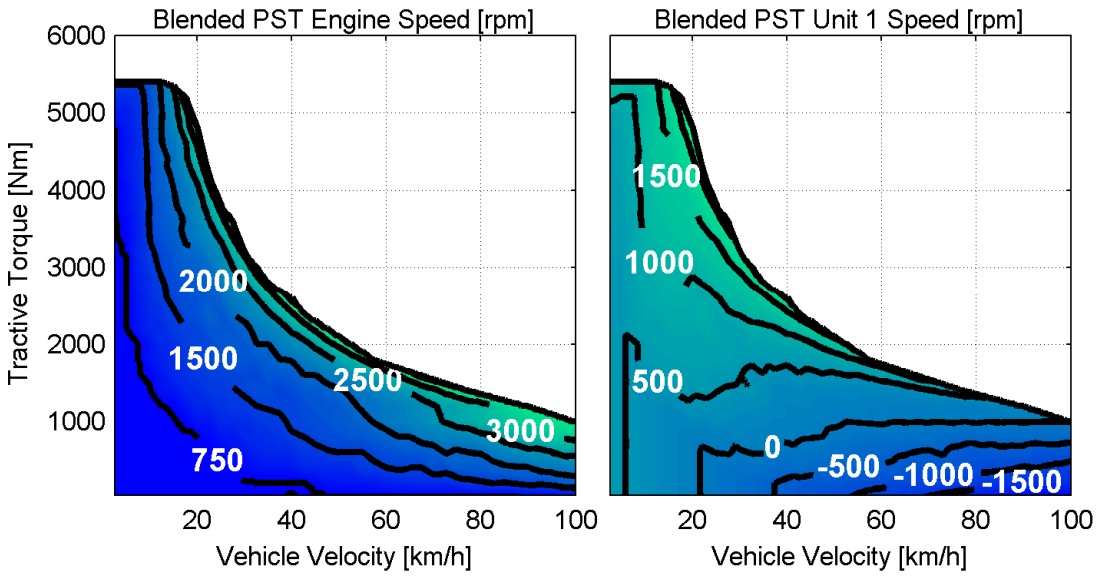

Figure 6.13 Steady state optimal operation

Figure 6.14 shows the steady state optimal power flowing through both the mechanical and hydraulic paths. Values less than zero and greater than 100% stem from power recirculation which causes power to flow through the mechanical and hydraulic paths multiple times.

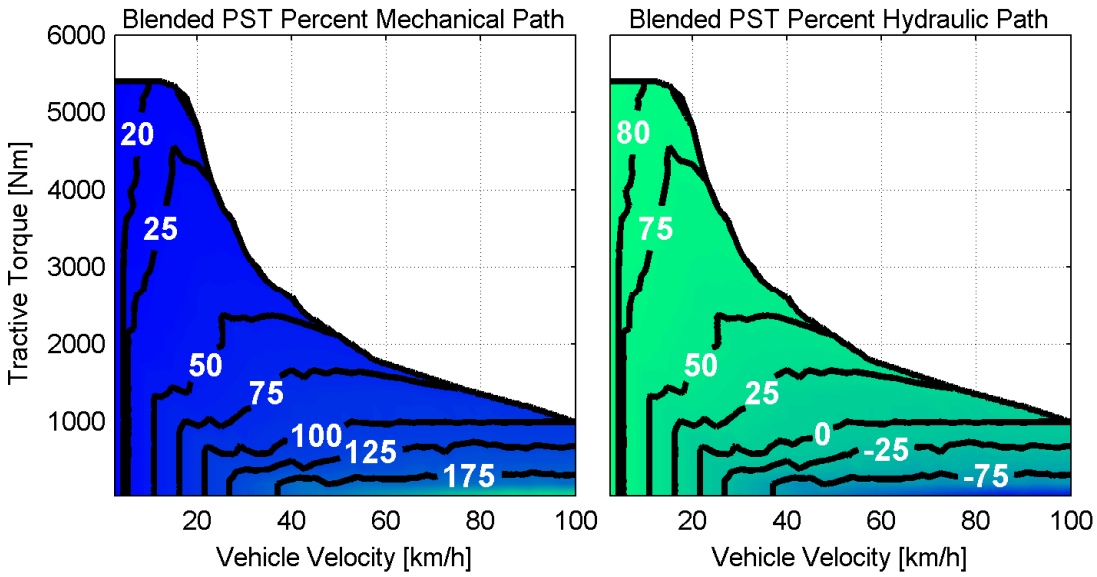

Figure 6.14 Steady state optimal operation

Figure 6.15 shows the steady state optimal Unit 1, 2, and 3 displacements. As with the blended hybrid, the blended hybrid PST is most efficiently operated when Unit 1 is at 100% displacement whenever possible. Optimal Unit 2 and 3 displacements generally reduces as tractive force decreases then move over center as required to pump fluid for the power recirculation mode.

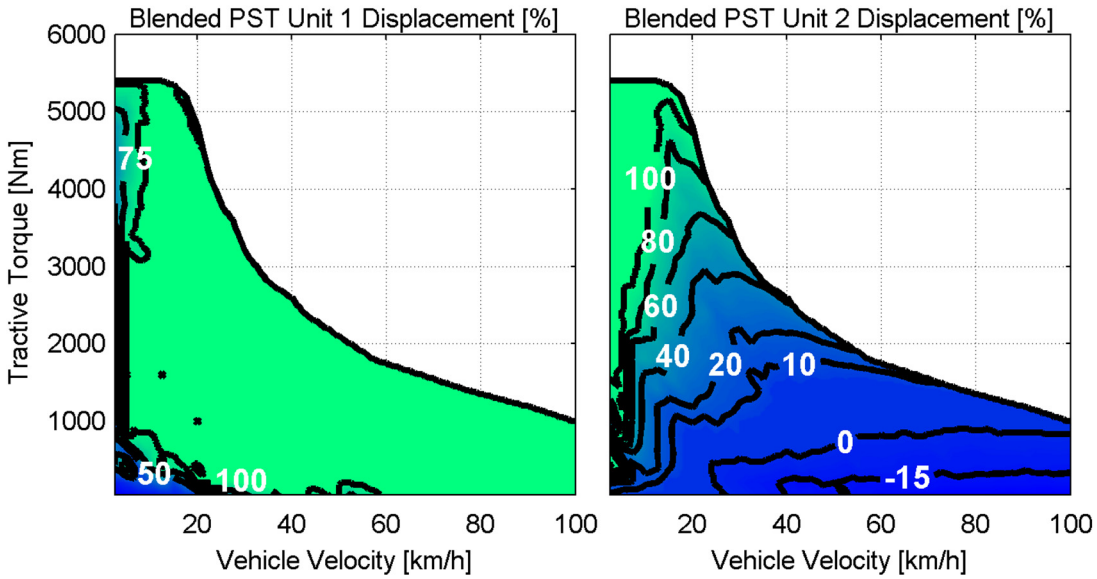

Figure 6.15 Steady state optimal operation

6.3.2 Control Strategies for Conventional Transmissions

When developing control strategies for a new transmission it is important to take drivability into account. Drivability is a general term covering such vehicle performance metrics as acceleration, braking, shift quality, engine speed, and NVH (Noise, Vibration, and Harshness) among others. Further, in order for a new transmission to gain wide spread acceptance it must possess a positive and familiar user feel. To date multiple series and power split hydraulic hybrids have been successfully demonstrated in on-road applications. In these architectures the units connected to the axle/wheels operate under secondary (torque) control, this is the same manner in which the engine in a conventional transmission operates. Consequently so long as the accumulator is sufficiently charged these vehicles should respond in a manner which is familiar to the driver. In contrast the

blended hybrid often functions as a hydrostatic transmission operating in flow (speed) control. Using the standard HST control methodology designed for off-highway applications in an automotive setting results in a markedly different driver feel. Thus the aim of the control schemes detailed in Sections 6.3.3 and 6.3.4 are to replicate the feel of a conventional automotive transmission with the blended hybrid architecture.

A firm grasp of how existing transmissions are controlled leads to a better understanding of how to control the blended hybrid transmission. Following are three common transmission architectures which provide insight and direction for two novel blended hybrid control schemes.

Mechanical Transmission

Mechanical transmissions are by far the most common type of vehicle transmission on the road today. As such it is the mechanical transmission's behavior and feel that should serve as a benchmark for the blended hybrid. For clarity only a manual transmission, and not the more complex automatic transmission, will be considered. In a mechanical transmission the driver adjusts the engine's combustion torque via the throttle pedal (also commonly referred to as the accelerator pedal). The engine power then travels through the selected discrete gear ratio before acting on the vehicle dynamics. An outline of this control structure is shown in Figure 6.16.

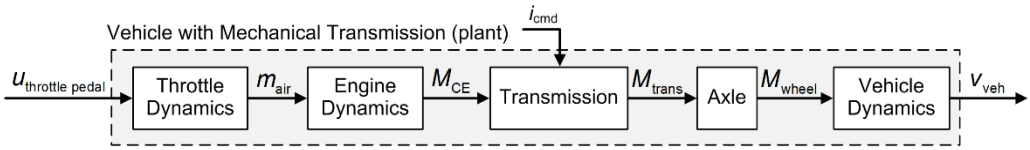

Figure 6.16 Mechanical transmission control structure

A greater understanding of how a driver interacts with a mechanical transmission, and specifically which aspects should be replicated by the blended hybrid, can be gained by examining the typical relationship between throttle pedal motion and vehicle speed. Figure 6.17 (a) shows a throttle pedal in its nominal positon. When the vehicle is at rest manual transmissions produce no output torque while automatic transmissions produce

some output torque due to the torque converter. Once the throttle pedal is depressed (b) the engine begins producing net output torque as a function of engine speed and pedal position which is propagated through the powertrain. The vehicle will then accelerate based on vehicle dynamics until the propulsive torque is balanced with the vehicle's resistive torque (aerodynamic drag, rolling resistance, grading force, etc.). When the pedal position is decreased (c) the vehicle will either continue to accelerate, or begin to decelerate, depending on the vehicle's current speed and external loads until a torque balance is reached. Finally once the throttle pedal returns to its nominal position (d) the vehicle speed will decrease aided by engine braking.

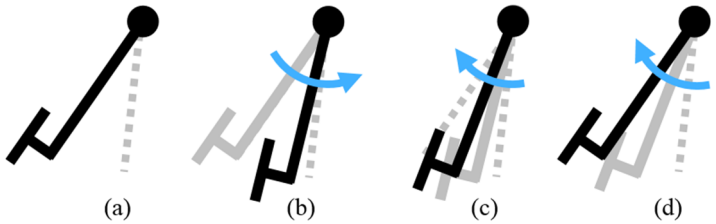

Figure 6.17: Throttle pedal positions

Series Hybrid

An understanding of a series hybrid's control methodology is useful as it is a common hydraulic hybrid architecture. Due to the large capacitance provided by the high pressure accumulator a series hybrid may be split into two semi-decoupled subsystems. On one side the engine and Unit 1 are coupled while on the other side the wheels and Unit 2 are coupled. Typically a speed controlled engine is employed with the reference engine speed provided by a supervisory controller. Unit 1's displacement is then set by another controller which seeks to maintain a reference pressure in the accumulator.

Driver input is provided through the throttle and brake pedals. The throttle pedal either directly adjusts the displacement of Unit 2 (0 to 100%), or provides a reference torque commanded to a separate Unit 2 controller. Similarly the activation of the brake pedal causes Unit 2 to move over center while the brake pedal's position provides a reference regenerative braking torque. Because of its semi-decoupled state, power for Unit 2 can

be thought of as coming from the accumulator. With this view the driver directly controls the power flowing to and from the wheels by adjusting Unit 2's displacement. As a result both series hybrids and mechanical transmissions possess a similar feel since in both cases the driver directly controls power flowing to the wheels. An outline of this control structure can be found in Figure 6.18.

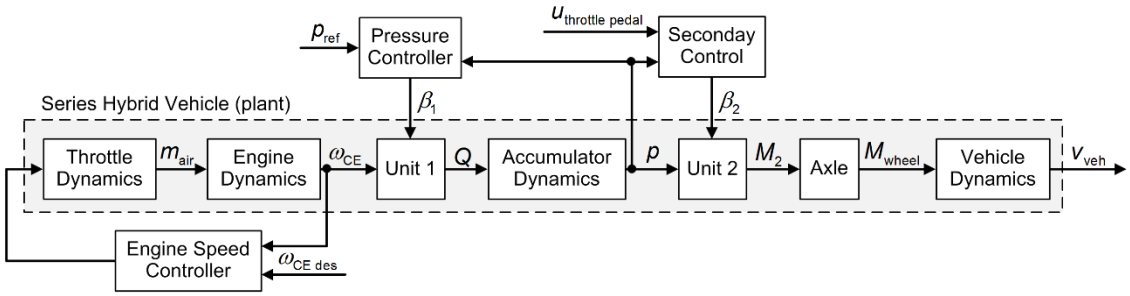

Figure 6.18 Series hybrid control structure

Hydrostatic Transmission

The blended hybrid often operates as a hydrostatic transmission so it is beneficial to understand how a HST is typically controlled. Like the series hybrid, hydrostatic transmission's typically use a speed controlled engine. However without an accumulator the HST's engine cannot be decoupled from the wheels as was done in the series hybrid. Driver input provided through the throttle pedal adjusts the displacements of Unit's 1 and 2. Unlike the previous two transmissions, this action does not directly control the power flowing to the wheels. Instead is best to think of adjusting the displacements as adjusting the overall transmission ratio. The engine's governor (i.e. speed controller) then adjusts the engine's combustion torque in order to compensate for any changes in the engine's speed. In this manner power following from the engine to the wheels is indirectly controlled by the driver. An outline of the HST control structure is located in Figure 6.19.

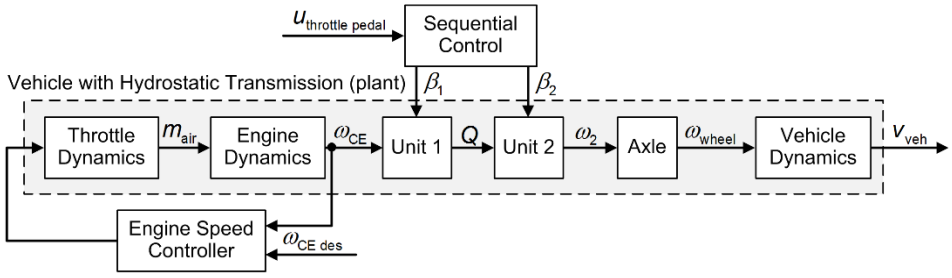

Figure 6.19 Hydrostatic transmission control structure

6.3.3 Speed Controlled Strategy for Blended Hybrid Transmissions

One method of replicating the feel of a mechanical transmission with the blended hybrid architecture involves first determining how a mechanical transmission would respond to the measured driver inputs. The blended hybrid can then be controlled similarly to a conventional HST (i.e. speed control) such that the vehicle's velocity matches the driver's expectations. This method of estimating the driver's intent is referred to in this work as path planning. The overall path planning control scheme for the blended hybrid relies on several distinct modes of operation, each with dedicated controllers. On the highest level of the path planning controller there is a supervisory control scheme which switches between the distinct controllers depending on a set of predefined conditions. This top level controller can be seen in Figure 6.20.

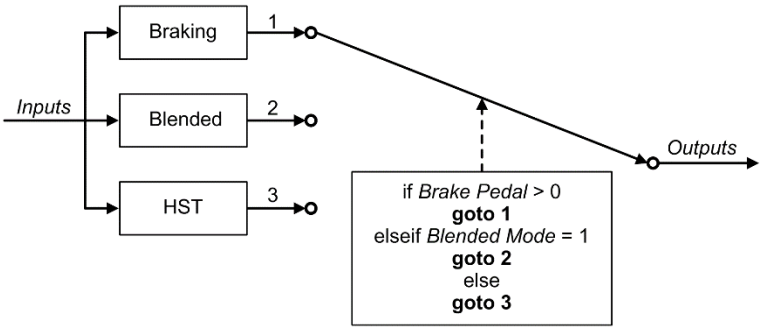

Figure 6.20: Path planning top level control scheme

Hydrostatic Driving

Desired vehicle speed is predicted by first estimating the intended torque applied to the transmission by the engine based on measured throttle pedal position (Eq. 6.5). In the path planning controller the transmission's current ratio is calculated using sequential control along with the current engine and desired wheel speeds (Eqs. 6.6, 6.9-6.12). From here the estimated torque applied to Unit 1 is passed through the transmission's current ratio before being applied to a vehicle dynamics model (Eq. 6.7). The vehicle's estimated wheel torque is then integrated to predict the driver's desired wheel speed (Eq. 6.8).

$$M_{\text{CE}} = M_{\text{WOT}}\left(\omega_{\text{CE}}\right) u_{\text{throttle pedal}} \tag{6.5}$$

$$i_{\text{HST}} = \frac{\beta_2 V_2 + \beta_3 V_3}{\beta_1 V_1} \tag{6.6}$$

$$M_{\text{wheel}} = M_{\text{CE}} i_{\text{HST}} i_{\text{axle}} \eta_{\text{hm}}^2 \tag{6.7}$$

$$\omega_{\text{wheel des}} = \int \frac{M_{\text{wheel}} - F_{\text{d}} r_{\text{dyn}} - F_{\text{rr}} r_{\text{dyn}} - F_{\text{g}} r_{\text{dyn}}}{m_{\text{veh}} r_{\text{dyn}}^2} dt \tag{6.8}$$

Once the desired wheel speed is estimated the blended hybrid transmission can be controlled like a conventional hydrostatic transmission. However now instead of the driver's throttle pedal directly controlling unit displacement, the unit displacements are calculated based on the measured engine speed and the desired wheel speed. An overview of this control methodology for hydrostatic driving can be found in Figure 6.21. Here, and throughout the next section, desired engine speed is specified by a supervisory engine speed controller which will be discussed in Section 6.3.5.

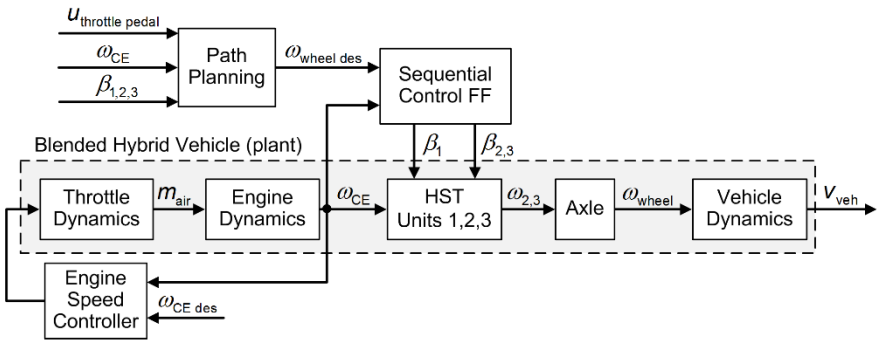

Figure 6.21: Path planning hydrostatic driving

During hydrostatic driving the hydraulic unit displacements are controlled using sequential control based on measured engine speed and desired wheel speed (Eqs. 6.9-6.12). For the path planning control strategy it was determined that only feed forward control should be used in determining unit displacements. This approach was chosen such that the transmission would respond promptly to changes in the driver's desired wheel speed. This eliminates potentially undesirable behavior if the measured wheel speed were to lag significantly behind the desired wheel speed and feedback counteracted the driver's changing commands. The controller's reduced tracking performance due to the absence of feedback is not a hindrance though as the driver has no knowledge of the reference wheel speed based on their measured throttle pedal input.

$$Q_{\text{Unit1 max}} = \omega_{CE} V_1 \eta_{\text{vol}} \tag{6.9}$$

$$Q_{\text{Unit2,3 max}} = \frac{\omega_{\text{wheel des}} i_{\text{axle}} \left(V_2 + V_3\right)}{\eta_{\text{vol}}} \tag{6.10}$$

$$\beta_1 = \begin{cases} \dfrac{Q_{\text{Unit2,3 max}}}{Q_{\text{Unit1 max}}} & ; Q_{\text{Unit1 max}} \geq Q_{\text{Unit2,3 max}} \\ 1 & ; Q_{\text{Unit1 max}} < Q_{\text{Unit2,3 max}} \end{cases} \tag{6.11}$$

$$\beta_{2,3} = \begin{cases} 1 & ; Q_{\text{Unit1 max}} \geq Q_{\text{Unit2,3 max}} \\ \dfrac{Q_{\text{Unit1 max}}}{Q_{\text{Unit2,3 max}}} & ; Q_{\text{Unit1 max}} < Q_{\text{Unit2,3 max}} \end{cases} \tag{6.12}$$

Blended Driving

During blended driving Unit 3 is disconnected from the Units 1 and 2 and connected to the high pressure accumulator. Units 1 and 2 are still operated in sequential control based on desired wheel speed, however the absence of flow to Unit 3 must be taken into account in the equations. Unit 3, operating in secondary control, is then controlled to provide some percentage (e.g. 50%) of the estimated axle torque. An overview of this control approach is shown in Figure 6.22.

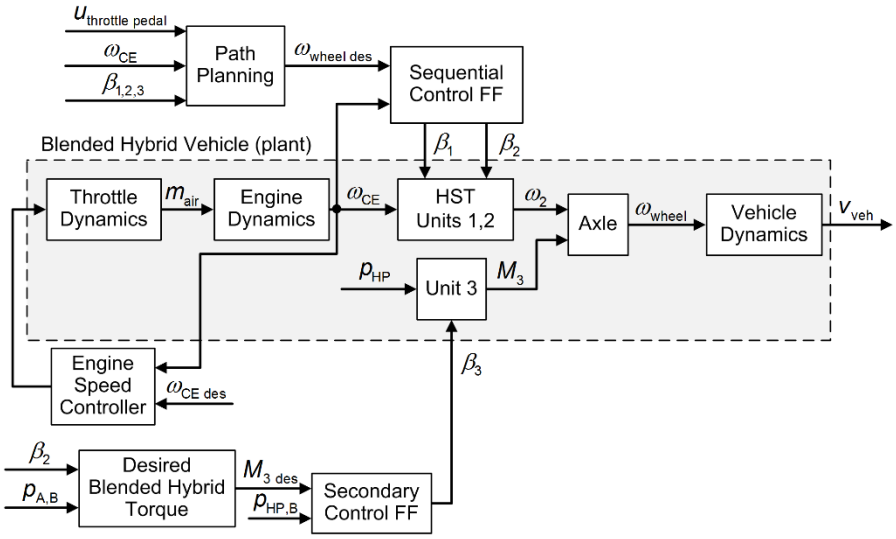

Figure 6.22: Path planning blended driving

Sequential control of the hydrostatic transmission during blended driving involves only Units 1 and 2 (Eqs. 6.13-6.16).

$$Q_{\text{Unit1 max}} = \omega_{CE} V_1 \eta_{\text{vol}} \tag{6.13}$$

$$Q_{\text{Unit2 max}} = \frac{\omega_{\text{wheel des}} i_{\text{axle}} V_2}{\eta_{\text{vol}}} \tag{6.14}$$

$$\beta_1 = \begin{cases} \dfrac{Q_{\text{Unit2 max}}}{Q_{\text{Unit1 max}}} & ; Q_{\text{Unit1 max}} \geq Q_{\text{Unit2 max}} \\ 1 & ; Q_{\text{Unit1 max}} < Q_{\text{Unit2 max}} \end{cases} \tag{6.15}$$

$$\beta_2 = \begin{cases} 1 & ;Q_{\text{Unit1 max}} \geq Q_{\text{Unit2 max}} \\ \dfrac{Q_{\text{Unit1 max}}}{Q_{\text{Unit2 max}}} & ;Q_{\text{Unit1 max}} < Q_{\text{Unit2 max}} \end{cases} \tag{6.16}$$

During blended driving the desired Unit 3 torque is calculated by first estimating the torque applied to the axle by Unit 2 (Eq. 6.17). In Section 6.3.5 it will be shown that a 50-50 torque split between Units 2 and 3 in blended driving mode is near optimal. Therefore Unit 3 is commanded here to provide the same torque as Unit 2. Though a gain (k_{split}) has still been included in the controller if a different torque split is desired (Eq. 6.18). Once the desired Unit 3 torque is determined, secondary control is used to specify Unit 3's displacement based primarily on the high pressure accumulator's current pressure (Eq. 6.19).

$$M_2 = \frac{\beta_2 V_2 \left(p_{\text{A}} - p_{\text{B}}\right)\eta_{\text{hm}}}{2\pi} \tag{6.17}$$

$$M_{3\text{ des}} = M_2 k_{\text{split}} \tag{6.18}$$

$$\beta_3 = \frac{M_{3\text{ des}} 2\pi}{V_3 \left(p_{\text{HP}} - p_{\text{B}}\right)\eta_{\text{hm}}} \tag{6.19}$$

Braking

Desired regenerative braking torque is given by a lookup table based on brake pedal position and current accumulator pressure (Eq. 6.20). More details on the brake pedal mapping are given in Section 8.4. While braking Unit 1 is set to zero displacement while Units 2 and 3 are controlled to provide the desired braking torque (Eq. 6.21).

$$M_{2,3\text{ des}} = M_{\text{brake torque map}}\left(u_{\text{brake pedal}}, p_{\text{HP}}\right) \tag{6.20}$$

$$\beta_{2,3} = \frac{M_{2,3\text{ des}} 2\pi}{\left(V_2 + V_3\right)\left(p_{\text{HP}} - p_{\text{A}}\right)\eta_{\text{hm}}} \tag{6.21}$$

One of the principle benefits offered by the path planning approach is the ability to operate the blended hybrid in a speed controlled manner similar to conventional HSTs. This may be beneficial in certain applications where a speed controlled engine is already present such as is commonly found in the off-highway segment. It also has the benefit of performing well during startup and low speed operation, a mode which is challenging for the torque controlled approach presented in the next section. However the path planning approach does rely heavily on having an accurate vehicle dynamics model and will not fully capture the expected vehicle dynamics resulting from varying external loads such as driving up or down a hill.

6.3.4 Torque Controlled Strategy for Blended Hybrid Transmissions

An alternative control methodology which addresses the aforementioned deficiencies of the path planning approach is proposed below. Instead of needing to estimate the driver's desired response in order to remain in a speed controlled configuration, the blended hybrid can be operated in a torque controlled mode quite similar to a conventional mechanical transmission. Here the throttle pedal directly adjusts combustion torque while a transmission controller adjusts the unit displacements according to some supervisory control scheme. This can be thought of as the same way in which an automatic transmission determines the appropriate gear ratio based on efficiency and drivability metrics. Torque control of the blended hybrid requires several distinct modes of operation as seen in Figure 6.23.

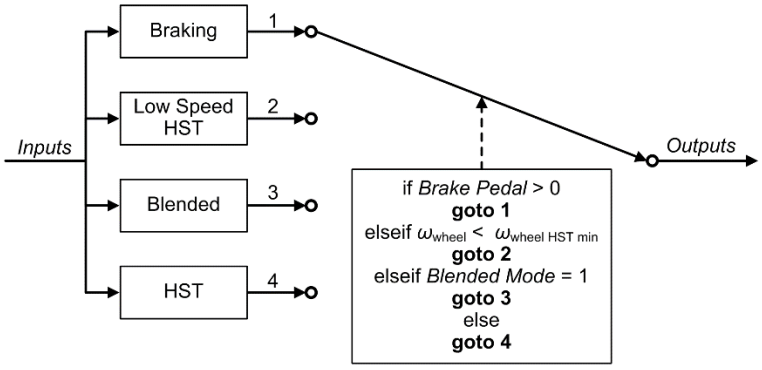

Figure 6.23: Torque control top level control scheme

Hydrostatic Driving

During hydrostatic driving the unit displacements are set using sequential control based on measured wheel speed and desired engine speed (as opposed to the measured engine speed and desired wheel speed used in the path planning approach). The transmission controller used for HST driving can also be thought of as the engine speed controller. During HST operation adjusting the unit displacements alters the transmission's ratio between the engine and wheels. Due to the vehicle's inertia being substantially greater than the engine's inertia, and because the engine's combustion torque is not being controlled to maintain a desired engine speed, modifying the unit displacements changes primarily the engine's speed rather than the vehicle's speed. An overview of the torque controlled approach for hydrostatic driving of a blended hybrid is shown in Figure 6.24.

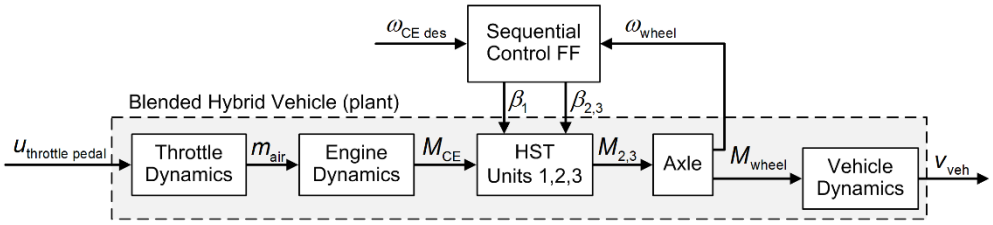

Figure 6.24: Torque controlled hydrostatic driving

Unit displacements during torque controlled hydrostatic driving are calculated using Equations 6.22-6.25.

$$Q_{Unit1\ max} = \omega_{CE\ des} V_1 \eta_{vol} \tag{6.22}$$

$$Q_{Unit2,3\ max} = \frac{\omega_{wheel} i_{axle} \left(V_2 + V_3\right)}{\eta_{vol}} \tag{6.23}$$

$$\beta_1 = \begin{cases} \dfrac{Q_{Unit2,3\ max}}{Q_{Unit1\ max}} & ; Q_{Unit1\ max} \geq Q_{Unit2,3\ max} \\ 1 & ; Q_{Unit1\ max} < Q_{Unit2,3\ max} \end{cases} \tag{6.24}$$

$$\beta_{2,3} = \begin{cases} 1 & ;Q_{\text{Unit1 max}} \geq Q_{\text{Unit2,3 max}} \\ \dfrac{Q_{\text{Unit1 max}}}{Q_{\text{Unit2,3 max}}} & ;Q_{\text{Unit1 max}} < Q_{\text{Unit2,3 max}} \end{cases} \tag{6.25}$$

A PID (Proportional, Integral, Derivative) feedback controller may be added to the hydrostatic transmission controller to improve engine speed tracking beyond the capabilities of feed forward sequential control. An overview of the torque controlled HST driving approach with PID feedback can be found in Figure 6.25.

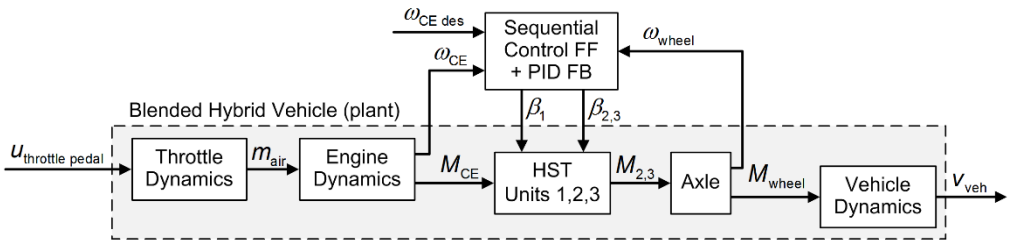

Figure 6.25: Torque controlled hydrostatic driving with PID feedback

This PID controller acts on the error between desired and measured engine speed with the controller's output $u_{\omega_{CE}}$ serving to account for differences between the units' estimated and actual volumetric efficiencies. This improved control scheme is contained in Equations 6.26-6.31.

$$e_{\omega_{CE}} = \omega_{CE\ des} - \omega_{CE} \tag{6.26}$$

$$u_{\omega_{CE}} = 1 - \left(k_p e_{\omega_{CE}} + k_i \int e_{\omega_{CE}} dt + k_d e_{\omega_{CE}} \frac{d}{dt} \right) \tag{6.27}$$

$$Q_{\text{Unit1 max}} = \omega_{CE\ des} V_1 \eta_{vol} u_{\omega_{CE}} \tag{6.28}$$

$$Q_{\text{Unit2,3 max}} = \frac{\omega_{wheel} i_{axle} (V_2 + V_3)}{\eta_{vol}} \frac{1}{u_{\omega_{CE}}} \tag{6.29}$$

$$\beta_1 = \begin{cases} \dfrac{Q_{\text{Unit2,3 max}}}{Q_{\text{Unit1 max}}} & ;Q_{\text{Unit1 max}} \geq Q_{\text{Unit2,3 max}} \\ 1 & ;Q_{\text{Unit1 max}} < Q_{\text{Unit2,3 max}} \end{cases} \tag{6.30}$$

$$\beta_{2,3} = \begin{cases} 1 & ;Q_{\text{Unit1 max}} \geq Q_{\text{Unit2,3 max}} \\ \dfrac{Q_{\text{Unit1 max}}}{Q_{\text{Unit2,3 max}}} & ;Q_{\text{Unit1 max}} < Q_{\text{Unit2,3 max}} \end{cases} \tag{6.31}$$

Another aspect of powertrain operation which is anticipated and expected by the driver is a coasting mode when the throttle pedal is released (Figure 6.17). Coasting often occurs as a vehicle is slowing down, such as approaching a stop, but the driver has yet to depress the brake pedal. In these cases the vehicle's inertia provides power to the powertrain and unloads the engine. While coasting vehicle speed decreases slowly based on the vehicle's inertia in combination with internal powertrain losses and external loads such as aerodynamic drag, rolling resistance, and grading force (though grading can be either a resistive or aiding load). Achieving a coasting mode is somewhat difficult in the previously described path planning approach due to differences between the vehicle's actual and simulated dynamics (used to generate the reference vehicle speed). However coasting happens automatically during hydrostatic driving in the torque controlled approach. In this case once the throttle is released the transmission remains in the HST driving mode with unit displacements set to track the reference engine speed. However now Units 2 and 3 act as pumps while Unit 1 acts as a motor and provides power to the engine. Pressure in Line B is thus based on the resistive load of the engine, Unit 1, and all of the connected axillary loads. During coasting the pressure in Line B is generally significantly lower than the HP accumulator such that the check valve connecting Line B to the accumulator remains closed and the transmission remains in a flow controlled mode.

Low Speed Hydrostatic Driving

While the proposed HST control methodology works quite well above a certain vehicle speed, there are some difficulties in starting the blended hybrid from rest using the torque controlled approach. These difficulties can be likened to those experience when starting a manual transmission. That is under a certain vehicle speed manual transmissions are unable to stay in gear as even the lowest gear ratio would cause the engine to operate at a speed below the safe operating range. Thus a friction clutch must

be used in manual transmissions and allowed to slip in order to partially decouple the engine speed from the vehicle speed. Unlike a conventional manual transmission, the blended hybrid's hydrostatic transmission is capable of a much greater range of transmission ratios. However these large ratios require a very small Unit 1 displacement to the point where controlling engine speed based on vehicle speed no longer functions properly.

To address this issue a separate control strategy is proposed for vehicles during startup. Most on-road engines feature a throttle bypass valve which is used to control the engine during low idle (as seen in Figure 8.21). This additional integrated controller and actuator removes the need for controlling engine speed via the hydrostatic transmission under all circumstance. Instead while the vehicle is a rest, and during braking, the engine is controlled at the low idle speed by the bypass valve.

In order to begin driving the driver depresses the throttle pedal which opens the engine's throttle valve resulting in increased combustion torque. Unit 1's displacement is set by first estimating the torque applied to Unit 1 by the engine (Eq. 6.32). Simultaneously the throttle pedal position is converted into a reference pressure for the HST (Eq. 6.33). Unit 1's displacement is then controlled such that the torque applied by the engine yields the desired pressure within the hydrostatic transmission (Eq. 6.34). Controlling the transmission in this manner results in the vehicle, and consequently the engine, increasing in speed up until the point where the measured engine speed reaches the reference engine speed at which time control is passed to the primary hydrostatic driving controller.

$$M_{\mathrm{CE}} = M_{\mathrm{WOT}}\left(\omega_{\mathrm{CE}}\right) u_{\text{throttle pedal}} \tag{6.32}$$

$$p_{\mathrm{ref}} = u_{\text{throttle pedal}} k_{\text{p ref}} \tag{6.33}$$

$$\beta_1 = \frac{M_{\mathrm{CE}} 2\pi}{V_1\left(p_{\mathrm{ref}} - p_{\mathrm{B}}\right)\eta_{\mathrm{hm}}} \tag{6.34}$$

Blended Driving

An overview of the blended driving controller for the torque controlled approach is shown in Figure 6.26.

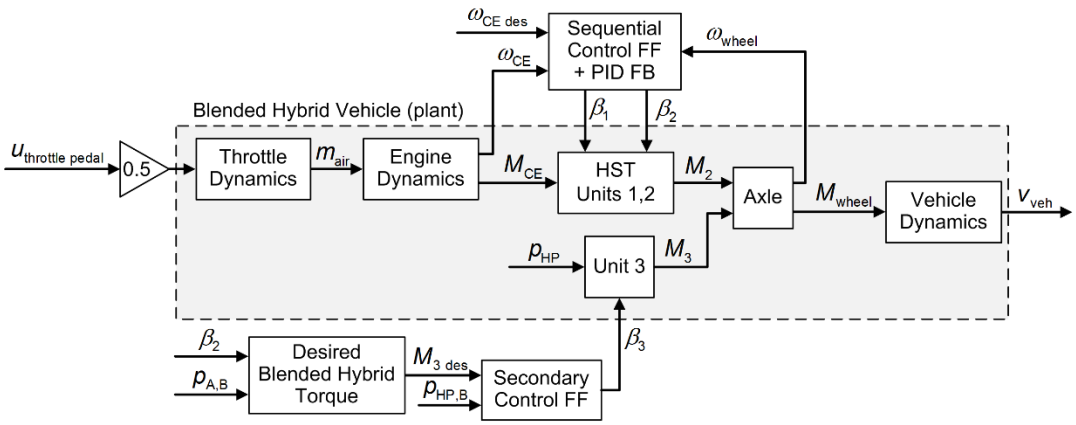

Figure 6.26: Torque controlled blended driving

During blended driving half of the power applied by the powertrain to the wheels comes from the engine while the second half is supplied by the high pressure accumulator. As during hydrostatic driving the driver continues to provide input into the system through the throttle pedal. However in order to maintain the same driver response as before the engine power must now be reduced by half. There are two methods to accomplish this; first the controller could reduce the measured throttle pedal position by 50% before actuating the throttle valve (shown in Figure 6.26). Alternatively the driver's commanded throttle position could be applied to the throttle valve unaltered while the engine's reference speed is cut in half. This second approach is superior from an efficiency perspective but is more difficult to consistently implement as reducing the engine speed by 50% is not always possible such as while operating at low engine speeds.

During blended driving Units 1 and 2 are adjusted using sequential control plus PID feedback in order to control the engine speed (Equations 6.35-6.40).

$$e_{\omega_{CE}} = \omega_{CE\ des} - \omega_{CE} \tag{6.35}$$

$$u_{\omega_{CE}} = 1 - \left(k_p e_{\omega_{CE}} + k_i \int e_{\omega_{CE}} dt + k_d e_{\omega_{CE}} \frac{d}{dt} \right) \tag{6.36}$$

$$Q_{\text{Unit1 max}} = \omega_{\text{CE des}} V_1 \eta_{\text{vol}} u_{\omega_{CE}} \tag{6.37}$$

$$Q_{\text{Unit2 max}} = \frac{\omega_{\text{wheel}} i_{\text{axle}} V_2}{\eta_{\text{vol}}} \frac{1}{u_{\omega_{CE}}} \tag{6.38}$$

$$\beta_1 = \begin{cases} \dfrac{Q_{\text{Unit2 max}}}{Q_{\text{Unit1 max}}} & ; Q_{\text{Unit1 max}} \geq Q_{\text{Unit2 max}} \\ 1 & ; Q_{\text{Unit1 max}} < Q_{\text{Unit2 max}} \end{cases} \tag{6.39}$$

$$\beta_2 = \begin{cases} 1 & ; Q_{\text{Unit1 max}} \geq Q_{\text{Unit2 max}} \\ \dfrac{Q_{\text{Unit1 max}}}{Q_{\text{Unit2 max}}} & ; Q_{\text{Unit1 max}} < Q_{\text{Unit2 max}} \end{cases} \tag{6.40}$$

During blended driving Unit 3 is controlled to provide the same torque to the wheels as Unit 2 (Eqs. 6.41-6.43).

$$M_2 = \frac{\beta_2 V_2 \left(p_A - p_B \right) \eta_{\text{hm}}}{2\pi} \tag{6.41}$$

$$M_{3\,\text{des}} = M_2 k_{\text{split}} \tag{6.42}$$

$$\beta_3 = \frac{M_{3\,\text{des}} 2\pi}{V_3 \left(p_{HP} - p_B \right) \eta_{\text{hm}}} \tag{6.43}$$

Braking

During regenerative braking Unit 1 is set to zero displacement while Units 2 and 3 are controlled (Eq. 6.45) to provide the desired braking torque (Eq. 6.44).

$$M_{2,3\,\mathrm{des}} = M_{\mathrm{brake\ torque\ map}}\left(u_{\mathrm{brake\ pedal}}, p_{\mathrm{HP}}\right) \tag{6.44}$$

$$\beta_{2,3} = \frac{M_{2,3\,\mathrm{des}} 2\pi}{\left(V_2 + V_3\right)\left(p_{\mathrm{HP}} - p_{\mathrm{A}}\right)\eta_{\mathrm{hm}}} \tag{6.45}$$

6.3.5 Power Management

Two different system level control strategies were proposed above for the blended hybrid. In addition two implementable power management strategies which take into account the blended hybrid's hybrid functionality will be discussed here. These power management strategies can be used in conjunction with either one of the system level control strategies yielding a more complete powertrain controller.

A novel neural network based power management control strategy was presented in Chapter 4 which demonstrated relatively good performance for a series hybrid. However because the blended hybrid is incapable of directly charging the accumulator from the engine, as series hybrids can, using an optimal pressure control strategy does not make sense for this application. Rather the blended hybrid often operates as a hydrostatic transmission thus control strategies such as instantaneous optimization are more appropriate. Instantaneous optimization strategies work well for HSTs because the optimal control of a HST has very little to do with past or future driving events. One downside of instantaneous optimization though is the high level of knowledge required about the specific system before an optimization can be conducted. Consequently instantaneous optimal control strategies lack generality so both an instantaneous optimal, and a more general engine centric, control strategy are proposed and investigated in this section.

One common method of powertrain control is an engine centric approach whereby the powertrain is controlled such that the engine operates along its minimum BSFC curve. That is the engine operates at its point of greatest efficiency for a given power demand. From the engine's perspective this is indeed the most efficient manner of operation.

However it does not take into account the influence engine speed has on the efficiency of other component within the powertrain. Nevertheless this approach has the advantage of not requiring any specific information about the drivetrain and therefore is more general than instantaneous optimization. Figure 6.27 shows the minimum BSFC curve for the base vehicle used throughout much of this chapter.

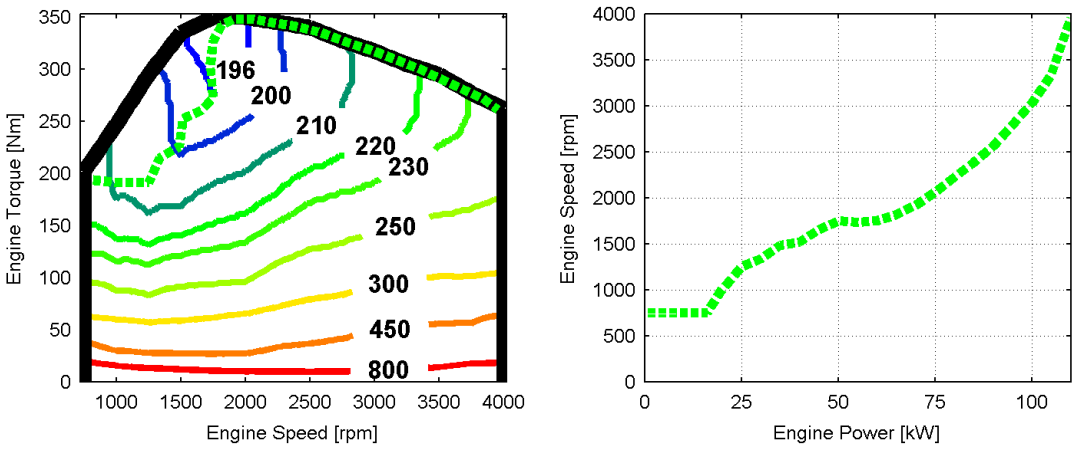

Figure 6.27: Minimum brake specific fuel consumption curve

A power management controller for the blended hybrid was created utilizing this minimum BSFC curve (Eq. 6.48). In the controller engine power is estimated based on measured engine speed and throttle in conjunction with a wide open throttle map (Eqs. 6.46-6.47). To ensure the driver is always capable of increasing engine speed if desired, the reference speed increases whenever the measured throttle pedal position exceeds 95% (Eq. 6.49).

$$M_{CE} = M_{WOT}\left(\omega_{CE}\right)u_{\text{engine throttle}} \tag{6.46}$$

$$P_{CE} = M_{CE}\omega_{CE} \tag{6.47}$$

$$\omega_{\text{CE des map}} = \text{Minimum BSFC map}\left(P_{CE}\right) \tag{6.48}$$

$$\omega_{\text{CE des}} = \begin{cases} \omega_{\text{CE des map}} & ;u_{\text{throttle pedal}} \le 0.95 \\ \omega_{\text{CE des map}} + \left(u_{\text{throttle pedal}} - 0.95\right)k & ;u_{\text{throttle pedal}} > 0.95 \end{cases} \tag{6.49}$$

A simple rule-based controller is proposed for the hybrid energy storage system. Whenever the following conditions are met the blended hybrid is switched from hydrostatic driving to blended driving:

- Accumulator pressure is greater than minimum accumulator pressure
- Accumulator pressure is greater than Line A pressure
- Vehicle speed is greater than some minimum value (e.g. 10 km/h)
- Throttle pedal is depressed

When all of these conditions are met the enabling valve is opened and Unit 3 is controlled to provide the same torque as Unit 2.

The minimum BSFC strategy combined with rule-based blended mode control was evaluated in the same blended hybrid transmission and vehicle used in the dynamic programming analysis. Over the UDDS cycle the proposed power management strategy achieved a fuel consumption rate of 9.01 l/100 km, only 7.60% greater than the DP globally optimal fuel consumption rate of 8.37 l/100 km.

Prior works have shown the benefits of using instantaneous optimization for power management of hydrostatic transmissions. In one example Ossyra, 2004 used instantaneous optimization to control an off-highway HST and estimated a 10-22% reduction in fuel consumption against a baseline control strategy. However he ran this optimization online using a Fibonacci search which resulted in a high computational demand. A different approach is used in this work which takes advantage of a steady state optimization similar to that presented in Section 6.3.1. However instead of optimizing powertrain control to maximize transmission efficiency, an optimization was conducted to minimize fuel consumption. In the proposed approach an optimal engine speed reference (Eq. 6.51) is determined based on measured vehicle speed and estimated tractive torque (Eq. 6.50) using the steady state optimization shown in Figure 6.28 as a lookup table. The instantaneous optimal engine speed controller also features a control

element which increases the reference engine speed whenever a throttle pedal input greater than 95% is measured (Eq. 6.52).

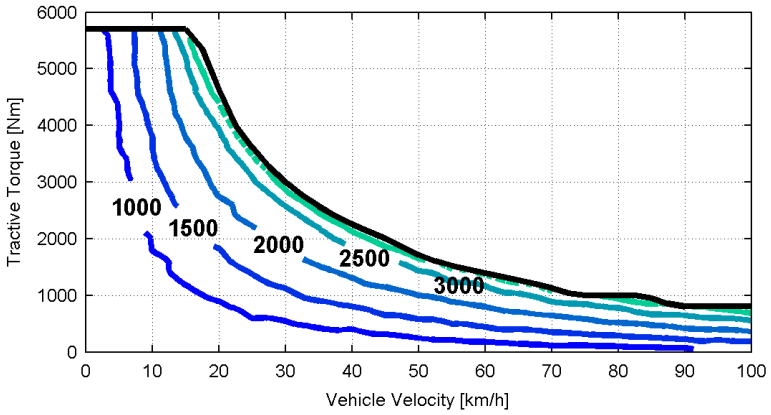

Figure 6.28: Instantaneous optimal engine speed

$$M_{\text{wheel}} = \frac{\left(\beta_2 V_2 + \beta_3 V_3\right)\left(p_{\text{A}} - p_{\text{B}}\right) i_{\text{axle}} \eta_{\text{hm}}}{2\pi} \tag{6.50}$$

$$\omega_{\text{CE des map}} = \text{Instantaneous optimization map}\left(M_{\text{wheel}}, \omega_{\text{wheel}}\right) \tag{6.51}$$

$$\omega_{\text{CE des}} = \begin{cases} \omega_{\text{CE des map}} & ;u_{\text{throttle pedal}} \le 0.95 \\ \omega_{\text{CE des map}} + \left(u_{\text{throttle pedal}} - 0.95\right)k & ;u_{\text{throttle pedal}} > 0.95 \end{cases} \tag{6.52}$$

The instantaneous optimal control approach was evaluated in the same blended hybrid reference vehicle as the minimum BSFC strategy. Combined with the rule-based hybrid strategy the proposed power management controller achieved a fuel consumption rate of 8.51 l/100 km, only 1.65% greater than the DP globally optimal fuel consumption rate of 8.37 l/100 km.

The results here are interesting for several reasons. First it shows that simply using the energy stored within the accumulator whenever possible, that is without regards to future driving events, is roughly optimal. Similarly using a 50-50 torque split between Units 2 and 3 also yields near optimal results. Additionally these results show that a blended hybrid power management controller does not need a pure hybrid driving mode

to achieve near optimal fuel efficiency. This assertion is supported by an examination of the DP optimal control trajectories which rarely places the blended hybrid in a pure hybrid mode, and then for only very short periods of time. Most important though is the knowledge that the blended hybrid can achieve near optimal fuel consumption results using a simple power management control scheme with no need to account for the broader drive cycle. Previous work by Kumar, 2010 showed instantaneous optimization of a series hybrid PST yielded a fuel consumption rate 11.7% higher than DP for the UDDS cycle. For the same application a stochastic dynamic programming based power management controller (also proposed by Kumar, 2010) was able to achieve a fuel consumption rate 5.4% higher than DP. However the SDP approach is highly complex and involved first training the power management controller on the test cycle. Ultimately this shows that the blended hybrid is far easier to control in terms of fuel efficiency than conventional hydraulic hybrids. It also indicates that differences in fuel efficiency estimated by DP would in fact be greater when these architectures are implemented in physical vehicles due to inherent differences in the relative ease of their power management. Finally it should be stated that the proposed power management controllers could be improved by optimizing the torque split between the two units as well as determining the optimal time to use the stored energy. However in this case the additional complexity and effort required to develop such a controller is likely not worthwhile due to the relatively small increase in fuel efficiency which could be obtained.

6.4 Hardware-in-the-Loop Evaluation

While modeling, simulation, and optimal control provide valuable insight, they are not a replacement for proof of concept testing. To further explore the proposed architecture a blended hybrid transmission was implemented on a hardware-in-the-loop transmission dynamometer. More information on this test rig is detailed in Chapter 7.

6.4.1 Hardware-in-the-Loop Transmission Dynamometer

The same vehicle and transmission component sizings used in the neural network investigation were also used to investigate the blended hybrid on the HIL test rig. For reference select vehicle and transmission parameters are repeated below in Table 6.2.

Table 6.2: Select parameters for the blended hybrid HIL transmission dynamometer

Tire rolling radius:	0.321 m	Engine:	103 kW @ 6300 rpm
Frontal area:	2.2 m^2	Engine:	170 Nm @ 3800 rpm
Drag coefficient:	0.31	Fuel:	Gasoline
Rolling resistance:	0.01	Mass:	1680 kg
Transmission:	Manual	Axle ratio:	3.94:1
HP/LP accumulator volume:	18.4 l	Unit 1,2,3:	42 cc/rev
HP accumulator precharge:	130 bar	Charge:	15 cc/rev
HP accumulator min pressure:	140 bar	Max pressure:	350 bar
LP accumulator precharge:	10 bar	Low pressure:	20 bar

The principle difference between the HIL configurations used in the NN and blended hybrid investigations was the hydraulic circuit used to connect the various components. A schematic of the blended hybrid HIL circuit is shown in Figure 6.29.

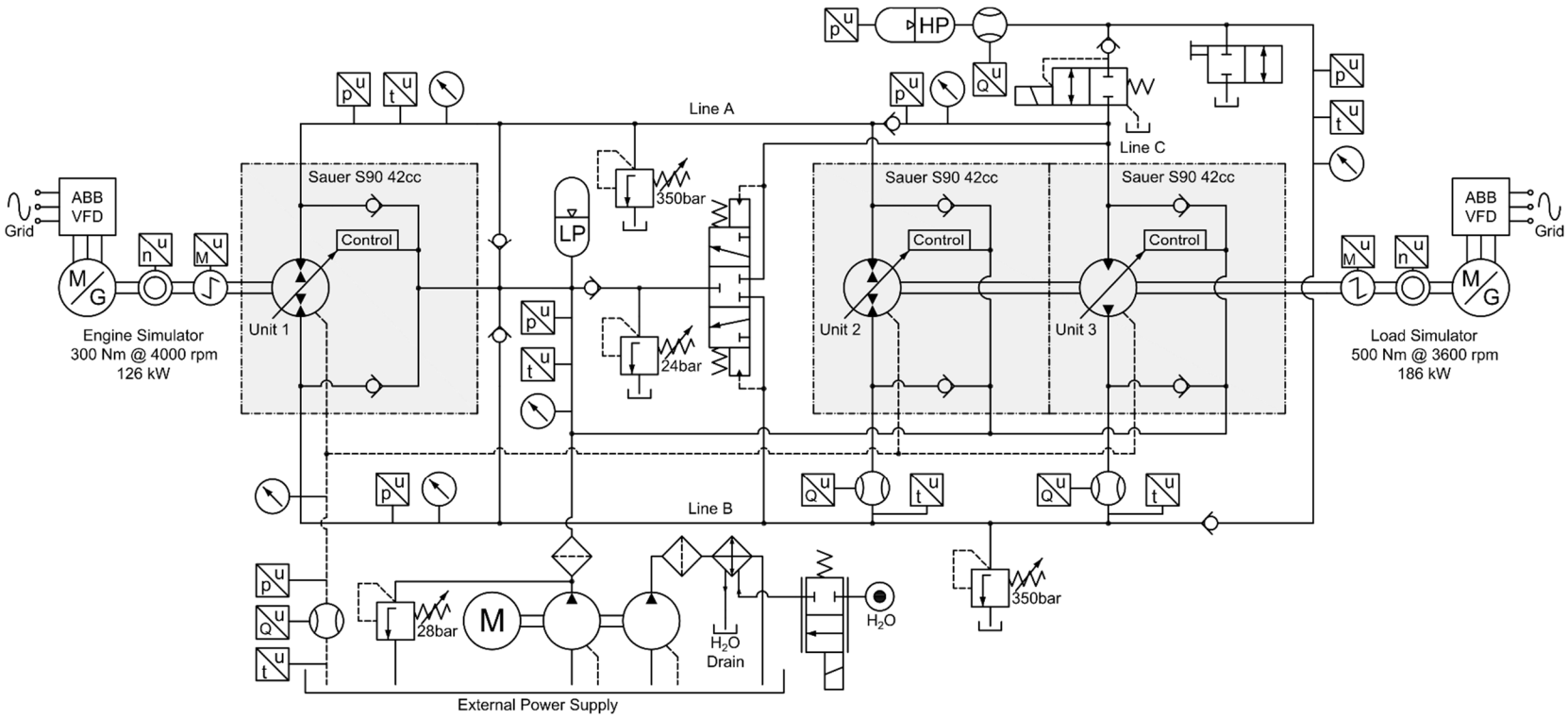

Figure 6.29: Blended hybrid hardware-in-the-loop test rig circuit

6.4.2 Control Methodology

One of the principle differences in operation between an on-road vehicle and the HIL transmission dynamometer is that on a HIL dynamometer vehicle inertia must be simulated. This means that both the speed and torque controlled approaches presented in Section 6.3 would be difficult to safely apply to the test rig. Instead it was decided that the test rig would be initially operated in such a manner as to validate the blended hybrid architecture. This meant that certain controller flows were not the same as would be found in an on-road vehicle, however this modified control scheme helped to ensure the test rig's safe operation.

When determining which parameters to control it is beneficial to consider the principles expressed in bond graph methodology (as proposed by Paynter, 1961). Two of these concepts are especially useful for control. First all power flow, regardless of physical domain, can be expressed in terms of effort and flow variables (summarized in Table 6.3). And second many mechanical components, including positive displacement machines, act as transformers. That is they convert effort to effort variables and flow to flow variables.

Table 6.3 Bond graph energy domains

Energy Domain:	Effort Variable:	Flow Variable:
Translational	Force	Velocity
Rotational	Torque	Angular velocity
Fluid (hydrostatic)	Pressure	Flow rate

Two more concepts are useful for determining controller flow through the HIL test rig. First any component which supplies (sources) or removes (sinks) power from the system must have a control loop placed around either the effort or the flow variable. Second a pair of sourcing and sinking components must have control loops placed around alternating variables in order to prevent the system from going unstable. For example if the sourcing component has a control loop placed around the flow variable then the sinking component must have a control loop placed around the effort variable (the

opposite combination is also possible). Due to the blended hybrid's discrete modes of operation, certain control loops within the HIL test rig must transition between effort and flow control in order to maintain balance between sourcing and sinking components.

Independent of these control loops the HIL test rig's objective was for the transmission to follow a predefined drive cycle. This drive cycle consisted solely of a defined velocity vs. time profile. The tractive torque required to track this cycle was based on specific vehicle characteristics and determined using Equations 6.53 and 6.54.

$$\alpha_{\text{wheel}} = \frac{v_{\text{veh}}}{3.6 r_{\text{dyn}}} \frac{d}{dt} \tag{6.53}$$

$$M_{\text{wheel}} = \alpha_{\text{wheel}} m_{\text{veh}} r_{\text{dyn}}^2 + \left(F_{\text{d}} + F_{\text{rr}} + F_{\text{g}} \right) r_{\text{dyn}} \tag{6.54}$$

Equations 6.55 and 6.56 were used to determine the load simulator's required speed and torque in order to simulate the powertrains missing axle ratio and wheels.

$$\omega_{\text{load des}} = \frac{v_{\text{veh}} 30 i_{\text{axle}}}{3.6 r_{\text{dyn}} \pi} \tag{6.55}$$

$$M_{\text{load des}} = \frac{M_{\text{wheel}}}{i_{\text{axle}}} \tag{6.56}$$

Controlling the blended hybrid on the HIL test rig required a separate control strategy for each discrete mode of operation (Figure 6.30). A supervisory control scheme switched between driving and braking whenever a negative load torque was commanded. Similarly the controller switched between HST, blended, and hybrid driving using predefined rules based on vehicle velocity and accumulator pressure.

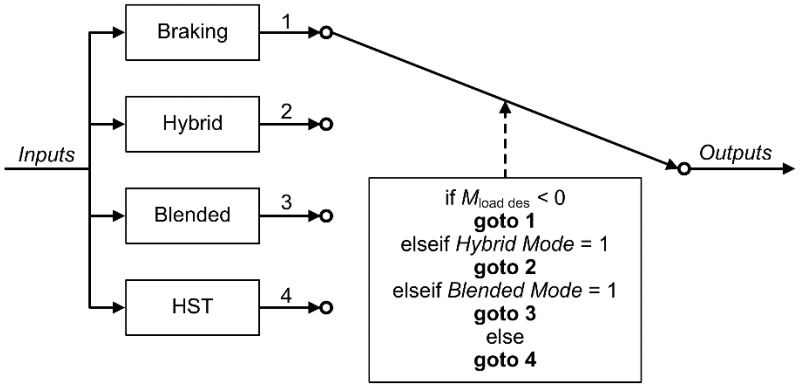

Figure 6.30: Blended hybrid HIL top level control scheme

Hydrostatic Driving

A block diagram of the control strategy used during hydrostatic for the complete HIL test rig is shown in Figure 6.31. A block diagram which shows information transfer through both physical quantities (i.e. speed, torque, flow rate, pressure) and control signals (i.e. commanded speed, torque, and unit displacements) was used to emphasize how control selection (effort or flow) propagates throughout the system.

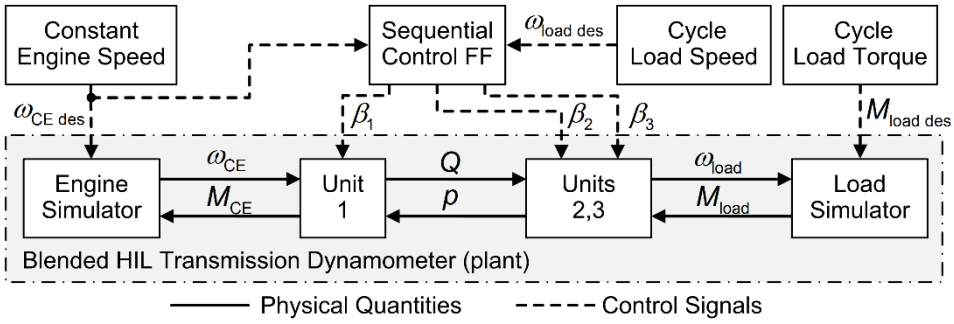

Figure 6.31: HIL hydrostatic driving block diagram

For all modes of operation the engine simulator was placed in a speed controlled mode and commanded to maintain a constant speed. During HST driving Units 1, 2, and 3 were operated in sequential control in order to track the desired vehicle velocity (Eqs. 6.57-6.60).

$$Q_{Unit1\ max} = \omega_{CE\ des} V_1 \eta_{vol} \tag{6.57}$$

$$Q_{\text{Unit2,3 max}} = \frac{\omega_{\text{load des}}\left(V_2 + V_3\right)}{\eta_{\text{vol}}} \tag{6.58}$$

$$\beta_1 = \begin{cases} \dfrac{Q_{\text{Unit2,3 max}}}{Q_{\text{Unit1 max}}} & ;Q_{\text{Unit1 max}} \geq Q_{\text{Unit2,3 max}} \\ 1 & ;Q_{\text{Unit1 max}} < Q_{\text{Unit2,3 max}} \end{cases} \tag{6.59}$$

$$\beta_{2,3} = \begin{cases} 1 & ;Q_{\text{Unit1 max}} \geq Q_{\text{Unit2,3 max}} \\ \dfrac{Q_{\text{Unit1 max}}}{Q_{\text{Unit2,3 max}}} & ;Q_{\text{Unit1 max}} < Q_{\text{Unit2,3 max}} \end{cases} \tag{6.60}$$

During HST driving the control loop placed around speed on the engine simulator was converted into a flow rate by Unit 1 before being converted back into speed at the load simulator by Units 2 and 3. The load simulator was then commanded to resist the torque required by the reference cycle (Eq. 6.56). This resistive torque was converted into pressure by Units 2 and 3 before being converted back into torque at the engine simulator by Unit 1. In this manner flow variables propagated from the power source to the power sink while the effort variables propagated from the power sink to the power source.

Blended Driving

A block diagram of the HIL controller used during blended driving is shown in Figure 6.32.

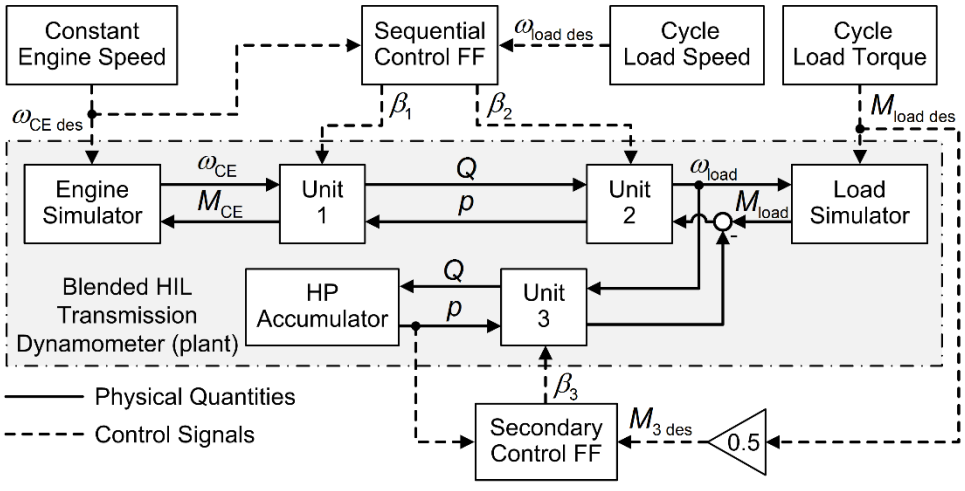

Figure 6.32: HIL blended driving block diagram

During blended driving Units 1 and 2 were operated as before using sequential control to control the load simulator's speed (Eqs. 6.61-6.64).

$$Q_{\text{Unit1 max}} = \omega_{\text{CE des}} V_1 \eta_{\text{vol}} \tag{6.61}$$

$$Q_{\text{Unit2 max}} = \frac{\omega_{\text{load des}} V_2}{\eta_{\text{vol}}} \tag{6.62}$$

$$\beta_1 = \begin{cases} \dfrac{Q_{\text{Unit2 max}}}{Q_{\text{Unit1 max}}} & ;Q_{\text{Unit1 max}} \geq Q_{\text{Unit2 max}} \\ 1 & ;Q_{\text{Unit1 max}} < Q_{\text{Unit2 max}} \end{cases} \tag{6.63}$$

$$\beta_2 = \begin{cases} 1 & ;Q_{\text{Unit1 max}} \geq Q_{\text{Unit2 max}} \\ \dfrac{Q_{\text{Unit1 max}}}{Q_{\text{Unit2 max}}} & ;Q_{\text{Unit1 max}} < Q_{\text{Unit2 max}} \end{cases} \tag{6.64}$$

Likewise the load simulator was controlled to resist the required cycle torque. However Unit 3 was now operated in secondary (torque) control to provide half of the required cycle torque (Eqs. 6.65-6.66).

$$M_{3\,\text{des}} = 0.5 M_{\text{load des}} \tag{6.65}$$

$$\beta_3 = \frac{M_{3\,\text{des}} 2\pi}{V_3 \left(p_{\text{HP}} - p_{\text{B}} \right) \eta_{\text{hm}}} \tag{6.66}$$

The torque provide by Unit 3 to the load simulator reduced the torque required from Unit 2 resulting in a lower torque being propagated back to the engine simulator.

Hybrid Driving

A block diagram of the HIL hybrid driving controller is shown in Figure 6.33. During hybrid driving both Units 1 and 2 were commanded to zero displacement. Because no flow passed between Units 1 and 2 the control loop placed around speed on the engine simulator could no longer propagate to the load simulator as occurred during HST and blended driving. With Unit 3 operating under torque control the load simulator had to be

switched to speed control in order to maintain the control balance between sink and source. While power was still flowing into the load simulator (sinking), the load simulator was now controlled to track the desired vehicle velocity while Unit 3 was controlled to provide the required tractive torque (Eq. 6.67).

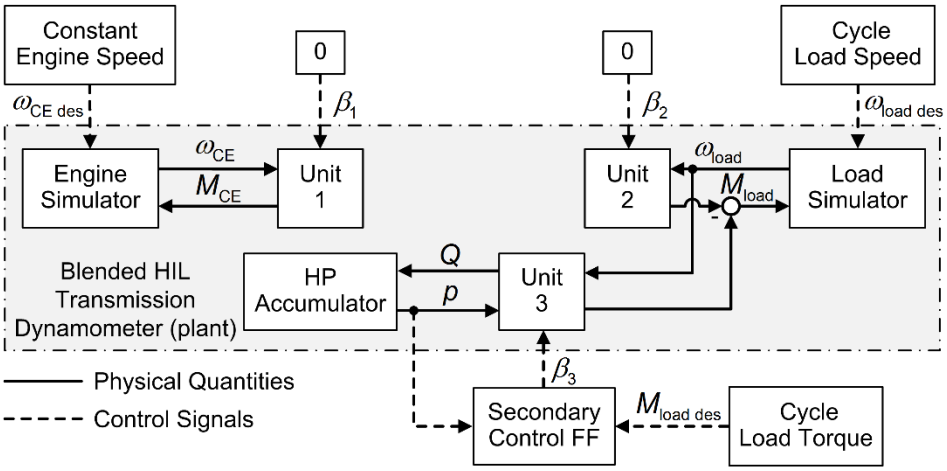

Figure 6.33: HIL hybrid driving block diagram

$$\beta_3 = \frac{M_{\text{load des}} 2\pi}{V_3 \left(p_{\text{HP}} - p_{\text{B}} \right) \eta_{\text{hm}}} \tag{6.67}$$

Braking

While braking Unit 1 was commanded to zero displacement while Units 2 and 3 were controlled to resist the required tractive torque (Eq. 6.68). Once again because Unit 1 was at zero displacement, and Units 2 and 3 were operated under torque control, the load simulator had to be placed in a speed controlled mode with a reference speed defined by the drive cycle. During braking the load simulator becomes the power source provide power to Units 2 and 3 which operate as sinks. A block diagram of the HIL braking control scheme can be found in Figure 6.34.

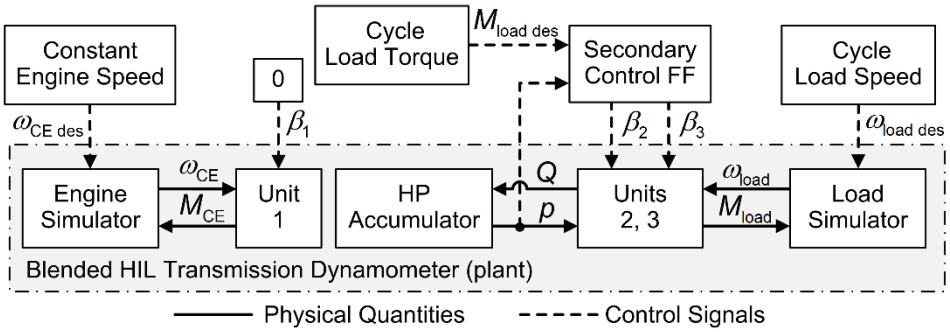

Figure 6.34: HIL braking block diagram

$$\beta_{2,3} = \frac{M_{load\ des} 2\pi}{(V_2 + V_3)(p_{HP} - p_A)\eta_{hm}} \tag{6.68}$$

6.4.3 Measurement Results

Transmission measurements provided some degree of validation to what had previously been only a concept evaluated in simulation. The primary purpose of the HIL test rig was to demonstrate the feasibility of the blended hybrid architecture and to provide a platform for future investigations. For these initial measurements the HIL test rig was controlled to follow a section of the UDDS cycle chosen to highlight the blended hybrid's distinct modes of operation. Further a constant engine speed was commanded in lieu of a more advanced power management strategy. A plot of these measurement results is located in Figure 6.35.

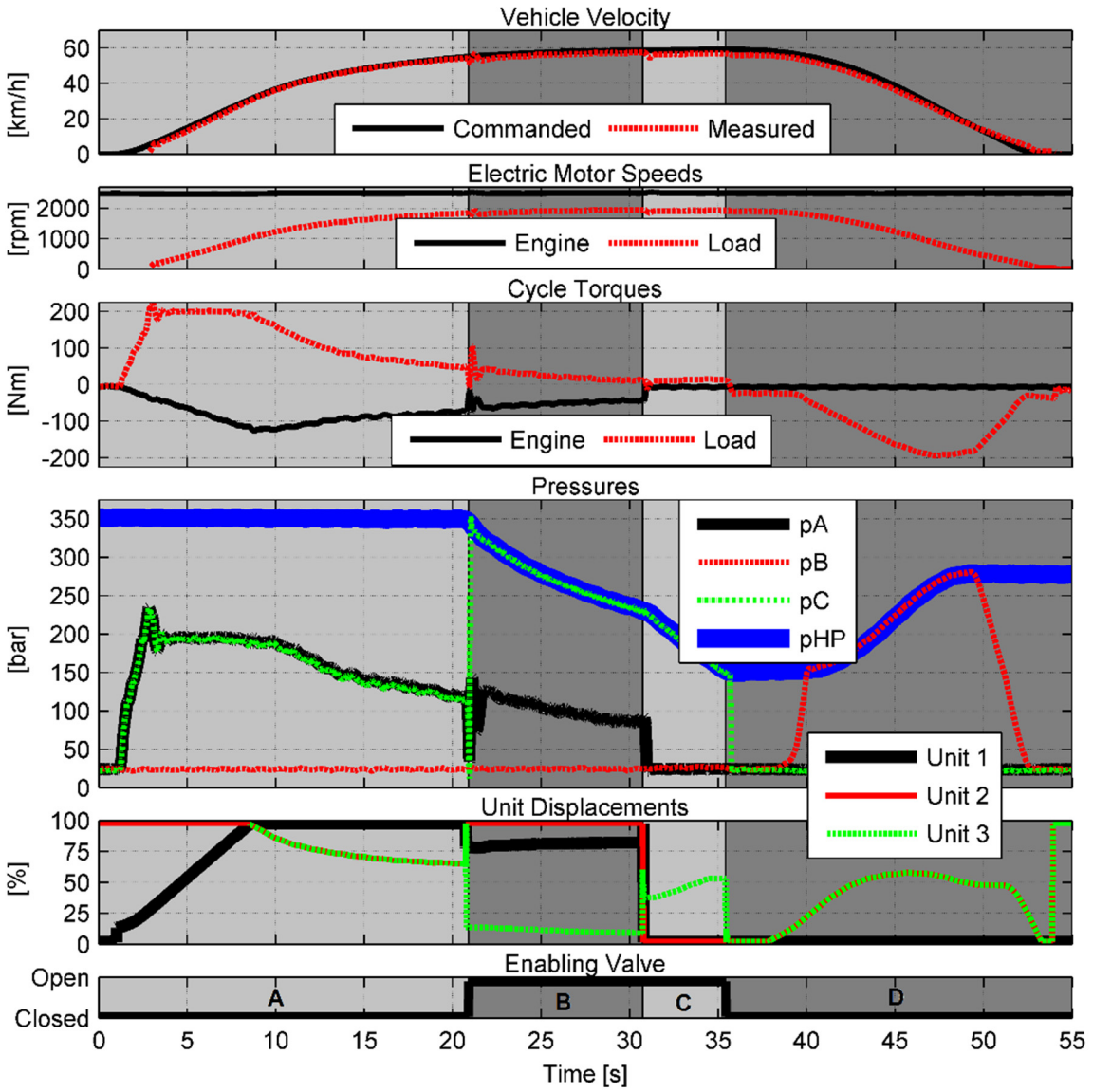

Figure 6.35 Hardware-in-the-loop measurement results

The drive cycle was split into four sections to illustrate the blended hybrid's distinct modes of operation (as denoted by letters in the final plot). First in Section A the transmission was operated as a hydrostatic transmission. Note how Units 2 and 3 operate at the same displacement and the same pressure effectively operating as a single unit.

In Section B the blended hybrid transitioned to blended driving. With the enabling valve open the pressure in Line C increased to that of the HP accumulator. As Unit 1 no longer provided flow to Unit 3 the displacements of Units 1 and 2 changed according to

sequential control in order to maintain the desired vehicle speed. To continue providing half of the required load torque Unit 3 was adjusted to a lower displacement than Unit 2 due to the higher pressure in Line C than Line A.

In Section C the blended hybrid transitioned to hybrid driving. In this mode Units 1 and 2 were commanded to zero displacement and consequently the pressure in Line A dropped to low pressure. Unit 3 was then controlled to provide the entire required load torque.

In Section D the transmission was switched into the braking mode. While Unit 1 remained at zero displacement, the enabling valve was closed and Units 2 and 3 were commanded to provide the required braking torque based on the pressure in the HP accumulator. Note the short dwell between when the enabling valve was closed and Units 2 and 3 were commanded to displace. During this period very little braking torque was required to track the drive cycle as the vehicle was coasting. Once the units began to displace pressure was built up in Line B until the check valve connecting Line B to the HP accumulator opened and the vehicle's simulated kinetic energy was stored in the accumulator. Towards the end of the cycle the pressure in Line B began to drop below the HP accumulator even though Units 2 and 3 were still displaced and the vehicle was moving. This was due to high leakage which occurred in the chosen units when they are operated at very low displacements and high pressures. Specifically Unit 1 leaked significantly during this operation and Unit 2 and 3 were not able to provide sufficient flow to make up for the losses. This issues is not inherent with the blended hybrid architecture and could be remedied by selecting units designed for this condition.

6.5 Chapter Summary

- Chapter 6 detailed an investigation into two novel transmission architectures termed the blended hydraulic hybrid and the blended hydraulic hybrid power split transmission. These architectures seek to address the inherent deficiencies of series hybrids and series hybrid PST's by partially separating power transmission from energy storage yielding a more efficient and higher performing system.

- An energetic analysis was performed on both blended hybrid architectures by optimally controlling each transmission in a compact SUV over a predefined drive cycle. Results from these simulations were compared with a similar study detailed in Chapter 4. In this investigation both the blended hybrid, and the blended hybrid PST achieved higher fuel efficiencies than either conventional mechanical transmission or their respective conventional hydraulic hybrid architectures.

- A steady state optimization of several different transmission architectures provided a deeper insight into the efficient operation of hydraulic hybrid transmissions.

- Two system level control strategies were proposed for the blended hybrid which aimed to reproduce the feel and drivability of conventional vehicles. First a speed controlled approach was presented which used path planning to estimate how a driver intends the vehicle to operate. The advantage of this approach is that it permits the use of speed controlled engines such as those commonly found in off-highway applications. A torque controlled approach was also proposed which closely replicated the operation and feel of a conventional mechanical transmission.

- Two implementable power management strategy were proposed for the blended hybrid with the more effective control strategy yielding a fuel consumption rate within 1.65% of the globally optimal value. An interesting finding was the relative ease of achieving near optimal power management of the blended hybrid especially when compared to the difficulties faced in obtaining effective power management of conventional hydraulic hybrids. This indicates the differences in fuel efficiency between the blended hybrid and conventional hydraulic hybrids estimated in the DP energetic analysis would in fact be greater when implemented in actual vehicles.

- The blended hybrid concept's feasibility was demonstrated through dynamic testing on a hardware-in-the-loop transmission dynamometer.

CHAPTER 7. HARDWARE-IN-THE-LOOP TRANSMISSION DYNAMOMETER

A hardware-in-the-loop transmission dynamometer was used to evaluate the neural network based power management controller presented in Chapter 5 as well as the blended hybrid concept presented in Chapter 6. Chapter 7 details this test rig's physical structure along with its data acquisition and control systems. This same test rig was used for both investigations with only minor changes being made to the hydraulic circuit. In interest of clarity this chapter focuses on the HIL test rig configured to investigate the blended hybrid, though much of the information applies to both configurations.

7.1 Hardware-in-the-Loop Transmission Dynamometer Structure

The HIL test rig was composed of two separate but interconnected subsystems. One subsystem contained the engine and load simulators while the second subsystem contained the transmission being tested. Figure 7.1 shows a schematic of a simplified HIL test rig while a picture of the completed blended hybrid HIL test rig can be found in Figure 7.2.

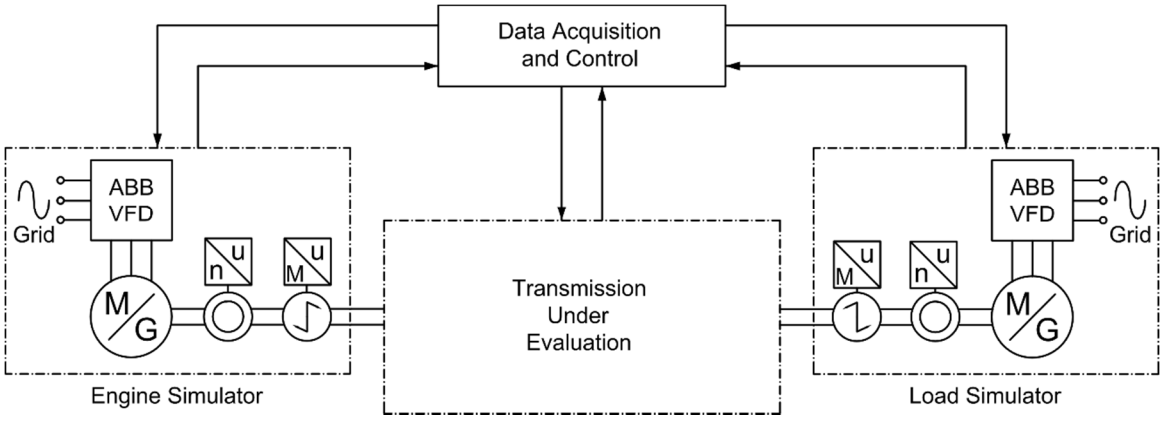

Figure 7.1: Simplified Hardware-in-the-loop transmission dynamometer

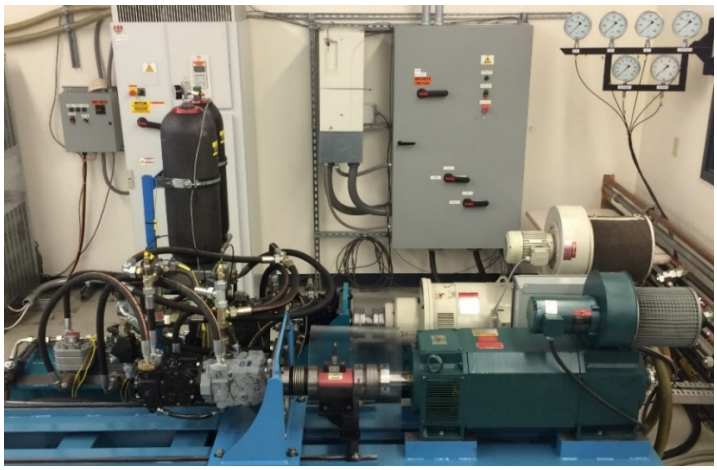

Figure 7.2: Hardware-in-the-loop transmission dynamometer

7.1.1 Engine and Load Simulators

Two electric motor/generators played a key role in simulating the system's virtual components (Figure 7.3). A 126 kW Schenck three-phase induction motor replicated the combustion engine while a 186 kW Baldor Reliance three-phase induction motor mimicked the road loads. The Schenck motor was capable of producing 300 Nm of torque at 4000 rpm (speeds up to 7000 rpm were possible at reduced torque) and was sufficient to fully replicate the reference engine. The Reliance motor was more powerful producing up to 500 Nm of torque at 3600 rpm and was capable of emulating all but the most aggressive driving events.

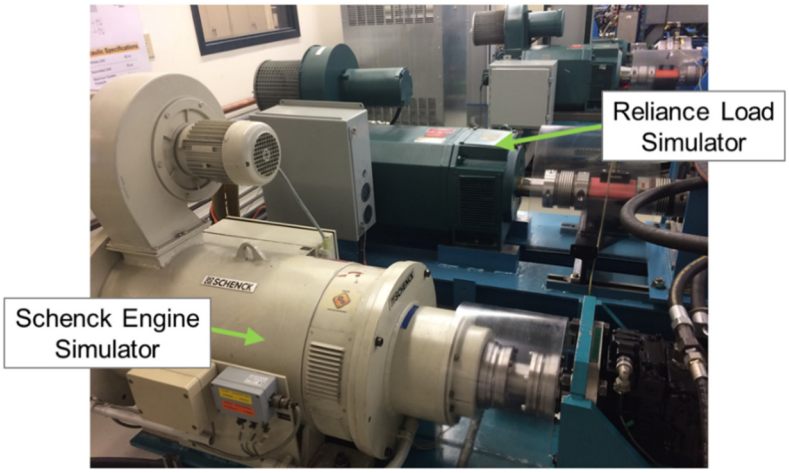

Figure 7.3: Engine and load simulators

The Reliance motor could meet the torque requirements of the road load largely because it was coupled directly to the transmission as opposed to the axle's output shaft. The axle ratio simulated was 3.94:1, meaning the electric motor only had to apply ~25% of the road torque, albeit at a higher speed.

The Schenck engine simulator operated as a typical electric motor, supplying rotational power to the transmission. This is in contrast to the load simulator which operated in two distinct modes. During normal driving the Reliance motor functioned as a generator, serving as a load and removing power for the transmission. Electricity produced by the generator was dissipated in a 4.5Ω resistor rated at 112 kW. The resistor's dissipative capacity created an upper bound for aggressive acceleration events but due to the transmission's size this limit was rarely approached. While braking the Reliance transitioned to a motoring mode and supplied rotational power to the transmission, mimicking the vehicle's inertia. Because the dissipative resistor was no longer in use the Reliance motor could supply up to 186 kW of power to the transmission.

Both electric motors were coupled to individual high performance ABB ACS800 Variable Frequency Drives (VFDs) (Figure 7.4). These drives rectified AC line voltage (460 V) and frequency (60 Hz) to DC before remodulating and sending the resulting AC power to the electric motors. Control over output frequency and voltage enabled the drives to accurately control both the electric motor's speed and torque. The ABB drives had a speed control accuracy of 0.01% and 0.1% of nominal speed for static and dynamic cases respectively. In torque control mode the drives were capable of a 0-100% torque step in <5 ms with an accuracy of 1% of nominal torque. Further integrated control algorithms enabled smooth transitioning between speed and torque control modes while under load. These features yielded in a highly capable HIL transmission dynamometer able to accurately replicate the loads present in an on-road vehicle.

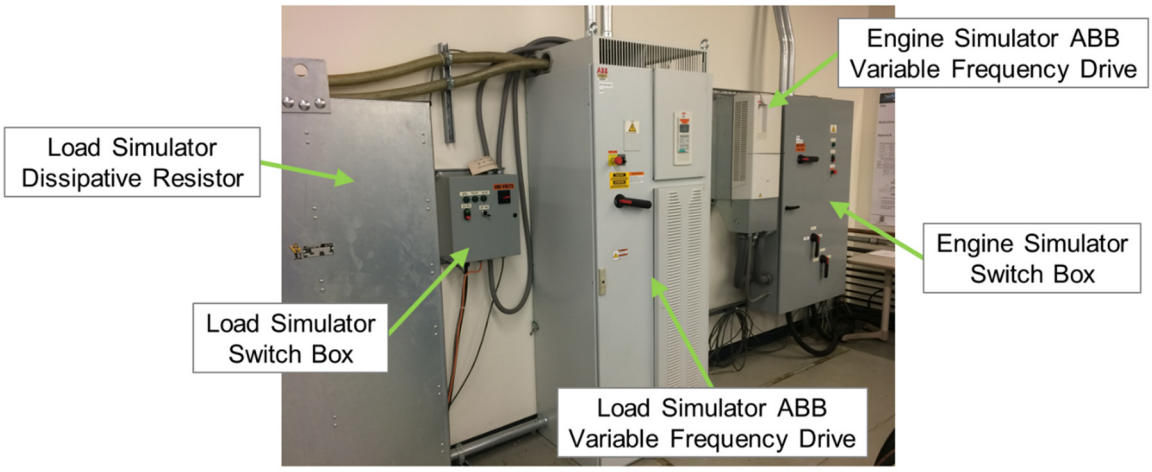

Figure 7.4: Engine and load simulator power electronics

7.1.2 Evaluated Transmission

The primary physical difference between the series and blended hybrids transmissions implemented on this test rig were the hydraulic circuits (series hybrid: Figure 5.9, blended hybrid: Figure 6.29) used to connect together the various hydraulic components. For both architectures the same hydraulic components were employed. Hydraulic Units 1, 2, and 3 were 42 cc/rev Sauer S90 swashplate style positive displacement machines (Figure 7.5). These units were rated to 4200 rpm and 450 bar with through shafts enabling Units 2 and 3 to be connected in tandem.

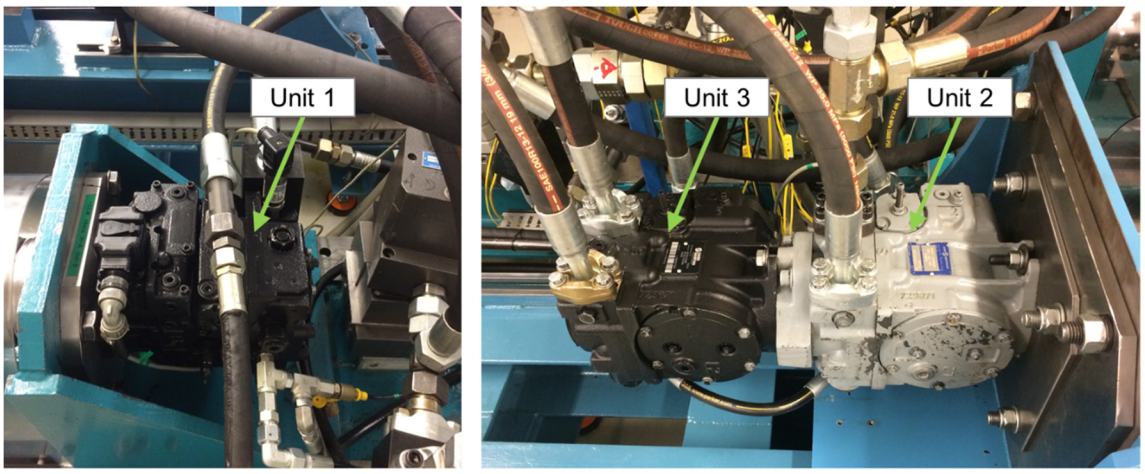

Figure 7.5: Hydraulic Units 1, 2, and 3

Both the high and low pressure accumulators were HYDAC bladder type accumulators (Figure 7.6). Both accumulators had an effective gas volume of 18.4 l with a precharge of 10 and 130 bar for the low and high pressure accumulators respectively. The rated maximum operating pressures for low and high pressure accumulators was 260 and 420 bar respectively.

Figure 7.6: High and low pressure accumulators

Flow for the low pressure system, cooling, and filtration was provided by an external hydraulic power supply (Figure 7.7).

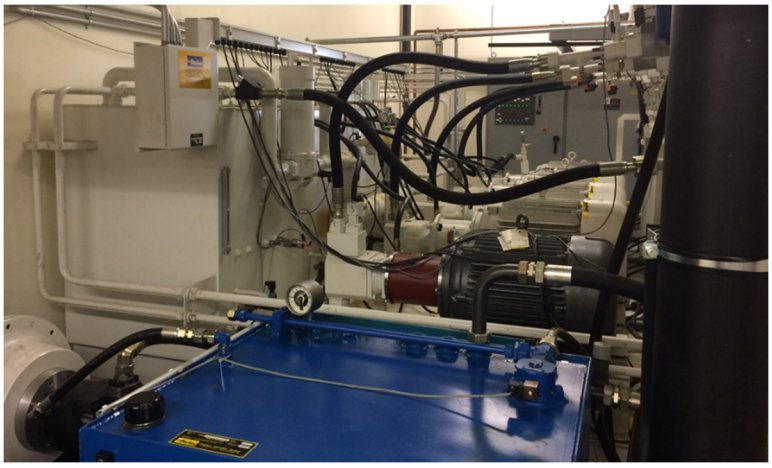

Figure 7.7: External hydraulic power supply

7.2 Instrumentation, Data Acquisition, and Control

To fully characterize the hybrid transmission under evaluation a number of sensors were included on the HIL test rig. With the exception of several pressure, temperature, and speed sensors none of this instrumentation would be required in an actual vehicle. Data acquisition and control was carried out using a National Instruments cRIO controller. This controller featured a modular design allowing the system to be fully customized with up to eight input/output cards. A list of the DAQ cards used is located in Table 7.1.

Table 7.1: National Instruments controller information

NI cRIO-9074	Controller
NI 9213	16 channel thermocouple input
NI 9201 x2	8 channel analog voltage input
NI 9269 x2	4 channel analog voltage output
NI 9265	4 channel analog current output
NI 9474	8 channel digital output
NI 9481	4 channel SPST relay

NI Veristand software was coupled with the NI cRIO hardware to complete the data acquisition and control package. NI Veristand enabled controller development in the MATLAB Simulink environment. Once a controller was developed in Simulink it could be uploaded onto the cRIO controller through Veristand. Once on the cRIO, the Simulink controller read in measured values and output control signals to various analog and digital outputs. The cRIO also had the advantage of dedicated embedded hardware for data acquisition and control. This embedded architecture ensured a consistently high cycle frequency to enable real time control. Real time refers to systems capable of reading, calculating, and acting on system inputs in a sufficiently short time such that the control system's performance is not limited by the cycle frequency of the controller. For the HIL test rig a cycle frequency of 100 Hz proved to be sufficient. A simplified wiring schematic for the HIL data acquisition and control system is shown in Figure 7.8.

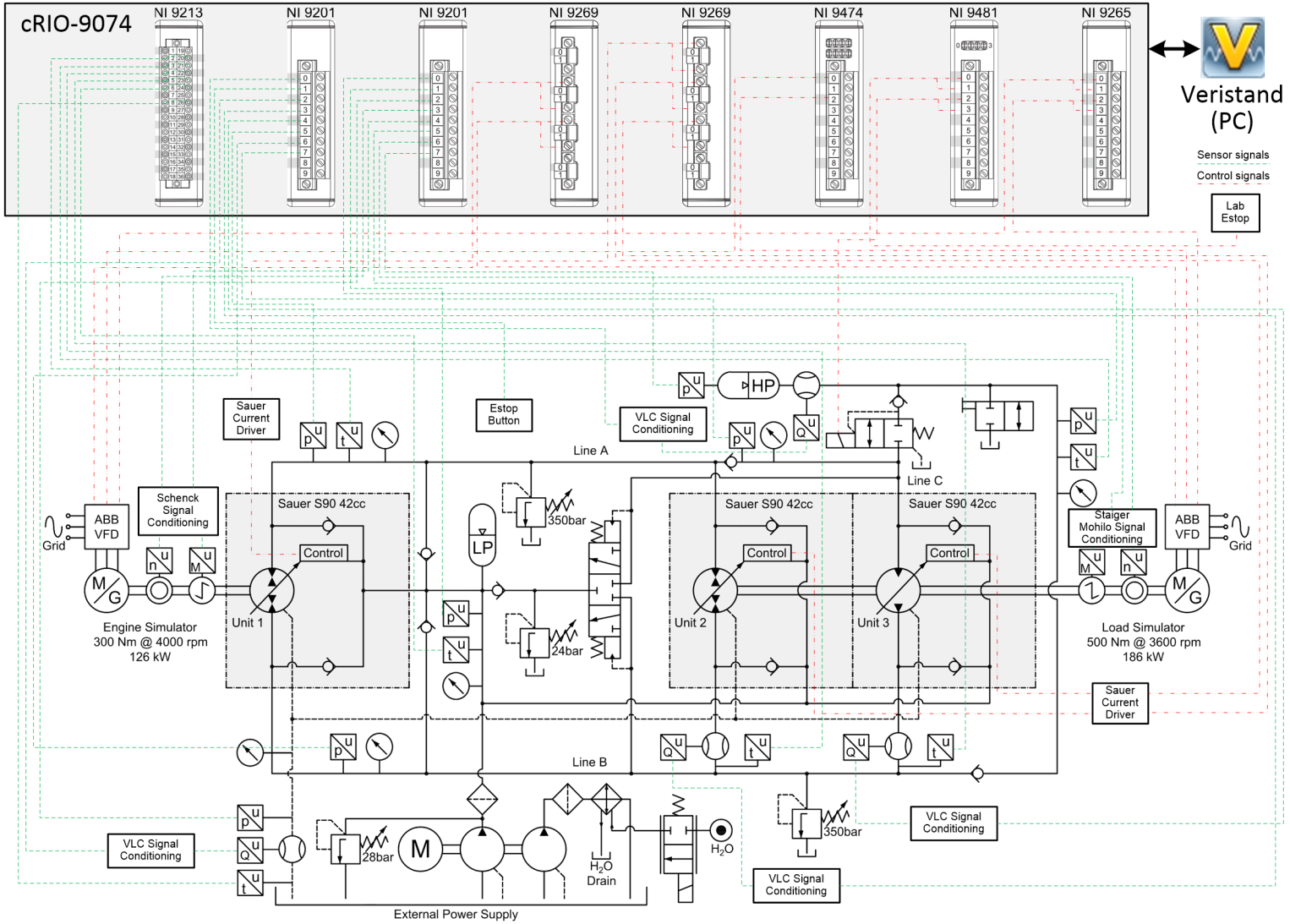

Figure 7.8: Blended HIL data acquisition and control wiring schematic

Most of the data acquisition and control equipment was contained in a room adjacent to the HIL transmission dynamometer. A picture of the control room can be seen in Figure 7.9.

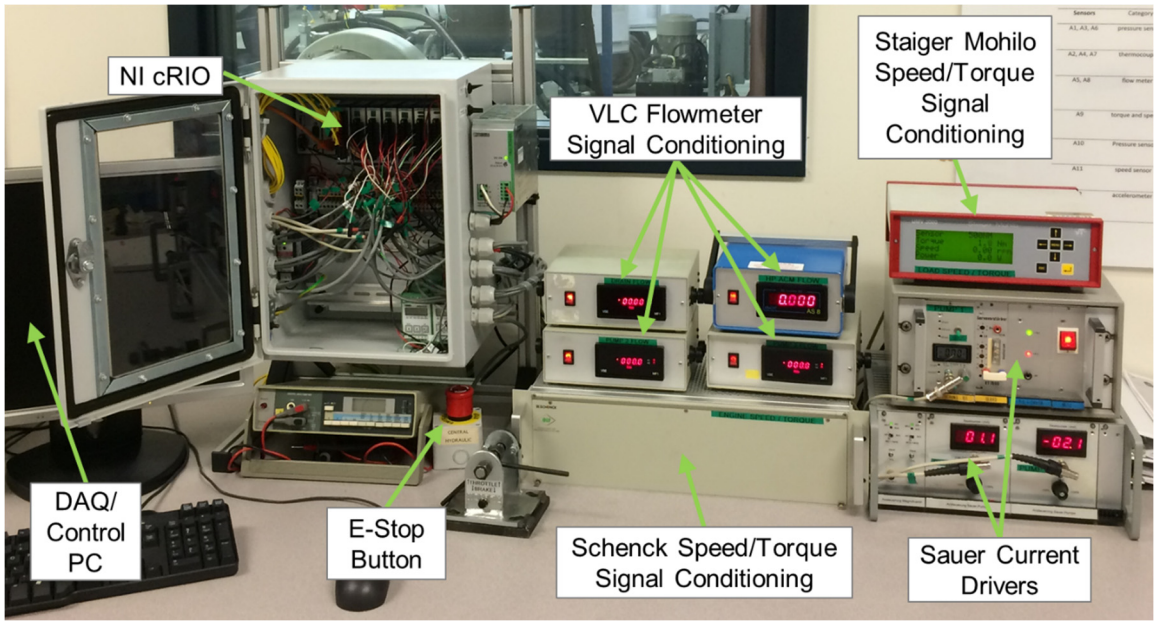

Figure 7.9: HIL transmission dynamometer control room

A significant amount of power was contained within the HIL test rig and controlled by the cRIO controller. If care was not taken a poorly scaled or timed control signal could damage or destroy both the HIL test rig and the transmission. In interest of safety, and to protect valuable components, a fault detection system was implemented. This system monitored a variety of sensor inputs including speeds, torques, pressures, flows, and temperatures and compared them against limit values. If one of the parameters fell below or exceeded a limit value then the fault detection system would trigger a lab wide emergency stop. In addition to safety shutting down both electric motors and the external hydraulic supply, the emergency stop closed the transmission's enabling valve thereby confining the high pressure accumulator's energy.

CHAPTER 8. BLENDED HYBRID DEMONSTRATION VEHICLE

Despite all of the modeling, simulations, optimizations, and hardware-in-the-loop validations which have been conducted up until this point, driver experience has yet to be investigated for the blended hybrid concept. The only way to explore this highly subjective experience was to build a blended hybrid demonstration vehicle. It must be noted that the design, optimization, and construction of this demonstration vehicle was a highly collaborative effort between many members of the Maha Fluid Power Research Center including this author. Tyler Bleazard led the effort and detailed much of the work in his master's thesis (Bleazard, 2015). In interest of brevity only an overview of the design and construction of the blended hybrid demonstration vehicle is included in this work.

8.1 Vehicle Platform

A 1999 Land Rover Range Rover (Figure 8.1) served as a platform for implementing the blended hybrid. This SUV was selected with regards to several considerations including among others ample seating for four evaluators, large quantities of available kinetic energy during braking, and a relatively spacious packaging environment. Select parameters for the base vehicle are given in Table 8.1.

Table 8.1: Select vehicle parameters

Engine:	142 kW @ 4750 rpm	Axle ratio:	3.54:1
Engine:	320 Nm @ 2600 rpm	Tire rolling radius:	0.358 m
Fuel:	Gasoline	Frontal area:	2.78 m^2
GVM:	2780 kg	Drag coefficient:	0.4

Figure 8.1: Blended hybrid demonstration vehicle

8.2 Blended Hybrid Conversion

Designing a blended hybrid transmission for an actual vehicle required taking more practical considerations into account than were required for simulation or HIL testing. First the existing vehicle used a full time four wheel drive configuration. To replicate this functionality both Units 2 and 3 could be connected to the existing transfer case/ center differential. Alternatively each unit could be connect to its own axle. Due to packaging constraints, and to demonstrate that a center differential was unnecessary, Unit 2 was connect to the rear axle while Unit 3 was connect to the front axle. Another practical consideration was the safe operating speed range of a moderately sized swashplate style hydraulic unit for Unit 1. In mobile applications hydraulic units are typically coupled to diesel engines which generally operate at substantially slower speeds than gasoline engines. In order to safely operate Unit 1 at the engine's maximum power point located at 4750 rpm, a speed reducing pump drive (i.e. gear box) with a ratio of 1.48:1 was added. Reducing Unit 1's speed also had the advantage of improving NVH (Noise, Vibration, Harshness) through lower noise generation. A schematic of the modified blended hybrid architecture can be found in Figure 8.2.

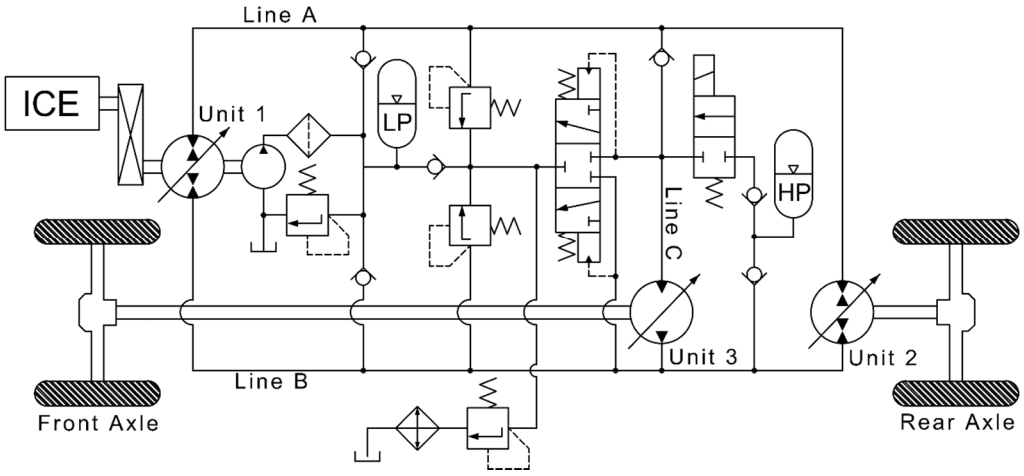

Figure 8.2: Four wheel drive blended hybrid architecture

Ensuring a high quality transmission sizing was of great importance given the considerable effort which went into constructing the demonstration vehicle. A good transmission sizing balances fuel efficiency with performance and driver perception. It would be a mistake to maximize fuel efficiency at the expense of poor vehicle performance, especially when one of the purposes of the demonstration vehicle was to showcase the technology to those unfamiliar with hydraulic hybrids. Transmission sizing began by instrumenting and baselining the existing vehicle to determine performance metrics such as acceleration. Next a large scale design of experiments was conducted by Bleazard where various combinations of hydraulic unit sizes, high pressure accumulator volumes, and high pressure accumulator precharges were evaluated (Bleazard et al., 2015) along the UDDS cycle. Dynamic programming was once again used to eliminate the influence of control on fuel efficiency thereby ensuring a fair comparison. Further dynamic simulations were run for each design combination evaluating their acceleration performance. Any design which did not meet or exceed the baseline vehicle's performance was discarded. After evaluating 735 design combinations an optimal compromise between efficiency and performance was chosen (Table 8.2).

Table 8.2: Select transmission parameters

Unit 1:	100 cc/rev	Max pressure:	450 bar
Unit 2,3:	75 cc/rev	HP accumulator effective gas volume:	32 l
Charge:	27 cc/rev	LP accumulator effective gas volume:	40 l
Low pressure:	30 bar	HP accumulator precharge:	130 bar

Modifications to the demonstration vehicle began by removing the existing automatic transmission, transfer case, and gas tank. Next a CAD model was created of the vehicle's underbody to define packaging constraints. This allowed components to be arranged in the CAD model and also enabled supporting structures to be designed. The finalized CAD model is shown in Figure 8.3. Ultimately only the low pressure accumulator had to be placed in the passenger compartment (behind the rear seats), all others components were fit under the vehicle.

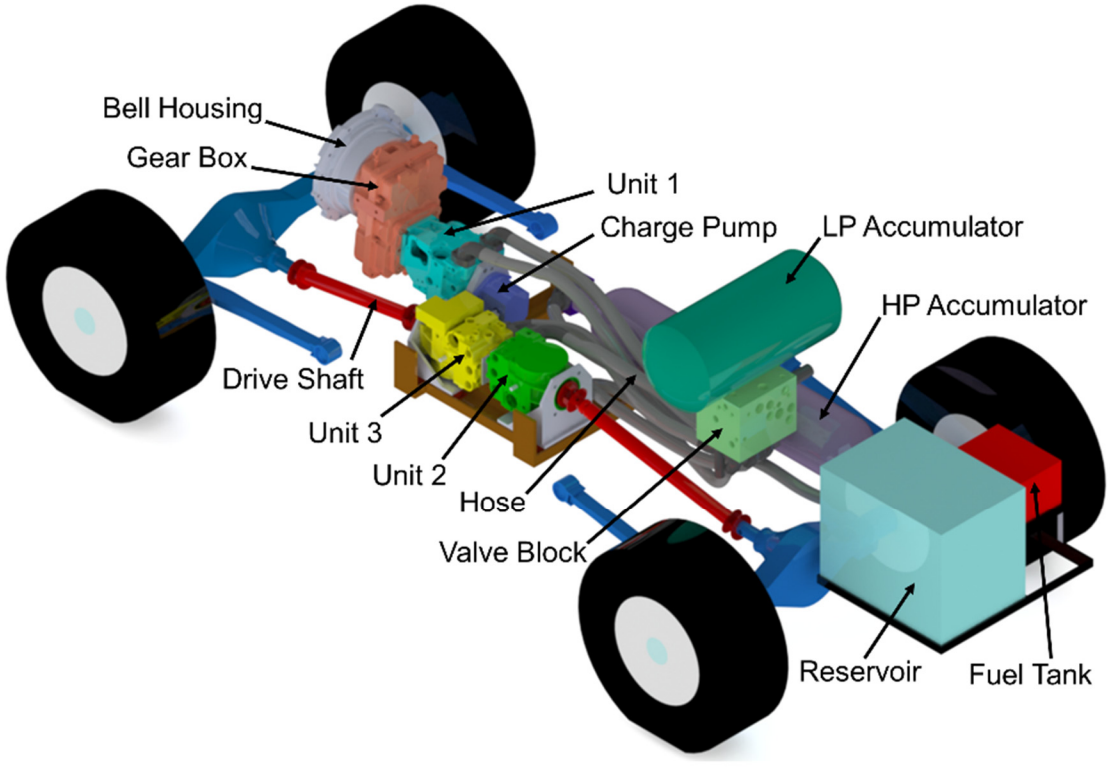

Figure 8.3: Vehicle CAD packaging

In order to create a clean and compact packaging, a valve block was designed to hold all of the system's valves as well as a majority of the component interconnections (Figure 8.6). A CAD model of the valve block is shown in Figure 8.4.

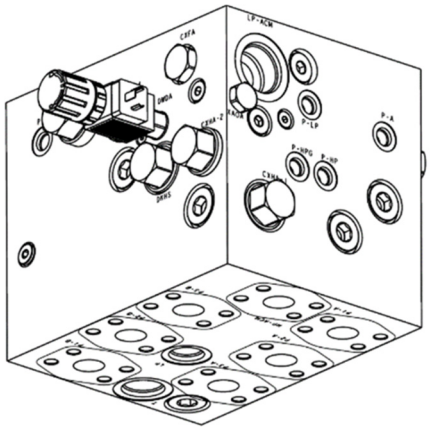

Figure 8.4: Valve block

The valve block was mounted to two transverse supporting structures attached to the vehicle's frame rails. A vibration isolating pad was sandwiched between the transverse supporting structures and the valve block to minimize NVH. A picture of the installed valve block can be seen in Figure 8.5.

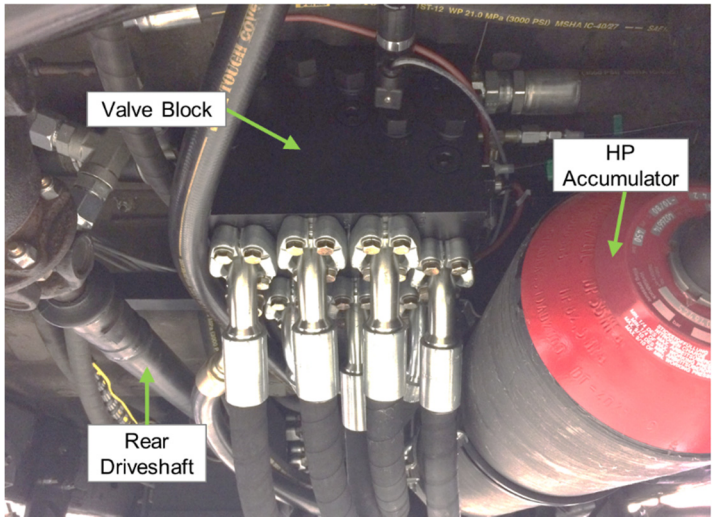

Figure 8.5: Installed valve block

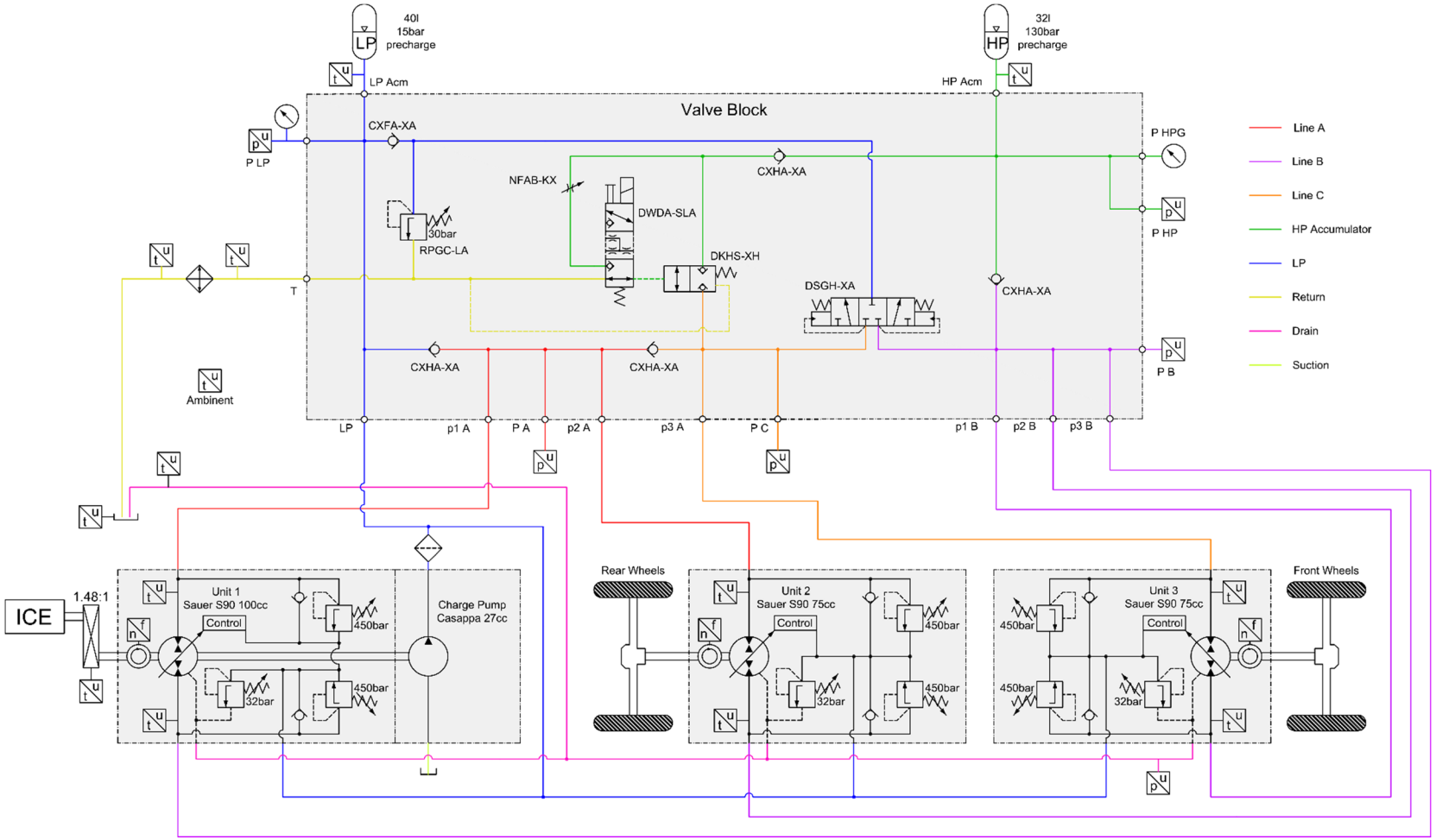

Figure 8.6 Demonstration vehicle hydraulic circuit

The pump drive, Unit 1, and the charge pump form the primary assembly which extracts power from the engine. In order to couple this assembly to the engine a custom bell housing and adapter plate were designed and fabricated. This adapter plate coupled the engine's existing flywheel with a flex plate provided by the pump drive manufacturer. Additionally this adapter plate was designed with external teeth which were sensed by a hall effect sensor providing speed feedback to the engine speed controller. A custom adapter plate was also designed and fabricated in order to connect the charge pump to Unit 1. An exploded CAD render of this assembly is shown in Figure 8.7.

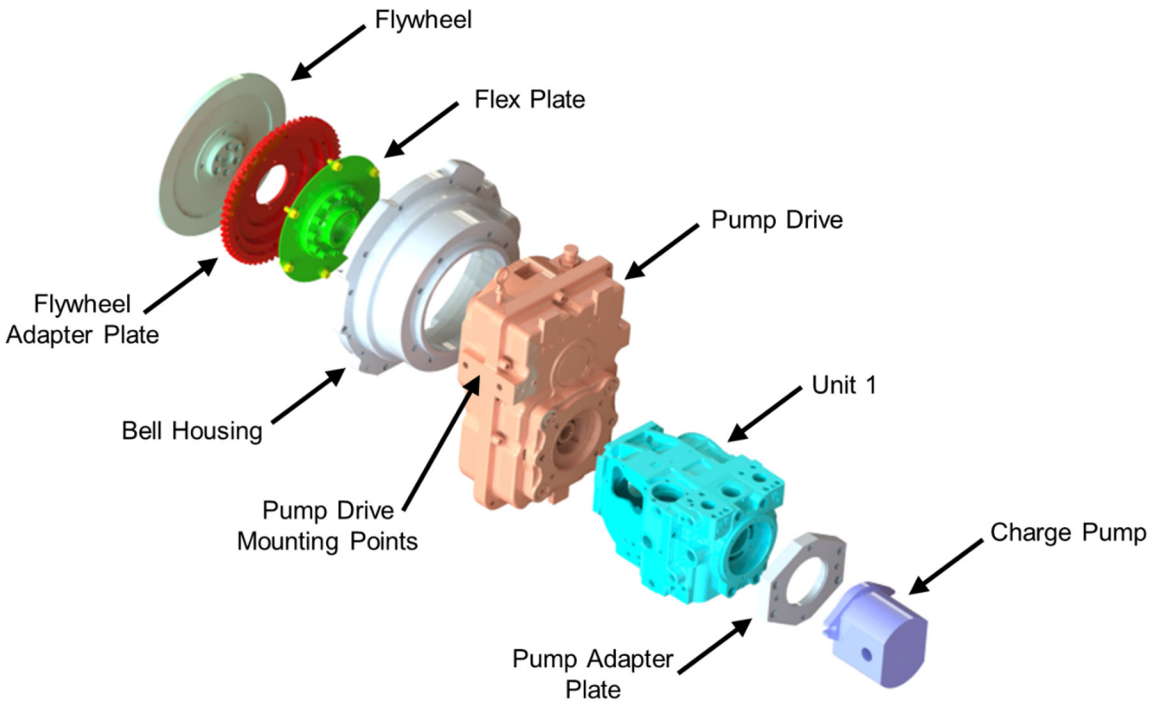

Figure 8.7: Pump drive, unit 1, charge pump assembly

The demonstration vehicle's original powertrain was supported by two longitudinally symmetric mounting points located below the engine (which were kept) and two longitudinally symmetric mounting points located below the transmission (which were removed). In order to support the new powertrain, mounting brackets were fabricated to connect the pump drive the vehicle's frame. Vibration isolators were included in the mounting structure to minimize NVH and provide some flex within the system.

Units 2 and 3 were supported by a custom structure which was connected to the vehicle's primary frame rails. Custom mounts were designed and fabricated which supported both units by their mounting flanges. These unit mounts were then connected to the frame by a series of four vibration isolators. The front end of the high pressure accumulator was mounted above this frame using a strap mount while the rear of the accumulator was attached to a transverse supporting member shared by the valve block. An exploded view of this assembly can be seen in Figure 8.8.

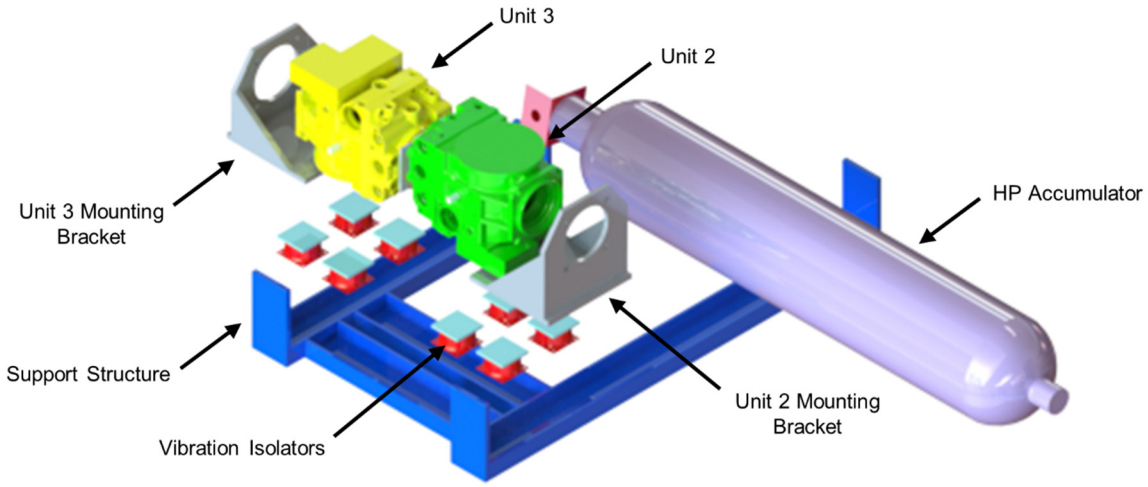

Figure 8.8: Units 2 and 3 assembly

An early picture of Units 2 and 3 installed in the vehicle can be found in Figure 8.9.

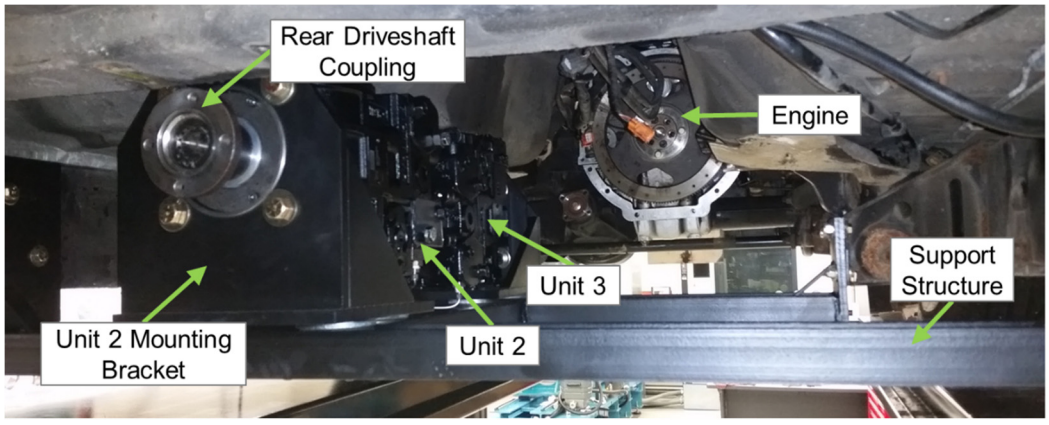

Figure 8.9: Units 2 and 3 installed

Custom drive shafts were required to link the hydraulic units to the axles. Figure 8.10 shows the driveshaft at the suspension's extreme high and low points.

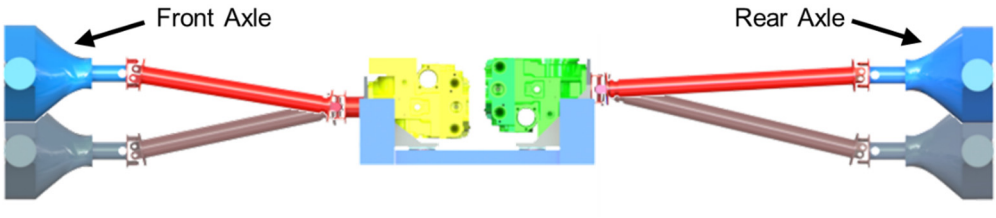

Figure 8.10: Driveshafts

The low pressure accumulator was the only hydraulic component which did not fit underneath the vehicle and had to be placed in the rear of the passenger compartment (Figure 8.11).

Figure 8.11: Low pressure accumulator

Both the hydraulic oil reservoir and modified fuel tank were placed in a cavity previously occupied by the spare tire. A small fuel tank was chosen to enable gravimetric fuel consumption measurements (i.e. measuring net fuel mass before and after a drive cycle). To facilitate these measurements a no spill quick disconnect was installed between the fuel tank and fuel line. A picture of the reservoir and fuel tank (which can be accessed through the trunk) is included in Figure 8.12.

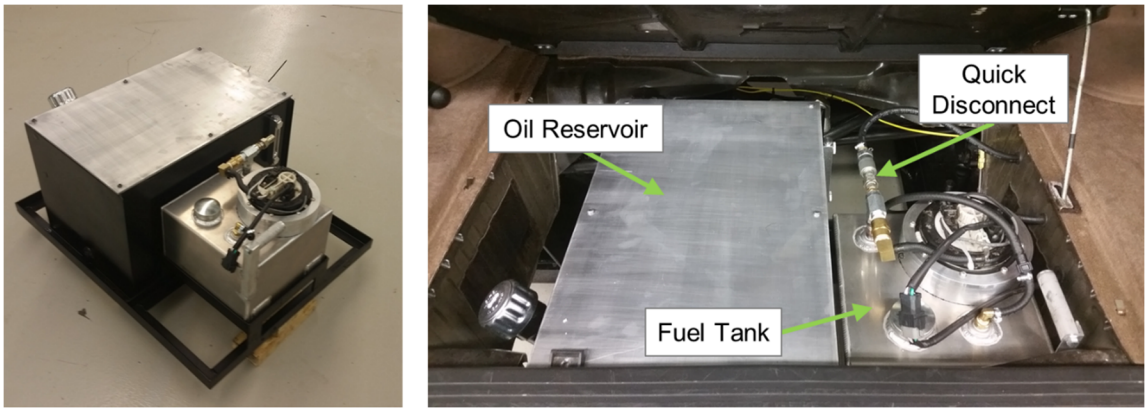

Figure 8.12: Hydraulic oil reservoir and fuel tank

A hydraulic oil cooler was placed in the engine compartment in front of the engine radiator (Figure 8.13). A single speed fan on the oil cooler was controlled by the transmission controller allowing moderate control over oil temperature.

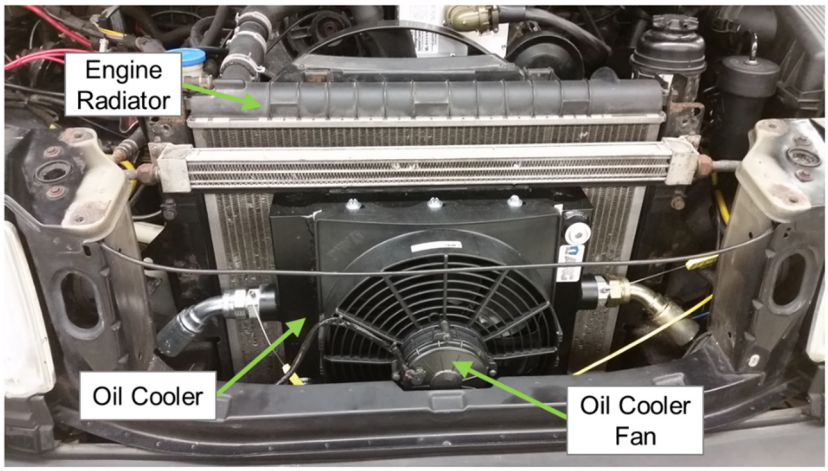

Figure 8.13: Hydraulic oil cooler

A picture of the completed demonstration vehicle's underbody can be seen in Figure 8.14.

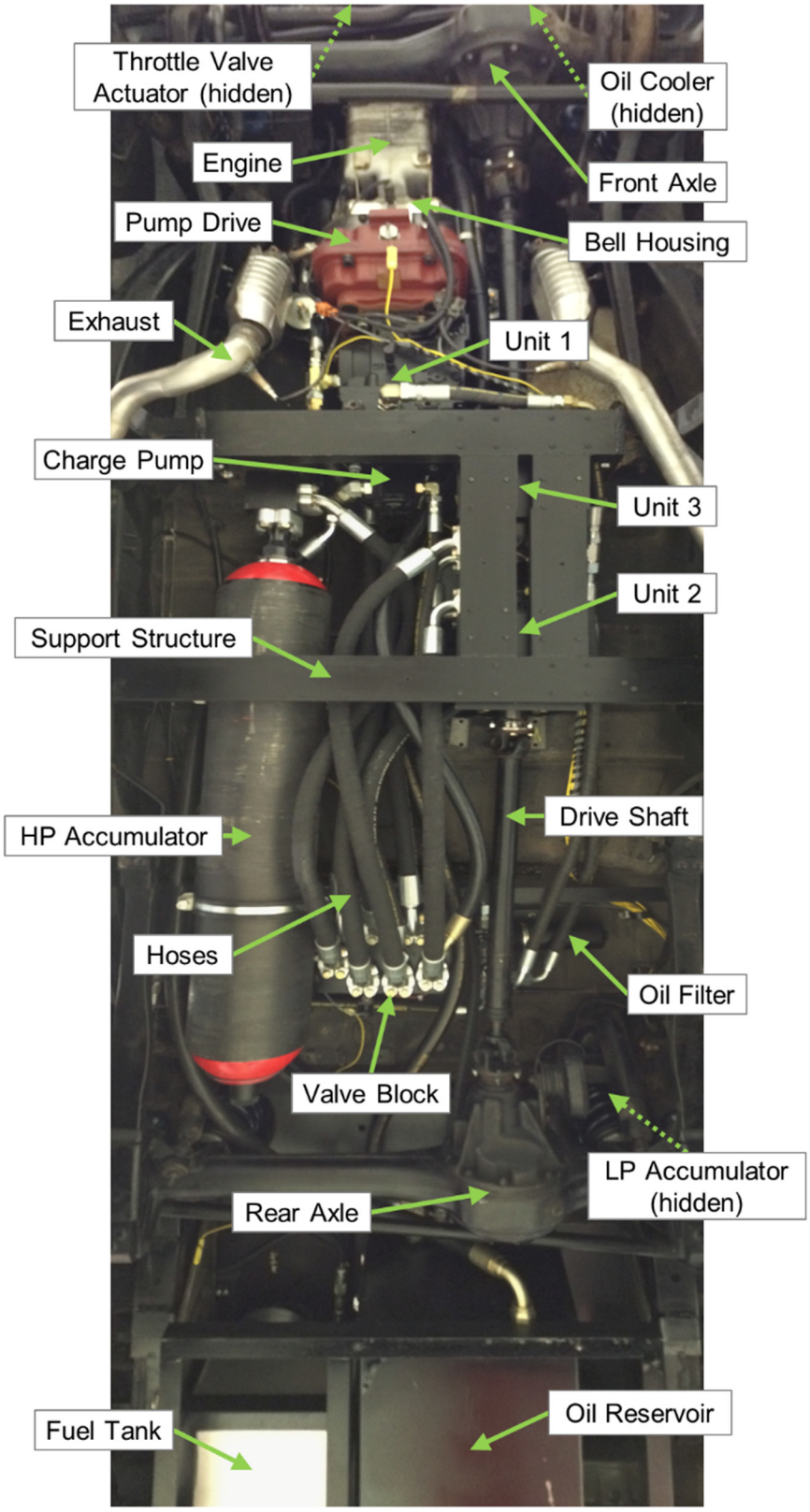

Figure 8.14: Demonstration vehicle underbody

8.3 Instrumentation, Data Acquisition, and Control

Sensors and actuators installed throughout the demonstration vehicle provided means for the driver and transmission controller to interact with the powertrain. A National Instruments CompactRIO system connected the various sensors and actuators together and provided real time powertrain control along with data acquisition. A simplified wiring schematic of the DAQ and control system can be found in Figure 8.15.

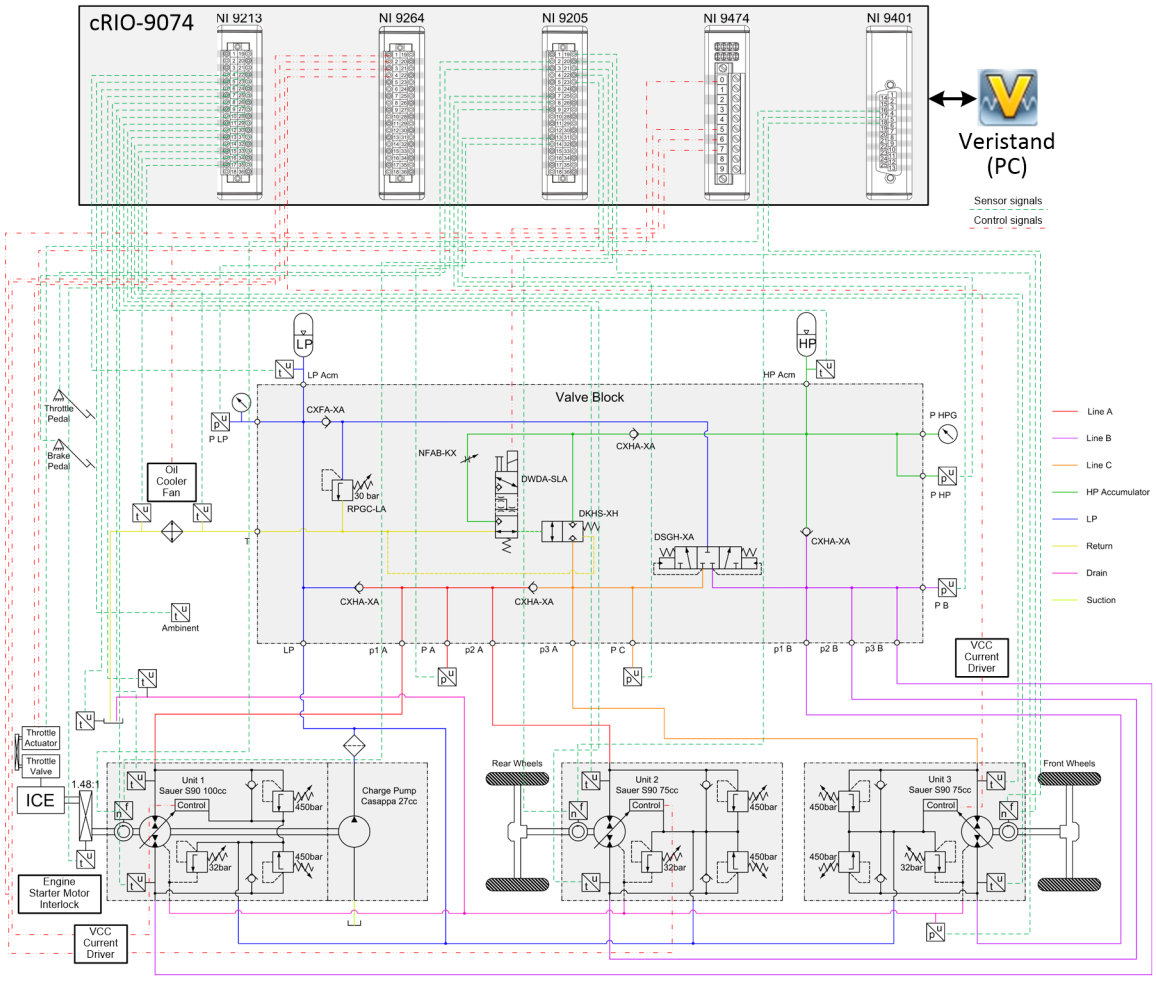

Figure 8.15: Data acquisition and control wiring schematic

The cRIO along with various terminals, relays, and current drivers (for the swashplate control valves) were contained in an enclosure located in the vehicle's trunk (Figure 8.16 left). Various fuses, a 12-24V power converter, and a Wi-Fi router used to connect to the cRIO were also located in the trunk (Figure 8.16 right).

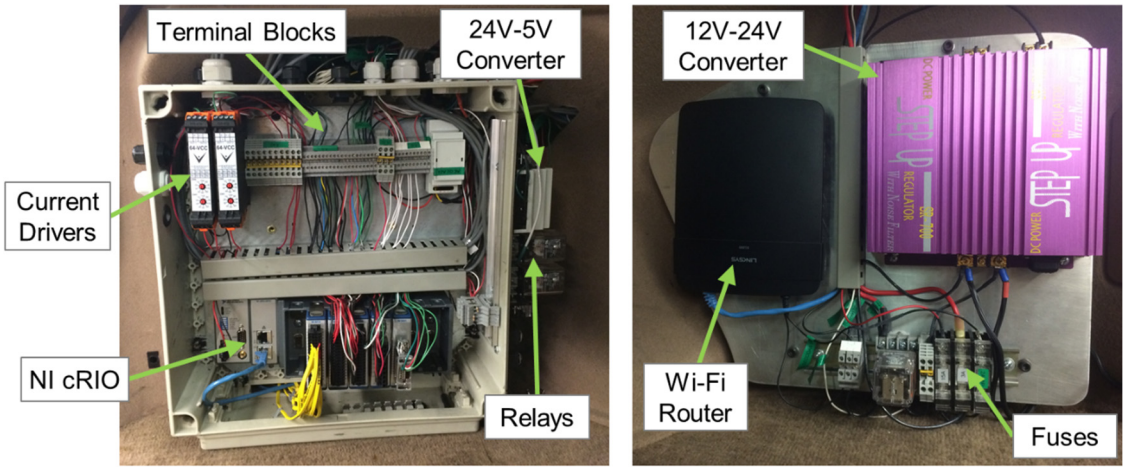

Figure 8.16: Controller enclosure

While cranking (i.e. starting) an engine the starter motor pulls a significant amount of current causing any connected battery's voltage to drop. To prevent this voltage drop from interfering with the controller a separate 12V battery was installed for the data acquisition and control system. A battery separator was installed which connected the two batteries together anytime a voltage of at least 13.5V was sensed across the primary battery enabling the auxiliary battery to be charged by the alternator. This minimum 13.5V was generated by the alternator and would be present as long as the primary battery was sufficiently charged. A schematic of the wiring diagram for both batteries as well as various other components is included in Figure 8.17.

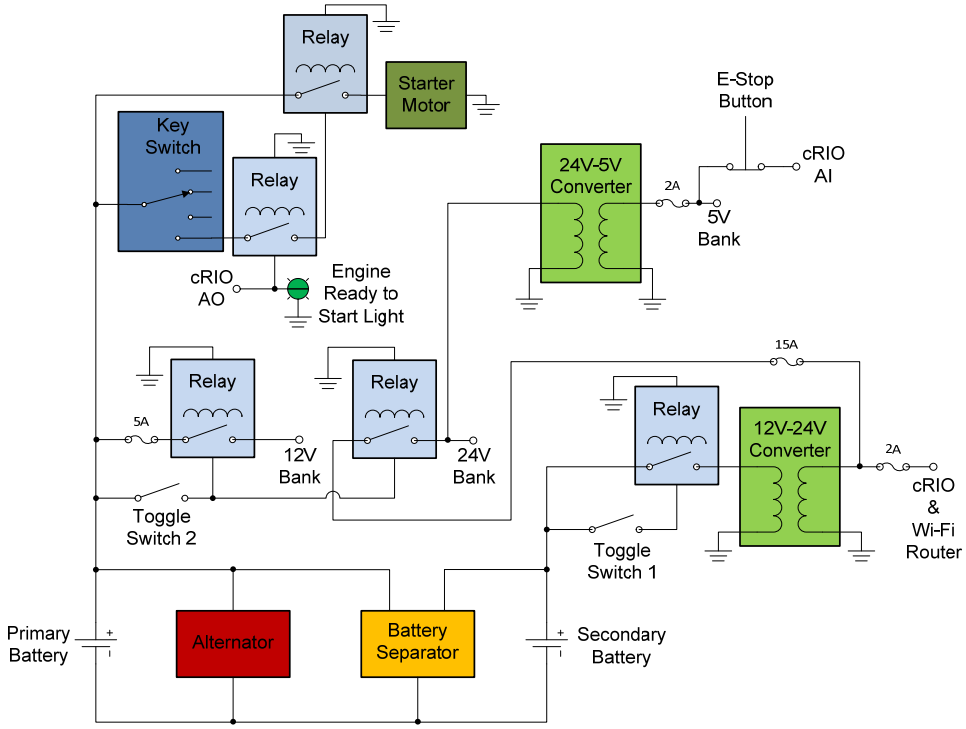

Figure 8.17: Electrical wiring diagram

An instrument panel installed in the center console displayed important information as well as provided the driver with several inputs into the controller (Figure 8.18). Included in this console were physical gages displaying the current pressure in both the low and high pressure accumulators, as well as a light indicating the controller was loaded and the vehicle was ready to start. Also included in the console were switches controlling power to the sensors and controller, an E-stop button, and a three position rocker switch for forward, neutral, and reverse.

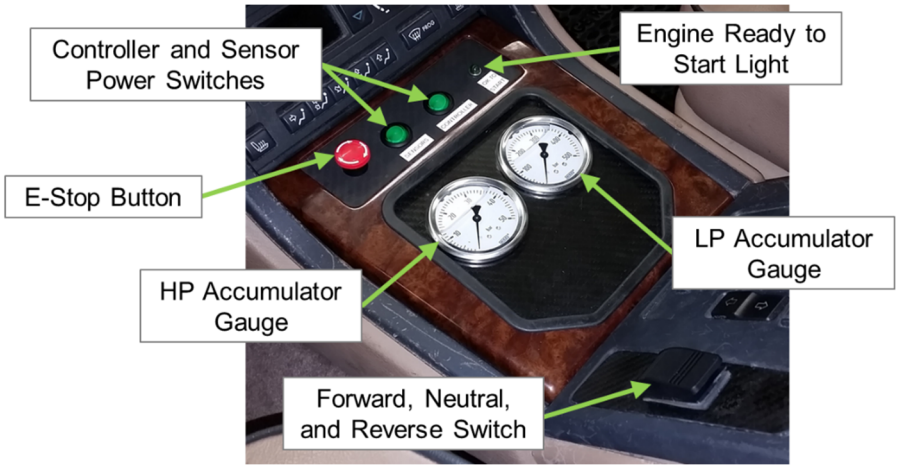

Figure 8.18: Instrument panel

Driver input to the powertrain was provided primarily though the throttle and brake pedals. In order to realize the blended hybrid concept it was necessary to move to a throttle and (partial) brake by wire system. This conversion began by adding linear potentiometers to measure the position of both pedals (Figure 8.19).

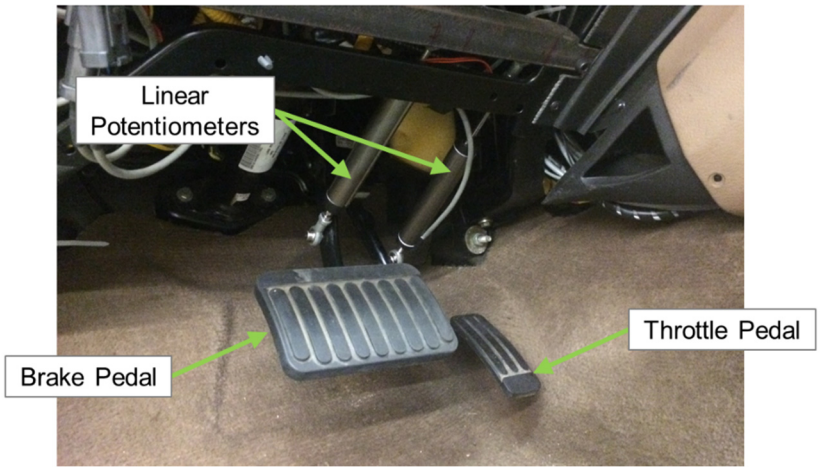

Figure 8.19: Throttle and brake pedals

In interest of safety a full brake by wire system was not implemented. Instead the brake pedal mechanism was modified to enable additional pedal travel which was sensed purely electronically and used as a control input for the regenerative braking system. This additional pedal travel was achieved by adding a prismatic joint to the existing revolute joint between the pedal arm and master cylinder's pushrod. Once modified the brake

pedal could travel 35% of its rotation before beginning to act on the master cylinder which then proportionally actuated the existing dissipative friction brakes. A CAD render of the original and modified brake pedals can be found in Figure 8.20.

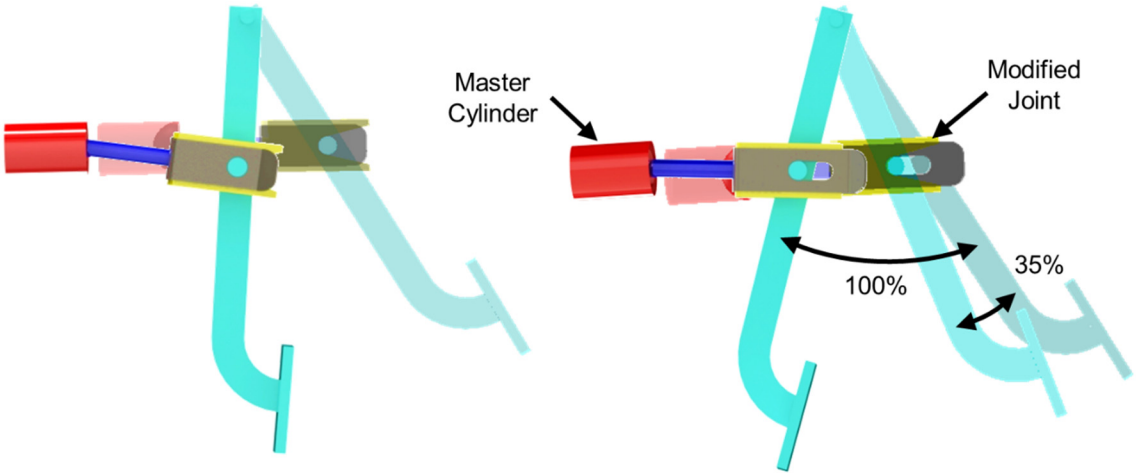

Figure 8.20: Original (left) and modified (right) brake pedals

In order to achieve a throttle by wire system the push-pull cable linking the throttle pedal to the throttle valve was removed. In its place an actuator was installed to actuate the throttle valve. Contained within this throttle actuator was a sensor and position controller which took in a normalized reference angle from the cRIO controller and adjusted the throttle valve in a closed loop position control mode.

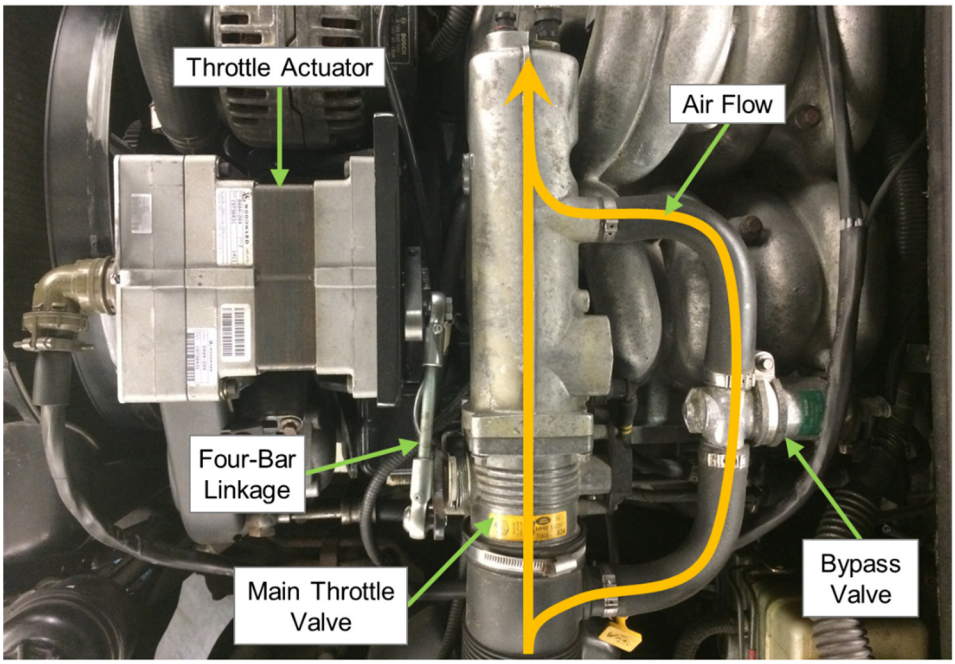

Figure 8.21: Throttle actuator

Though specifically designed as a throttle actuator, the actuator only possessed a range of motion of 0-75 degrees. In order to achieve the requisite 0-90 degree motion a four-bar linkage was designed to couple the throttle actuator and throttle valve (Figure 8.22).

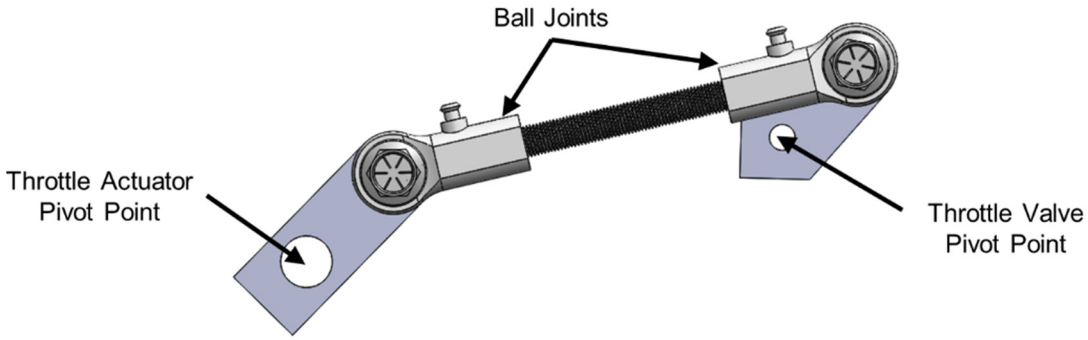

Figure 8.22: Throttle actuator/valve four-bar linkage

8.4 Blended Hybrid Control

In prior work by Bleazard and this author the path planning approach presented in Section 6.3.3 was implemented and evaluated on the blended hybrid demonstration vehicle

(Bleazard, 2015 and Sprengel et al., 2015). While the path planning controller worked relatively well, its reliance on an accurate vehicle dynamics model to estimate the driver's desired vehicle speed was not ideal. In this work the torque controlled approach described in Section 6.3.4 was implemented in the demonstration vehicle. This approach has the advantage of more closely replicating the conventional manner in which a driver interacts with a vehicle's powertrain by allowing the driver to directly adjust the engine's combustion torque under most circumstances.

Controls implemented in the blended hybrid demonstration vehicle were modified from those presented in Section 6.3.4 to account for changes in the blended hybrid's architecture. As before distinct controllers were employed for low speed HST driving, HST driving, blended driving, and braking (Figure 8.23).

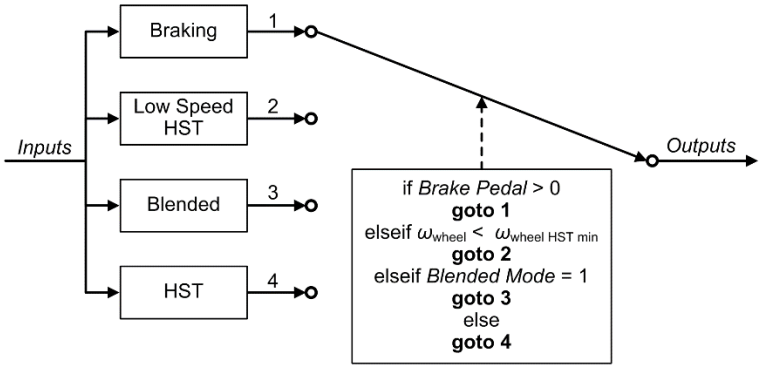

Figure 8.23: Torque control top level control scheme

A supervisory controller switched between the various control strategies based on measured parameters and predefined criteria. From rest the powertrain was initially controlled using the low speed HST controller. Once the vehicle reached either a predefine vehicle speed, or the reference engine speed, the powertrain was switched to HST control. From here the powertrain was moved to blended control once the vehicle reached a predefined speed and sufficient pressure was present in the HP accumulator. The blended control mode was maintained as long as the throttle pedal was depressed and the HP accumulator maintained a sufficient pressure after which it switch back to the

HST controller. Finally the powertrain was switch to the braking controller once the brake pedal was depressed.

Low Speed Hydrostatic Driving

During low speed driving the driver controlled engine throttle via the throttle pedal while Units 2 and 3 were set to 100% displacement. Simultaneously Unit 1 was controlled to provide some arbitrary pressure (e.g. 200 bar) based on the estimated combustion torque applied to Unit 1 (Eqs. 8.1-8.3). Modifications from the controller presented in Section 6.3.4 include consideration of the pump drive as well as a constant reference pressure.

$$M_{\text{CE}} = M_{\text{WOT}}\left(\omega_{\text{CE}}\right)u_{\text{throttle pedal}} \tag{8.1}$$

$$p_{\text{ref}} = 2\text{e}7 \text{ pa} \tag{8.2}$$

$$\beta_1 = \frac{M_{\text{CE}} i_{\text{pmp drv}} 2\pi}{V_1\left(p_{\text{ref}} - p_{\text{B}}\right)\eta_{\text{hm}}} \tag{8.3}$$

Hydrostatic Driving

During hydrostatic driving the driver continued to control engine throttle via the throttle pedal while the transmission controller adjusted unit displacements in order to track the reference engine speed. For the blended hybrid demonstration vehicle the reference engine speed was provided by a minimum BSFC control strategy similar to that described in Section 6.3.5. However the reference speed was artificially increased beyond what was optimal in order to better illustrate how the transmission controller tracked a varying reference engine speed. A block diagram of the hydrostatic driving controller for the blended hybrid is shown in Figure 8.24.

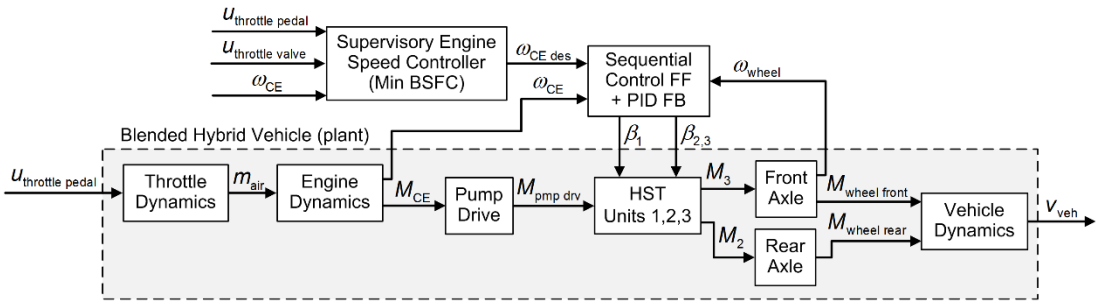

Figure 8.24: Torque controlled hydrostatic driving

The primary modifications made to the HST controller for use in the demonstration vehicle involved consideration of the pump drive as well as showing Units 2 and 3 connected to separate axles in the block diagram. Control of the units during HST driving is given by Equations 8.4-8.9.

$$e_{\omega_{CE}} = \omega_{CE\ des} - \omega_{CE} \tag{8.4}$$

$$u_{\omega_{CE}} = 1 - \left(k_p e_{\omega_{CE}} + k_i \int e_{\omega_{CE}} dt + k_d e_{\omega_{CE}} \frac{d}{dt} \right) \tag{8.5}$$

$$Q_{Unit1\ max} = \frac{\omega_{CE\ des} V_1 \eta_{vol}}{i_{pmp\ drv}} u_{\omega_{CE}} \tag{8.6}$$

$$Q_{Unit2,3\ max} = \frac{\omega_{wheel} i_{axle} \left(V_2 + V_3 \right)}{\eta_{vol}} \frac{1}{u_{\omega_{CE}}} \tag{8.7}$$

$$\beta_1 = \begin{cases} \dfrac{Q_{Unit2,3\ max}}{Q_{Unit1\ max}} & ; Q_{Unit1\ max} \geq Q_{Unit2,3\ max} \\ 1 & ; Q_{Unit1\ max} < Q_{Unit2,3\ max} \end{cases} \tag{8.8}$$

$$\beta_{2,3} = \begin{cases} 1 & ; Q_{Unit1\ max} \geq Q_{Unit2,3\ max} \\ \dfrac{Q_{Unit1\ max}}{Q_{Unit2,3\ max}} & ; Q_{Unit1\ max} < Q_{Unit2,3\ max} \end{cases} \tag{8.9}$$

Blended Driving

As during low speed and hydrostatic driving, the driver continued to supply input into the system by means of the throttle pedal. However during blended driving half of the power supplied by the powertrain to the wheels was provided by the engine while the second half was provided by the high pressure accumulator. In order to maintain a similar driver feel during blended driving the engine throttle valve was set to half the displacement commanded by the driver. A block diagram of the blended driving controller used in the demonstration vehicle is shown in Figure 8.25.

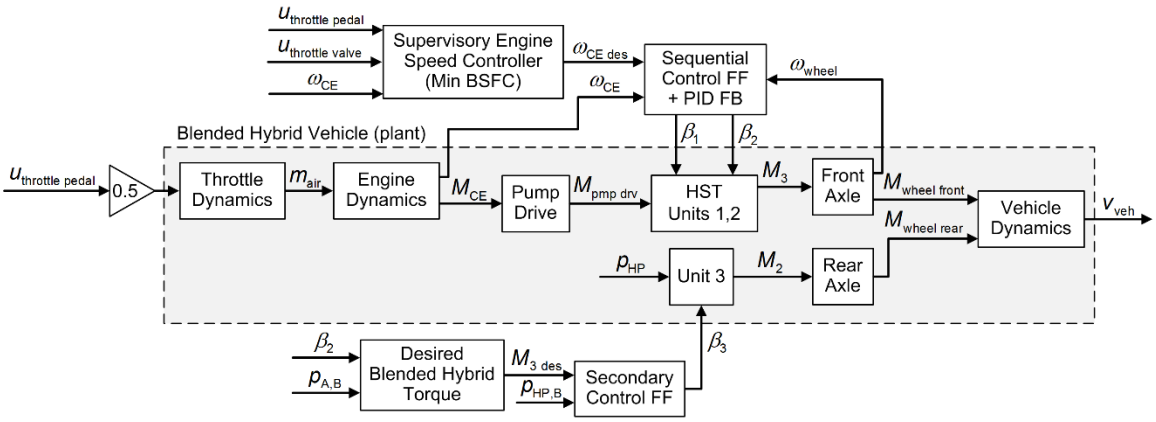

Figure 8.25: Torque controlled blended driving

During blended driving Units 1 and 2 were adjusted using sequential control plus PID feedback in order to control the engine speed (Equations 8.10-8.15).

$$e_{\omega_{CE}} = \omega_{CE\ des} - \omega_{CE} \tag{8.10}$$

$$u_{\omega_{CE}} = 1 - \left(k_p e_{\omega_{CE}} + k_i \int e_{\omega_{CE}} dt + k_d e_{\omega_{CE}} \frac{d}{dt} \right) \tag{8.11}$$

$$Q_{\text{Unit1 max}} = \frac{\omega_{CE\ des} V_1 \eta_{vol}}{i_{pmp\ drv}} u_{\omega_{CE}} \tag{8.12}$$

$$Q_{\text{Unit2 max}} = \frac{\omega_{wheel} i_{axle} V_2}{\eta_{vol}} \frac{1}{u_{\omega_{CE}}} \tag{8.13}$$

$$\beta_1 = \begin{cases} \dfrac{Q_{\text{Unit2 max}}}{Q_{\text{Unit1 max}}} & ;Q_{\text{Unit1 max}} \geq Q_{\text{Unit2 max}} \\ 1 & ;Q_{\text{Unit1 max}} < Q_{\text{Unit2 max}} \end{cases} \tag{8.14}$$

$$\beta_2 = \begin{cases} 1 & ;Q_{\text{Unit1 max}} \geq Q_{\text{Unit2 max}} \\ \dfrac{Q_{\text{Unit1 max}}}{Q_{\text{Unit2 max}}} & ;Q_{\text{Unit1 max}} < Q_{\text{Unit2 max}} \end{cases} \tag{8.15}$$

During blended driving Unit 3 was controlled to provide the same torque to the wheels as Unit 2 (Eqs. 8.16-8.18).

$$M_2 = \frac{\beta_2 V_2 \left(p_{\text{A}} - p_{\text{B}}\right)\eta_{\text{hm}}}{2\pi} \tag{8.16}$$

$$M_{3\,\text{des}} = M_2 \tag{8.17}$$

$$\beta_3 = \frac{M_{3\,\text{des}} 2\pi}{V_3 \left(p_{\text{HP}} - p_{\text{B}}\right)\eta_{\text{hm}}} \tag{8.18}$$

Braking

During regenerative braking Unit 1 was set to zero displacement while Units 2 and 3 were controlled (Eq. 8.20) to provide the desired braking torque (Eq. 8.19).

$$M_{2,3\,\text{des}} = M_{\text{brake torque map}}\left(u_{\text{brake pedal}}, p_{\text{HP}}\right) \tag{8.19}$$

$$\beta_{2,3} = \frac{M_{2,3\,\text{des}} 2\pi}{\left(V_2 + V_3\right)\left(p_{\text{HP}} - p_{\text{A}}\right)\eta_{\text{hm}}} \tag{8.20}$$

Desired regenerative braking torque was determined using the measured brake pedal position along with a predefined mapping. In interest of safety the brake pedal in the demonstration vehicle was modified such that the first 35% of travel was sensed purely electronically and used as in input into the regenerative braking system. However as the brake pedal was pressed past 35% the existing friction brakes began to be activated and combined with the regenerative braking torque. The brake pedal position to regenerative

braking torque mapping was designed with two key considers: first over a given range the same brake pedal position should always result in the same regenerative braking torque regardless of accumulator pressure (to maintain a consistent response). Second regenerative braking torque should be maximized before applying friction brakes (to maximize energy recovery). These considerations led to the mapping seen in Figure 8.26.

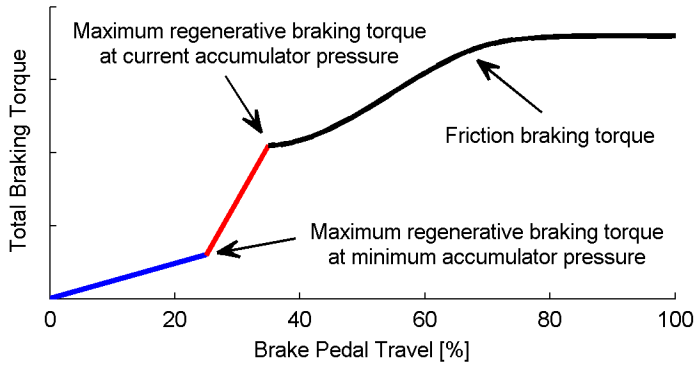

Figure 8.26: Desired regenerative braking torque mapping

Here 0 to 25% pedal travel corresponds to 0 to 100% of the braking torque available when the high pressure accumulator is at its minimum pressure and Units 2 and 3 are at full displacement. In this way the first 25% of pedal travel always corresponds to the same regenerative braking torque regardless of accumulator pressure. At 35% the hydraulic units are commanded to provide the maximum braking torque at the current accumulator pressure (i.e. Units 2 and 3 are at 100% displacement). Between 25 and 35% pedal travel the regenerative braking torque command is linearly interpolated between the maximum torque available at the minimum accumulator pressure, and the maximum torque available at the current accumulator pressure. Finally after 35% Units 2 and 3 remain at 100% while the dissipative frication brakes are applied.

8.5 Blended Hybrid Vehicle Testing

A mild acceleration and braking cycle was conducted to highlight the blended hybrid vehicle's distinct modes of operation using the control approach described in Section 8.4. A plot of these measurements can be found in Figure 8.27.

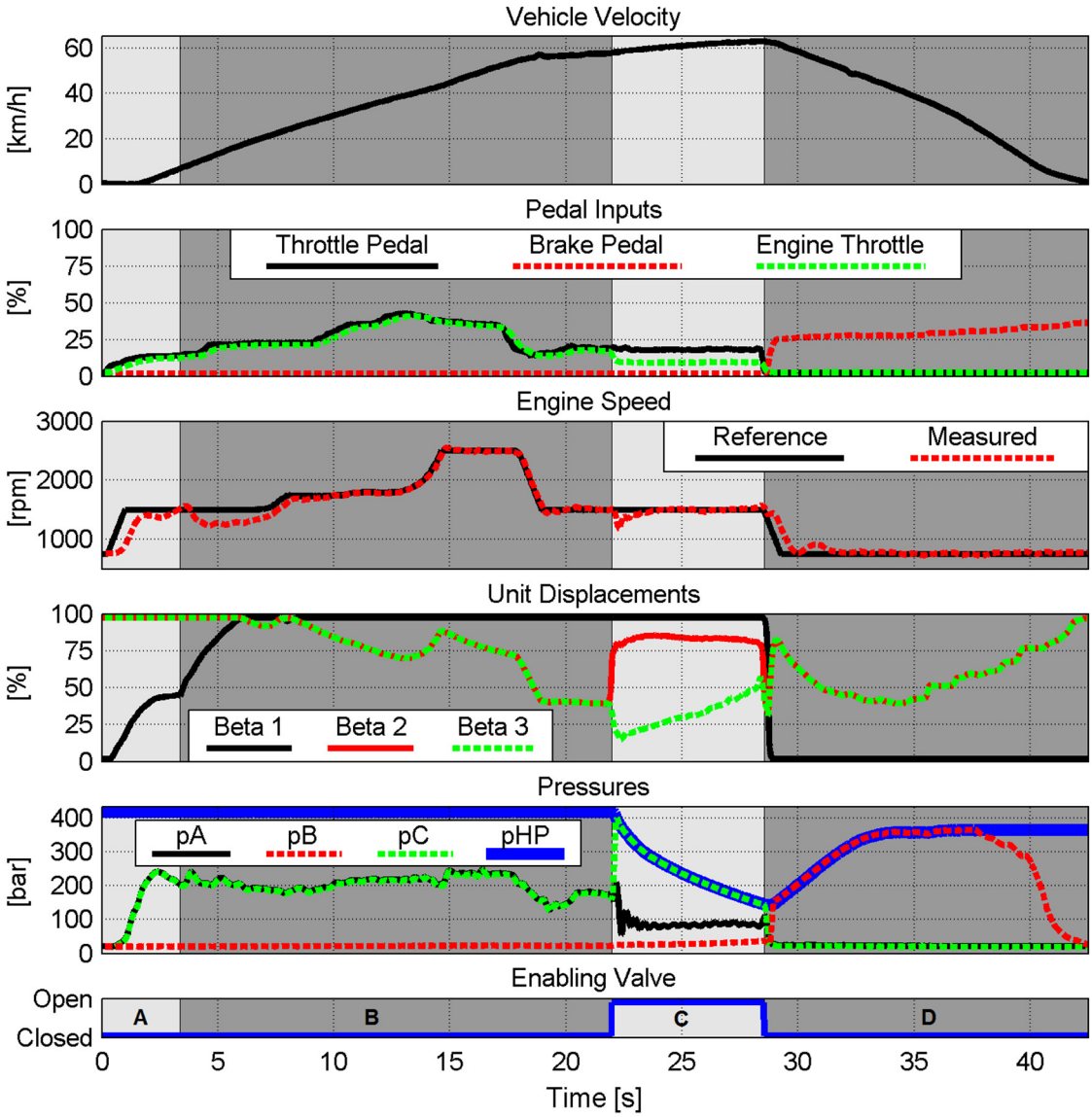

Figure 8.27: Blended hybrid demonstration vehicle measurement results

Measurements of the acceleration and braking cycle are split into four distinct sections (as denoted by letters in the final plot). In Section A the vehicle began at rest with an integrated throttle bypass valve maintaining the engine at a low idle speed of 750 rpm. To begin driving the driver depressed the throttle pedal which opened the engine's throttle valve in a 1-1 ratio. It should be noted that for this engine a throttle valve opening of 30% corresponded to roughly 85% of the available combustion torque. Therefore the throttle pedal commands seen in these measurements represent a relatively high

percentage of the engine's available torque. During startup the transmission was controlled using the low speed HST controller described above. In this control scheme Unit 1's displacement was controlled to generate some arbitrary pressure based on the applied combustion torque estimated using measured engine speed and throttle valve position. This low speed control strategy worked relatively well as seen in Figure 8.27 and felt natural to the driver. The low speed control strategy was maintained until the measured engine speed reached the desired engine speed at which point control of the units was transferred to the primary HST driving controller.

In Section B the demonstration vehicle was operated as a hydrostatic transmission. The driver continued to provide input into the system by adjusting the engine's combustion torque by means of the throttle pedal. Now though the unit displacements were set based primarily on measured vehicle speed in order to obtain the desired engine speed specified by the supervisory engine speed controller. A PID controller (tuned using the Ziegler-Nichols methodology) served to modify the unit displacements based on measured engine speed feedback in order to better track the reference engine speed. Figure 8.27 shows that for the most part engine speed was relatively well tracked using the proposed control methodology. However immediately following the transition from low speed control to HST control there was roughly a 250 rpm drop in engine speed as sequential control began and the PID controller was initialized. Controlling engine speed in this manner is made somewhat difficult due to the highly nonlinear volumetric losses of the hydraulic units which are influence by speed, pressure, and displacement. All three of these parameters were continuously changing for multiple units within the transmission leading to the errors in engine speed tracking seen in the measurements. A more advanced control methodology which can better handle the nonlinear characteristics of the transmission would quite likely improve the engine speed tracking for the proposed torque controlled approach.

In Section C the transmission was switched from hydrostatic to blended driving. Once the switch command was initiated Units 1 and 2 were commanded to begin changing their

displacements such that the reference engine speed would be maintained using the transmission ratio formed by Units 1 and 2 (instead of Units 1, 2, and 3 as before). Simultaneously Unit 3 was commanded to begin changing its displacement to provide the same torque produced by Unit 2, albeit at the high pressure accumulator's current pressure. A short period after the switching command was initiated the enabling valve was commanded to open providing Unit 3 with flow/pressure from the high pressure accumulator. It was determined experimentally that a 10 ms delay in commanding the enabling valve to open provided the smoothest transition between hydrostatic and blended driving. During blended driving the driver continued to supply input into the powertrain by means of the throttle pedal. However in this mode of operation only half of the power supplied by the powertrain to the wheels came from the engine as the second half was provided by the high pressure accumulator. In order for the driver's throttle pedal input to continue providing the same vehicle response experienced during hydrostatic driving, the engine's power must be reduced by half. There are two methods to accomplish this, first the reference engine speed could be cut in half (or close to this if differences in the WOT are taken into account). However in Section C the reference engine speed was already at 1500 rpm which was the lower limit set for the demonstration vehicle to prevent the engine from bogging down while driving. The second option for reducing engine power was to reduce the engine's combustion torque by half at the given engine speed. This second approach was used successfully in the demonstration vehicle resulting in a similar driver feel in both hydrostatic and blended modes of operation.

In Section D the blended hybrid transmission was switched from blended driving to regenerative braking. This process was initiated when the driver began depressing the brake pedal. Once the brake pedal was depressed Unit 1 was commanded to zero displacement and the enabling valve was commanded to close. Simultaneously Units 2 and 3 were adjusted to provide the desired regenerative braking torque specified by the brake pedal mapping. The blended hybrid then began to recover and store the vehicle's

kinetic energy resulting in an increasing pressure within the high pressure accumulator. From roughly 29-35s the measured brake pedal input, and consequently the commanded regenerative braking torque, remained relatively constant. To adapt to the rising pressure the displacements of Units 2 and 3 were decreased during this time period as seen in the figure. At around 37s pressure in Line B began to drop below the accumulator's pressure. Below a certain vehicle speed the flow leaving Units 2 and 3 was no longer sufficient to make up for the leakage across Unit 1. This is not a limitation of the blended hybrid architecture in general but rather the specific hydraulic unit chosen for Unit 1. This unit was never designed to operate at zero displacement while being exposed to high pressure and specifics of its design result in significant leakage under these conditions to the case drain. This issue could be remedied by simply using a different hydraulic unit which was designed to operate in such conditions. From 37s until the vehicle came to rest the pressure in Line B was thus determined by the pressure dependent volumetric losses of all three units. Regardless of this low vehicle speed issue, the regenerative braking system in the demonstration vehicle yielded a smooth and intuitive driver feel. The only other main change desirable in future iterations would be to redesign the braking system such that a longer percentage of the brake pedal travel could be dedicated to regenerative braking with friction brakes applied later in the travel.

Ultimately the blended hybrid demonstration vehicle proved to be quite successful. The torque controlled approach proposed in the work yielded a driving experience similar to conventional on-road vehicle and could potentially be used as an alternative to speed controlled hydrostatic transmissions in the off-highway segment as well. Speed control of the engine by means of the HST worked relatively well however more advanced control strategies which address the highly nonlinear volumetric losses of the units would likely improve tracking and performance. Further both hydrostatic and blended driving modes possessed a similar and familiar driver feel. The transition between hydrostatic and blended driving was also relatively smooth. Though this transition could be further improved by incorporating a pressure compensated flow control valve on the pilot stage

of the enabling valve thereby ensuring consistent opening characteristics regardless of accumulator pressure. Finally the regenerative braking system performed quite well and replicated the feel of a conventional friction braking system. The author would like to especially thank several industrial sponsors including Casappa, Danfoss, Durst, ExxonMobil, Hydac, and Sun Hydraulics for making this demonstration vehicle possible.

8.6 Chapter Summary

- A four wheel drive SUV was converted into a blended hybrid demonstration vehicle. This chapter detailed the circuit design, component design, packaging, and instrumentation required to implement the blended hybrid in an on-road vehicle.
- The driver torque controlled approach proposed in Section 6.3.4 was modified for use in the demonstration vehicle. This system level controller was combined with a minimum BSFC engine speed controller and a rule-based controller for the hybrid energy storage system to complete the powertrain control strategy.

- The ability to physically drive a blended hybrid vehicle allowed various control methodologies to be investigated from the perspective of driver perception. It was found that the proposed torque controlled approach worked quite well in replicating the driver feel of a conventional on-road vehicle.
- On-road measurements detailed in the work demonstrated the feasibility of the blended hybrid concept in real world conditions.

CHAPTER 9. CONCLUSIONS AND FUTURE WORK

This work aimed to discover how the performance, fuel efficiency, and controllability of hydraulic hybrid powertrains can be improved through novel hybrid architectures. To that end the following original contributions were made to advance the state of the art in fluid power:

- The relative fuel efficiencies of four transmissions including a manual, automatic, series hydraulic hybrid, and series hydraulic hybrid power split transmission were compared to one another when the influence of control on fuel efficiency was removed through dynamic programming. Evaluating the fuel efficiencies of these transmissions in a single vehicle over a defined cycle provided a benchmark for comparing novel hybrid transmission architectures.
- A novel neural network based power management strategy was proposed and investigated for conventional hydraulic hybrid transmissions. This implementable control strategy sought to replicate the performance of dynamic programming on new and untrained drive cycle. Experimental validation demonstrated that the proposed power management strategy improved fuel efficiency over baseline control strategies.
- Two novel transmission architectures termed the Blended Hydraulic Hybrid and the Blended Hydraulic Hybrid Power Split Transmission were proposed and investigated. Optimally controlled simulation studies showed these novel architectures were able to improve fuel efficiency over baseline mechanical and conventional hydraulic hybrid transmissions.

- Two novel system level control schemes were proposed and investigated for the blended hybrid. These control schemes sought to replicated the feel of a traditional mechanical transmission by uniquely controlling what is in essence a hydrostatic transmission in an on-road environment. On-road testing in a blended hybrid demonstration vehicle showed these control schemes yielded a driver feel similar to conventional vehicles.

- Two novel implementable power management control schemes were proposed and investigated for the blended hybrid. The more fuel efficient control scheme combined instantaneous optimization of the hydrostatic path with rule-based control of the hybrid energy storage system. Simulation studies showed this power management controller was able to achieve near globally optimal fuel efficiency without requiring knowledge of past driving events, or an estimation of future cycle demands. As an alternative an engine centric minimum BSFC power management control strategy was also proposed and investigated. While this control strategy achieved slightly lower fuel efficiency than the instantaneous optimization approach, it required little information about the transmission resulting in a more generally applicable approach.

- A hardware-in-the-loop transmission dynamometer was constructed to evaluate both the neural network based power management control strategy and the blended hybrid transmission architecture. This test rig enabled repeatable and accurate measurements on dynamic drive cycles providing a highly effective platform for original research.

- A four wheel drive SUV was modified into an on-road blended hybrid demonstration vehicle. This research platform demonstrated the blended hybrid concept's feasibility as well as enabling an exploration into driver perception of the various proposed control methodologies.

For conventional hydraulic hybrids the goals of this dissertation were addressed through a novel neural network based power management control scheme. Although the NN approach's potential was demonstrated within this research, future work could further improve the NN's performance and generality in real world environments. Specifically research could further investigate the NN's optimal size and configuration, the breadth vs. depth of training data, and whether any cycle data other than velocity would help to improve the network's predictive performance. Greater potential for increasing the NN's performance likely lies with online training of the NN. A control scheme can be envisioned where recently passed driving events are optimized off-line (though still in the transmission's controller) with these optimal controls being used to slowly retrain the NN. In this manner the NN could adapt to changes in driving style and vehicle characteristics.

To further improve the performance, fuel efficiency, and controllability of hydraulic hybrid transmissions two novel blended hybrid architectures were proposed in this work. The original research presented in this dissertation largely details the origination of the blended hybrid concept all the way through to successful prototype testing. Work is still needed though to bring the blended hybrid architectures into a form suitable for commercial production. Several areas of work remain: first more robust controllers are needed to handle aggressive driving and mode switching in order to maximize the transmission's performance. Improved transmission control can then be combined with one of the power management control schemes proposed in this work and evaluated in on-road vehicles. Thorough testing will then finally demonstrate the improved fuel efficiency potential offered by the blended hybrid concept. Second, a commercially viable blended hybrid would not take the form seen in the demonstration vehicle. Rather it would combined all of the rotating groups (i.e. hydraulic units) and valves into a single transmission housing in preferably a power split configuration. Regardless of the work remaining, the blended hybrid concept investigated in this dissertation has sufficient benefits over conventional hydraulic hybrid transmissions as to merit future study.

LIST OF REFERENCES

LIST OF REFERENCES

ANL 2015. Argonne National Laboratory, PSAT (Powertrain Systems Analysis Toolkit), http://www.transportation.anl.gov.

Artemis Intelligent Power. New Vehicle Technology Delivers 30% Carbon Savings. Artemis Intelligent Power, 2008.

Baseley, S., Ehret, C., Greif, E. and Kliffken, M. 2007. Hydraulic Hybrid systems for Commercial Vehicles. SAE Technical Paper 2007-01-4150.

Bauer, F., Field, D. and Grün, S. 2011. Double Piston Accumulator, Innovative Hydraulic Accumulator for Mobile Equipment. Proceedings of the Third Symposium, Hybrid Drives for Mobile Equipment, Karlsruhe, Germany. (Originally in German)

Bellman, R. 1956. Dynamic Programming and Lagrange Multipliers. Proceedings of the National Academy of Sciences of the United States of America, 42(10), 767.

Bender, F., Kaszynski, M. and Sawodny, O. 2013. Drive Cycle Prediction and Energy Management Optimization for Hybrid Hydraulic Vehicles. Vehicular Technology, IEEE Transactions on, 62(8), 3581-3592.

Bleazard, T. 2015. Hydraulic Hybrid Four Wheel Drive Sport Utility Vehicle - Utilizing the Blended Hybrid Architecture. MS thesis, Purdue University.

Bleazard, T., Hirai, H., Sprengel, M. and Ivantysynova, M. 2015. Optimal Control and Performance Based Design of the Blended Hydraulic Hybrid. ASME/Bath Symposium on Fluid Power and Motion Control. Oct. 12-14, 2015, Chicago, IL, USA.

Bowns, D., Vaughan, N. and Dorey, R. 1981. Design Study of a Regenerative Hydrostatic Split Power Transmission for a City Bus. IMechE Hydrostatic Transmissions for Vehicle Application. pp 29-38. Coventry, England.

Buchwald, P., Christensen, G., Larsen, H. and et al. 1979. Improvement of City Bus Fuel Economy Using a Hydraulic Hybrid Propulsion System – a Theoretical and Experimental Study. SAE Technical Paper 790305.

Clark, N., Zhen, F., Wayne, W. and Lyons, D. 2007. Transit Bus Life Cycle Cost and Year 2007 Emissions Estimation. No. FTA-WV-26-7004.2007.1.

Davies, A. 1987. Fuel Economy and Emissions Potential of a City Bus, Regenerative Power Train. SAE Technical Paper 872267.

Davies, A. 1989. The Reduction of City Bus Exhaust Emissions by Means of a Regenerative Powertrain. SAE Technical Paper 890267.

Davis, S., Diegel, S. and Boundy, R. 2014. Transportation Energy Data Book: Edition 33 (No. ORNL 6990). United States. Department of Energy.

Dewey C., Elder, F. and Otis, D. 1974. Accumulator-Charged Hydrostatic Drive for Cars Saves Energy. Hydraulics and Pneumatics, pp. 180-183.

Dorey, R. and Vaughan, N. 1984. Computer Aided Design of Split Power Hydrostatic Transmission Systems. ImechE. 198B(2):61-69.

Dunn, H. and Wojcienchowski, P. 1972. High-Pressure Hydraulic Hybrid with Regenerative Braking. 7th Intersociety Energy Conversion Engineering Conference, pp 989-995.

Dunn, H. and Wojcienchowski, P. 1974. Energy Storage and Conversion Efficiency in a Hydraulic/Gas–Turbine Hybrid. ASME, 74-GT-107.

Dunn, H. and Wojcienchowski, P. 1975. Energy Regeneration and Conversion Efficiency in a Hydraulic-Hybrid Propulsion System. High Speed Ground Transportation Journal, 9:383-392.

Dziuba, F. and R. Honzek 1997. Neues Stufenloses Leistungsverzweigtes Traktorgetriebe. (A new power-split transmission). Agrartechnische Forschung Vol. 3 No.1: 19-27.

Eaton 2010. Eaton's Hydraulic Hybrid System Deployed in Ann Arbor; City Takes Delivery of Recycling Trucks that Reduce Fuel Consumption, Emissions by 30 Percent http://www.eaton.com/Eaton/OurCompany/NewsEvents/NewsReleases/PCT_199871

Elder, F. and Otis, D. 1973. Simulation of a Hydraulic Hybrid Vehicle Powertrain. ASME, 73-ICT-50.

Environmental Protection Agency (EPA) 2015. http://www3.epa.gov/nvfel/testing/dynamometer.htm

Gray, C. 2004. The United States of America as represented by the Administrator of the Environmental Protection Agency. Hydraulic Hybrid Vehicle. Washington, DC USA. US 6,719,080 B1.

Hamblin H.J. 1952. Hydraulic Propulsion. Farm Mechanization Vol. 4, No. 38: 229-230.

Heggie, W. and Sandri R. 1979. An Energy-Saving Hydro-Pneumatic Power Plant for the Automobile. ASME, (79-WAIDSC-15).

Heskitt, M., Smith, T. and Hopkins, J. 2012. Design & Development of the LCO-140H Series Hydraulic Hybrid Low Floor Transit Bus: BUSolutions Final Technical Report (No. FTA Report No. 0018).

Hippalgaonkar, R. 2014. Power Management Strategies for Hydraulic Hybrid Multi-Actuator Mobile Machines with DC actuators. PhD thesis, Purdue University.

Hugosson, C. 1993. Cumulo Hydrostatic Drive – A Vehicle Drive with Secondary Control. 3rd Scandinavian International Conference on Fluid Power. Linkoping, Sweden.

Ivantysynova, M., Carl, B. and Williams, K. 2012. Power Split Transmission with Energy Recovery. U.S. Patent No. 8,277,352.

Jacobsen, R., Stewart, R. and Jahangiri, M. 1986. Thermodynamic Properties of Nitrogen from the Freezing Line to 2000 K at Pressures to 1000 MPa. Journal of Physical and Chemical Reference Data, 15(2), 735-909.

Johri, R., Baseley, S. and Filipi, Z. 2011. Simultaneous Optimization of Supervisory Control and Gear Shift Logic for a Parallel Hydraulic Hybrid Refuse Truck Using Stochastic Dynamic Programming. In ASME 2011 Dynamic Systems and Control Conference and Bath/ASME Symposium on Fluid Power and Motion Control (pp. 99-106). American Society of Mechanical Engineers.

Kepner, R. 2002. Hydraulic Power Assist – A Demonstration of Hydraulic Hybrid Vehicle Regenerative Braking in a Road Vehicle Application. SAE Technical Paper 2002-01-3128.

Kim, Y. and Filipi, Z. 2007. Series Hydraulic Hybrid Propulsion for a Light Truck-Optimizing the Thermostatic Power Management. SAE Technical Paper 2007-24-0080.

Kumar, R. and Ivantysynova, M. 2010. Investigation of Various Power Management Strategies for a Class of Hydraulic Hybrid Powertrains: Theory and Experiments Proc. of the 6th FPNI PhD Symposium, West Lafayette, USA, pp 87 - 99.

Kumar, R. 2010. A Power Management Strategy for Hybrid Output Coupled Power-Split Transmission to Minimize Fuel Consumption. PhD thesis, Purdue University.

Lammert, M., Burton, J., Sindler, P. and Duran, A. 2014. Hydraulic Hybrid and Conventional Parcel Delivery Vehicles' Measured Laboratory Fuel Economy on Targeted Drive Cycles. SAE Technical Paper 2014-01-2375.

Liebherr, 2015. Pactronic Hybrid Drive System. www.liebherr.com

Lin, C., Kang, J., Grizzle, J. and Peng, H. 2001. Energy Management Strategy for a Parallel Hybrid Electric Truck. Proceedings of the American Control Conference, Arlington, USA.

Linde. 2015. Linde History from 1904 to 2014. http://www.lindehydraulics.com/en-gb/about/timeline.aspx

Liu, J. and Peng, H. 2006. Control Optimization for a Power-Split Hybrid Vehicle. American Control Conference.

Martini, S. 1984. The M.A.N. Hydrobus: A Drive Concept with Hydrostatic Brake Energy Recovery. International Symposium on Advanced and Hybrid Vehicles.

Matheson, P. and Stecki, J. 2003. Development and Simulation of a Hydraulic-Hybrid Powertrain for use in Commercial Heavy Vehicles. SAE Technical paper 2003-01-3370.

Meile 1961. Hydrostatic Drives for Tractors. ASAE paper No. 61-632. St Joseph, MI: American Society of Agricultural Engineers.

Mikeska, D. and Ivantysynova, M. 2002. Virtual Prototyping of Power Split Drives. Proc. Bath Workshop on Power Transmission and Motion Control PTMC. Bath, UK. 95-111.

Molly, H. 1966. Hydrostatische Fahrzeugantriebe–ihre Schaltung und konstruktive Gestaltung. (Hydrostatic Vehicle Drives - Their Control and Engineering. Part I and II). ATZ, 68(4), 103-110.

Morris, W. 1967. The IHC Hydrostatic. Farm Mechanization and Buildings Vol. 19, No. 215:79.

Musardo, C., Rizzoni, G., Guezennec, Y. and Staccia, B. 2005. A-ECMS: An Adaptive Algorithm for Hybrid Electric Vehicle Energy Management. European Journal of Control, 11(4), 509-524.

Nakazawa, N., Kono, Y., Takao, E. and Takeda, N. 1987. Development of a Braking Energy Regeneration System for City Bus. SAE Technical Paper 872265.

Ossyra, Jean-Claude 2004. Control Concepts for Vehicle Drive Line to Reduce Fuel Consumption. PhD thesis, TUHH Hamburg.

Pacala, S. and Socolow, R. 2004. Stabilization Wedges: Solving the Climate Problem for the Next 50 Years with Current Eechnologies. Science, 305 (5686), 968-972.

Paynter, H. 1961. Analysis and Design of Engineering Systems. M.I.T. Press, Cambridge, Massachusetts, USA.

PSA-Peugeot-Citroen, 2015. Hybrid Air, an Innovative Full Hybrid Gasoline System. http://www.psa-peugeot-citroen.com.

Renius, K. and Resch, R. 2005. Continuously Variable Tractor Transmissions. ASAE Distinguished Lecture Series.

Reynolds, W., Ross, L. and Gantzer, C. 1966. Starter-Drive System. U.S. Patent No. 3,274,855.

Ross, W. 1972. Designing a Hydromechanical Transmission for Heavy Duty Trucks. SAE Technical Paper 720725.

Schneider, K. and Krautler, W. 2012. Hydraulic Drive System. U.S. Patent No. 8,151,563.

Shiber, S. 1979. Automotive Energy Management System. National Conference on Fluid Power. 141-147.

Shiber, S. 1980. Multi-Mode Transmission. U.S. Patent No. 4,196,587.

Sprengel, M. and Ivantysynova, M. 2012a. Energy Saving System Architecture for Hydraulic Hybrid Off-Highway Vehicles. Proceedings of the 7th FPNI PhD Symposium. June 27-30, 2012. Reggio Emilia, Italy.

Sprengel, M. and Ivantysynova, M. 2012b. Novel Transmission Configuration for Hydraulic Hybrid Vehicles. Proceedings of the International Sci-Tech Conference “Machine Dynamics and Vibro Acoustics”. Sept. 5-6, 2012. Samara, Russia.

Sprengel, M. and Ivantysynova, M. 2012c. Coupling Displacement Controlled Actuation with Power Split Transmissions in Hydraulic Hybrid Systems for Off-Highway Vehicles. Bath Workshop on Power Transmission and Motion Control (PTMC2012). Sept. 12-14, 2012. Bath, UK.

Sprengel, M. and Ivantysynova, M. 2013a. Investigation and Energetic Analysis of a Novel Hydraulic Hybrid Architecture for On-Road Vehicles. Proceedings of the 13th Scandinavian International Conference on Fluid Power (SICFP2013). June 3-5, 2013. Linkoping, Sweden.

Sprengel, M. and Ivantysynova, M. 2013b. Control Strategies for a Novel Blended Hydraulic Hybrid Transmission. Proceedings of the 22nd International Conference on Hydraulics and Pneumatics. Oct. 24-25, 2013. Prague, Czech Republic.

Sprengel, M. and Ivantysynova, M. 2014a. Investigation and Energetic Analysis of a Novel Blended Hydraulic Hybrid Power Split Transmission. Proceedings of the 9th IFK International Fluid Power Conference. March 24-26, 2014. Aachen, Germany.

Sprengel, M. and Ivantysynova, M. 2014b. Hardware-in-the-Loop Testing of a Novel Blended Hydraulic Hybrid Transmission. Proceedings of the 8th FPNI PhD Symposium on Fluid Power (FPNI2014). June 11-13, 2014. Lappeenranta, Finland.

Sprengel, M. and Ivantysynova, M. 2014c. Recent Developments in a Novel Blended Hydraulic Hybrid Transmission. SAE 2014 Commercial Vehicle Engineering Congress. Oct. 7-9, 2014. Rosemont, IL, USA. SAE Technical Paper 2014-01-2399.

Sprengel, M., Bleazard, T., Haria, H. and Ivantysynova, M. 2015. Implementation of a Novel Hydraulic Hybrid Powertrain in a Sports Utility Vehicle. Proceedings of the 2014 IFAC Workshop on Engine and Powertrain Control, Simulation and Modeling. Aug. 23-26, 2015. Columbus, OH, USA.

Tollefson, S., Beachley, N. and Fronczak, F. 1985. Studies of an Accumulator Energy-Storage Automobile Design with a Single with a Single Pump/Motor Unit. SAE Technical Paper 851677.

Wadman, B. 1973. Responder Automatic Transmission Ready for Market. Diesel and Gas Turbine Progress Vol. 39, No. 6: 32-35.

Wendel, G., Baseley, S., O'Brien, J., Kargul, J. and Ellis, M. 2007. Hydraulic Hybrid Vehicle System Panel. Michigan Clean Fleet Conference.

Wu, B., Luo, N., Fronczak, F. and Beachley, N. 1985. Fuel Economy and Operating Characteristics of a Hydropneumatic Energy Storage Automobile. SAE Technical Paper 851678.

Zimmerman, J. 2012. Toward Optimal Multi-Actuator Displacement Controlled Mobile Hydraulic Systems. PhD thesis, Purdue University.

VITA

VITA

Michael Sprengel

Department of Agricultural and Biological Engineering, Purdue University

Education

B.S. Mechanical Engineering, May 2010, Missouri University of Science and Technology (formally University of Missouri Rolla), Rolla, Missouri.

M.S. Mechanical Engineering, May 2013, Purdue University, West Lafayette, Indiana.
Major Professor: Monika Ivantysynova

Ph.D. Engineering, December 2015, Purdue University, West Lafayette, Indiana.
Thesis: Influence of Architecture Design on the Performance and Fuel Efficiency of Hydraulic Hybrid Transmissions
Major Professor: Monika Ivantysynova

Awards

Backe Medal – 8th FPNI PhD Symposium, Lappeenranta, Finland

Department of Energy H3CoE Fellowship – Department of Energy and hybrid vehicle industrial partners

PUBLICATIONS

PUBLICATIONS

Sprengel, M. and Ivantysynova, M. 2016. Neural Network Based Power Management of Hydraulic Hybrid Vehicles. International Journal of Fluid Power. (In Review)

Bleazard, T., Hirai, H., Sprengel, M. and Ivantysynova, M. 2015. Optimal Control and Performance Based Design of the Blended Hydraulic Hybrid. ASME/Bath Symposium on Fluid Power and Motion Control. Oct. 12-14, 2015. Chicago, IL, USA.

Sprengel, M., Bleazard, T., Haria, H. and Ivantysynova, M. 2015. Implementation of a Novel Hydraulic Hybrid Powertrain in a Sports Utility Vehicle. Proceedings of the 2014 IFAC Workshop on Engine and Powertrain Control, Simulation and Modeling. Aug. 23-26, 2015. Columbus, OH, USA.

Sprengel, M. and Ivantysynova, M. 2014. Recent Developments in a Novel Blended Hydraulic Hybrid Transmission. SAE 2014 Commercial Vehicle Engineering Congress. Oct. 7-9, 2014. Rosemont, IL, USA. SAE Technical Paper 2014-01-2399.

Sprengel, M. and Ivantysynova, M. 2014. Hardware-in-the-Loop Testing of a Novel Blended Hydraulic Hybrid Transmission. Proceedings of the 8th FPNI PhD Symposium on Fluid Power (FPNI2014). June 11-13, 2014. Lappeenranta, Finland.

Sprengel, M. and Ivantysynova, M. 2014. Investigation and Energetic Analysis of a Novel Blended Hydraulic Hybrid Power Split Transmission. Proceedings of the 9th IFK International Fluid Power Conference. March 24-26, 2014. Aachen, Germany.

Sprengel, M. and Ivantysynova, M. 2013. Control Strategies for a Novel Blended Hydraulic Hybrid Transmission. Proceedings of the 22nd International Conference on Hydraulics and Pneumatics. Oct. 24-25, 2013. Prague, Czech Republic.

Sprengel, M. and Ivantysynova, M. 2013. Investigation and Energetic Analysis of a Novel Hydraulic Hybrid Architecture for On-Road Vehicles. Proceedings of the 13th Scandinavian International Conference on Fluid Power (SICFP2013). June 3-5, 2013. Linkoping, Sweden.

Sprengel, M. and Ivantysynova, M. 2012. Coupling Displacement Controlled Actuation with Power Split Transmissions in Hydraulic Hybrid Systems for Off-Highway Vehicles. Bath Workshop on Power Transmission and Motion Control (PTMC2012). Sept. 12-14, 2012. Bath, UK.

Sprengel, M. and Ivantysynova, M. 2012. Novel Transmission Configuration for Hydraulic Hybrid Vehicles. Proceedings of the International Sci-Tech Conference “Machine Dynamics and Vibro Acoustics”. Sept. 5-6, 2012. Samara, Russia.

Sprengel, M. and Ivantysynova, M. 2012. Energy Saving System Architecture for Hydraulic Hybrid Off-Highway Vehicles. Proceedings of the 7th FPNI PhD Symposium. June 27-30, 2012. Reggio Emilia, Italy.